REMOVAL OF SELECTED TOXIC ELEMENTS BY SURFACE MODIFIED MULTI-WALLED CARBON NANOTUBES FROM CONTAMINATED GROUNDWATER IN SEKHUKHUNE, LIMPOPO

BY

RUTH DIPUO THOBAKGALE

DISSERTATION

Submitted in fulfilment of the requirements for the degree of

MASTER OF SCIENCE

in

CHEMISTRY

in the

FACULTY OF SCIENCE AND AGRICULTURE

(School of Physical and Mineral Sciences)

at the

UNIVERSITY OF LIMPOPO

SUPERVISOR: PROF T. MAGADZU

CO-SUPERVISORS: DR A.A AMBUSHE (UJ)

DR L.E MACEVELE

2022

DECLARATION

I declare that the work presented in this dissertation for the degree of Master of Science in chemistry at the University of Limpopo was written by me under the supervision of Prof T Magadzu. It has not been previously submitted before for any degree at any other university. It is my design and all the materials for the references contained have been fully acknowledged.

Signature: 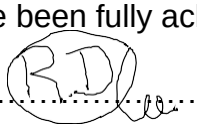 ..... Date: 03/08/2022

DEDICATION

This dissertation is sincerely dedicated to my son Katlego Thobakgale for being the strength and light that keeps me going. I also dedicate this work to my sister Julia Kholofelo Thobakgale for her support throughout my study.

ACKNOWLEDGEMENTS

I would like to express my sincere gratitude to my supervisor Prof T Magadzu for allowing me to do research, providing invaluable guidance throughout this research and for the constant remarks you always made to improve my work. To both my supervisor and co-supervisors (Dr LE Macevele and Dr AA Ambushe), I am grateful for their support, advice and encouragement throughout this research project in which I gained knowledge from their expertise. I am grateful to them for reviewing and commenting on the entire dissertation with patience and guidance as my supervisors.

I would also like to appreciate my co-supervisor Dr LE Macevele for her bright and insightful comments and ideas. I am also thankful as she shaped and gave direction to my research and tremendous endurance even when the pressure of the work was mounting. To Dr AA Ambushe, your suggestions regarding the research focus, sampling methods, financial assistance and assistance with nanocomposite characterisations at the University of Johannesburg were duly acknowledged.

Special thanks go to my lab mates and associates, Veronica Ramollo and Dinah Thole for their assistance during the research and for making our lab a friendly environment to work in. I would also like to extend my gratitude to Veronica Ramollo and Stuart Mamabolo for taking their time to accompany and assist me in water sampling at Sekhukhune. Thank you all for being there for me.

Sincere thanks also go to Prof RM Mampa and Dr TC Leboho for their continuous assistance and suggestions at the department no matter how minor. To Ms Ramakadi, the one person who made sure we were not short of reagents and other supplies needed in our lab, I am thankful for her kindness and always willing to help. I am also thankful to the University of Limpopo and the chemistry department for allowing me the opportunity to further my studies at this institution.

I would like to thank my late grandparents (John and Martinah Thobakgale), who without their wisdom and faith I would have not made it this far, and to my loving and supporting mother (Rachel Motubasa Thobakgale), for your support, strength and patience shaped me into the person I am today and made it possible for me to reach the level in which I am at currently.

To my younger sister (Julia Kholofelo Thobakgale), no number of words can express how thankful and how much I appreciate your endless support. You took a heavy load of weight off my shoulders with the financial assistance you provided me to be able to complete my degree. I thank you for all the time you took to read my work and gave the necessary suggestions. If it was not for you, it would have taken me longer to complete my work and for that, I am deeply grateful.

The funding provided by the Water Research Commission (WRC) Project Number K5/2515//1 is greatly acknowledged.

I am thankful to the maker of heaven and earth for the strength I had through him to persevere throughout my studies.

In all your ways acknowledge Him and He shall direct your paths.

Proverbs 3:6

Whatever you ask for in prayer, believe

that you have received it, and it will be yours.

Mark 11:12 (NIV)

CONFERENCE PRESENTATIONS

Oral presentation

- R.D. Thobakgale, L.E. Macevele, A.A. Ambushe and T. Magadzu. Removal of Cr(III) and Cr(VI) by surface-modified multi-walled carbon nanotubes from contaminated groundwater in Sekhukhune, Limpopo, presented at the University of Limpopo research day, Bolivia lodge, South Africa, October 2021.

ABSTRACT

Water contamination caused by toxic elements has serious human health and ecological implications. The increasing quantity of toxic elements in surface and groundwater is currently an area of greater concern, especially since many industries are discharging their metal containing effluents into freshwater without any adequate treatment. The mineral dissolution in mining regions is highly enhanced by mining and smelting activities. The mine waste and drainage in areas surrounding mines have high levels of toxic element contamination above the permissible limits. Contamination of groundwater by toxic elements such as As, Fe, Mn, Al, Cr, Zn and Co due to operational activities of surrounding mines in the Sekhukhune district was reported by several researchers. Removal of toxic elements from contaminated water is a big challenge. The affected communities need to attain a safe water supply source for daily usage, hence there is an urgent need of technologies for the treatment of water supplies contaminated with these toxic elements to ensure the safety of potable water.

The study was undertaken by modifying nitrogen-doped multi-walled carbon nanotubes (N-MWCNTs) and investigating the removal of chromium, nickel and lead from anthropogenic contaminated groundwater in the Sekhukhune area, in Limpopo. The as-prepared N-MWCNTs functionalised with metal oxide, thiol and amino functional groups are expected to increase the surface area of the nanocomposite, which can facilitate high adsorption of contaminants from water samples. The adsorption capabilities for the removal of these toxic elements by modified N-MWCNTs nanocomposites were investigated in batch studies as a function of different parameters. The parameters studied included pH, contact time, adsorbent dosage, initial concentration, temperature, competing ions and reusability. The optimum condition was then acquired for removal of selected toxic elements from real water studies. The removal efficiencies of the as-prepared nanocomposites were pH dependent and the optimal pH values for adsorption was 5.5, 1.5, 11 and 6 at optimum contact time of 10, 80, 60 and 120 min and dosage of 0.30, 0.35, 0.05 and 0.6 g/L for Cr(III), Cr(VI), Ni(II) and Pb(II), respectively.

The prepared nanocomposites were characterised using various techniques such as Fourier transform infrared (FTIR) spectroscopy, powder X-ray diffraction (PXRD), scanning electron microscopy (SEM), transmission electron microscopy (TEM),

Brunauer-Emmet-Teller (BET) and thermogravimetric analysis (TGA). The FTIR analysis confirmed the presence of Fe_3O_4, -SH and -NH_2 groups on the functionalised MWCNTs. The PXRD analysis further supported that the synthesized nanocomposites consisted of hexagonal graphite structure of MWCNTs. Furthermore, SEM and TEM results showed that the introduced functional groups were uniformly attached on the surface of the MWCNTs. The BET analysis indicated that the surface area of the modified MWCNTs nanocomposites increased significantly as compared to the acid-treated MWCNTs. In addition, TGA showed that the M-MWCNTs (M = modified) nanocomposites possess high thermal stability. Raw N-MWCNTs showed higher stability as compared to oxidised N-MWCNTs, which decomposes at lower temperatures of 200 °C. No weight loss was observed below 800 °C for the hydrazine-functionalised nanocomposites as compared to the triethylenetetramine (TETA)-substituted nanocomposites, which showed weight loss at 300 °C.

Toxic elements in solutions before and after treatment were quantified using flame-atomic absorption spectrometry (F-AAS). The adsorption isotherms of the as-prepared nanocomposites for chromium, nickel and lead removal fitted both the Langmuir and Freundlich model depending on the adsorbent used, which suggest that the adsorption process met both monolayer and heterogeneous adsorption. Thermodynamic analysis showed that the adsorption of Cr(III), Cr(VI), Ni(II) and Pb(II) ions are spontaneous and endothermic. The as-prepared nanocomposites showed an outstanding regeneration performance retaining over 50% toxic elements removal. Thus, the as-prepared nanocomposites are promising for practical application in toxic element treatment. Analysis of the collected river and borehole water in Sekhukhune indicated that the concentration of total chromium, nickel and lead before treatment varied from (0.207 to 0.286 mg/L), (0.226 to 0.380 mg/L) and (3.301 to 8.017 mg/L), respectively which were above acceptable levels recommended by the South African National Standards (SANS), United States Environmental Protection Agency (USEPA) and World Health Organisation (WHO), i.e., 0.05 mg/L, 0.07 mg/L and 0.01 mg/L. After treatment, the nanocomposites were able to remove 100% of the metal ions from the water. TETA-functionalised nanocomposites showed greater removal efficiencies in comparison to the hydrazine-functionalised nanocomposites for all the studies done.

TABLE OF CONTENTS

LIST OF FIGURES

LIST OF TABLES

LIST OF ABBREVIATIONS AND ACRONYMS

AMD	Acid mine drainage
BET	Brunauer-Emmet-Teller
CNTs	Carbon nanotubes
CSIR	Council for scientific and industrial research
EC	Electrical conductivity
DWAF	Department of Water and Sanitation
F-AAS	Flame-atomic absorption spectrometry
f-MWCNTs	Functionalised MWCNTs
FTIR	Fourier transform infrared spectroscopy
HA	Humic acid
HABs	Harmful algal blooms
HFeO	Hydrous ferric oxide
HMs	Heavy metals
HRTEM	High resolution transmission electron microscopy
HSAB	Hard and soft acids and bases
ICP-MS	Inductively coupled plasma-mass spectrometry
MPL	Maximum permissible level
MSPE	Magnetic solid phase extraction
MWCNTs	Multi-walled carbon nanotubes
M-MWCNTs	Modified multi-walled carbon nanotubes
PAC	Powdered activated carbons
PAHs	Polycyclic aromatic hydrocarbons
PXRD	Powder x-ray diffraction

NMs	Nanomaterials
NPs	Nanoparticles
N-MWCNTs	Nitrogen-doped multi-walled carbon nanotubes
SANS	South African National Standards
SEM	Scanning electron microscopy
SF	Surface functionalisation
SS	Sampling site
SWCNTs	Single-walled carbon nanotubes
TEM	Transmission electron microscopy
TETA	Triethylenetatramine
TGA	Thermogravimetric analysis
WBP	Waterborne protozoa
USEPA	United States Environmental Protection Agency
WHO	World Health Organisation
R^2	Square of correlation coefficient

CHAPTER 1: INTRODUCTION

1.1 BACKGROUND

South Africa is ranked the 30th driest country in the world due to its water scarcity and is often subjected to extreme climate and rainfall fluctuations. Due to the influx of urban populations and the economic pressure from industrial development, including mining, the demand for access to drinkable water is expected to continue escalating. Sekhukhune has been chosen as the primary research area because it has experienced a significant increase in mining activities [1].

Toxic elements are frequent contaminants in the environment from mining operations. All of these operations contaminate the environment in significant amounts. As well as hydro-chemical factors such as the mineral composition of the rocks and the characteristics of the soil, toxic elements in natural water are affected by anthropogenic activities [2]. Biochemical processes, such as biomethylation and assimilation of pollutant metals, lead to new bond types such as the conversion of mercury to methyl mercury; both being processes that lead to the formation of more toxic metal species. Using processes of assimilation, bioaccumulation and biomethylation, polluted metals are incorporated into the food chain from water bodies [2]. Due to the toxic properties of toxic elements, the maximum permissible levels (MPLs) of these elements in water intended for human consumption was strictly set by the World Health Organisation (WHO) and guidelines by many countries [3].

Toxic elements cause environmental problems due to their non-oxidative nature. They provide a long-term source of contamination [4]. Hexavalent chromium (Cr(VI)) for instance is among the most toxic elemental species and is considered a significant groundwater contaminant, worldwide [5]. About seventy countries including South Africa, have reported serious health hazards such as skin lesions, cardiovascular and neurological effects because of using water contaminated with toxic elements [6]. To date, various studies have been carried out on the water quality in different parts of the Sekhukhune district [1]. Conventional methods are usually time-consuming, labour-intensive, and susceptible to interferences [7]. Various physical and chemical methods have been applied for the remediation of toxic elements such as adsorption,

membrane filtration, chemical coagulation, ion exchange, leaching and photocatalysis [8,9]. Among them, adsorption is the most explored because of the simplicity, effectiveness and economics of this method. In this direction, nanotechnology plays an important role to develop nano-adsorbents. Nanomaterials offer a greater specific surface area, which directly enhances the adsorption capacity [9].

Recent studies have shown that magnetic nanostructures have potential applications for the effective removal of toxic elements. They have been found to show excellent adsorption for various types of toxic elements such as As(III), As(V), Cr(VI) and Pb(II) [10]. Carbon nanotubes provide a chemically inert atmosphere for physical adsorption. Their structure at the atomic scale is far more defined than any of the other adsorbents. They are highly porous and have strong interactions with pollutants [11]. Iron oxide nanoparticles and their modified surfaces with a variety of functional groups as nanosorbents are promising in the removal of toxic elements from groundwater near industrial areas [12]. Surface modification by the attachment of inorganic or organic molecules, not only stabilizes the nanoparticles and prevents them from oxidation but also provides specific functional groups or reaction sites that can be selective and specific for ions uptake and tremendously enhance the capacity for toxic element uptake in water treatment procedure [12].

However, there are not many findings on the adsorption of toxic elements onto multi-walled carbon nanotubes (MWCNTs) modified with a couple of functional groups namely iron oxide, thiol and amino groups (N_2H_4-SH-Fe_3O_4/o-MWCNTs or $C_6H_{18}N_4$-SH-Fe_3O_4/o-MWCNTs). Iron oxides can be easily separated from water under a magnetic field and also allow easy isolation from aqueous solutions for regeneration [13]. Due to Lewis acid-base interactions with the thiol groups, they exhibit a strong affinity for various heavy metal ions and exhibit very selective adsorption [14], while the amino groups can also selectively remove heavy metal ions via coordination interactions [15].

1.2 PROBLEM STATEMENT

The contamination of water by toxic elements has become a major environmental concern resulting from rapid growth in urbanisation, industrialisation and agricultural practices. Many elements are vital nutrients in small amounts; however, they pose serious threats to the environment and the health of the people at high concentrations [3]. For example, neurological, mental and other hostile effects are caused by subjection and accumulation of toxic elements [16]. Among these toxic elements, arsenic, chromium in its hexavalent form, mercury and nickel; are significant groundwater contaminants worldwide [17,18]. As an example, contamination of groundwater by arsenic and other toxic elements due to operational activities of Foskor phosphate and Phalaborwa copper mines downstream of Greater Letaba was reported by Letsoalo et al. [19]. In the Sekhukhune area, surrounding mines such as the Tubatse Chrome mine developed a new slag dump disposal facility near the village of Steelpoort adding to possible sources of water contamination [20]. Although studies have been done on speciation of toxic elements in the selected areas, no study has focused on the removal of such toxic elements.

Several methods of removing toxic elements already exist, which includes precipitation, adsorption and ion exchange [21]. From these methods, adsorption is preferred due to its versatility and ease of operation [16,22]. Among a variety of carbon nanomaterials, the study proposes to use amine treated modified MWCNTs with the additions of thiol functional groups for the removal of toxic elements [23].

1.3 MOTIVATION

Sekhukhune area is one of the five districts in the Limpopo province with towns such as Burgersfort and Steelpoort surrounded by mining operations. These operations develop slag dumps and hazardous waste disposal to the water supply. Tubatse Municipality has recorded about 232 villages that still depend on boreholes for water supply, which imply that reliance on boreholes must be reduced as they get contaminated [24]. The study is influenced by the scarcity of safe potable water in rural

areas on account of toxic element contamination from industrial and mining activities. Toxic elements are non-biodegradable and can accumulate in the environment and living creatures [25,5]. For example, a maximum permissible concentration for arsenic, as recommended by the WHO, in portable water is 10 µg/L [26]. The toxicity of mercury is based upon its chemical form; hence organic species are more toxic than inorganic species [27]. Chromium is a naturally abundant element with three different states of oxidation, that is, Cr(II), Cr(III) and Cr(VI). Hexavalent chromium, Cr(VI) is formed in small quantities as an unintentional by-product during ferrochrome production and airborne exposure to Cr(VI) being correlated with respiratory cancer [28].

MWCNTs are an efficient sorbent for removing organic, inorganic and biological pollutants [29]. Nowadays, MWCNTs are used in multidisciplinary areas due to their optical, electronic, thermal and outstanding mechanical properties [30]. For example, Hadavifar et al. [31] have reported that thiol treated MWCNTs improve the adsorption capacity of mercury ions. This is because of their ability to stabilise MWCNTs (due to the presence of magnetic species) while providing more active sites for adsorption [24].

The use of metal oxides such as titanium dioxide ($TiO_{2)}$ and cobalt oxide (Co_3O_4) have been reported to enhance the reactivity of materials due to higher surface ratio and they are less toxic [32]. Hence, this study will investigate the adsorption capabilities of surface-modified MWCNTs and the effects of their modification with amino and thiol groups towards the simultaneous removal of toxic elements such as Cr, Ni and Pb.

1.4 AIM AND OBJECTIVES

1.4.1 Aim

The aim of the study is to investigate the adsorption capabilities of modified MWCNTs for the removal of toxic elements from anthropogenic contaminated groundwater.

1.4.2 Objectives

The objectives of the study will be to:

i. synthesise amine treated metal oxides-MWCNTs nanocomposites,
ii. characterise the prepared nanocomposites using techniques such as Fourier transform infrared (FTIR) spectroscopy, thermogravimetric analysis (TGA), scanning electron microscopy (SEM) and transmission electron microscopy (TEM),
iii. optimise the adsorption conditions with hydrazine and thiol for the removal of Cr, Ni and Pb using the modified MWCNTs nanocomposites,
iv. quantify toxic elements in simulated solutions and water before and after treatment using flame-atomic absorption spectrometry (F-AAS) and inductively coupled plasma-mass spectrometry (ICP-MS).
v. screen for multi-elements in borehole water using ICP-MS.

1.5 SCIENTIFIC CONTRIBUTIONS

Various communities in the Limpopo province are enclosed by mining activities which enhance mineral dissolution; hence the water supply and drainages in these areas have elevated levels of toxic elements. This study will assist in developing improved materials and systems for treating toxic element contaminated water. At least one article will be published in peer-reviewed local and international journals. Also, the output of this study will be presented at local and international conferences.

1.6 ETHICAL CONSIDERATION

No ethical issues are to be considered within the scope of this research since there is no animal or human involvement.

1.7 OUTLINE OF THE DISSERTATION CHAPTERS

Chapter 1 gives insight into the proposed research which includes the introduction, problem statement, motivation of the study, aim and objectives.

The literature review is presented in chapter 2 which entails the selected study areas, water scarcity in Sekhukhune district, occurrence and distribution of toxic elements, water contaminants, looking at inorganic contaminants in detail, current methods for toxic element remediation and modification of nanomaterials for water treatment.

Chapter 3 gives a detailed methodology for the preparation of the MWCNTs nanocomposites, characterisation techniques, description of the study areas and sample collection procedures followed for this study.

Chapter 4 presents discussed characterisation results as well as results and discussions for adsorption studies.

Conclusions and recommendations are outlined in chapter 5 based on the findings from the study. A list of references is provided at the end of each chapter.

REFERENCES

1. Guidone, A., 2019. Whose Knowledge, Whose Water, Whose Life: A Case Study of Water Governance and Mining in Sekhukhune, South Africa (Doctoral dissertation, Queen's University (Canada), Department of Environmental Studies).
2. Sedibe, M., Achilonu, M.C., Tikilili, P., Shale, K. and Ebenebe, P.C., 2017. South African mine effluents: Heavy metal pollution and impact on the ecosystem. Int J Chem Sci. 2017;15(4):198.
3. Xu, J., Cao, Z., Zhang, Y., Yuan, Z., Lou, Z., Xu, X. and Wang, X., 2018. A review of functionalized carbon nanotubes and graphene for heavy metal adsorption from water: Preparation, application, and mechanism. Chemosphere, 195, pp.351-364.
4. Hashim, M.A., Mukhopadhyay, S., Sahu, J.N. and Sengupta, B., 2011. Remediation technologies for heavy metal contaminated groundwater. Journal of environmental management, 92(10), pp.2355-2388.
5. Xu, L., Wang, J., Lu, A., 2017. Occurrence, speciation and transportation of heavy metals in 9 coastal rivers from watershed of Laizhou Bay, China. Chemosphere 173, pp.61-68.
6. Omwene, P.I., Çelen, M., Öncel, M.S. and Kobya, M., 2019. Arsenic removal from naturally arsenic contaminated ground water by packed-bed electrocoagulator using Al and Fe scrap anodes. Process Safety and Environmental Protection, 121, pp.20-31.
7. Jabłońska-Czapla, M., 2015. Arsenic, antimony, chromium, and thallium speciation in water and sediment samples with the LC-ICP-MS technique. International journal of analytical chemistry, 2015.
8. Fu, F. and Wang, Q., 2011. Removal of heavy metal ions from wastewaters: a review. Journal of environmental management, 92(3), pp.407-418.
9. Pandey, L.M., 2020. Surface engineering of nano-sorbents for the removal of heavy metals: Interfacial aspects. Journal of Environmental Chemical Engineering, p.104586.
10. Abdullah, N.H., Shameli, K., Abdullah, E.C. and Abdullah, L.C., 2019. Solid matrices for fabrication of magnetic iron oxide nanocomposites: synthesis, properties, and application for the adsorption of heavy metal ions and dyes. Composites Part B: Engineering, 162, pp.538-568.

11. Verma, B. and Balomajumder, C., 2020. Surface modification of one-dimensional Carbon Nanotubes: A review for the management of heavy metals in wastewater. Environmental Technology & Innovation, 17, p.100596.
12. Neyaz, N., Siddiqui, W.A. and Nair, K.K., 2014. Application of surface functionalized iron oxide nanomaterials as a nanosorbents in extraction of toxic heavy metals from ground water: a review. International Journal of Environmental Sciences, 4(4), p.472.
13. Hua, M., Zhang, S., Pan, B., Zhang, W., Lv, L. and Zhang, Q., 2012. Heavy metal removal from water/wastewater by nanosized metal oxides: a review. Journal of hazardous materials, 211, pp.317-331.
14. Zhang, C., Sui, J., Li, J., Tang, Y. and Cai, W., 2012. Efficient removal of heavy metal ions by thiol-functionalized superparamagnetic carbon nanotubes. Chemical Engineering Journal, 210, pp.45-52.
15. Zhan, Y., Hu, H., He, Y., Long, Z., Wan, X. and Zeng, G., 2016. Novel amino-functionalized Fe 3 O 4/carboxylic multi-walled carbon nanotubes: one-pot synthesis, characterization and removal for Cu (II). Russian Journal of Applied Chemistry, 89(11), pp.1894-1902.
16. Masindi, V. and Muedi, K.L., 2018. Environmental contamination by heavy metals. Heavy metals, 10, pp.115-132.
17. Kobya, M., Soltani, R.D.C., Omwene, P.I. and Khataee, A., 2020. A review on decontamination of arsenic-contained water by electrocoagulation: Reactor configurations and operating cost along with removal mechanisms. Environmental Technology & Innovation, 17, pp.100519.
18. Almeida, J.C., Cardoso, C.E., Tavares, D.S., Freitas, R., Trindade, T., Vale, C. and Pereira, E., 2019. Chromium removal from contaminated waters using nanomaterials–a review. TrAC Trends in Analytical Chemistry, 118, pp.277-291.
19. Letsoalo, M.R., Godeto, T.W., Magadzu, T. and Ambushe, A.A., 2018. Quantitative Speciation of Arsenic in Water and Sediment Samples from the Mokolo River in Limpopo Province, South Africa. Analytical Letters, 51(17), pp.2763-2777.
20. Pistorius, J.C.C. 2012. A phase I heritage impact assessment (HIA) study for Tubatse Chrome (PTY) LTD: expansion of a slag dump and the development of a new hazardous waste site in the Steelpoort valley in the Limpopo province

of South Africa. Unpublished report prepared for Tubatse Chrome (PTY) LTD and Golder Associates Africa (Pty) Ltd.

21. Mohan, D. and Pittman, C.U., 2007. Arsenic removal from water/wastewater using adsorbents—a critical review, J. Hazard. Mater. 142, pp.1–53.
22. Mishra, T. and Mahato, D.K., 2016. A comparative study on enhanced arsenic (V) and arsenic (III) removal by iron oxide and manganese oxide pillared clays from groundwater. Journal of Environmental Chemical Engineering, 4(1), pp.1224-1230.
23. Jiang, L., Li, S., Yu, H., Zou, Z., Hou, X., Shen, F., Li, C. and Yao, X., 2016. Amino and thiol modified magnetic multi-walled carbon nanotubes for the simultaneous removal of lead, zinc, and phenol from aqueous solutions. Applied Surface Science, 369, pp.398-413.
24. Sekhukhune District Municipality. 2018. Draft Integrated Development Plan (IDP) Review for 2018/2019. Groblersdal. Retrieved from: https://doi.org/http://www.sekhukhunedistrict.gov.za/sdm-admin/documents/Draft IDP 2018-2019.pdf. (accessed 07 August 2020).
25. Hashim, M.A., Mukhopadhyay, S., Sahu, J.N. and Sengupta, B., 2011. Remediation technologies for heavy metal contaminated groundwater. Journal of environmental management, 92(10), pp.2355-2388.
26. World Health Organization, 2003. Arsenic in drinking-water: Background document for development of WHO guidelines for drinking-water quality (No. WHO/SDE/WSH/03.04/75). World Health Organization.
27. Ricardo, A.I.C., Sánchez-Cachero, A., Jiménez-Moreno, M., Bernardo, F.J.G., Martín-Doimeadios, R.C.R. and Ríos, A., 2018. Carbon nanotubes magnetic hybrid nanocomposites for a rapid and selective preconcentration and clean-up of mercury species in water samples. Talanta, 179, pp.442-447.
28. Beukes, J.P., Van Zyl, P.G. and Ras, M., 2012. Treatment of Cr (VI)-containing wastes in the South African ferrochrome industry-a review of currently applied methods. Journal of the Southern African Institute of Mining and Metallurgy, 112(5), pp.347-352.
29. Ahmad, J., Naeem, S., Ahmad, M., Usman, A.R. and Al-Wabel, M.I., 2019. A critical review on organic micropollutants contamination in wastewater and removal through carbon nanotubes. Journal of environmental management, 246, pp.214-228.

30. Robati, D., Mirza, B., Ghazisaeidi, R., Rajabi, M., Moradi, O., Tyagi, I., Agarwal, S. and Gupta, V.K., 2016. Adsorption behaviour of methylene blue dye on nanocomposite multi-walled carbon nanotube functionalized thiol (MWCNT-SH) as new adsorbent. Journal of Molecular Liquids, 216, pp.830-835.
31. Hadavifar, M., Bahramifar, N., Younesi, H. and Li, Q., 2014. Adsorption of mercury ions from synthetic and real wastewater aqueous solution by functionalized multi-walled carbon nanotube with both amino and thiolated groups. Chemical Engineering Journal, 237, pp.217-228.
32. Yaqoob, A.A., Parveen, T., Umar, K. and Mohamad Ibrahim, M.N., 2020. Role of nanomaterials in the treatment of wastewater: A review. Water, 12(2), p.495.

CHAPTER 2: LITERATURE REVIEW

2.1 INTRODUCTION

The rapid expansion of urbanisation, industrialisation, and agricultural practices has made high-quality drinking water scarcer [1]. The contaminants found in water have become among the most important environmental concerns of the 21st century, posing a serious risk to human health as well as the environment [2]. Due to their adverse health effects, toxic elements have gained attention among various water contaminants [2,3]. Different methods of treating water and wastewater containing toxic elements have been developed over many years in order to decrease the amount of water and wastewater that contains toxic elements and improve the quality of treated effluents [4,5].

2.2 WATER SCARCITY IN SEKHUKHUNE DISTRICT

The Sekhukhune District Municipality in Limpopo Province, South Africa is made up of five local municipalities, namely: Greater Tubatse, Elias Motsoaledi, Fetakgomo, Makhuduthamaga and Ephraim Mogale. Sekhukhune is commonly recognized as being a water-scarce region, having few surface and ground water reserves. Despite this, the district uses a variety of sources such as groundwater, rivers, wells, pools, and dams. However, access to water remains an unfulfilled priority in Sekhukhune, despite recent infrastructure investments. The majority of households either lack piped water or have to travel outside their homes to obtain water [6].

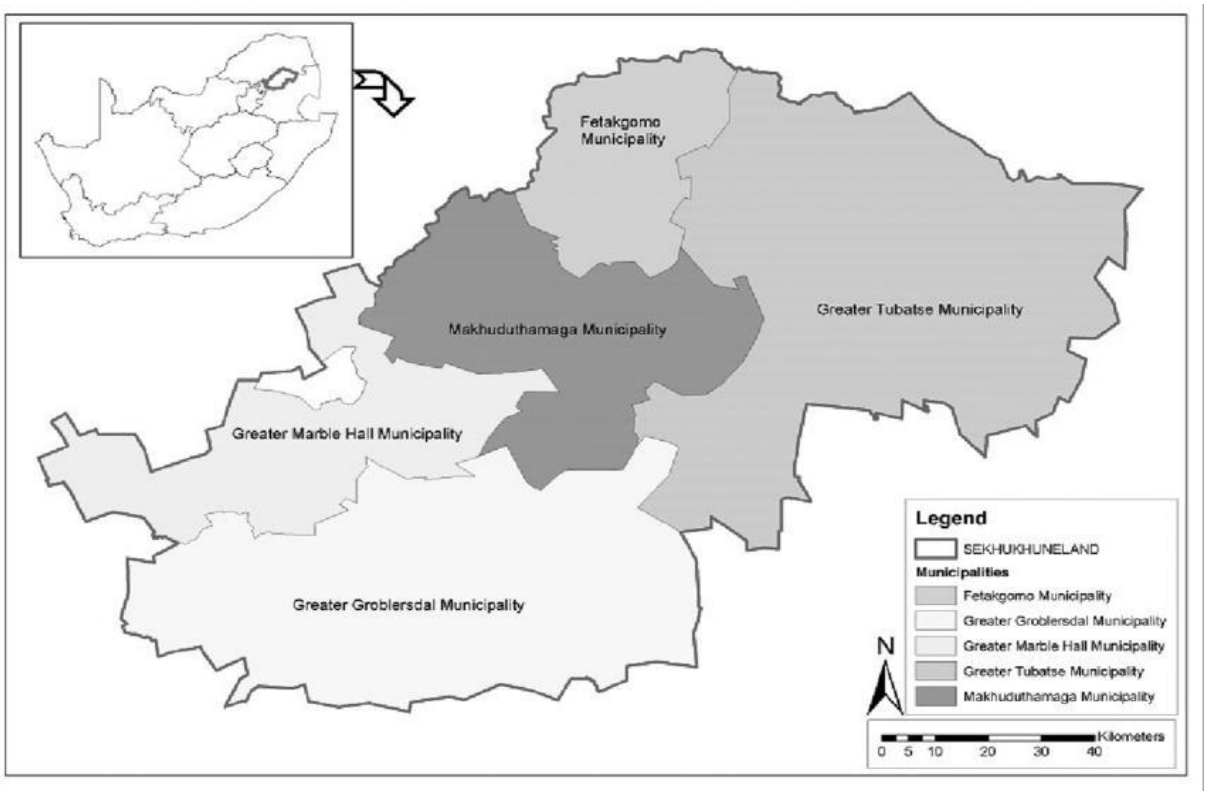

Figure 2. 1: Photo showing the five municipalities making up the Sekhukhune district [7].

Rural communities in Sekhukhune struggle with water access and quality issues related to bulk water infrastructure and service provision, in addition to living right next to active mining operations. Community perceptions about access to water depend on a variety of contextual factors and concluded from research done in Sekhukhune by Meissner et al. [8], water security is mainly understood and interpreted differently by people with varying lifestyles and relates mostly to the availability, accessibility and quality of water resources.

2.3 MINING ACTIVITIES IN LIMPOPO PROVINCE

Mining for valuable mineral resources is practised in various countries such as China, India, South Africa, Australia, the United States of America and European Union countries. The production of mining materials like copper, lead, and others have

increased in the last few decades. This practice helps stimulate economic growth and development in developing nations. Mining activities like deep mining or auxiliary projects and opencast mining usually impact water quality hydrology [9].

Mineral resources are abundant in the Limpopo Province. There are over 70 mines in the province, with a total of 50 small to medium scale mines as recorded by the Minerals Bureau [10]. It was also recorded that there are more mining activities in Sekhukhune District Municipality than in any other district municipality in Limpopo Province. Mining has been identified as an important contributor to enterprise development, job creation, economic growth and the empowerment of the local population in the Limpopo Province 11]. The platinum sector in South Africa is responsible for producing up to 80% of the world's platinum group metals (PGMs) supplies with more than 75% of the world's output [6]. The province has the biggest reserves of PGMs, which include rich deposits of nickel, vanadium, titanium, iron ore, chrome, diamonds, copper and coal [11]. A study conducted in the area found that the economy of the Sekhukhune District Municipality is heavily dependent on these minerals and irrigated agriculture; all of which require a lot of water, which is currently insufficient in the area. Mining activities are known to contaminate underground water supplies because metals in mine effluent are washed into rivers rendering it unfit for human consumption [12].

2.4 IMPACT OF MINING ON THE ENVIRONMENT AND HUMAN HEALTH

Some effluents produced by mining activities contain large amounts of toxic materials, such as heavy metals and cyanides, which have serious ecological and health consequences. In addition to contributing significantly to a region's economic activity, mining is also a major polluter and degrader [10].

According to past studies on mining impact, aquifers below mining operations can be contaminated resulting from infiltration of low-quality mine water. A variety of toxic elements can also be found in mining waste, including arsenic, chromium, cadmium, copper, fluoride, zinc, nickel, and lead. Groundwater may become contaminated with these toxic contaminants if they accumulate in water bodies [9]. Several studies

conducted from Limpopo, South Africa [13], Musina, Limpopo [10], Sekhukhune, Limpopo [14], Mokolo and Greater Letaba Rivers, Limpopo [15] and Tubatse Municipality, Sekhukhune [16] have reported these areas to be having high groundwater toxic element contamination. A study conducted by Singh et al. [9] concluded that almost 19,300 km of rivers watercourses and more than 72,000 hectares of reservoirs and lakes around the world may be seriously impacted by mine effluents from discarded coal and metal mines.

Due to its diverse mineral deposits, the Limpopo Province is quickly becoming South Africa's leading mining province. Many aspects of mining are negative for the environment, even though mining generally generates prosperity and economic wealth. Consequently, toxic elements are becoming more prevalent as a result of mining and smelting of ores *via* dust emissions, mine tailings, and sewage. In addition to land surface contamination, mining also contaminates surface- and groundwater [13]. As an example, contamination of groundwater by arsenic and other toxic metals due to operational activities of Phalaborwa copper and Foskor phosphate mines downstream of Greater Letaba was reported by Letsoalo et al. [15]. Another study was reported by Mathipa [16] for contamination of groundwater by toxic elements due to operational activities of surrounding mines in the Tubatse municipality.

Water scarcity is currently experienced in the Sekhukhune District Municipality among other areas in Limpopo Province as a result of mining activities. Furthermore, a mining operation's effect on water quality and air quality can lead to food insecurity in communities around the mines as well [11]. Furthermore, statistics on river and dam water access were presented by the research focused on agriculture in Sekhukhune. The study showed that 7.3% of households had access to water from a dam, while 12.9% relied on rivers [14]. In addition to soil erosion and toxic element contamination, mining diminishes the usability of land. Mining damages groundwater with chemicals, reducing the availability of clean water and leading to conflict between local communities and mining companies [11]. Drimie et al. reported that toxic element contamination in Greater Tubatse Local Municipality makes it difficult to access clean water for agricultural production and human consumption [7].

In mining, water is contaminated in various ways, for example by toxic elements, processing chemicals, erosion, and sedimentation. Another concern is acid mine drainage (AMD) from historic and present mines. To balance a load of contaminated water disposed into containment facilities, mining and industrial sectors discharge polluted or contaminated water to rivers. Poorly designed and inadequately operated water treatment facilities cause both sectors to fail to treat affected water, anions and cations also predominate in the discharged affected water [17].

2.4.1 Environmental impacts

Mining is linked to several environmental impacts, including erosion, acid mine drainage, land degradation and toxic element contamination. Eventually, these lead to problems with health, safety and sociality [10]. Mining operations contribute to the contamination of the environment with toxic elements at almost every stage of their activities, including processes such as the excavation of land, drilling, quarrying, crushing, grinding, and concentrating of ores, as well as their disposal. Environmental contamination is a consequence of all these operations [18]

A combination of intensive land use and poor environmental management practices have led to an increasing threat to rivers and streams from anthropogenic pollution such as toxic elements. The biogeochemical cycle naturally produces most elements, but many are released into inland waterways as effluents from mining, industrial, agricultural, and domestic sources, and may have adverse effects on aquatic systems. Benthic macroinvertebrates inhabit river sediments, which function as sinks for elements such as heavy metals. Some benthic organisms burrow, which exposes them to chemical elements contaminated sediments through a chronic exposure process [19].

2.4.2 Impacts on human health

Toxic elements can interfere with the metabolic functions of the human body in a variety of ways. For example, they can accumulate in important organs like the brain, the heart, the liver, and the kidneys, impairing normal biological functions. As toxic

elements can be absorbed by the human body through various routes, including by ingesting contaminated food and water or inhaling them, a variety of effects may occur in the body [20]. Upon entering living organisms, these metals react with enzymes, proteins, and DNA molecules, forming highly stable bio-toxic compounds, interfering with their normal functions and impeding their biochemical reactions. As a result, disproportional amounts of toxic elements adversely impact the metabolism of humans and also lead to imbalances in antioxidation. Additionally, numerous hormones are affected as well as enzymes and enzyme functions [20,21]. The accumulation of toxic elements in the body and their substitution for essential elements can cause an imbalance in the body when exposed to toxic elements repeatedly [20].

2.5 STUDY AREAS

2.5.1 Steelpoort River

Besides its ecological and social importance, the Steelpoort River is a major tributary of the Olifants River. Water from the Steelpoort River is mostly used for agricultural and domestic activities. Animals from the area also drink water from the Steelpoort River. The Steelpoort River may be affected by various anthropogenic activities in the area such as agriculture, mining, and other industrial activities. Collectively, dams and other anthropogenic alterations to rivers reduce river health [22]. Mining has experienced rapid growth in the Steelpoort region. Several opencast quarries also exist in the Steelpoort area, which exploits different sources of construction materials for buildings and roads. Mine expansion or development in the area, therefore, depends entirely on the quality and quantity of water [22].

The main tributaries of the Steelpoort River are the Sperkboom and Groot Dwars Rivers. A water quality study by DWAF [23] on the Steelpoort basin states that surface and groundwater resources in the Steelpoort basin are further threatened by increasing levels of contaminants from agricultural, industrial, residential and mining sources. The same reports conclude that in the area of the Steelpoort River in the central Steelpoort basin: surface water is potable with nominal treatment (filtration and chlorination) and It was found that out of 25 boreholes studied, most of the samples were not suitable for drinking water [24].

2.5.2 Olifants River

Catchment of Olifants River is part of Limpopo River Basin, which forms part of an international drainage basin that stretches across Botswana, Mozambique, South Africa and Zimbabwe. A catchment as large as the Olifants River contributes nearly 40% of the water flowing into Limpopo River, meaning it plays an important role in the water supply system. The main tributaries of the Olifants River are the Blyde, Elands, Ga-Selati, Klaserie, Klein Olifants, Steelpoort, Timbavati Wilge, Rivers [24].

2.6 TYPES OF WATER CONTAMINANTS

There are three various types of contaminants associated with water pollution in Sekhukhune area, biological contaminants, organic contaminants and inorganic contaminants.

2.6.1 Biological contaminants

A biological contamination of water occurs when there are living organisms in it, such as bacteria, algae, protozoans or viruses. Every one of them can have distinct effects on water [25]. Drinking water contaminated with microbial pathogens beyond the recommended limits cause serious human health hazards which can lead to waterborne diseases, such as cholera, vomiting, dysentery, typhoid fever, and polio, which have been defined as the world’s leading killers by the WHO [26,27].

Public health remains a major concern regarding bacterial infections caused by drinking contaminated water as it is linked to fatal illnesses such as diarrhoea. Diarrhoeal disease is believed to be caused by unsafe drinking water, according to the WHO [28]. By assessing the water's colour, odour, turbidity, and taste, contaminants can often be easily detected. Many of these contaminants cannot be detected at first sight and must be tested to determine whether the water is contaminated. Thus, the contaminants may cause an unpleasant taste or smell, staining and health effects [25].

Algae are in general single-celled and microscopic [25]. The presence of cyanotoxins produced by harmful algal blooms (HABs) is a serious threat to drinking water sources and an urgent global challenge. Continued eutrophication and climate change have

led to significant increases in HABs and the associated cyanotoxin contamination of drinking water sources [29]. Many organisms may produce freshwater HABs, including cyanobacteria (formerly known as blue-green algae), haptophytes, macroalgae, euglenophytes, dinoagellates, and others. Cyanobacteria are typically the taxa of greatest concern with respect to HABs in freshwater systems and include organisms such as Anabaena, Microcystis, Nodularia, Cylindrospermopsis, and others [30].

Protozoans are also single-celled and microscopic organisms [25]. There are a variety of parasites causing diarrheal illnesses, including waterborne protozoa (WBP). The diversity of WBP can be found in water [31]. A virus is the smallest living organism capable of causing diseases and producing infection [25]. Human enteric viruses commonly occur in subsurface water supplies and are generally understood to contribute to a significant number of waterborne outbreaks of gastroenteritis related to groundwater consumption. Consistent with this, they are generally more prevalent in the subsurface than other pathogens such as protozoan cyst [32].

2.6.2 Organic contaminants

The term organic contamination describes biodegradable contaminants that can be found in an environment. Anthropogenic activity has also contributed to the intensive production of these sources of pollution to meet human needs, even though they are naturally found and caused by the environment. Compounds such as human waste, food waste, organochlorine pesticides (OCPs), polychlorinated biphenyls (PCBs), pharmaceuticals, polybrominated diphenyl ethers (PBDEs), and polycyclic aromatic hydrocarbons (PAHs) have been noted to be contributing to organic contamination [33]. There has been increased attention paid to organic contaminants since they have become a major environmental problem. Organic contaminants are found to be persistent due to their properties which include stability, hydrophilicity, lipid solubility and lipophilicity. Because of these properties, organic contaminants are able to bioaccumulate in the environment, which can lead to toxicological effects. Domestic waste, pesticides and industrial waste are the most common anthropogenic sources of organic contamination. Contamination with organic materials can result in serious health concerns like cancer, hormonal disturbances, and nervous system problems [26].

Metal toxicity can reduce biodegradation of organic components. It appears that metals have a significant effect on organic biodegradation by affecting both the physiology and ecology of microorganisms involved in the degradation process. Industrial wastewater from various industries such as glass production, leather tanning, metal coating, pigments and dyes, mining activities and battery manufacture contains toxic elements. Besides being heavily contaminated, tannery wastewater contains high organic loadings. Organic contents are produced owing to the existence of soluble protein, fertilizer, hair, flesh and blood particles [34].

2.6.3 Inorganic contaminants

Human and animal health is adversely affected by the contamination of the environment caused by industrial, agricultural, and domestic waste. From such sources, inorganic contaminants are released. Metals, salts, and minerals are inorganic contaminants that typically have mineral origins [33,35]. A variety of anthropogenic and natural processes, as well as mine drainage, smelting, metallurgical and chemical processes, lead to inorganic substances entering the environment.

The presence of several inorganic contaminants has been detected in drinking water throughout the world and often at levels beyond the standards recommended by the WHO. Water sources containing inorganic pollutants are a cause for concern due to their impact on human health [36]. This section explains in detail the properties of the selected inorganic contaminants from this study.

2.6.3.1 Chromium

Physical and chemical properties

Naturally, Cr is found mostly in the trivalent state Cr(III). In nature, it occurs as chromate, a white transition metal that appears steely-grey, glossy, and brittle. Among the nine valence states, Cr(VI) and Cr(III) have an impact on the environment because

they are unstable in the natural environment [37]. In general, the common valence states of chromium in nature are trivalent chromium (Cr(III)) and hexavalent chromium (Cr(VI)). Cr(III) is a trace metal that has little mobility and toxicity in soil and water; the chromate Cr(VI) is highly soluble in water and has very high mobility and toxicity [34,37,38]. In aqueous systems, Cr(VI) occurs mostly in the form of chromate (CrO_4^{2-}, $Cr(OH)^{2+}$, $Cr(OH)_3$ and $Cr(OH)_4^-$) and dichromate ($Cr_2O_7^{2-}$, $HCrO_4^-$ and CrO_4^{2-}) [37]. Compounds containing Cr(III) are generally insoluble in water, such as $Cr(OH)_3$, which precipitate at neutral pH; Cr(VI) is highly soluble in water throughout the pH range. It is important to note that the ratio between chromium hexavalent, Cr(VI), and trivalent, Cr(III), is highly dependent on the pH of the solution, oxidative properties (redox potential), and kinetics of the reaction. Chromium can therefore change oxidation states in water based on these conditions. When pH is > 6.5, CrO_4^{2-} becomes the predominant form, while $HCrO_4^-$ becomes the predominant form at pH 2.0 to 6.5. There are four main forms of Cr(III) in aqueous solution, in which soluble Cr^{3+} complexes are predominant at pH < 4.0, and Cr(III) precipitates as $Cr(OH)_3$ between pH = 5.5 and 12.5 [39].

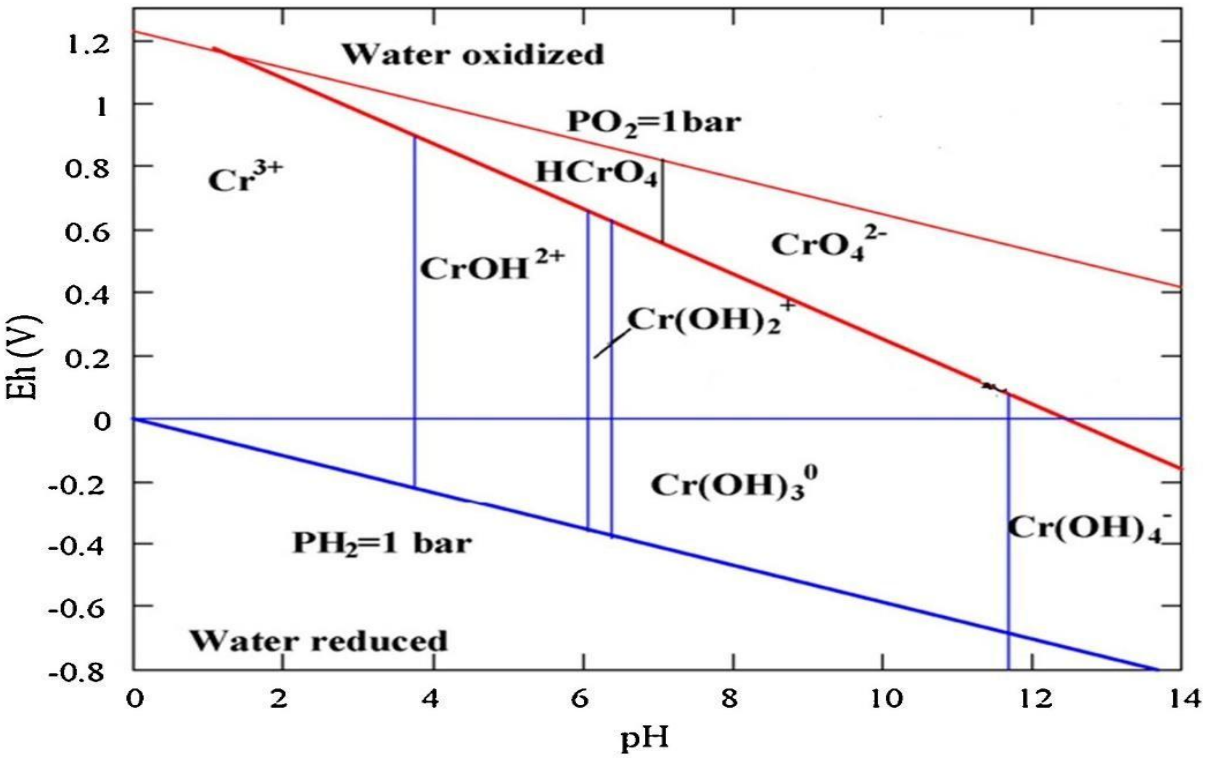

Figure 2. 2: Eh-pH diagram of chromium [37].

Occurrence and distribution of chromium

The ample use of chromium in industrial applications, such as metal electroplating, metallurgy, chromate manufacturing, textile dyeing, tanneries, wood preservation, metal electroplating and refractory, makes it one of the more noxious traces in surface and groundwater [34,37-40]. To create stainless steel, chromium is consumed in the form of ferrochromium, which contributes greatly to its corrosion resistance. South Africa is particularly affected by this problem given the atmospheric concentration of Cr(VI) [37]. Heavy metals (HMs) often occur in developing country water systems due to anthropogenic emissions and natural processes [37]. For example, several natural processes are implicated in increasing the amount of chromium released to oceans, rivers, lakes, and estuaries, including soil erosion and the weathering of rock. These processes happen by means of mineral dissolution, precipitation and adsorption/desorption of chemical species, evolving to contaminants in groundwater and soils [37].

Health threats associated with chromium contamination

Various health issues have been reported since Cr(VI) easily penetrates biological membranes, causing it to be carcinogenic by nature. Once accumulated in the body, it poses serious effects, disrupting blood and nerve circulation [34,37,38]. Humans can suffer internal haemorrhage, liver damage, dermatitis, respiratory disorders, skin ulcerations, chromosome abnormalities, lung cancer, tissue necrosis, bronchitis, diarrhoea, and other conditions as a consequence of inhaling Cr(VI) ions from the contaminated environment [34,37-40,41]. In the bloodstream, Cr(VI) is toxic due to its high oxidative properties, which can cause damage to blood cells [41]. When the skin comes into contact with Cr(VI), it inhibits the healing of cuts and scrapes and may cause poisoning damage or severe burns. Both the exposure time and inhaled amount can pose the risk of nasal, lung and sinus cancer including eye damage [41]. Thus, the United States Environmental Protection Agency (USEPA) has listed chromium as one of 129 contaminants of main concern and 14 most toxic elements. Its concentration in industrial wastewater ranges from 0.5 to 270, 000 mg/L [37] and the allowable Cr(VI) maximum concentration in drinking water according to the South

African National Standards (SANS), USEPA and WHO should not exceed 0.1 mg/L for drinking water [42-44].

2.6.3.2 Lead

Physical and chemical properties

Lead is listed among some of the most toxic metals with bioaccumulative features. It has four stable isotopes: ^{204}Pb, ^{206}Pb, ^{207}Pb, ^{208}Pb and one common radioactive isotope ^{202}Pb. It is formed in the earth by the decay of thorium and uranium. South Africa is known for its lead-zinc deposits such as that in the Leeuwbosch lead deposits, north of Thabazimbi in Limpopo Province and the Pering mine in the Northwest Province [13].

Occurrence and distribution of lead

Lead is distributed into the environment in various ways such as through crust weathering, motor vehicle emissions, paint pigments and industrial emissions. Natural contamination with lead can occur in soil and earth crust due to the dissolution of lead. [13]. Lead is usually found in agriculture (insecticide as lead arsenate), batteries, pigment printing, ceramic products, manufacturing, pipe solder and paints and photographic materials [34,45]. Water containing a substantial amount of lead contains the majority of lead in the human body. In the beginning, it enters the body through the digestive tract and lungs and spreads by the blood [34,46]. Industrialisation and urbanisation are among the factors contributing to increased levels of heavy metal water contamination although there are many sources of contamination. Run-off from heavy metal-producing industries, cities, and towns can transport toxic elements [33]. The leaching of metals occurs when water washes over the rock surface. Leaching of metals occurs at moderate pH conditions, but at low pH conditions, the process is accelerated. Mining companies use cyanide and sulfuric acid to separate the target mineral from the ore, which causes pollution when the chemical agents they are using spill, leak, or leach into nearby waterways [16].

Health threats associated with lead contamination

Pollutants such as lead are widely distributed and have no biological benefits. Depending on the amount of exposure, it can cause anything from minor biochemical or physiological disturbances to serious pathological conditions in which organs or systems can be damaged or altered. Lead affects mainly the nervous system especially the central nervous system (CNS) [13]. Lead is a non-biodegradable hazardous toxic element that simply accumulates in the human body. The presence of a significant amount of lead in drinking water eventually leads to cancer, anaemia, nervous system damage, renal kidney disease and mental retardation [34,46]. The presence of lead in water can lead to serious health problems, particularly in growing children. The symptoms of acute lead poisoning are abdominal pain, headache, irritability and various symptoms associated to the nervous system [45,47,48]. Sleeplessness and restlessness characterize lead encephalopathy. Learning, behavioural disturbances and concentration difficulties mostly affect children. When lead encephalopathy is severe, the patient may suffer acute psychosis as well as confusion and reduced consciousness [45,47,48]. People who have been exposed to lead for a long time may suffer from prolonged reaction time, memory deterioration and reduced ability to understand. If blood lead levels are under 3 µmol/L, individuals may manifest peripheral nerve symptoms such as reduced nerve conduction velocity and reduced skin sensitivity [45,47,48].

2.6.3.3 Nickel

Physical and chemical properties

In the periodic table, nickel belongs to group VIIIb, the first transition series metal, as well as having relatively high thermal and electrical conductivities, and is ferromagnetic [49]. The siderophile nickel properties facilitate the formation of nickel-iron alloys. In addition to being a member of the transition elements, nickel is resistant to corrosion by water, air and alkalis, but readily dissolves in dilute oxidizing acids. Nickel salts of strong acids and organic acids are soluble in water, unlike nickel salts of weak inorganic acids [49].

Occurrence, distribution and uses of nickel in various industries

Nickel is used in alloys, nickel plating for corrosion prevention, and battery manufacture [50-52]. Industrial sources and agriculture are the sources of nickel pollution in water. Its toxicity is enhanced in the existence of other metals such as iron, cobalt, zinc and copper in drinking water [50]. Nickel is considered among various metal ions to be a notorious water contaminant and is commonly detected in various industrial wastewaters like batteries, coins, copper sulfate, electroplating, enamelling, metallic alloys, nonferrous metals, porcelain, stainless steel, steam-electric power plants, super-alloys, etc. If wastewater is not adequately treated, nickel-metal ions may enter the aquatic environment [51]. Adding to environmental contamination, Ni can also be present in food processed in stainless-steel vessels during drying, canning, and cooking. Thus, the Ni content in food contents is low (below 0.2 mg/kg) [53].

Health threats associated with nickel contamination

Nickel is considered an essential trace metal; for the production of blood cells, it is low in quantity. High concentrations of nickel, however, cause toxic effects [38-40]. It is considered carcinogenic to humans. Nickel sensitivity in humans has been studied in some studies. The cause of hair loss can be linked to contaminated drinking water, and nickel toxicity can cause dermatitis in hypersensitive people [50]. The WHO and SANS have set a MPL for nickel in drinking water at less than 0.02 mg/L and 0.07 mg/L, respectively [42,52]. Nickel metal ions at higher concentrations give rise to short term issues including diarrhoea, chest pain, nausea, vomiting, shortness of breath, inhibition of oxidative enzyme activity, etc. [51]. Long-term exposure gives rise to decreased bodyweight, lung cancer, pulmonary fibrosis, renal oedema, skin dermatitis and cause damage to the heart and liver [51,52]. The consumption of Ni-containing ingredients is generally considered safe because they comprise a normal part of the diet [53].

2.7 CURRENT METHODS FOR TOXIC ELEMENT REMEDIATION

Industrial runoffs containing toxic elements must be effectively disposed of to satisfy the rising demand for pure water with a low metal concentration before their release into the ecosystem [58]. Chemical, physical, and biological processes (or a combination thereof) are the three main types of toxic element removal treatment. Each type includes a variety of sub-methods. To decontaminate water and wastewater, various conventional approaches are available, including ion exchange, reverse osmosis, solvent extraction, chemical precipitation, membrane filtration, etc. [58-63]. Unfortunately, most of these methods are very costly, have low removal efficiency, and require further treatment [89]. In light of the various drawbacks associated with the methods mentioned above, new methods and technologies are needed. At present, coagulation-flocculation, precipitation, adsorption, membrane separation and ion exchange are the popular methods for removing toxic elements from water [58-63].

2.7.1 Chemical precipitation

Through this process, metal ions are transformed into insoluble precipitates of either carbonate, hydroxide, phosphate or sulphide. Filtration is used later to separate the solid precipitate. This is a simple method that has a high degree of selectivity and precipitants are relatively inexpensive [64]. However, it is ineffective in treating water containing a high concentration of toxic elements, requires numerous precipitate agents, production of a substantial amount of toxic sludge and chemical stabilisation [47,64].

2.7.2 Coagulation flocculation

In this process, a positively charged coagulant is presented to reduce the surface negative charge of particles so that they can aggregate. To fuse the positively charged aggregates together, an ionic flocculant is then added, resulting in a larger group that can be separated through filtration. This is a simple operation, relatively economical as alum and uses inexpensive coagulant. However, toxic elements are not completely

removed, and the production of sludge is insufficient for ensuring the effective removal of toxic elements [64].

2.7.3 Ion-exchange

A large part of toxic element removal from aqueous environments has been done with the ion exchange process, which has been used primarily to remove toxic elements from drinking water. The success of ion exchange is dependent on the exchange of surface ions, so the medium must be highly porous and have a high specific surface area. Acrylic, methacrylic, zeolite, and sodium silicate resins are typical examples. pH, contact time, resin dosage, initial concentration, and temperature are all important variables affecting the performance of ion exchange resins. The level of hydronium ions in the solution may be an influential factor in the ion-exchange process. Typically, resin removal efficiency decreases with increasing pH as a result of the formation of hydroxide anions (OH^-). As a consequence of these conditions, metal hydroxides can precipitate and hydrolyse. Increased resin concentration logically results in increased metal ion sorption [61]. The advantages of this process include its fast kinetics, convenience, and economics due to its low-cost materials and regenerated resin. Some of the disadvantages are being designed for low concentrations of metals, fouling of metal ions on ion exchange media, being highly sensitive to pH, and having a poor binding affinity if free acids are present [35,64].

2.7.4 Adsorption

It has been demonstrated that adsorption is a suitable technique to remove toxic elements from water because it removes pollutants even at low concentrations, consumes little energy, and allows the use of a wide variety of adsorbent types. By utilizing structures with adsorptive properties (e.g., functional groups, highly porous, large surface area) this process entraps metal ions through chemical or physical interactions [59-624,64]. Following the filtration process, the adsorbents are separated from the solution and undergo a regeneration process [64]. As part of the adsorption process, soluble liquids and gases attach themselves to an adsorbent. There are two main types of adsorption. The physical process of physisorption occurs when the van

der Waals force joins the absorbent and adsorbate (material to be absorbed and removed). In contrast, chemisorption occurs when molecules of the adsorbate are chemically bonded to the adsorbent surface. For an effective adsorption process to occur, the adsorption capacity must be high, which is directly associated with the characteristics of the adsorbent surface and how they interact with the specific contaminants being adsorbed. With respect to different pollutants, functional groups, surface charge, and surface area may produce different levels of activity [47].

Out of the listed methods, adsorption is the most flexible method in design and operation, as well as the most efficient at enriching and allowing phase separation [65]. Despite the above-mentioned approaches being efficient and achieving discharge standards, the majority of them create secondary waste [58]. Adsorption technique excels over other conventional methods because it is easier to implement, less expensive, far more capable of processing large volumes of water, effective at removing toxic metal ions even at low concentrations, readily available adsorbents, the flexibility of regeneration, and the relative simplicity of the process [47,59-62,66,67,68]. There are several disadvantages of this approach, including an extensive post-treatment process, a lack of promise for nanosized adsorbents due to very strong Van der Waal forces, and the need to hybridize various types of adsorbents for optimal binding ability [64]. Adsorption is used for water purification in combination with various adsorbents including activated carbon and synthetic carbon compounds such as carbon nanotubes and zeolite, cow dung, silicon oxide and titanium dioxide [69].

2.8 NANOMATERIALS

Materials science research is advancing rapidly, and nanomaterials are gaining application in our everyday lives, for example in life science, energy and environmental fields [67]. Nanomaterials (NMs) developed by the research community offer a diversity of cost-effective, resourceful, and recyclable approaches to decontaminate groundwater, surface water, and drinking water of manufacturing wastes [37]. The surface chemistry, high specific surface area, and related active adsorption sites of nanomaterials allow them to overcome the drawbacks of conventional adsorbents in wastewater treatment. They can adsorb toxic substances by adsorption, ion exchange

and ion precipitation [70]. Carbon nanomaterials have remained at the forefront of nanotechnology due to their high specific surfaces and large pores. Most commonly, carbon nanotubes (CNTs) and graphene have been applied to remove metal ions from water, including As(III)/(V), Cr(VI), Cd(II), Hg(II), Co(II), Pb(II), U(VI), and many others [67]. Compared to conventional adsorbents such as iron oxide, zero-valent iron, zeolite, silica, chitosan, titanium dioxide, and polymer, CNTs and graphene nanomaterials carry higher surface areas, tunable surface chemistry, scalable production, surface oxygen-containing functional groups and non-corrosive property [67].

As the nanoadsorbent is added into toxic element-containing water, toxic elements diffuse on the nanoadsorbent's external surface, due to diffusion potential, which is determined by the concentration of toxic elements and the external surface area of the nanoadsorbent. The toxic element diffuses on the available pores of the adsorbent following diffusion on the external surface. In the adsorption process, the metals occupy the exposed active sites of the nanocomposite through physisorption or chemisorption. Nanoadsorbents can be divided into various categories, such as carbon-based, metal-based, and polymeric nanoadsorbents [70]. Pure nanomaterials, however, have some limitations, and carbon-based nanocomposites, as well as carbon-hybrids with more and controlled functions, are attracting attention for use in environmental applications. Nanomaterials, which are increasingly important in environmental applications, pose challenges to scientific and technological research due to their durability, functionality, and performance [67,70].

2.8.1 Carbon nanotubes

A carbon molecule can take on a wide variety of molecular forms, also known as allotropes. Different structures of carbon elements are constitutive of these allotropes. The carbon nanotube (CNT) consists of cylindrical graphite sheets (a form of allotropic carbon) rolled into a tube-like configuration [71]. In addition to having unique structural, electrochemical, optical, mechanical, optoelectronic, semiconductor, and physiochemical properties, CNTs are some of the most promising carbon-based nanomaterials discovered by Iijima [72].

A carbon nanotube is a cylindrical carbon nanostructure made from rolled graphite sheets whose carbon atoms have an sp2 hybridisation. It has a hexagonal carbon atom array with a highly hydrophobic surface and a structure consisting of π-π conjugation. Since CNTs are hydrophobic, they can readily interact with nonpolar substances and are therefore ideally suited for use as a sorbent in the removal of nonpolar contaminants. Nevertheless, due to the high porosity structure of CNTs, some materials such as polar compounds and ionic compounds may also be absorbed into the pores of CNTs [45]. There are two types of CNTs based on their superstructure: single-walled and multiwall. A single-walled carbon nanotube (SWCNT) consists of one sheet of graphene rolled into a cylindrical form with a diameter of 1–2 nm [45,71,72]. The multi-wall CNTs, on the other hand, are made from multiple layers of graphene sheets rolled over one another in a cylindrical shape with a space between adjacent layers of 0.34 nm. The contact surface of SWCNTs with pollutants is more than MWCNTs because SWCNTs consist of a single cylindrical layer. Because SWCNTs are more difficult and more expensive to synthesize, they are not as often used for removing contaminants as MWCNTs [45]. By functionalising CNTs with different types of metals, CNTs can exhibit improved properties, including increased oxygen, nitrogen, and other surface functional groups that increase dispersibility and specific surface area [72].

Studies have shown that CNT can remove toxic elements from water in a variety of scenarios [72]. In addition to removing toxic elements such as lead, cadmium, nickel, copper, and arsenic, CNT has excellent capability to remove other metals as well [57,71]. To enhance the sorption capacities, CNTs can be modified by oxidation, coupling with organic compounds and combining with other metal ions or metal oxides. Electrostatic and chemical interactions between metal ions and the surface functional groups of CNT are attributed to the process of metal ion adsorption on CNTs [71]. As a result of the strong Van-der-Waals interactions (and the large bundles formed between the CNTs), CNTs exhibit a hydrophobic nature, which tends to cause them to aggregate in aqueous solutions. Specifically, CNT aggregation reduces the accessible adsorption sites, selectivity, sensitivity, and removal efficiency, which are all detrimental to the prospective use of CNTs for contaminants and toxic elements

removal [57]. Thus, their functionalisation process can be beneficial in surmounting the CNTs bundle configuration [57].

2.8.2 Modifications of CNTs

Surface functionalisation (SF) is a promising procedure to control agglomeration, which greatly improves the adsorption capacity of CNTs, their high reactivity and dispersion. This is accomplished using several chemical species, such as amino groups together with oxygen that serve as electrostatic and coordination sites for transition metal adsorption [57,73]. The functionalisation also enhances solubility and reformed cellular interface trails, following a substantial decrease in the effects of cytotoxic [57].

Chemical modification of MWCNT surfaces can occur through the formation of chemical bonds between modifying species and nanocarbon surfaces. Surface modification of CNTs is typically achieved by treatment with various mineral acids (HNO_3 or H_2SO_4 [74], $KMnO_4$ [75], H_2O_2 [74], KOH or a combination of these acids, such as HNO_3 + H_2O_2 [74,76], HNO_3 + H_2SO_4 [77,74], yielding hydrophilic groups, such as hydroxyl −OH, carboxyl −COOH or carbonyl > CO groups [80]. Another technique involves the impregnation of metals (such as Fe) or metal oxides (such as Fe_2O_3, MnO_2, α-Al_2O_3, ZrO_2) [78]. In the adsorption process, modifying the CNT structure is considered a crucial step for improved efficiency and selectivity in removing toxic elements [57,78]. The modified structure of MWCNTs increases the specific surface area of the adsorbent and improves the adsorptivity towards toxic metal ions in comparison to raw nanotubes [78].

2.8.3 Modified of CNTs by introducing functional groups

Through chemical covalent bonding, functional groups such as carboxyl, hydroxyl, iron oxide, nitrogen, amino and thiol may be added to CNTs to enhance their adsorption affinities and improve their active adsorption sites.

2.8.3.1 Metal oxide-functionalisation

The various types of metal and metal oxide-based nanoparticles and their composites, such as silver nanoparticles (NPs), Fe_3O_4, copper oxide (CuO), cerium oxides, magnesium oxide (MgO), titanium dioxide (TiO_2), manganese oxides and zinc oxide (ZnO), play an important role in a wide range of scientific and industrial applications, like magnets, catalyst and in the treatment of wastewater [37]. It has been found that they exhibit excellent adsorption for various types of toxic elements, such as As(III), As(V), Cr(VI), and Pb(II) [64]. Although these materials are quite effective as adsorbents, their main limitations are their easy oxidation/dissolution in acidic media and difficulties recycling the nanoparticles due to their small size. To overcome these limitations, solid or polymeric substrates were employed in order to regulate the particle size and to prevent materials from oxidising [64].

Among the numerous iron materials studied, magnetic magnetite (Fe_3O_4) nanoparticles with unique physical and chemical properties have received the most attention [79]. For example, studies using Fe_3O_4-MWCNTs for the adsorption of toxic elements were conducted for the removal of Cr(III) [80] and Ni(II) [81]. Its large surface area, strong magnetic properties and highly porous nature have enabled it to exhibit impressive sorption capacities in recent years. By controlling and managing its magnetic properties, factors like surface defects, size and the proportion of ferromagnetic and antiferromagnetic particles, the morphology can be significantly stabilised [62]. Therefore, carbon nanotubes combined with magnetite (Fe_3O_4) nanoparticles would be an attractive choice for removing toxic elements from wastewater. Adsorbents composed of Fe_3O_4 nanoparticles are effective and economical for removing metal ions rapidly from wastewater effluents. Magnetic nanoparticles are popular in adsorption because they are easily separated with an external magnetic field and consume less energy and are cheaper to recycle [60].

2.8.3.2 Amino-functionalisation

Due to their unique properties which result from the presence of amino groups, amino-containing materials have attracted significant attention. In combination with other

functional groups, amino functionalities play a critical role in the construction of complex structures [82]. In the case of amino-functionalisation of CNTs, amino (-NH_2) functional groups are produced on the surface of the CNTs, either by covalent bonding or by non-covalent bonding. A nitrogen atom and two hydrogen atoms make up the chemical structure of the amino-functional group. Having a lone pair of electrons on the nitrogen atom in the structure of an amino-functional group, it is a chemical electron donor, which gives it a unique chemical property. As a result, the amino-functional group is considered a very good nucleophile due to the presence of this atom. Nucleophilicity and donation characteristics of amino-functional groups grafted onto surfaces of carbon nanotubes cause the surface of the CNTs to be activated, which can then lead to many potential applications for NH_2-CNTs [83].

The modification of amino groups in CNTs (CNTs-NH_2) is essential for improving CNT extraction efficiency. Based on the following mechanisms, amino-functionalisation can effectively improve CNT adsorptivity and selectivity. It could form hydrogen bonds between CNTs and analytes with the exception of the known p-p stacking and hydrophobic interactions. Moreover, it improved the hydrophilicity of CNTs, thereby facilitating their dispersion and, subsequently, making more contact with analytes. Further, this process can encourage the aggregation of CNTs, allowing for more sorption sites between CNT bundles, such as external grooves, interstitial channels, and exterior surfaces [84].

Different amino groups have been applied to CNTs for toxic element treatment. Huang et al. [85] used polyethyleneimine (PEI) and ethylenediamine (EDA) for adsorption of Cu(II) and Pb(II); aminopropyl trimethoxysilane (APTMS) for Pb(II) was used by Kunlun et al. [86]. MWCNTs treated with ethylenediamine (EDA) for preconcentration of Cr(III) and Pb(II) have been studied [87] as well as with EDA, diethylenetriamine (DETA) and triethylenetetramine (TETA) for removal of Pb(II) [82].

2.8.3.3 Thiol-functionalisation

Material science has made extensive use of thiol-functionalised adsorbents as a means of treating pollutants. Hard and soft acids and bases (HSAB) theory state that

thiol is a soft alkali that can readily combine with metal ions in water to remove metal ions [88]. It's Lewis acid-base interactions enable it to have a high affinity for various toxic metal ions, making the thiol group an excellent ligand. Thiol-functionalised Fe_3O_4 nanoparticles, hollow silica spheres, magnetic mesoporous silica, and Fe_3O_4-poly(3,4-ethylenedioxythiophene) core-shell nanoparticles have been synthesised and have shown high selective adsorption capabilities to a variety of toxic metal ions (Ag(I), Pb(II), Hg(II), Cu(II), As(III), etc.) [89].

The thiol-functionalised CNTs (CNTs-SH) have been found to exhibit improved adsorption capacity, selectivity, and efficiency for adsorption of toxic elements, dyes, and phenols. In addition, CNTs-SH were studied for magnetic micro-solid phase extraction of antibiotics in water, milk products, and chicken meat products before HPLC analysis, and the results showed that thiol modification improved the reactivity of CNTs and provided additional active sites, which were conducive to improving their adsorptivity. The results also strengthened the selectivity of the established magnetic solid phase extraction (MSPE) technology and further broadened its applications [86]. Researchers have used thiol-functionalised nanoparticles to treat aqueous solutions contaminated with toxic elements, Hg(II) [88,89], Pb(II) [89] and methylene blue [92].

2.8.3.4 Nitrogen functionalisation

The nitrogen-functionalised carbon nanotubes (N-CNTs) have been explored as potential extractants that have unique structures and exceptional properties. Nitrogen is incorporated into the graphitic lattice of CNTs as a dopant, leading to the localized electronic state, which disrupts the p-clouds of CNTs, thus creating defect sites on the wall. Consequently, N-CNTs exhibit a greatly enhanced chemical activity and surface hydrophilicity, and their affinity to analytes is significantly increased. As a result of the addition of Lewis-basic nitrogen to CNTs, their active sites are more basic, and their positively charged surface area increases, potentially causing increased adsorption interactions with analytes such as dipole-dipole, hydrogen bonding and electrostatic interactions [84]. MSPE studies have shown that N-CNTs are a versatile and efficient extractant to determine polycyclic aromatic hydrocarbons (PAHs) from environmental water samples. Adsorption experiments and density functional theory have shown that

N-CNTs have superior adsorption capacity to metal ions such as Pb(II) and Zn(II). As compared to pure CNTs, functional CNTs have significantly improved adsorption capabilities. Furthermore, apart from the increased adsorption affinity to analytes, the functional groups introduced onto CNTs can also serve as complexing functional groups to capture MNPs. The introduction of functional groups can lay the foundation for CNT modification in the future [84].

N-doped multi-walled carbon nanotubes (N-MWCNTs)

A nitrogen substitution doping has been controversial because it has been predicted that chemical reactivity, electrical conductivity and mechanical properties will be significantly altered [75,91]. As electron-rich nitrogen replaces carbon in a graphitic layer, the band gap of CNTs is reduced, leading to metallic CNTs [75,91]. Nitrogen doping produces a three-dimensional texture that is referred to as "bamboo or stacked cup" MWCNTs [75,91] and their surfaces are highly reactive with a variety of accessible interaction points [91], thus facilitating chemical functionalisation [75].

2.8.3.5 Combination of CNTs with several functional groups

For removing toxic elements from wastewater and/or water, carbon nanotubes combined with magnetite nanoparticles (Fe_3O_4) are an attractive option. In one example, Zhan et al. [89] developed a hybrid material formed from Fe_3O_4 and multi-walled carbon nanotubes through the use of $FeCl_3{\cdot}6H_2O$ as a single ion source, multiwalled carbon nanotubes as templates and 3-aminophenoxyphthalonitrile as an amino group source. It has been shown that the process provides an efficient means of adding Fe_3O_4, amino, and thiol groups to nanotube sidewalls. Using trimethoxysilylpropanethiol (MPTs), hydrazine, ammonium ferric sulfate and ammonium ferrous sulfate,, Jiang et al. [77] synthesised functionalised multi-walled carbon nanotubes.

2.9 EFFECT OF IONIC STRENGTH AND COEXISTING ANIONS

Both natural water and industrial wastewater contain different kinds of ions such as Mg(II), Ca(II), Na(I), K(I), Cu(II), chloride, carbonate, and sulphate [92,93]. The composition of natural water can include a number of ions and organic compounds, which might coexist with metal ions and influence their removal [86]. There is a possibility that these metal ions will affect the efficiency of metal ion removal in the adsorption process [86]. It is generally the case that wastewater contains a certain level of salt. Increasing the salt concentration would weaken the electrostatic interactions between the adsorbate and adsorbent, which in turn would influence the adsorption process [94].

Several works are found in the literature for the treatment of aqueous solutions contaminated with chromium, lead and nickel using modified MWCNTs. The main techniques for removing these contaminants involve adsorption. The removal mechanism of Cr(VI) in aqueous environments mostly involves ionic attraction between positively charged adsorbents and $HCrO_4^-$, $Cr_2O_7^{2-}$, or CrO_4^{2-} species. Therefore, the presence of background anions in solution at low pH values is sure to compete with Cr(VI) anionic species [95]. The study conducted by Huang et al. [96] assumes that the monovalent anions Cl^- and NO_3^- compete in a small way on the surface of chitosan/MWCNTsCOOH with the chromium anions; whereas PO_4^{3-} and SO_4^{2-} are multivalent anions, and they compete more extensively with Cr(VI) for the positively charged sorption sites.

In a similar study, chloride ions were selected as a potential competing anion, since chloride ions are frequently used in industrial effluent water treatment and have already shown a potential to inhibit Cr(VI) adsorption on activated carbon. The other ion was selected as the sulphate ion. Chemically, this ion resembles dichromate ions with respect to its charge [97]. Pillay et al. [97] explained that the presence of potentially competitive anions leads to the inhibition of dichromate ion adsorption. The negatively charged chloride and sulfate ions repel the negatively charged dichromate ions. Adsorption is greatly inhibited by the ions of sulphate rather than chloride. This may be attributable to chemical similarity between dichromate ions and sulphate ions,

in addition to the sulphate ion's extra negative charge. An affinity for chloride and sulphate ions may be stronger on the nanotube surface than for dichromate ions [97].

In the presence of a ligand or a metal ion, Cr(VI) adsorption is influenced by the interaction between the metal ion, anion, and substrate sites, as well as the concentration and order of addition. In previous studies, ligand or metal ion adsorption to mineral surfaces has been studied with findings suggesting that Cr(VI) adsorption can be either decreased, enhanced, or unaffected by Cr(VI). Most of the time, Cr(VI) adsorption was significantly reduced when organic compounds were present compared to when Cr(VI) was in solution. Various studies have reported different results regarding the interaction of Cr(VI) and humic acid (HA) [98].

2.10 RECENT STUDIES ON THE REMOVAL OF TOXIC ELEMENTS USING MODIFIED CNTS

There are very few studies reported on the adsorption of Cr(III), Cr(VI), Ni(II) and Pb(II) onto modified CNTs and most of these have been conducted recently [40,73,77,78,81,82,92,96,99-103]. Dokmaj et al. [40] found that 98% Cr(VI) and 99% Cr(III) is adsorbed onto MWCNTs-CTAB at optimum conditions. Huang et al. [98], on the other hand achieved removal efficiencies of 98-100% Cr(VI) onto Chitosan/MWCNTs-COOH. Obayomi et al. [99] achieved 90% Cr(VI) onto MWCNTs from Co–Fe/AC. Finally, Alguacil et al. [100] reported 84% Cr(III) removal efficiency onto MWCNTs-COOH. The above mentioned adsorbents were reported to have a great potential in dealing with Cr(VI) contamination. Wang et al. [101] recorded 98% Ni(II) removal efficiency onto γ-PGA-Fe_3O_4-GO-(o-MWCNTs while Egbosiuba et al. [73] achieved 100% removal efficiency for both Ni(II) and Pb(II) ions onto MWCNTs of different diameters.

Rahmati et al. [104] found 93% Ni(II) onto DES-MWCNTs (KTMWCNTs) and 92% Ni(II) removal efficiency was achieved by Ahmadi et al. [105]. Furthermore, the removal efficiency of 98% Pb(II) was obtained by Jiang et al. [77] under the same experimental conditions as those of the current study. In addition to most of the studies, Wang et al. [92] found that 80% Pb(II) is adsorbed onto Magnetic

hydroxypropyl chitosan/oxidised multi-walled carbon nanotubes (MHC/OMCNTs). Consequently, 92.5% Pb(II) removal efficiency was achieved onto MWCNTs–$SeP(O)(O\text{-}t\text{-}Bu)_2$ by Kończyk et al. [78]. Finally, the removal efficiency of 99.6% Pb(II) onto MWCNTs/polyrhodanine was reported by Alizadeh et al. [103]. The modified adsorbents for the adsorption Ni(II) and Pb(II) were found to be efficient in water and wastewater decontamination. A series of recent studies have indicated that removal of toxic elements by functionalisation of MWCNTs increases the effectiveness of the nanotubes with increased surface area and adsorption sites [77,88,90]. The functionalisation of sorbent using a chemical bond between the sorbent and the new functional groups can significantly enhance the sorbent's chemical stability [45].

REFERENCES

1. Biswas, P., Karn, A.K., Balasubramanian, P. and Kale, P.G., 2017. Biosensor for detection of dissolved chromium in potable water: A review. Biosensors and Bioelectronics, 94, pp.589-604.
2. Xu, J., Cao, Z., Zhang, Y., Yuan, Z., Lou, Z., Xu, X. and Wang, X., 2018. A review of functionalized carbon nanotubes and graphene for heavy metal adsorption from water: Preparation, application, and mechanism. Chemosphere, 195, pp.351-364.
3. Mohan, D. and Pittman, C.U., 2007. Arsenic removal from water/wastewater using adsorbents—a critical review, J. Hazard. Mater. 142, pp.1–53.
4. Abbas, A., Al-Amer, A.M., Laoui, T., Al-Marri, M.J., Nasser, M.S., Khraisheh, M. and Atieh, M.A., 2016. Heavy metal removal from aqueous solution by advanced carbon nanotubes: critical review of adsorption applications. Separation and Purification Technology, 157, pp.141-161.
5. Khan, F.S.A., Mubarak, N.M., Tan, Y.H., Khalid, M., Karri, R.R., Walvekar, R., Abdullah, E.C., Nizamuddin, S. and Mazari, S.A., 2021. A comprehensive review on magnetic carbon nanotubes and carbon nanotube-based buckypaper-heavy metal and dyes removal. Journal of Hazardous Materials, p.125375.
6. Minerals Council South Africa. (2017). Platinum. Key Facts and Figures. Accessed July 14, 2021, from https://www.mineralscouncil.org.za/sa-mining/platinum
7. Drimie, S., Germishuyse, T., Rademeyer, L. and Schwabe, C., 2009. Agricultural production in Greater Sekhukhune: the future for food security in a poverty node of South Africa?. Agrekon, 48(3), pp.245-275.
8. Meissner, R., Funke, N., Nortje, K., Jacobs-Mata, I., Moyo, E., Steyn, M., … Nohayi, N. (2018). Water security at local government level in South Africa: a qualitative interview-based analysis. The Lancet Planetary Health, 2, S17. https://doi.org/10.1016/s2542- 5196(18)30102-5
9. Singh, U.K., Ramanathan, A.L. and Subramanian, V., 2018. Groundwater chemistry and human health risk assessment in the mining region of East Singhbhum, Jharkhand, India. Chemosphere, 204, pp.501-513.

10. Singo, N.K., 2013. An assessment of heavy metal pollution near an old copper mine dump in Musina, South Africa. (Doctoral dissertation, University of South Africa, Department of Environmental Management).
11. Tsebe, M.R., 2018. Impact of mining on agriculture and socio-economic aspects in the rural communities of Greater Tubatse Local Municipality (Doctoral dissertation, University of South Africa, Department of Agriculture).
12. Ziervogel, G. and Taylor, A., 2008. Feeling stressed: integrating climate adaptation with other priorities in South Africa. Environment: Science and Policy for Sustainable Development, 50(2), pp.32-41.
13. Ali, Y.D., 2010. Toxic elements in foodchain: exposure pathways to infants in selected areas of Limpopo Province (Doctoral dissertation, University of South Africa, Department of Environmental Science).
14. Guidone, A., 2019. Whose Knowledge, Whose Water, Whose Life: A Case Study of Water Governance and Mining in Sekhukhune, South Africa (Doctoral dissertation, Queen's University (Canada), Department of Environmental Studies).
15. Letsoalo, M.R., Godeto, T.W., Magadzu, T. and Ambushe, A.A., 2018. Quantitative Speciation of Arsenic in Water and Sediment Samples from the Mokolo River in Limpopo Province, South Africa. Analytical Letters, 51(17), pp.2763-2777.
16. Mathipa, M.M., 2016. Analysis of the bio-physicochemical quality of surface and ground water in the Tubatse Municipality (Doctoral dissertation, University of Limpopo, Department of Microbiology).
17. Ratombo, A.P., 2019. Determination of coal mine impacts on surface water bodies (Olifants River) (Doctoral dissertation, North-West University (South Africa)).
18. Sedibe, M., Achilonu, M.C., Tikilili, P., Shale, K. and Ebenebe, P.C., 2017. South African mine effluents: Heavy metal pollution and impact on the ecosystem.
19. Addo-Bediako, A. and Malakane, K., 2020. Preliminary Assessment of Chemical Elements in Sediments and Larvae of Gomphidae (Odonata) from the Blyde River of the Olifants River System, South Africa. International Journal of Environmental Research and Public Health, 17(21), p.8135.

20. Fu, Z. and Xi, S., 2020. The effects of heavy metals on human metabolism. Toxicology mechanisms and methods, 30(3), pp.167-176.
21. Mishra, S., Bharagava, R.N., More, N., Yadav, A., Zainith, S., Mani, S. and Chowdhary, P., 2019. Heavy metal contamination: an alarming threat to environment and human health. In Environmental biotechnology: For sustainable future (pp. 103-125). Springer, Singapore.
22. Magala, M., 2015. Aquatic Health Assessment of the Steelpoort River System, Limpopo, South Africa. University of Johannesburg (South Africa).
23. DWAF (Department of Water Affairs and Forestry). 1995. Middle Steelpoort Catchment, groundwater management plan; Volume 1-6. Pretoria: DWAF.
24. Stimie, C., Richters, E., Thompson, H., Perret, S., Matete, M., Abdallah, K., Kau, J. and Mulibana, E., 2001. Hydro-institutional mapping in the steelpoort river basin.
25. Sharma, S. and Bhattacharya, A., 2017. Drinking water contamination and treatment techniques. Applied Water Science, 7(3), pp.1043-1067.
26. Rengaraj, S., Cruz-Izquierdo, Á., Scott, J.L. and Di Lorenzo, M., 2018. Impedimetric paper-based biosensor for the detection of bacterial contamination in water. Sensors and Actuators B: Chemical, 265, pp.50-58.
27. Singh, R., Bhadouria, R., Singh, P., Kumar, A., Pandey, S. and Singh, V.K., 2020. Nanofiltration technology for removal of pathogens present in drinking water. In Waterborne Pathogens (pp. 463-489). Butterworth-Heinemann.
28. Gwimbi, P., George, M. and Ramphalile, M., 2019. Bacterial contamination of drinking water sources in rural villages of Mohale Basin, Lesotho: exposures through neighbourhood sanitation and hygiene practices. Environmental health and preventive medicine, 24(1), pp.1-7.
29. Jaramillo, M. and O'Shea, K.E., 2019. Analytical methods for assessment of cyanotoxin contamination in drinking water sources. Current Opinion in Environmental Science & Health, 7, pp.45-51.
30. Walker, H.W., 2019. Harmful algae blooms in drinking water: removal of cyanobacterial cells and toxins. CRC Press.
31. Ahmed, S.A., Guerrero Flórez, M. and Karanis, P., 2018. The impact of water crises and climate changes on the transmission of protozoan parasites in Africa. Pathogens and global health, 112(6), pp.281-293.

32. Emelko, M.B., Schmidt, P.J. and Borchardt, M.A., 2019. Confirming the need for virus disinfection in municipal subsurface drinking water supplies. Water research, 157, pp.356-364.

33. Masindi, V., and Muedi, K.L., 2018. Environmental Contamination by Heavy Metals. Heavy Metals, 10, pp.115-132.

34. Yahya, M.D., Obayomi, K.S., Abdulkadir, M.B., Iyaka, Y.A. and Olugbenga, A.G., 2020. Characterization of cobalt ferrite-supported activated carbon for removal of chromium and lead ions from tannery wastewater via adsorption equilibrium. Water Science and Engineering, 13(3), pp.202-213.

35. Rananga, L.E., 2013. Synthesis, characters and application of silver-doped cabon Nanotubes and nanoporous polymers for purification of water samples (Doctoral dissertation, University of Limpopo (Turfloop Campus), Department of Chemistry).

36. Kurwadkar, S., 2019. Occurrence and distribution of organic and inorganic pollutants in groundwater. Water Environment Research, 91(10), pp.1001-1008.

37. Aigbe, U.O. and Osibote, O.A., 2020. A review of hexavalent chromium removal from aqueous solutions by sorption technique using nanomaterials. Journal of Environmental Chemical Engineering, p.104503.

38. Xu, H., Liu, Y., Liang, H., Gao, C., Qin, J., You, L., Wang, R., Li, J. and Yang, S., 2021. Adsorption of Cr (VI) from aqueous solutions using novel activated carbon spheres derived from glucose and sodium dodecylbenzene sulfonate. Science of The Total Environment, 759, p.143457.

39. Almeida, J.C., Cardoso, C.E., Tavares, D.S., Freitas, R., Trindade, T., Vale, C. and Pereira, E., 2019. Chromium removal from contaminated waters using nanomaterials–a review. TrAC Trends in Analytical Chemistry, 118, pp.277-291.

40. Dokmaj, T., Ibrahim, T., Khamis, M., Abouleish, M. and Alam, I., 2020. Chemically Modified Nanoparticles Usage for Removal of Chromium from Sewer Water. Environmental Nanotechnology, Monitoring & Management, p.100319.

41. Prasad, S., Yadav, K.K., Kumar, S., Gupta, N., Cabral-Pinto, M.M., Rezania, S., Radwan, N. and Alam, J., 2021. Chromium contamination and effect on

environmental health and its remediation: A sustainable approaches. Journal of Environmental Management, 285, p.112174

42. Nthunya, L.N., Masheane, M.L., Malinga, S.P., Nxumalo, E.N., Mamba, B.B. and Mhlanga, S.D., 2017. Determination of toxic metals in drinking water sources in the Chief Albert Luthuli Local Municipality in Mpumalanga, South Africa. *Physics and Chemistry of the Earth, Parts A/B/C*, *100*, pp.94-100.
43. Gebrekidan, M. and Samuel, Z., Concentration of Heavy Metals in Drinking Water from Urban Areas of the Tigray Region, Northern Ethiopia, vol. 3. *CNCS, Mekelle University ISSN*, pp.105-121.
44. Kinuthia, G.K., Ngure, V., Beti, D., Lugalia, R., Wangila, A. and Kamau, L., 2020. Levels of heavy metals in wastewater and soil samples from open drainage channels in Nairobi, Kenya: Community health implication. Scientific reports, 10(1), pp.1-13.
45. Ghorbani, M., Seyedin, O. and Aghamohammadhassan, M., 2020. Adsorptive removal of lead (II) ion from water and wastewater media using carbon-based nanomaterials as unique sorbents: A review. Journal of environmental management, 254, p.109814.
46. kumar Das, S., singh Grewal, A. and Banerjee, M., 2011. A brief review: Heavy metal and their analysis. Organization, 11(1), p.003.
47. Fiyadh, S.S., AlSaadi, M.A., Jaafar, W.Z., AlOmar, M.K., Fayaed, S.S., Mohd, N.S., Hin, L.S. and El-Shafie, A., 2019. Review on heavy metal adsorption processes by carbon nanotubes. Journal of Cleaner Production, 230, pp.783-793.
48. Järup, L., 2003. Hazards of heavy metal contamination. British medical bulletin, 68(1), pp.167-182.
49. Barceloux, D.G. and Barceloux, D., 1999. Nickel. Journal of toxicology: clinical Toxicology, 37(2), pp.239-258.
50. Sankhla, M.S., Kumari, M., Nandan, M., Kumar, R. and Agrawal, P., 2016. Heavy metals contamination in water and their hazardous effect on human health-a review. Int. J. Curr. Microbiol. App. Sci (2016), 5(10), pp.759-766.
51. Siddiqui, M.N., Ali, I., Asim, M. and Chanbasha, B., 2020. Quick removal of nickel metal ions in water using asphalt-based porous carbon. Journal of Molecular Liquids, 308, p.113078.

52. Ahmadi, S., Igwegbe, C.A., Rahdar, S. and Asadi, Z., 2019. The survey of application of the linear and nonlinear kinetic models for the adsorption of nickel (II) by modified multi-walled carbon nanotubes. Applied Water Science, 9(4), pp.1-7.
53. Peeters, K., Zuliani, T., Žigon, D., Milačič, R. and Ščančar, J., 2017. Nickel speciation in cocoa infusions using monolithic chromatography–Post-column ID-ICP-MS and Q-TOF-MS. Food chemistry, 230, pp.327-335.
54. Raval, N.P., Shah, P.U. and Shah, N.K., 2016. Adsorptive removal of nickel (II) ions from aqueous environment: A review. Journal of Environmental Management, 179, pp.1-20.
55. Ukhurebor, K.E., Aigbe, U.O., Onyancha, R.B., Nwankwo, W., Osibote, O.A., Paumo, H.K., Ama, O.M., Adetunji, C.O. and Siloko, I.U., 2021. Effect of hexavalent chromium on the environment and removal techniques: a review. Journal of Environmental Management, 280, p.111809.
56. Bulgariu, L. and Bulgariu, D., 2018. Functionalized soy waste biomass-A novel environmental-friendly biosorbent for the removal of heavy metals from aqueous solution. Journal of Cleaner Production, 197, pp.875-885.
57. Onyancha, R.B., Aigbe, U.O., Ukhurebor, K.E. and Muchiri, P.W., 2021. Facile synthesis and applications of carbon nanotubes in heavy-metal remediation and biomedical fields: A comprehensive review. Journal of Molecular Structure, 1238, p.130462.
58. Yaqoob, A.A., Parveen, T., Umar, K. and Mohamad Ibrahim, M.N., 2020. Role of nanomaterials in the treatment of wastewater: A review. Water, 12(2), p.495.
59. Tshikovhi, A., Mishra, S.B. and Mishra, A.K., 2020. Nanocellulose-based composites for the removal of contaminants from wastewater. International Journal of Biological Macromolecules.
60. Fallah, Z., Zare, E.N., Ghomi, M., Ahmadijokani, F., Amini, M., Tajbakhsh, M., Arjmand, M., Sharma, G., Ali, H., Ahmad, A. and Makvandi, P., 2021. Toxicity and remediation of pharmaceuticals and pesticides using metal oxides and carbon nanomaterials. Chemosphere, p.130055.
61. Nazaripour, M., Reshadi, M.A.M., Mirbagheri, S.A., Nazaripour, M. and Bazargan, A., 2021. Research trends of heavy metal removal from aqueous environments. Journal of Environmental Management, 287, p.112322.

62. Kolluru, S.S., Agarwal, S., Sireesha, S., Sreedhar, I. and Kale, S.R., 2021. Heavy metal removal from Wastewater using Nanomaterials-Process and Engineering Aspects. Process Safety and Environmental Protection.
63. Ukhurebor, K.E., Aigbe, U.O., Onyancha, R.B., Nwankwo, W., Osibote, O.A., Paumo, H.K., Ama, O.M., Adetunji, C.O. and Siloko, I.U., 2021. Effect of hexavalent chromium on the environment and removal techniques: a review. Journal of Environmental Management, 280, p.111809.
64. Abdullah, N., Yusof, N., Lau, W.J., Jaafar, J. and Ismail, A.F., 2019. Recent trends of heavy metal removal from water/wastewater by membrane technologies. Journal of Industrial and Engineering Chemistry, 76, pp.17-38.
65. Dimpe, K.M. and Nomngongo, P.N., 2017. A review on the efficacy of the application of myriad carbonaceous materials for the removal of toxic trace elements in the environment. Trends in Environmental Analytical Chemistry, 16, pp.24-31.
66. Verma, B. and Balomajumder, C., 2020. Surface modification of one-dimensional Carbon Nanotubes: A review for the management of heavy metals in wastewater. Environmental Technology & Innovation, 17, p.100596.
67. Xu, J., Cao, Z., Zhang, Y., Yuan, Z., Lou, Z., Xu, X. and Wang, X., 2018. A review of functionalized carbon nanotubes and graphene for heavy metal adsorption from water: Preparation, application, and mechanism. Chemosphere, 195, pp.351-364.
68. Pandey, L.M., 2020. Surface engineering of nano-sorbents for the removal of heavy metals: Interfacial aspects. Journal of Environmental Chemical Engineering, p.104586.
69. Kariim, I., Abdulkareem, A.S., Tijani, J.O. and Abubakre, O.K., 2020. Development of MWCNTs/TiO2 nanoadsorbent for Simultaneous removal of Phenol and Cyanide from refinery wastewater. Scientific African, p.e00593.
70. Parvin, F., Rikta, S.Y. and Tareq, S.M., 2019. Application of nanomaterials for the removal of heavy metal from wastewater. In Nanotechnology in water and wastewater treatment (pp. 137-157). Elsevier.
71. Abbas, A., Al-Amer, A.M., Laoui, T., Al-Marri, M.J., Nasser, M.S., Khraisheh, M. and Atieh, M.A., 2016. Heavy metal removal from aqueous solution by advanced carbon nanotubes: critical review of adsorption applications. Separation and Purification Technology, 157, pp.141-161.

72. Lal, S., Singhal, A. and Kumari, P., 2020. Exploring carbonaceous nanomaterials for arsenic and chromium removal from wastewater. Journal of Water Process Engineering, 36, p.101276.
73. Egbosiuba, T.C., Abdulkareem, A.S., Tijani, J.O., Ani, J.I., Krikstolaityte, V., Srinivasan, M., Veksha, A. and Lisak, G., 2021. Taguchi optimization design of diameter-controlled synthesis of multi walled carbon nanotubes for the adsorption of Pb (II) and Ni (II) from chemical industry wastewater. Chemosphere, 266, p.128937.
74. Mkhondo, N.B. and Magadzu, T., 2014. Effects of different acid-treatment on the nanostructure and performance of carbon nanotubes in electrochemical hydrogen storage. Dig. J. Nanomater. Bios, 9(4), pp.1331-1338.
75. Kaur, A.P., 2013. N-doped Multiwalled Carbon Nanotubes: Functionalization, Characterization and Application in Li Ion Batteries.
76. Farghali, A.A., Tawab, H.A., Moaty, S.A. and Khaled, R., 2017. Functionalization of acidified multi-walled carbon nanotubes for removal of heavy metals in aqueous solutions. Journal of Nanostructure in Chemistry, 7(2), pp.101-111.
77. Jiang, L., Li, S., Yu, H., Zou, Z., Hou, X., Shen, F., Li, C. and Yao, X., 2016. Amino and thiol modified magnetic multi-walled carbon nanotubes for the simultaneous removal of lead, zinc, and phenol from aqueous solutions. Applied Surface Science, 369, pp.398-413.
78. Kończyk, J., Żarska, S. and Ciesielski, W., 2019. Adsorptive removal of Pb (II) ions from aqueous solutions by multi-walled carbon nanotubes functionalised by selenophosphoryl groups: Kinetic, mechanism, and thermodynamic studies. Colloids and Surfaces A: Physicochemical and Engineering Aspects, 575, pp.271-282.
79. Zhan, Y., Hu, H., He, Y., Long, Z., Wan, X. and Zeng, G., 2016. Novel amino-functionalized Fe 3 O 4/carboxylic multi-walled carbon nanotubes: one-pot synthesis, characterization and removal for Cu (II). Russian Journal of Applied Chemistry, 89(11), pp.1894-1902.
80. Gupta, V.K., Agarwal, S. and Saleh, T.A., 2011. Chromium removal by combining the magnetic properties of iron oxide with adsorption properties of carbon nanotubes. Water research, 45(6), pp.2207-2212.

81. Dong, P., Wu, X., Sun, Z., Hu, J. and Yang, S., 2014. Removal performance and the underlying mechanisms of plasma-induced CD/MWCNT/iron oxides towards Ni (II). Chemical Engineering Journal, 256, pp.128-136.
82. Vuković, G.D., Marinković, A.D., Škapin, S.D., Ristić, M.Đ., Aleksić, R., Perić-Grujić, A.A. and Uskoković, P.S., 2011. Removal of lead from water by amino modified multi-walled carbon nanotubes. Chemical Engineering Journal, 173(3), pp.855-865.
83. Yaghoubi, A. and Ramazani, A., 2018. Synthesis of amino-functionalized carbon nanotubes and their applications. Current Organic Chemistry, 22(15), pp.1505-1522.
84. Li, W.K. and Shi, Y.P., 2019. Recent advances and applications of carbon nanotubes based composites in magnetic solid-phase extraction. TrAC Trends in Analytical Chemistry, 118, pp.652-665.
85. Huang, Z., Huang, Z., Feng, L., Luo, X., Wu, P., Cui, L. and Mao, X., 2018. Modified cellulose by polyethyleneimine and ethylenediamine with induced Cu (II) and Pb (II) adsorption potentialities. Carbohydrate polymers, 202, pp.470-478.
86. Yang, K., Lou, Z., Fu, R., Zhou, J., Xu, J., Baig, S.A. and Xu, X., 2018. Multiwalled carbon nanotubes incorporated with or without amino groups for aqueous Pb (II) removal: Comparison and mechanism study. Journal of Molecular Liquids, 260, pp.149-158.
87. Zang, Z., Hu, Z., Li, Z., He, Q. and Chang, X., 2009. Synthesis, characterization and application of ethylenediamine-modified multiwalled carbon nanotubes for selective solid-phase extraction and preconcentration of metal ions. Journal of Hazardous Materials, 172(2-3), pp.958-963.
88. Chen, K., Zhang, Z., Xia, K., Zhou, X., Guo, Y. and Huang, T., 2019. Facile synthesis of thiol-functionalized magnetic activated carbon and application for the removal of mercury (II) from aqueous solution. ACS omega, 4(5), pp.8568-8579.
89. Zhang, C., Sui, J., Li, J., Tang, Y. and Cai, W., 2012. Efficient removal of heavy metal ions by thiol-functionalized superparamagnetic carbon nanotubes. Chemical Engineering Journal, 210, pp.45-52.
90. Robati, D., Mirza, B., Ghazisaeidi, R., Rajabi, M., Moradi, O., Tyagi, I., Agarwal, S. and Gupta, V.K., 2016. Adsorption behavior of methylene blue dye on

nanocomposite multi-walled carbon nanotube functionalized thiol (MWCNT-SH) as new adsorbent. Journal of Molecular Liquids, 216, pp.830-835.

91. Vanyorek, L., Prekob, A., Hajdu, V., Muranszky, G., Fiser, B., Sikora, E., Kristaly, F. and Viskolcz, B., 2020. Ultrasonic cavitation assisted deposition of catalytically active metals on nitrogen-doped and non-doped carbon nanotubes—A comparative study. Journal of Materials Research and Technology, 9(3), pp.4283-4291.
92. Wang, Y., Shi, L., Gao, L., Wei, Q., Cui, L., Hu, L., Yan, L. and Du, B., 2015. The removal of lead ions from aqueous solution by using magnetic hydroxypropyl chitosan/oxidized multiwalled carbon nanotubes composites. Journal of colloid and interface science, 451, pp.7-14.
93. Niu, J., Ding, P., Jia, X., Hu, G. and Li, Z., 2019. Study of the properties and mechanism of deep reduction and efficient adsorption of Cr (VI) by low-cost Fe3O4-modified ceramsite. Science of The Total Environment, 688, pp.994-1004.
94. Zhao, R., Li, X., Li, Y., Li, Y., Sun, B., Zhang, N., Chao, S. and Wang, C., 2017. Functionalized magnetic iron oxide/polyacrylonitrile composite electrospun fibers as effective chromium (VI) adsorbents for water purification. Journal of colloid and interface science, 505, pp.1018-1030.
95. Jung, C., Heo, J., Han, J., Her, N., Lee, S.J., Oh, J., Ryu, J. and Yoon, Y., 2013. Hexavalent chromium removal by various adsorbents: powdered activated carbon, chitosan, and single/multi-walled carbon nanotubes. Separation and Purification Technology, 106, pp.63-71.
96. Huang, Y., Lee, X., Macazo, F.C., Grattieri, M., Cai, R. and Minteer, S.D., 2018. Fast and efficient removal of chromium (VI) anionic species by a reusable chitosan-modified multi-walled carbon nanotube composite. Chemical Engineering Journal, 339, pp.259-267.
97. Pillay, K., Cukrowska, E.M. and Coville, N.J., 2009. Multi-walled carbon nanotubes as adsorbents for the removal of parts per billion levels of hexavalent chromium from aqueous solution. Journal of hazardous materials, 166(2-3), pp.1067-1075.
98. Islam, M.A., Angove, M.J. and Morton, D.W., 2019. Recent innovative research on chromium (VI) adsorption mechanism. Environmental Nanotechnology, Monitoring & Management, 12, p.100267.

99. Obayomi, K.S., Bello, J.O., Yahya, M.D., Chukwunedum, E. and Adeoye, J.B., 2020. Statistical analyses on effective removal of cadmium and hexavalent chromium ions by multiwall carbon nanotubes (MWCNTs). Heliyon, 6(6), p.e04174.

100. Alguacil, F.J. and López, F.A., 2020. On the Active Adsorption of Chromium (III) from Alkaline Solutions Using Multiwalled Carbon Nanotubes. Applied Sciences, 10(1), p.36.

101. Wang, L., Hu, D., Kong, X., Liu, J., Li, X., Zhou, K., Zhao, H. and Zhou, C., 2018. Anionic polypeptide poly (γ-glutamic acid)-functionalized magnetic Fe_3O_4-GO-(o-MWCNTs) hybrid nanocomposite for high-efficiency removal of Cd (II), Cu (II) and Ni (II) heavy metal ions. Chemical Engineering Journal, 346, pp.38-49.

102. Adolph, M.A., Xavier, Y.M., Kriveshini, P. and Rui, K., 2012. Phosphine functionalised multiwalled carbon nanotubes: a new adsorbent for the removal of nickel from aqueous solution. Journal of Environmental Sciences, 24(6), pp.1133-1141.

103. Alizadeh, B., Ghorbani, M. and Salehi, M.A., 2016. Application of polyrhodanine modified multi-walled carbon nanotubes for high efficiency removal of Pb (II) from aqueous solution. Journal of Molecular Liquids, 220, pp.142-149.

104. Rahmati, N., Rahimnejad, M., Pourali, M. and Muallah, S.K., 2021. Effective removal of nickel ions from aqueous solution using multi-wall carbon nanotube functionalized by glycerol-based deep eutectic solvent. Colloid and Interface Science Communications, 40, p.100347.

105. Ahmadi, S., Igwegbe, C.A., Rahdar, S. and Asadi, Z., 2019. The survey of application of the linear nonlinear kinetic models for the adsorption of nickel (II) by modified multi-walled carbon nanotubes. Applied Water Science, 9(4), pp.1-7.

CHAPTER 3: RESEARCH METHODOLOGY

This chapter presents the methodologies and instrumentation utilised for the analysis of water samples. Characterisation techniques used for the analysis of the as-prepared nanocomposites are also included. This chapter also justifies the selected study areas, sample preparation procedures, sample pre-treatment and sample collection.

3.1 MATERIALS

All chemicals were of analytical grade reagents and were used throughout this study as received. Solutions based on elements of interest with different concentrations were prepared in the laboratory using de-ionised water. Multi-walled carbon nanotubes (MWCNTs, > 98% purity with an average diameter of 20–40 nm) were purchased from Protea laboratories (Midrand, South Africa) and Nitrogen-doped (N-MWCNTs, > 98% carbon purity, 3-5wt. % N) were purchased from SABINANO (Randburg, South Africa). Sulphuric acid (H_2SO_4, 98%), nitric acid (HNO_3, 55%), hydrazine hydrate (N_2H_4, 50-60%), ammonium hydroxide (NH_4OH, 25 %), acetone ($(CH_3)_2CO$), ethanol (C_2H_5OH), acetic acid (CH_3COOH), ammonium ferrous sulphate ($(NH_4)_2Fe(SO_4)_2{\cdot}6H_2O$), ammonium ferric sulphate dodecahydrate ($NH_4Fe(SO_4)_2{\cdot}12H_2O$), hydrogen peroxide ($H_2O_2$, 30%), N,N-Dimethylformamide (DMF, 99.5%), triethylenetetramine ($C_6H_{18}N_4$, 60%), nickel(II) nitrate hexahydrate ($N_2NiO_6{\cdot}6H_2O$), potassium dichromate ($K_2Cr_2O_7$), chromium (III) chloride ($CrCl_3{\cdot}6H_2O$) and lead nitrate ($Pb(NO_3)_2$) were purchased from Sigma Aldrich (Darmstadt, Germany) and Rochelle chemicals (Johannesburg, South Africa). Thioglycolic acid ($C_2H_4O_2S$) was purchased from Merck chemical supplies (Germiston, South Africa).

3.2 PREPARATION OF ADSORBENTS

Each step of the adsorbent preparation involved both undoped MWCNTs and N-doped MWCNTs were used.

3.2.1 Synthesis of surface functionalised multi-walled carbon nanotubes [1]

To prepare the functionalised MWCNTs (f-MWCNTs), 0.5 g of MWCNTs were added to a beaker. Followed by the addition of concentrated solutions of sulphuric and nitric acid (3:1 v/v ratios). The mixture was sonicated for 3 h and then diluted with 150 mL of de-ionised water. The functionalised MWCNTs suspensions were then filtered using a nylon membrane and washed with de-ionised water several times until a pH of 7 was reached. The solids were vacuum dried in an oven at 80 °C overnight.

A similar procedure was followed by the addition of concentrated hydrogen peroxide and nitric acid (1:3 v/v ratios).

3.2.2 Preparation of iron oxide-modified MWCNTs nanocomposite [2]

Briefly, a solution of the required amount of $(NH_4)_2Fe(SO_4)_2{\cdot}6H_2O$ and $NH_4Fe(SO_4)_2{\cdot}12H_2O$ were prepared and stirred for a few minutes prior to a dropwise addition of ammonium hydroxide (8 M). When the pH had reached 11, the mixture was stirred for an additional 2 h at 70 °C. The prepared nanocomposites were filtered through a nylon membrane and then washed several times with de-ionised water. Thereafter the product was dried in a vacuum oven at 80 °C for overnight and then calcined at 300 $^{\circ}$C for 2 h.

3.2.3 Preparation of hydrazine and thiol modified M-MWCNTs nanocomposite [2]

Approximately 200 mg of Fe_3O_4-modified MWCNTs was dispersed in an alcohol solution at 25 °C. Then, a mixture of acetic acid and thioglycolic acid was added and stirred for 24 h under N_2 atmosphere. Thereafter, a solution of hydrazine was added and allowed to react for 10 min. The reaction mixture was quenched by addition of acetone, which was followed by filtration using a mixture of ethanol and de-ionised water. The as-prepared nanocomposite was vacuum dried at 80 °C overnight.

3.2.4 Preparation of triethylenetetramine-modified M-MWCNTs nanocomposite

About 100 mL of thionyl chloride ($SOCl_2$) and 30 mL tetrahydrofuran (THF) were mixed with the obtained thiol-modified MWCNTs. $SOCl_2$ was used to prepare acyl chloride MWCNTs. The mixture was sonicated for 30 minutes at room temperature, followed by refluxing while stirring at 80 °C for 24 h under N_2 atmosphere to convert the surface-bound carboxyl groups into acyl chloride groups. The MWCNTs were filtered, washed with anhydrous THF and dried at 80 °C for 24 h. These were denoted as Acyl chloride multi-walled carbon nanotubes (MWCNTs-COCl) [3]. The dried acyl chloride treated MWCNTs were ultrasonicated with N, N-Dimethylformamide(DMF) as the solvent and the binder for 2 h in a beaker containing 200 ml of triethylenetetramine (TETA). The mixtures were transferred in the round bottom flasks and refluxed for 72 h at 80 °C in the fuming cupboard. This was done to allow amide linkage between the amino group donors and the MWCNTs. The treated MWCNTs were then washed with anhydrous ethanol and de-ionised water to remove the excess amount of TETA. Finally, the nanocomposite was dried in an oven at 80 °C for 24 h. These were denoted as amino-functionalised MWCNTs [4].

3.3 CHARACTERISATION OF ADSORBENTS

3.3.1 Fourier-transform infrared spectroscopy

The FTIR spectroscopy analysis was conducted to identify the main functional groups present in the chemical structure of the materials used. The functional groups on the surface sites of MWCNTs were detected with the Agilent Cary 600 series equipment (California, USA) at the University of Limpopo with a 10 cm^{-1} resolution and 20 scans per analysis. Prior to analysis, the background was first measured to calibrate the instrument followed by cleaning the sample placement area with absolute alcohol. A small amount of the sample was then placed directly into the infrared (IR) beam for analysis. Spectra were recorded in the range 400–4000 cm^{-1}, and data were collected and processed with Origin 8.5 software.

3.3.2 Powder X-ray diffraction

The crystallographic information of the as-prepared nanocomposite materials was investigated using (Rigaku MiniFlex 600 powder X-ray) diffractometer (P-XRD MiniFlex, Hugenottenallee, Germany) at the University of Johannesburg under the conditions of radiation analysis Cu Kα (λ = 1.54056 nm) radiation source and power source with 30 kV and 10 mA, with a scan speed of 0.02 s^{-1} ranging from 5 to 65°. The diffracted X-rays patterns are presented as peak positions at two thetas (2θ) in degrees. The PXRD data were analysed using Origin 8.5 software. The mean crystallite size of the as-synthesised nanoparticles was measured through the most intense peak using the Scherrer equation.

$$D = \frac{0.9\,\lambda}{\beta COS\theta}$$

where D is the mean crystallite size, λ is the wavelength of Cu Kα, β is the full widthat medium height (FWHM) of the diffraction peaks and θ is the Bragg angle.

3.3.3 Scanning electron microscopy

Morphological analysis of M-N-MWCNTs was visualised using a Field Emission Scanning Electron Microscope, Model: JEOL JSM 7500F (Massachusetts, USA) at Council for Scientific and Industrial Research (CSIR) and Sefako Makgatho Health Science University, attached to secondary electron (SE) detectors to obtain the images. The samples were coated with gold (15 nm) *via* sputtering, using a current of 20 mA for 90 s. Magnifications of 100x and 300x were used with a 2 kV energy beam. The diameter of the M-N-MWCNTs was measured using the ImageJ software package.

3.3.4 Transmission electron microscopy

The morphology and microstructure of the products were examined utilising TEM. The samples were carried out on a Joel-Jem 2100F (Joel, Tokyo, Japan) at the University of Johannesburg operating at 200 kV equipped with an energy-dispersive. For that, a drop of the colloidal solution at 2 wt% was deposited on a copper grid for analysis.

3.3.5 Brunauer-Emmett-Teller

The specific surface area of the adsorbents was measured using the BET instrument (Tristar II. Manufactured by Micromeritics (Georgia, USA)) at the CSIR. Approximately 500 mg of the as-synthesised nanoparticles were degassed under nitrogen gas at specific operational conditions (time = 4 hrs, temp = 90 °C and flow rate = 60 cm^3 /min). BET surface area, pore size and volume were measured using nitrogen at 77 K.

3.3.6 Thermogravimetric analysis

Thermogravimetric analysis (TGA) allows the analysis of material mass loss (thermal stability) because of a progressive increase in temperature. The content of the M-N-MWCNTs in the nanoparticle samples was determined using TA Q500 thermogravimetric analyser from TA Instruments (New Castle, DE, USA) at the University of Johannesburg. Approximately 5-10 mg of the dried samples were heated. The instrument was used with a nitrogen atmosphere (N_2) at a flow rate of 50- and 100-mL min^{-1} at a heating rate of 10 °C min^{-1} and a temperature ranging from 25–1000 °C. Data were processed using Origin 8.0 software.

3.4 JUSTIFICATION AND DESCRIPTION OF THE SELECTED STUDY SITES

Sekhukhune District Municipality is among the areas experiencing water shortages. Due to mining activities, the quality of clean water and air is lowered [5]. Despite often being recognised as being a water-scarce region and having few ground and surface water reserves, the District does utilize water from various sources, including groundwater, wells, pools, rivers and dams [6]. Tubatse Municipality has recorded a vast number of villages that still depend on boreholes and rivers for water supply, which imply that their reliance must be reduced as they get contaminated [7] and this is one of the factors, which prompted the choice of the province as a study area. Illustrated below is the map of the study area and operational mines in the area (figure 3.1).

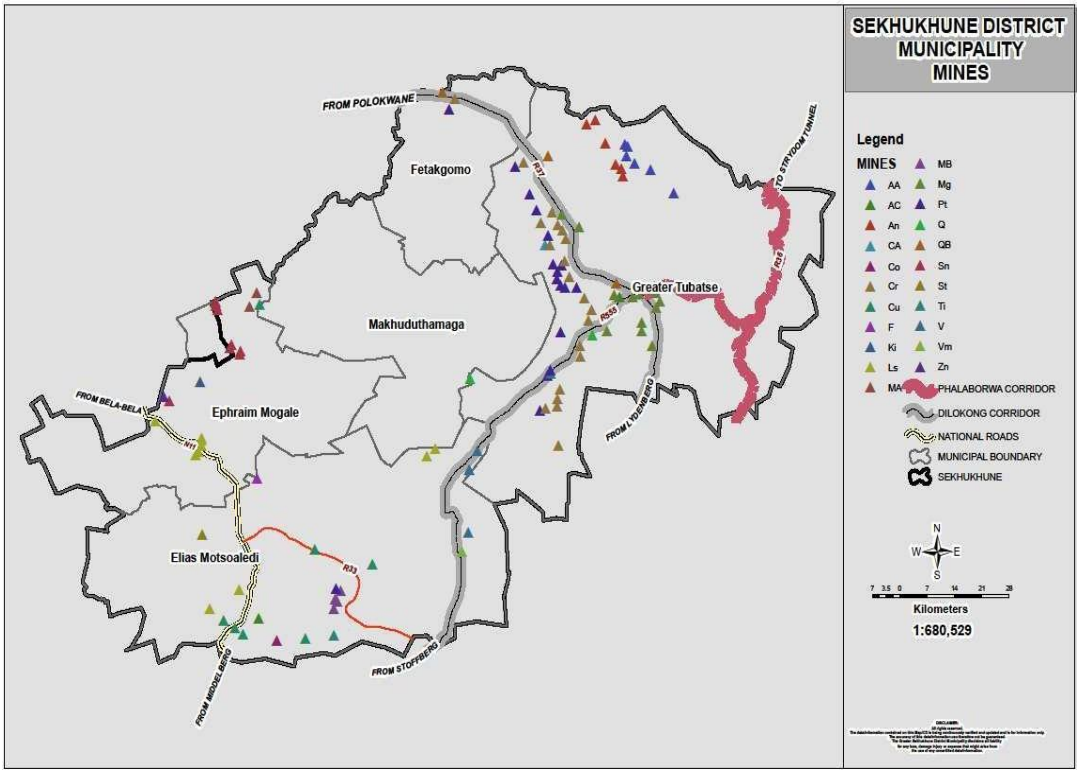

Figure 3. 1: Operational Mines in Sekhukhune District Municipality [8].

3.4.1 Sample collection and pre-treatment

Water samples were collected from upstream of the Steelpoort River near De Hoop dam (upstream of R555 bridge) descending through the midstream under Steelpoort bridge and downstream the Olifants River. The map showing 3 sampling sites from the Steelpoort and Olifants Rivers and 1 sampling point at a Burgersfort borehole is indicated in figure 3.2. The sample collection sites were selected at the Steelpoort River based on land use and mining activities and site 3 was selected based on the Steelpoort River being a tributary of the Olifants River. The mining and metal smelters were found in the proximity of the upstream and midstream of Steelpoort River. Water collection for washing laundry was observed during sampling at site 1 (upstream of Steelpoort River).

Before the collection of the samples at the rivers, sample bottles of 1000 mL with high density polyethylene were soaked in 10% (v/v) HNO_3 for 24 h before rinsing thoroughly

with deionized water. Following further rinsing with de-ionised water, the bottles were left to dry. At the sampling sites, bottles were rinsed with river water before collection of water samples and the pH (Mettler Toledo FE20-Kit FiveEasy™ Benchtop pH Meter) of the water samples was measured. During the sampling process, the bottles were kept at the bottom of the water surface and sealed to minimize air exposure to the sample. A cooler box with ice was used to keep samples while they were transported to the laboratory. The samples were filtered through with 0.45 µm nylon membranes and a 1% (v/v) HNO_3 solution was used to preserve the filtered water samples and stored in the refrigerator at 4 ^{0} C pending the analysis [9].

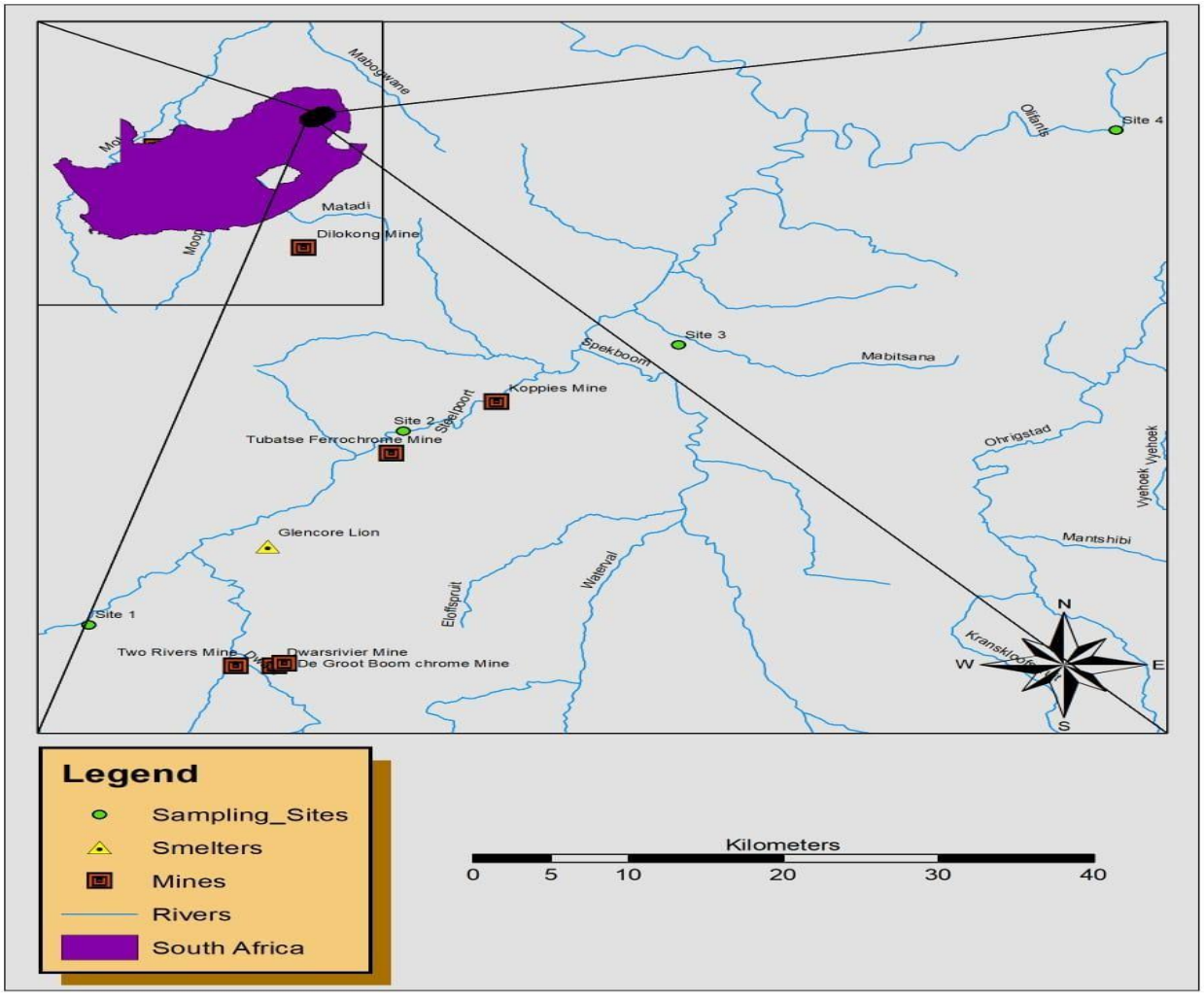

Figure 3.2: Map showing sampling sites from the Steelpoort River, Olifants River and Driekop borehole.

3.4.2 Borehole water sampling

Using 1000 mL polyethylene sampling bottles, samples were collected through a tap. Immediately after sampling, the pH of the water samples was measured. In a cooler box containing ice, water samples were stored, then transported to the laboratory. The samples were filtered through with 0.45 µm nylon membranes and 1% (v/v) HNO_3 was added to preserve all the metal ion content. The filtered water samples were stored in the refrigerator at 4 ^{0}C pending the analysis [10].

3.4.3 Analysis of collected water samples

Analysis of the real water samples was carried out before and after adsorption. To determine the total concentration of the elements of interest before adsorption, the pH of the water samples was not adjusted. The pH meter was calibrated using pH buffers of 4.29, 7.0 and 9.29. A water bath was used to raise the temperature to 40 °C. All the experiments were carried out by soaking a known amount of the adsorbent into 50 mL of the water samples. The optimum pH obtained from synthetic studies were adjusted using 0.1M HNO_3 and NaOH and vigorously stirred at an optimum time. Analysis was done at 25 ^{0} C and the obtained optimum temperature from laboratory simulation studies (40 ^{0} C). The F-AAS was used to measure the total concentrations of the analytes of interest, i.e., total chromium, nickel and lead. The samples were analysed in triplicates and the average of the measured values was recorded. The amount of the adsorbed metal ions was calculated using the following equation:

$$\% \text{ Removal} = \frac{(C_o - C_e)}{C_0} \text{ x } 100\%$$

and the adsorption capacity was calculated from the following equation:

$$qe = \frac{(C_o - C_e)V}{W}$$

where C_o and C_e (mg/L) represents the initial and equilibrium concentration of metal ions in the solution, respectively. q_e is the adsorption amount (mg/g); W is the mass of adsorbent (g) and V is the volume of metal ions in solution (L).

3.4.3.1 Determination of total concentrations of chromium, nickel and lead in water samples

Total chromium, nickel and lead concentrations in water samples were determined using Perkin Elmer Pinnacle 500 F-AAS (Massachusetts, United States) equipped with Syngistix Touch software. The operating conditions indicated for F-AAS are indicated in table 3.1.

Table 3.1: The operating condition for F-AAS

Operating Conditions	Cr	Ni	Pb
Measuring Wavelength (nm)	357.9	232.0	283.3
Lamp Current value (mA)	7	10	10
Slit Width (nm)	0.2	0.2	0.5
Oxidant(air) flow rate (L/min)	3.5	3.5	3.5
Flow rate of C_2H_2 (L/min)	2.0	2.0	2.0

3.5 PHYSICAL PROPERTIES OF GROUND AND SURFACE WATER

The multi-parameter analyser (HI 991300 pH/EC meter) was placed directly into the water samples to measure the pH and electrical conductivity.

3.6 ADSORPTION STUDIES

The procedures that follow below were used to study chromium(III), chromium(VI), nickel(II) and lead(II) adsorption.

3.6.1 Batch adsorption experiments for the selected elements

The adsorption of Cr(III), Cr(VI), Ni(II) and Pb(II) in solution by modified N-MWCNTs were investigated through batch experiments. The effect of pH on selected metal ions removal by 0.2 and 0.05 g L^{-1} (i.e., 2.5 and 10 mg mass of the sample/50 mL volume of the solution) was done at pH (2-8)Cr^{3+}, (0.5-8)Cr^{6+}, (3-12)Ni^{2+} and (1-9)Pb^{2+} for 30 min at 25°C. The pH of the metal ion solutions was adjusted using NaOH (0.5 M) and HNO_3 (0.5 M) and measured using a pH meter [11].

For time studies, respective dosages of M-MWCNTs and 50 mL of metal iron solution (50, 50, 20 and 40 mg/L) were added to a 250 mL conical flask and the pH was adjusted to obtain optimum values. The flask was stirred using a magnetic stirrer bar on a magnetic stirring plate at 120 rpm for different time intervals (1-180 min and continued for 24-72 h at 25°C) [11]. The efficiency of the removal of the selected metals was also investigated under the effect of the M-MWCNTs dosage (0.05-0.35 g/L) Cr, (0.01-0.05 g/L) Ni and (0.1-0.6 g/L) Pb. [12].

The effect of the initial metal concentration on adsorption by M-N-MWCNTs (optimum dosage) was studied using metal concentrations ranging from (20 to 250 mg/L) Cr, (20 to 120 mg/L) Ni and (20 to 100 mg/L) Pb at optimum pH, contact time and dosage [11]. The adsorption test was also carried out at varying temperatures (20, 25, 30, 35, 40°C) to investigate the effect of temperature on adsorption. These experiments were conducted at optimum pH, contact time, adsorbent dosage and initial concentration, and were stirred at 150 rpm [13].

In all the experiments, samples were filtered after the adsorption reactions and the concentrations of metal ions were measured by F-AAS. The adsorption capacity (q_e) and percentage removal (%) were calculated using the above mentioned formulae [11].

The experimental data were fitted to both Langmuir and Freundlich isotherms. The thermodynamics parameters were also evaluated.

3.6.1.1 Adsorption kinetics

The amount of metal ion adsorbed by the adsorbent depends on the contact time and thus, the kinetics of adsorption of the metal ions (Cr(III), Cr(VI), Ni(II) and Pb(II)) was explained through pseudo-first-order and pseudo-second-order kinetic models [14]. The studies were carried out at the optimum pH of 5.5, 1.5, 11 and 6 for Cr(III), Cr(VI), Ni(II) and Pb(II), respectively; and the solutions were equilibrated with 0.30, 0.35, 0.06 and 0.6 g/L of adsorbent at 25 °C for different time intervals (0–180 min). The solutions were withdrawn at predetermined times, and the concentrations were measured using

F-AAS. The kinetics of the adsorption of the metal ions by M-N-MWCNTs was investigated by measuring q_e as a function of time to investigate which model between the pseudo-first-order and pseudo-second-order model can fit the data best [12].

The pseudo-first-order kinetics and its linearised form are given by the equations below [12]:

$q_t = q_e(1-e^{-k1t})$

$\ln (q_e - q_t) = \ln q_e - k_1 t$

The pseudo-second-order equation is given as:

$$\frac{t}{qt} = \frac{1}{k_2 q_e^2} + \frac{t}{qe}$$

where q_t and q_e (mg/g) refer to the concentrations of Cr(III), Cr(VI), Ni(II) and Pb(II) adsorbed at equilibrium and at time t with the first-order rate constant k_1 (min^{-1}) and second-order rate constant k_2 (g/mg/min).

3.6.1.2 Langmuir and Freundlich isotherms

Batch experiments at different temperatures were conducted utilizing the optimum pH, dosage of adsorbents, contact time, and initial concentrations of adsorbate. The adsorption capacities (q) were calculated, and the results were fitted to Langmuir and Freundlich's adsorption isotherms [12]. Langmuir and Freundlich isotherms are often used to better understand adsorption processes. Langmuir isotherms assume a monolayer coverage of adsorbate over a homogeneous adsorbent surface, and that the adsorption of each molecule onto the surface has equal adsorption activation energy [15].

The Langmuir isotherm is mathematically expressed in terms of concentrations and adsorption capacities as shown below [15]:

$$q_e = \frac{qmaxbCe}{1+bCe}$$

$$\frac{1}{qe} = \frac{1}{qmax} + \frac{1}{bqmaxCe}$$

where q_e represent the maximum amount of adsorption (mg/g), q_{max} (mg/g) represents the maximum adsorption capacity or the theoretical monolayer saturation capacity, C_e is the equilibrium concentration of substrates in the solution (mg/L) and b (L/mg) is the adsorption constant for the Langmuir isotherm.

The essential features of the Langmuir isotherm indicating the favourability of the adsorption (R_L, also called equilibrium parameter) is expressed by equations below [16]:

$$R_L = \frac{1}{1+bCo}$$

where C_o (mg/L) is the initial metal concentration and b is Langmuir equilibrium constant for adsorption (L/mg). The value of R_L indicates the type of Langmuir isotherm to either be unfavourable adsorption (R_L>1), linear (R_L = 1), favourable (0 < R_L < 1) or irreversible (R_L = 0).

The Freundlich isotherm considers a heterogeneous surface with a non-uniform distribution of adsorption heat over the surface and multilayer adsorption can be formed.

The Freundlich isotherm is mathematically expressed as shown below [15]:

$$q_e = K_f C_e^{1/n}$$

$$\ln q_e = \ln K_f + \frac{1}{n} \ln C_e$$

where q_e is the maximum amount of adsorption (mg/g), C_e is the equilibrium concentration of substrates in the solution (mg/L). K_f is a constant representing adsorption capacity($mg^{1-1/n}$ $L^{1/n}$ g^{-1}) and n is a constant depicting the adsorption intensity.

3.6.1.3 Adsorption thermodynamics

Enthalpy change (ΔH′), Gibbs free energy change (ΔG′) and change in entropy (ΔS′) for the adsorption of Cr(III), Cr(VI), Ni(II) and Pb(II) on the modified MWCNTs were determined using the equation below [17]:

$\Delta G' = \Delta H' - T\Delta S'$

$\Delta G' = -RT \ln (K'_e)$ $\ln K_e =$

$\frac{\Delta S^\circ}{R} - \frac{\Delta H^\circ}{RT}$

$K_e = \frac{Cad}{Ce}$

where K'_e is the distribution coefficient. The universal gas constant (R) is 8.314 J/mol. K and T is the absolute temperature (K). C_e (mg/L) and C_{ad} (mg/L) represents the equilibrium concentration of metal adsorbed in the solution and the concentration of the metal in the adsorbent at equilibrium, respectively. ΔS^o, ΔH^o and ΔG^o represent changes in standard entropy (J/mol/K), standard enthalpy (kJ/mol) and the standard Gibbs free energy (kJ/mol), respectively. The values of ΔS^o and ΔH^o represents the intercept and slope from the plot of $\ln K_e$ versus 1/T.

3.6.2 Effect of competing anions on metal ion removal

The effect of competing anions on the ability of the as-prepared nanocomposite in adsorbing the selected metal ions (Cr(III), Cr(VI), Ni(II) and Pb(II)) was conducted in the presence of chloride (Cl^-), bicarbonate (HCO_3^-), dichromate ($Cr_2O_7^{2-}$), nitrate (NO_3^-), phosphate (PO_3^{4-}) and sulphate (SO_4^{2-}). Adsorption studies were carried out using the obtained optimum parameters (pH, contact time, adsorbent dosage, initial concentration and temperature). The metal ion solutions were mixed with competing ions solutions at different concentrations containing $[Cl^-]_0$ = 355 mg/L, $[HCO_3^-]_0$ = 610 mg/L, $[Cr_2O_7^{2-}]_0$ = 50 mg/L, $[NO_3^-]_0$ = 20 mg/L , $[PO_4^{3-}]_0$ = 20 mg/L and $[SO_4^{2-}]_0$ = 960 mg/L. The removal of the metal ions was evaluated in a binary-solute system containing the element of interest and a single competing anion for each of the selected anions at a time. The removal was also evaluated in a multi-solute system containing four different anions together with the metal of interest. By introducing a known mass of adsorbent into a conical flask, batch adsorption tests were conducted, followed by introducing a known concentration of either (Cr(III), Cr(VI), Ni(II) and Pb(II)) was added and the pH was adjusted to the desired pH using 0.1 M HNO_3 and NaOH. The samples were then stirred magnetically at the specified contact time at 150 rpm. The solutions were removed from the stirrer plates at predetermined times,

and the concentrations were measured using F-AAS to determine the extent of the interfering anions.

3.6.3 Reusability and regeneration studies

The reusability of the modified N-MWCNTs nanocomposites was investigated through sequential cycles of adsorption/desorption experiments. For the adsorption experiment, a known amount of the M-N-MWCNTs nanocomposite was equilibrated with 50mL of the metal solution under the obtained optimum parameters (pH, adsorbent dosage, contact time, initial concentration and temperature) of each element of interest. After filtration, the solution was analysed, and the final concentration of the metal ions was determined using the F-AAS. After adsorption of chromium, nickel and lead, the metal loaded M-N-MWCNTs nanocomposite was regenerated in 0.5mol/L of HCl solution and shook in a centrifuge at 25℃ for 2h. After 12 h of drying at 60 °C, the regenerated nanocomposite was used in the next adsorption cycle. Each experiment was carried out four times under the same conditions to test the reusability of the adsorbent [18].

REFERENCES

1. Farghali, A.A., Tawab, H.A., Moaty, S.A. and Khaled, R., 2017. Functionalization of acidified multi-walled carbon nanotubes for removal of heavy metals in aqueous solutions. Journal of Nanostructure in Chemistry, 7(2), pp.101-111.
2. Jiang, L., Li, S., Yu, H., Zou, Z., Hou, X., Shen, F., Li, C. and Yao, X., 2016. Amino and thiol modified magnetic multi-walled carbon nanotubes for the simultaneous removal of lead, zinc, and phenol from aqueous solutions. Applied Surface Science, 369, pp.398-413.
3. Soleimani, M., Ghahraman Afshar, M. and Sedghi, A., 2013. Amino-functionalization of multiwall carbon nanotubes and its use for solid phase extraction of mercury ions from fish sample. International Scholarly Research Notices, 2013.
4. Kashyap, A., Singh, N.P., Arora, S., Singh, V. and Gupta, V.K., 2020. Effect of amino-functionalization of MWCNTs on the mechanical and thermal properties of MWCNTs/epoxy composites. Bulletin of Materials Science, 43(1), pp.1-9.
5. Tsebe, M.R., 2018. Impact of mining on agriculture and socio-economic aspects in the rural communities of Greater Tubatse Local Municipality (Doctoral dissertation, University of South Africa, Department of Agriculture).
6. Minerals Council South Africa. (2017). Platinum. Key Facts and Figures. Retrieved June 23, 2017, from https://www.mineralscouncil.org.za/sa-mining/platinum
7. Sekhukhune District Municipality. 2018. Draft Integrated Development Plan (IDP) Review for 2018/2019. Groblersdal. Retrieved from: https://doi.org/http://www.sekhukhunedistrict.gov.za/sdm-admin/documents/Draft IDP 2018-20199.pdf. (accessed 07 August 2020).
8. Sekhukhune District Municipality. 2015. Draft Integrated Development Plan (IDP) Review for 2013/2014. Groblersdal. Retrieved from: https://doi.org/http://www.sekhukhunedistrict.gov.za/sdm-admin/documents/Draft IDP 2013-2014.pdf. (accessed 26 June 2020).
9. Letsoalo, M.R., Godeto, T.W., Magadzu, T. and Ambushe, A.A., 2019. Selective speciation of inorganic arsenic in water using nanocomposite based solid-phase extraction followed by inductively coupled plasma-mass

spectrometry detection. Journal of Environmental Science and Health, Part A, 54(9), pp.924-932.

10. Munyangane, P., Mouri, H. and Kramers, J., 2017. Assessment of some potential harmful trace elements (PHTEs) in the borehole water of Greater Giyani, Limpopo Province, South Africa: possible implications for human health. Environmental geochemistry and health, 39(5), pp.1201-1219.
11. Xu, H., Liu, Y., Liang, H., Gao, C., Qin, J., You, L., Wang, R., Li, J. and Yang, S., 2020. Adsorption of Cr (VI) from aqueous solutions using novel activated carbon spheres derived from glucose and sodium dodecylbenzene sulfonate. Science of The Total Environment, p.143457.
12. Dokmaj, T., Ibrahim, T., Khamis, M., Abouleish, M. and Alam, I., 2020. Chemically Modified Nanoparticles Usage for Removal of Chromium from Sewer Water. Environmental Nanotechnology, Monitoring & Management, p.100319.
13. Anupam, K., Dutta, S., Bhattacharjee, C. and Datta, S., 2011. Adsorptive removal of chromium (VI) from aqueous solution over powdered activated carbon: Optimisation through response surface methodology. Chemical Engineering Journal, 173(1), pp.135-143.
14. Kahu, S.S., Shekhawat, A., Saravanan, D. and Jugade, R.M., 2016. Two fold modified chitosan for enhanced adsorption of hexavalent chromium from simulated wastewater and industrial effluents. Carbohydrate polymers, 146, pp.264-273.
15. Huang, Y., Lee, X., Macazo, F.C., Grattieri, M., Cai, R. and Minteer, S.D., 2018. Fast and efficient removal of chromium (VI) anionic species by a reusable chitosan-modified multi-walled carbon nanotube composite. Chemical Engineering Journal, 339, pp.259-267.
16. Macevele, L.E., 2019. Preparation and application of multi-walled carbon nanotubes/poly (vinylidene fluoride-co-hexafluropropylene) composite membranes for filtration and adsorption of contaminants in water (Doctoral dissertation, University of Limpopo, Department of Chemistry).
17. Magadzu, T., Moganedi, K.L.M. and Macevele, L., 2020. Adsorption of Cadmium (II) ions from aqueous solutions using Poly (amidoamine)/multi-walled carbon nanotubes doped Poly (vinylidene fluoride-co-

hexafluoropropene) composite membrane. Journal of Membrane Science and Research, 7(3), pp.152-165.

18. Wang, L., Hu, D., Kong, X., Liu, J., Li, X., Zhou, K., Zhao, H. and Zhou, C., 2018. Anionic polypeptide poly (γ-glutamic acid)-functionalized magnetic Fe3O4-GO-(o-MWCNTs) hybrid nanocomposite for high-efficiency removal of Cd (II), Cu (II) and Ni (II) heavy metal ions. Chemical Engineering Journal, 346, pp.38-49.

CHAPTER 4: RESULTS AND DISCUSSION

4.1 INTRODUCTION

This chapter gives a detailed description of the obtained characterisations and research finding namely the adsorption results of the selected metal ions.

4.2 CHARACTERISATION OF SYNTHESISED MWCNTs AND N-DOPED MWCNTs NANOCOMPOSITE MATERIALS

4.2.1 Fourier transform infrared spectroscopy analysis

4.2.1.1 Fourier transform infrared spectra of raw-MWCNTs, o-MWCNTs and N_2H_4-SH-Fe_3O_4/o-MWCNTs nanocomposites

The FTIR spectra of raw-MWCNTs, o-MWCNTs and N_2H_4-SH-Fe_3O_4/o-MWCNTs nanocomposites are shown in figure 4.1. The raw MWCNTs (figure 4.1a) shows an absence of -OH and -CO functional groups as reported elsewhere [1]. Figure 4.1 (b) shows an additional peak at 1420 cm^{-1} which is attributed to C=O stretching confirming the presence of carboxylic groups as reported by Rananga et al. [2]. Figure 4.1 (c) shows functional groups after treatment with metal oxides, thiol and amino groups. Figure 4.4c confirmed the formation of amide groups on the MWCNTs surface. The strong peak at approximately 3432 cm^{-1} was attributed to O-H stretching vibration, which existed in water molecules or active groups on N_2H_4-SH-Fe_3O_4/o-MWCNTs after amino-functionalisation [3]. The peak located at 2813 cm^{-1} is attributed to the C-H stretching vibration of the (-CH_2-) group in the structure of hydrazine. The peaks at 1260 and 1448 cm^{-1} were ascribed to C–N stretching of amide groups, while the peaks at 1622 and 1371 cm^{-1} correspond to the N-H bending and C-N stretching of amine, respectively which are compatible with the bands confirmed by Singh et al. [4].

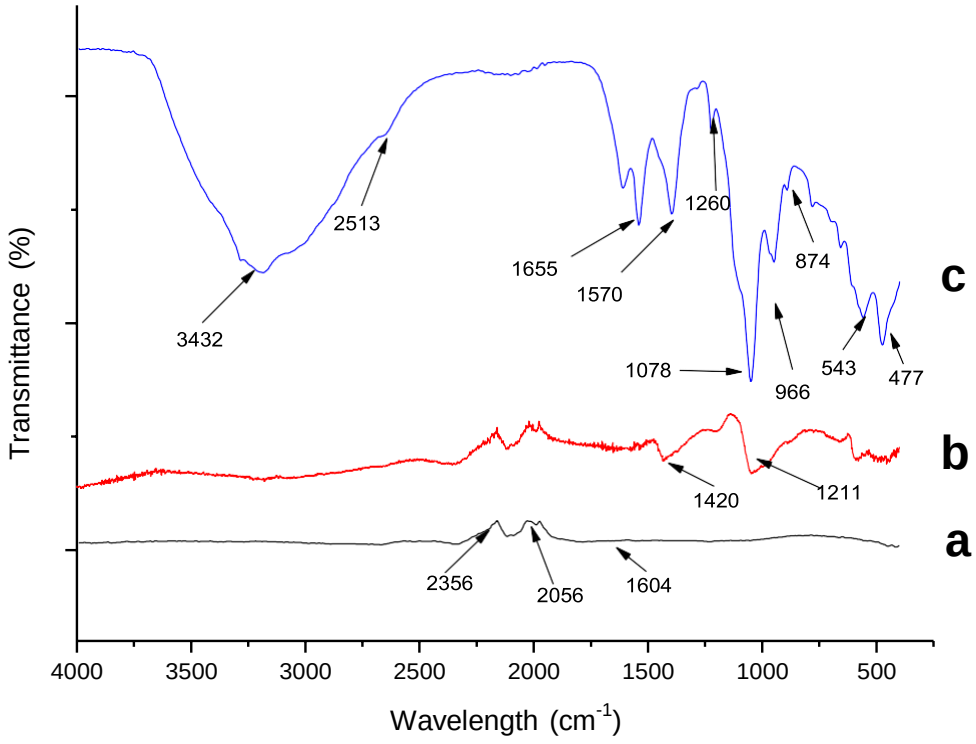

Figure 4.1: FTIR spectra of (a) raw MWCNTs, (b) o-MWCNTs and (c) N_2H_4-SH-Fe_3O_4/o-MWCNTs.

The appearance of a new peak at 966 cm^{-1} (figure 4.1c) is assigned to Si-N stretching vibration, which reveals that $C_2H_4O_2S$ and N_2H_4 are successfully coated [5]. The peak at 808 cm^{-1} is related to the -NH_2 groups which prove that the amino groups were successfully loaded onto the carbon nanotubes as observed by Yang et al. [3]. The Fe-O peak appears in the fingerprint region which makes it difficult to confirm especially with competing features from the structure, thus a characteristic peak at 477 cm^{-1} (figure 4.1c) for the Fe-O stretching vibration of Fe_3O_4 is observed. The peak at 1078 cm^{-1} showed an increase in intensity after iron oxide, thiol and amino-functionalisation, which was explained by Yang et al. [3] that many methylene groups from amino precursors may be attached to the surface of MWCNTs.

4.2.1.2 Fourier transform infrared analysis of raw and acidified N-doped MWCNTs nanocomposites

The FTIR spectra of raw N-MWCNTs and acid-treated N-MWCNTs are shown in figure 4.2. N-MWCNTs (figure 4.2a) show carbon graphite structure that is visible due to the presence of a shift wavenumber at 2311 cm^{-1}, which indicates the presence of alkyne absorption that is augmented by weak absorption between wavenumbers of 2056 and 1500 cm^{-1} [6].

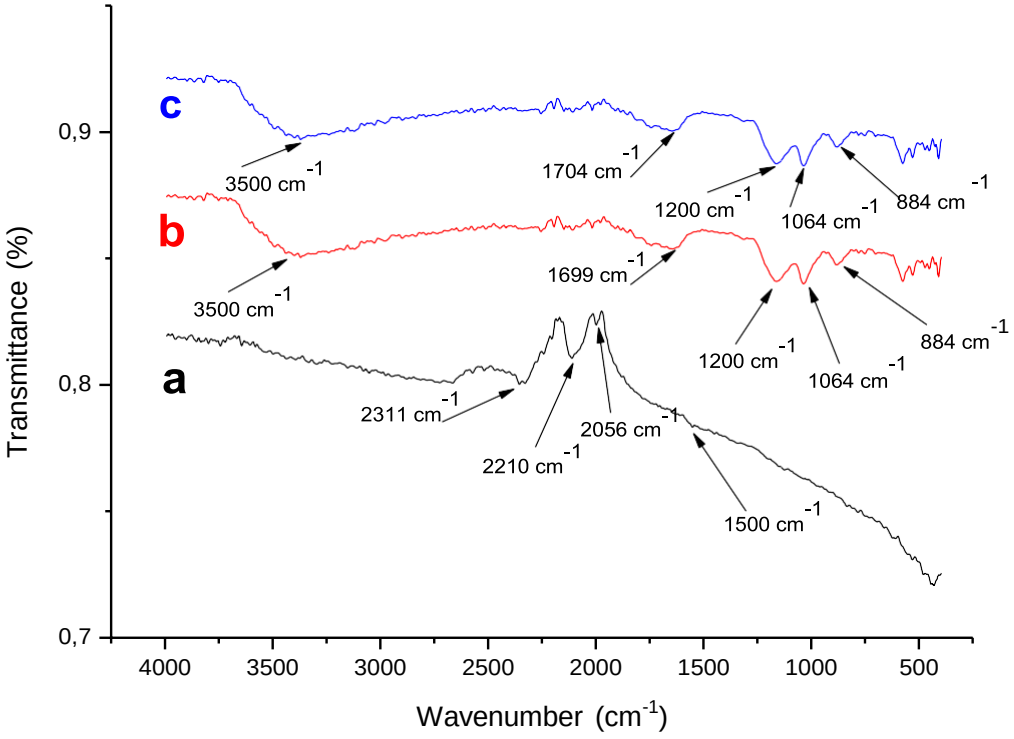

Figure 4.2: FTIR spectra of (a) raw N-MWCNTs, (b) H_2O_2-HNO_3 treated N-MWCNTs and (c) H_2SO_4-HNO_3 treated N-MWCNTs.

Spectra of acidified N-MWCNTs are shown in figure 4.2b and c indicating the acid treatment generated functional groups on the surface of N-MWCNTs. The corresponding band at 3500 cm^{-1} is attributed to hydroxyl groups on acidified N-MWCNTs surface [6-8]. The appearance of this peak is an indication of acid functionalisation [6-9]. On the other hand, the characterised peak at 1704 cm^{-1} could be attributed to carboxyl groups as observed by Fargali et al. [8]. The peak located at

1200 cm^{-1} was associated with symmetric COO^- stretching. Jung et al. [10] also observed CO stretching vibration on COH at 1064 cm^{-1}. Mkhondo et al. [1] noted that the mixture of H_2O_2:HNO_3 shows almost the same functional groups as the mixture of H_2SO_4:HNO_3. Almost similar intensity of the functional groups was introduced on the surface of N-MWCNTs from both nitric and hydrogen peroxide (H_2O_2:HNO_3) and nitric and sulphuric acid mixture (H_2SO_4:HNO_3) as observed from the obtained FTIR spectra. These results are compatible with the work done by Mkhondo et al. [1]. As explained by Fu et al. [11], introducing heteroatom N into the graphitic carbon structure contributes to tailoring the underlying catalyst–support interactions to boost the electrocatalytic activity and stability. The two types of MWNTs were found to possess similar strengths but different load-bearing abilities owing to the differences in their wall structures. As such, N-MWCNTs were selected because the sonication time has no particular effect on the fracture of N-MWCNTs when compared to the undoped MWCNTs [12].

4.2.1.3 Fourier transform infrared spectra of acid (H_2SO_4-HNO_3) treated N-doped MWCNTs nanocomposites

Figure 4.3 shows the deformation mode of NH_2 group at 1604 cm^{-1} in all the materials. The characteristic peaks of the modified o-N-MWCNTs in figure 4.3a appeared at 3420 cm^{-1} corresponding to O-H deformation vibration [3,5]. The peak at 1397 cm^{-1} (figure 4.3b) corresponds to the characteristic absorbance of single C–N bonds [6,13]. Figure 4.3b shows the appearance of a strong peak at 1064 cm^{-1} attributed to C=O stretching vibration in aromatic esters [9]. The results indicate that the alcohol groups on the surface of the M-N-MWCNTs are successfully esterified with thioglycolic acid as explained by Chen et al. [9]. The presence of the ring vibration peak at 1064 cm^{-1} in the chromatography of the as-prepared material was reported by Chen et al. [9], which attributed to the stretching vibration of C=O in aromatic esters. The results indicate that the alcohol hydroxyl groups on the surface of the nanotubes are successfully esterified with thioglycolic acid. As observed by Chen et al. [9], there is a weak peak at 2363 cm^{-1} which is due to the introduction of -SH, but the position of the peak shifts from 2560 cm^{-1}. The appearance of a weak peak (figure 4.3b) at 2500 cm^{-1} corresponds to the results reported by Chen et al. [9].

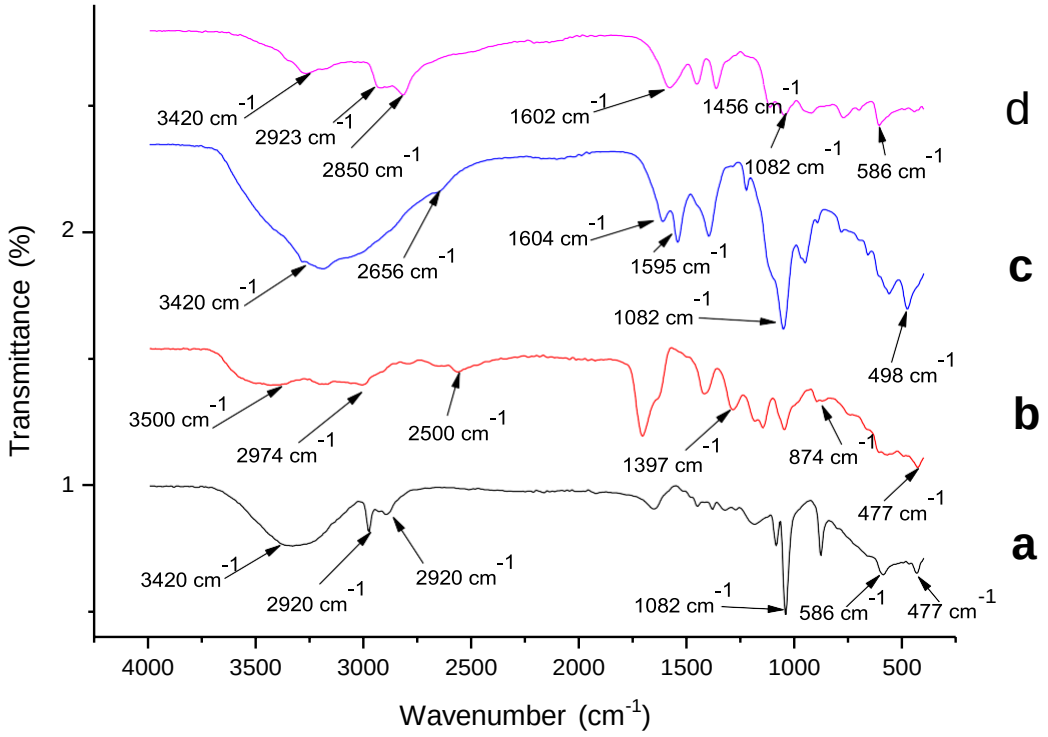

Figure 4.3: FTIR spectra of (a) Fe_3O_4/o-N-MWCNTs, (b) SH-Fe_3O_4/o-N-MWCNTs, (c) N_2H_4-SH-Fe_3O_4/o-N-MWCNTs and (d) $C_6H_{18}N_4$-SH-Fe_3O_4/o-N-MWCNTs nanocomposites treated with H_2SO_4-HNO_3.

Figure 4.3c shows the absorption peak at 1355 cm^{-1} assigned to the stretching peak of -CH on the CNTs surface [7]. The peak located at 1082 cm^{-1} is assigned to C-O stretching vibration [14] while the peak at 1595 cm^{-1} is attributed to C=N stretching modes [15]. Figure 4.3(c and d) show that OH stretching vibration is experiencing a shift in the spectrum of 3420 cm^{-1} and reinforced by the appearance of a sharp absorption at a wavenumber of 1082 cm^{-1} indicating the presence of carbonyl group (CO). The peak located at 2923 cm^{-1} attributed to the stretching vibration of C-H is reinforced by the appearance of peaks at 1456 and 1323 cm^{-1} indicating the presence of CH_2 and CH_3 [6]. Looking at N-MWCNTs, the obtained results provide evidence for the presence of incorporated nitrogen in CNTs. Consequently, the peak at 3420 cm^{-1} weakened after thiol-functionalisation then after hydrazine-functionalisation an increase in the intensity is observed which may be due to the amino groups attached to the surface of the adsorbent as observed by Kariim et al. [16]. Meanwhile, the same intense peak was supposed to be observed after TETA-functionalisation as it also

introduces amino groups. However, the peak was weakened which may have resulted from synthesis of the material. Ritter et al. [15] pointed out that substituting the N atom in place of a C atom in an sp^2 bonded carbon network will induce strong IR activity. Consequently, the absorption in the 1000–1750 cm^{-1} region is expected if the N atoms are bonded into the carbon network [15].

4.2.2 Powder X-ray diffraction Analysis

4.2.2.1 PXRD patterns of o-N-MWCNTs, Fe_3O_4/o-N-MWCNTs and N_2H_4-SH-Fe_3O_4/o-N-MWCNTs nanocomposites

The PXRD patterns of the as-synthesised carbon nanotubes are shown in figure 4.4. The intense peak at 26 degrees in all the samples can be assigned to the (002) plane of the graphitic structure of CNTs [13]. Figure 4.4(b-c) shows that the diffraction peaks of MWCNTs become weak at 26° and have a lower crystallinity than o-MWCNTs [5]. The PXRD pattern of the Fe_3O_4/o-N-MWCNTs (figure 4.4b) nanocomposite displayed characteristic peaks at 2θ = 26, 35.4, 42.9 and 62.92 degrees which are consistent with the (002), (311), (100) and (440) planes and are in line with the standard XRD data for the inverse spine crystalline structure of Fe_3O_4 (JCDS No. 19-0629) with a face-centered cubic (fcc) structure [7]. As explained by Luo et al. [17] the broad diffraction peaks exhibit the very small size of Fe_3O_4 nanoparticles which changed only a little after modification. No peaks of corresponding impurities were observed after thiol-functionalisation (not shown), indicating that the structure of MWCNTs/Fe_3O_4 nanocomposite remains unchanged. The study done by Chen et al. [9] reveals that the introduction of thiol groups does not affect the as-prepared magnetic Fe_3O_4/o-N-MWCNTs. This observation is in accordance with the study done by Zhang et al. [7].

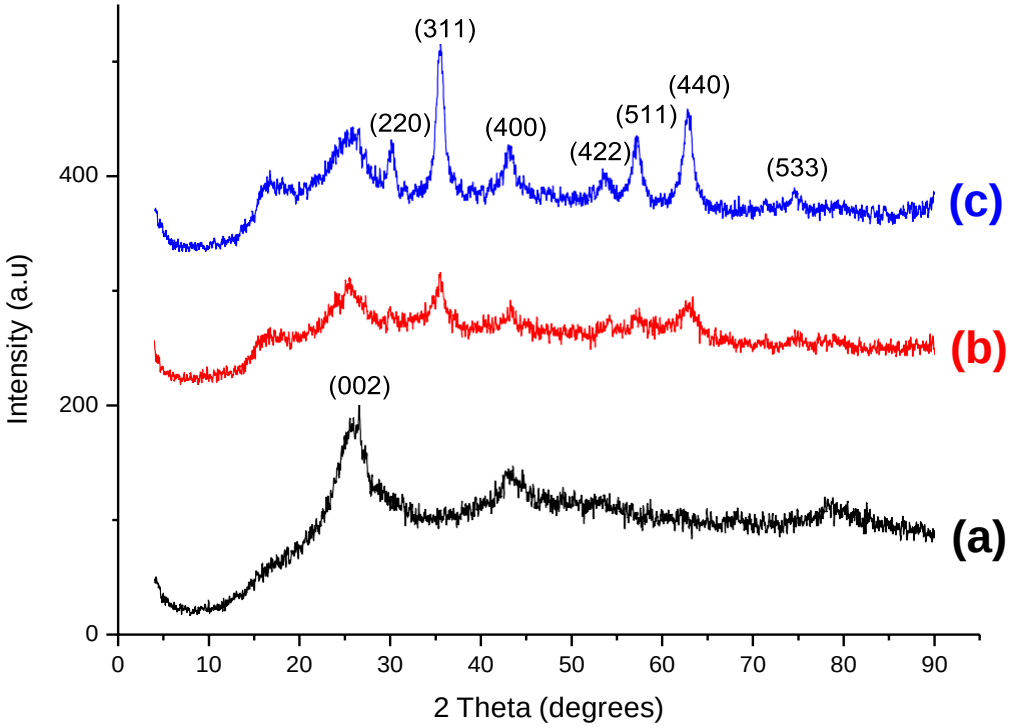

Figure 4.4: PXRD patterns of (a) o-N-MWCNTs, (b) Fe_3O_4/o-N-MWCNTs and (c) N_2H_4-SH-Fe_3O_4/o-N-MWCNTs.

New peaks appeared after amination of the N-MWCNTs (figure 4.4c) at 2θ = 55°, 56.9° and a weak peak at 73.93° corresponding to the (004), (511) and (533) planes respectively indicating the presence of Fe_3O_4 as observed elsewhere [18]. A study by Ritter et al. [15] showed that the PXRD pattern of N-MWCNT exhibits weak peaks, which can be ascribed to the hexagonal C_3N_4 (201) and (004) reflections whereas the iron oxide (202) reflection at 42.6° is superimposed by much stronger CNT (100) feature. The estimated particle size of the MWCNTs nanoparticles using the (002) and (311) peaks by the Scherrer equation are approximately 18.18 nm and 32.2 nm for theo-N-MWCNTs and Fe_3O_4/o-N-MWCNTs respectively, which is consistent with the TEM results in section 4.2.4. and 72.07 nm using the (311) peak for the N_2H_4-SH-Fe_3O_4/o-N-MWCNTs.

4.2.2.2 PXRD patterns showing the effect of hydrazine and triethylenetetramine (TETA) substituted SH-Fe_3O_4/o-N-MWCNTs nanocomposites

The PXRD patterns of the amino-functionalised carbon nanotubes are shown in figure 4.5. The intense peak at 26 degrees can be allocated to the (002) plane of the graphitic structure of CNTs [15]. The intensity of the diffraction peak at (002) plane for the TETA-functionalised SH-Fe_3O_4/o-N-MWCNTs (figure 4.5b) is more intense as compared to the hydrazine-functionalised SH-Fe_3O_4/o-N-MWCNTs (figure 4.6a). In comparison to the hydrazine-functionalised SH-Fe_3O_4/o-N-MWCNTs (figure 4.6a), the TETA-functionalised SH-Fe_3O_4/o-N-MWCNTs (figure 4.5b) showed disappearance of diffraction peaks at 2θ = 30.1°, 35.3° and 62.92° degrees which are consistent with the (220), (311) and (440) planes. The missing peaks in figure 4.6b may be due to distortion of typical fcc crystalline structure [18]. A few noisy peaks were observed (figure 4.5b), which may have resulted from impurities encountered during the synthesis of the nanocomposite material, thus the disappearance of the Fe_3O_4 determining peaks. The estimated particle size of the MWCNTs nanoparticles using the (311) and (002) peaks is approximately 72.07 nm and 10.67 for the hydrazine-functionalised SH-Fe_3O_4/o-N-MWCNTs and TETA-functionalised SH-Fe_3O_4/o-N-MWCNTs nanoparticles, respectively. Notably, the TETA-functionalised SH-Fe_3O_4/o-N-MWCNTs particle size corresponds to TEM results in section 4.2.4.2.

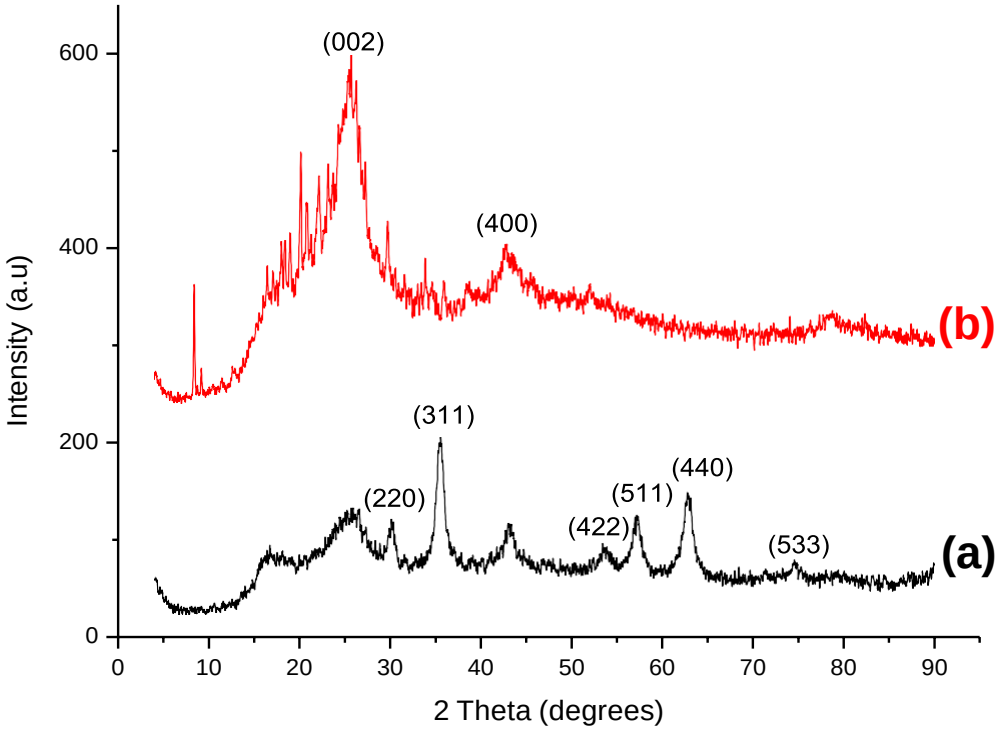

Figure 4.5: PXRD patterns showing the comparison of (a) hydrazine-functionalised and (b) TETA-functionalised SH-Fe_3O_4/o-N-MWCNTs.

4.2.2.3 PXRD patterns showing the effect of nitrogen doping on N_2H_4-SH-Fe_3O_4/o-MWCNTs nanocomposites

Figure 4.6 shows the PXRD patterns of hydrazine-functionalised MWCNTs and both figures 4.6(a and b) exhibit the same characteristic peaks [19]. The peak observed at 73.93° was also noticed by Jiang et al. [5], in their study for removal of lead, zinc, and phenol from aqueous solutions using thiol and amino modified magnetic MWCNTs. The peak changes in XRD patterns are related to the structural changes on the synthesized MWCNTs which may result from an increase or decrease in crystallite size. Compared to N_2H_4-SH-Fe_3O_4/o-MWCNTs (figure 4.6b), the N-doped N_2H_4-SH-Fe_3O_4/o-MWCNTs (figure 4.6a) had a broader (002) peak with other peaks depicting lower intensity, indicating a decrease of graphene crystallinity due to nitrogen doping induced structural damage [20].

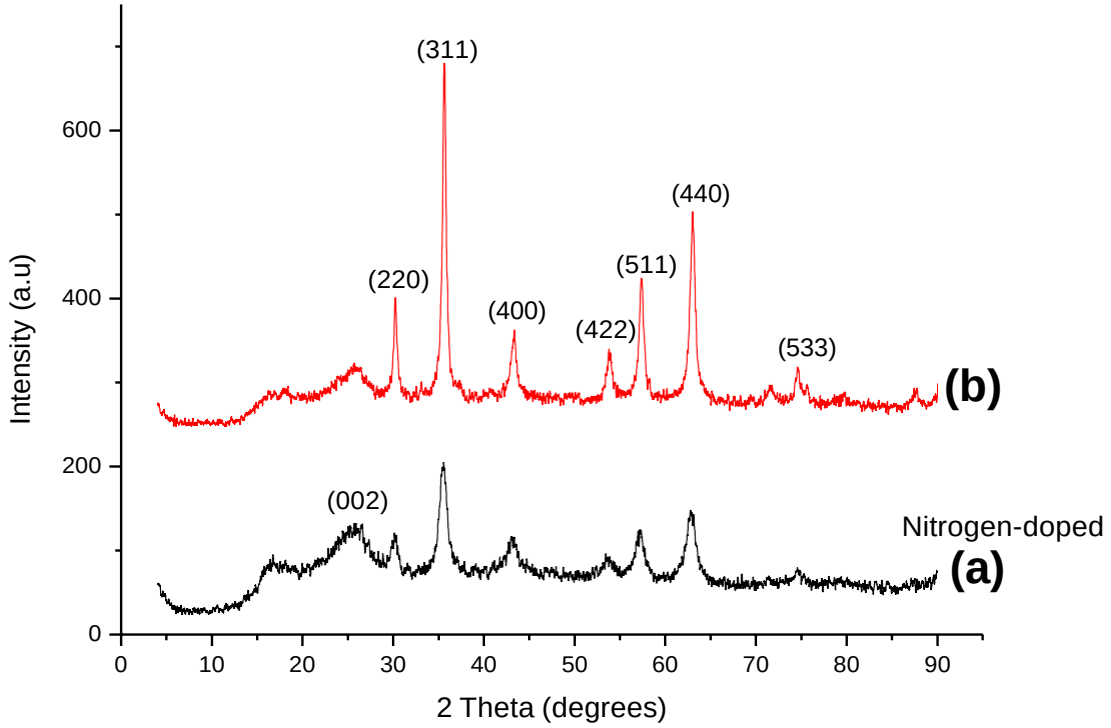

Figure 4.6: PXRD patterns showing a comparison of (a) Nitrogen-doped N_2H_4-SH-Fe_3O_4/o-MWCNTs and (b) undoped N_2H_4-SH-Fe_3O_4/o-MWCNTs.

The average crystallite size was calculated based on the highest intensity of each nanocomposite material using the Scherrer equation. A size of 160 nm was obtained for the N_2H_4-SH-Fe_3O_4/o-N-MWCNTs nanocomposite and 72.07 nm for the nitrogen-doped N_2H_4-SH-Fe_3O_4/o-MWCNTs nanocomposite was obtained.

4.2.3 Scanning electron microscopy analysis

4.2.3.1 SEM images of o-N-MWCNTs, Fe_3O_4/o-N-MWCNTs and SH-Fe_3O_4/o-N-MWCNTs nanocomposites

Scanning electron microscopy (SEM) was used to study morphology, surface structure and homogeneity of the modified N-MWCNTs nanocomposite. The SEM images in figure 4.7a show that raw N-MWCNTs are smoothed, well dispersed and possess characteristic flat tips with a diameter of about 20-30 nm (figure 4.7b) and 190-240 nm in length. After acidification, no significant changes to the structures and the sizes of

the N-MWCNTs were observed which was also confirmed by Tetana et al. [21]. Kaur [22] reported similar results showing that sonication of CNTs in H_2SO_4/HNO_3 (3:1) mixture produces tubes of shorter lengths. Simon et al. [23] also reported that as a result of oxidative treatment, the N-CNTs fibers were broken into shorter fibers, with about 200–800 nm sections in length. N-doped bamboo-like carbon nanotubes carry lower mechanical strengths than their non-doped counterparts, which explains why they are easily ruptured.

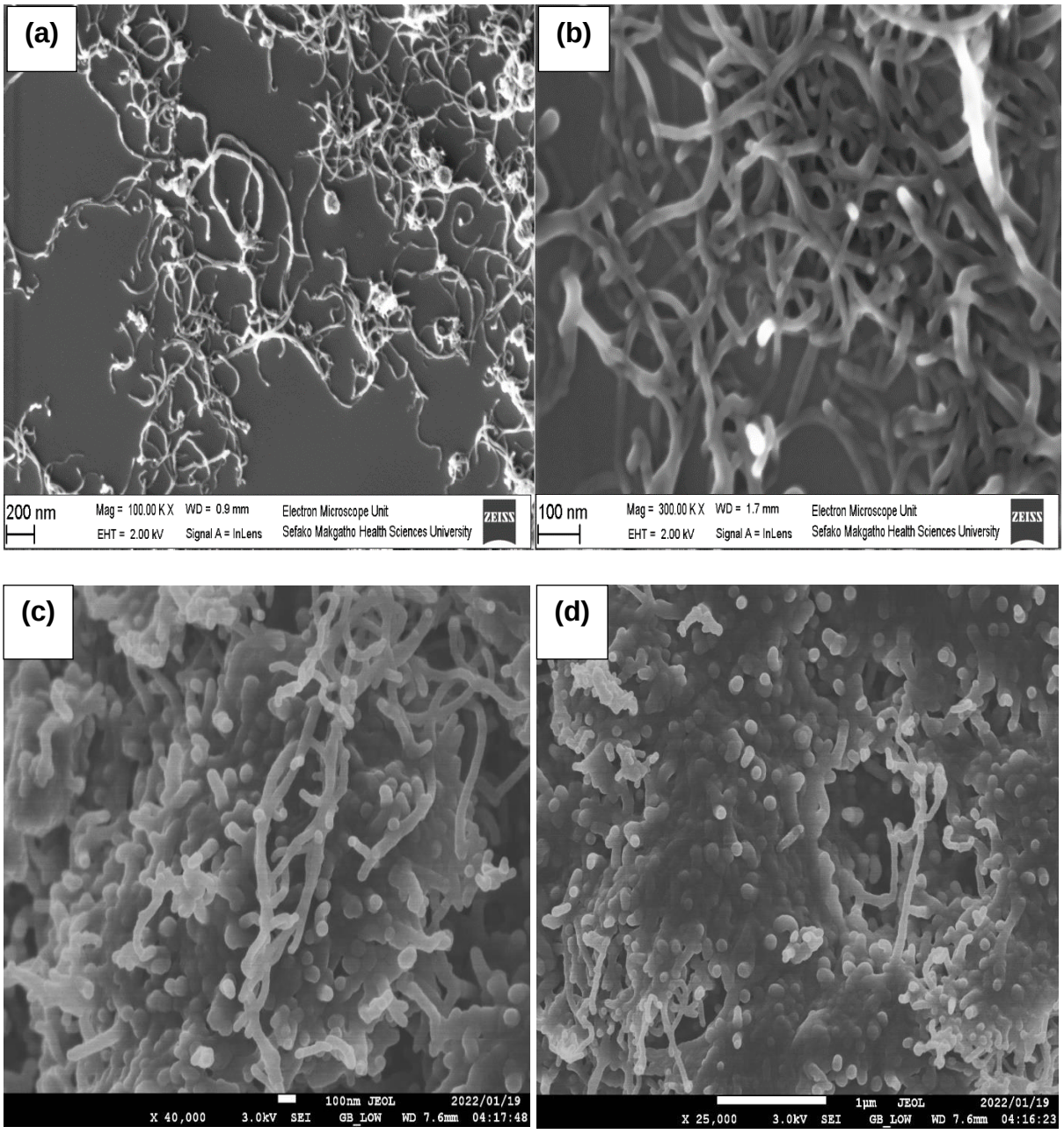

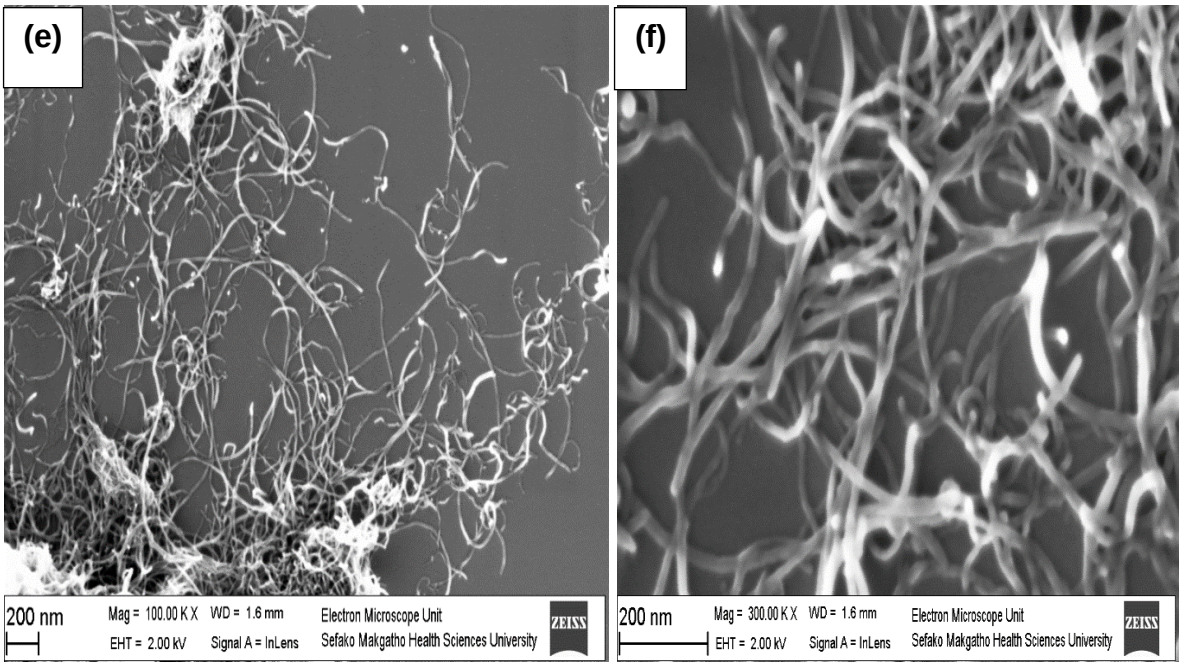

Figure 4.7: Low and high magnification SEM images of modified N-MWCNTs (o-N-MWCNTs (a and b), Fe_3O_4/o-N-MWCNTs (c and d) and SH-Fe_3O_4/o-N-MWCNTs (e and f).

As shown in figure 4.7(c and d), the nanoparticles indicate that Fe_3O_4 nanoparticles are deposited uniformly on the surface of the MWCNTs. A distinct agglomeration of the CNTs can be observed which due to the magnetic properties of iron oxide. Because the capillary tube force of MWCNTs can overcome the surface tension of water, Fe^{2+} and Fe^{3+} entered the MWCNTs. Moreover, nitric acid oxidation of MWCNTs caused the ends to open, which enabled iron ions to enter the interior of MWCNTs and to be adsorbed on their surface. [24]. The nanoparticles revealed the entangled nanotubes with an average diameter within the range of 5-15 nm. The morphological profile is in good agreement with the literature [25]. A study conducted by Egbosiuba et al. [25] suggested that due to the observed absence of metallic impurities and amorphous carbon on the surface, the morphology of the nanoadsorbents indicates that the purification process worked effectively. The SEM images of thiol-functionalised N-doped multi-walled carbon nanotube (SH-Fe_3O_4/o-N-MWCNTs) are shown in figure 4.7 (e and f). As shown in figure 4.7 (e and f). Figure 4.8 f reveals that CNT particles have a uniform distribution with average diameters of 25-30 nm. It can also be seen that the tubes have a twisted and entangled state with

a flattened surface [13]. An entangled network was observed for SH-CNTs, and no obvious change in sample morphology was detected after SH loading. Fe_3O_4 clusters attachment was shown in figure 4.7 e for SH-Fe_3O_4/CNTs. The observed large Fe_3O_4 aggregates may be formed *via* precipitation followed by the aggregation process. The carbon nanotube diameter was slightly increased due to the attached Fe_3O_4 on the outer surface [26]. After modification with thioglycolic acid, thiol-functionalisation of Fe_3O_4 composite attached on the surface of the carbon nanotubes are observed from SEM images in figure 4.7 f with an average length of 150-230 nm.

4.2.3.2 SEM images showing the effect of hydrazine and triethylenetetramine substituted SH-Fe_3O_4/o-N-MWCNTs nanocomposites

As shown in figure 4.8 (a and b), it is indicated that MWCNTs are usually curves [27] with an average external diameter of 30 nm. Figure 4.8 a shows that amino-functionalised CNTs are bonded to hydrazine and that the surface texture of the amino-MWCNTs shows a distinct agglomeration of CNTs. The diameter in figure 4.8 b was found to be 19 nm with 140-200 nm length. Also, the surface shows the formation of some agglomerated structures, particles of different shapes and sizes, which are arranged overlapping each other [28]. It appears that amino-functionalisation of MWCNTs helps in reducing the agglomeration and facilitates uniform dispersion of amino-MWCNTs in hydrazine-functionalised SH-Fe_3O_4/o-N-MWCNTs [29].

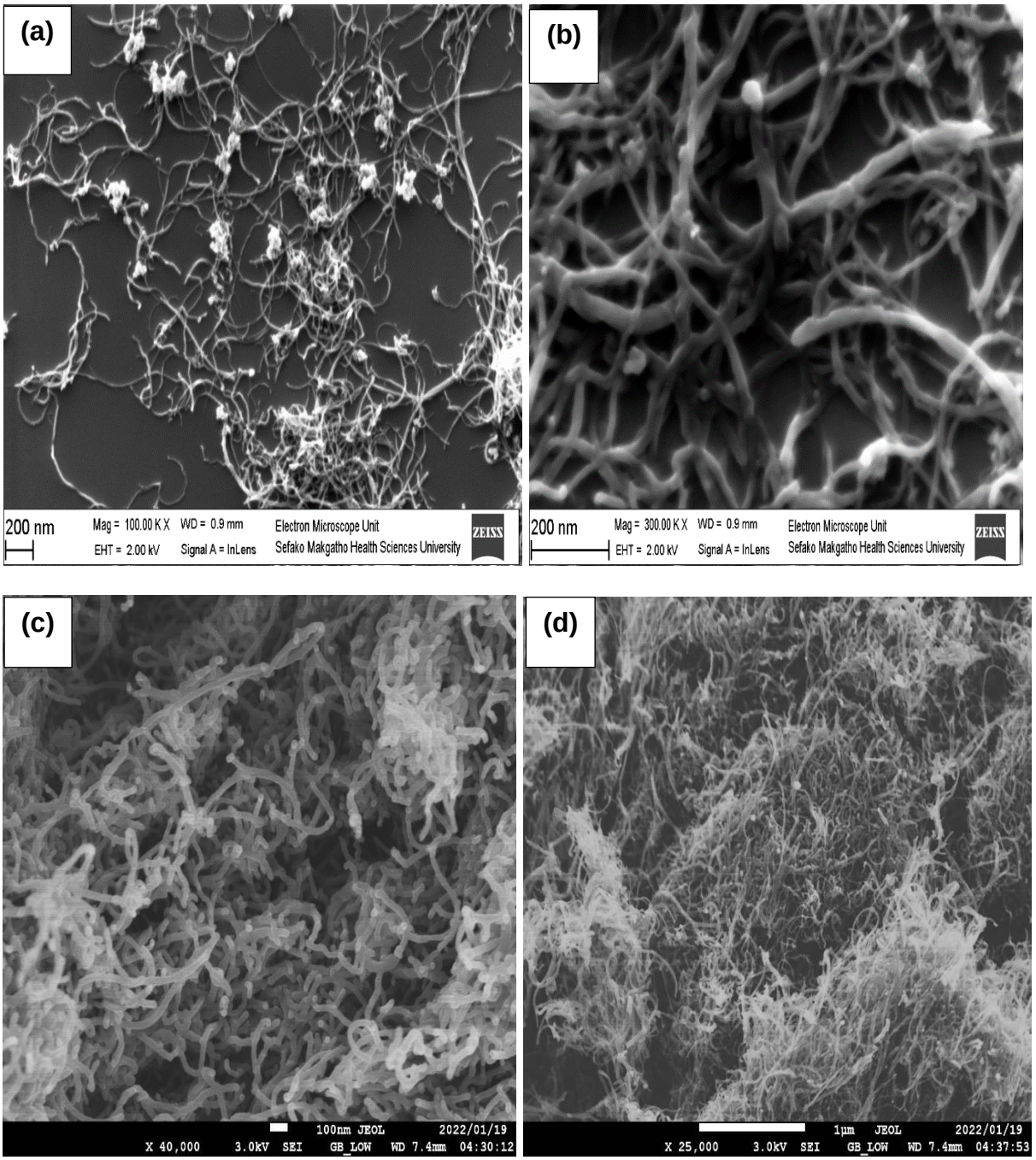

Figure 4.8: Low and high magnification SEM images of hydrazine-functionalised SH-Fe_3O_4/o-N-MWCNTs (a and b) and TETA-functionalised SH-Fe_3O_4/o-N-MWCNTs (c and d).

The SEM images of TETA-functionalised SH-Fe_3O_4/o-N-MWCNTs are shown in figure 4.8 (c and d). The images show that carbon nanotubes in MWCNTs are twined to each other, generating the abundant network structure of MWCNTs. In figure 4.8 (c and d),

the images of the hydrazine-functionalised SH-Fe_3O_4/o-N-MWCNTs proved that the TETA coating fully covered the surface of MWCNTs with varying outer diameters ranging from 16.3 nm to 25.86 nm. TETA improved the dispersity of as-prepared nanomaterials. After amination treatment, the surfaces of amino-functionalised MWCNTs are covered by a layer of nanoparticles becoming rougher than that of MWCNTs [3]. Due to intermolecular forces, MWCNTs aggregates of the entangled network are formed [4].

4.2.3.3 SEM patterns of modified M-MWCNTs (N_2H_4-SH-Fe_3O_4/o-N-MWCNTs) nanocomposite

SEM images are shown in figure 4.9 (a and b). Formation of MWCNTs in coiled-shaped was observed from the high magnification SEM image in figure 4.9 b. Similarity in results was obtained by Kariim et al. [16] for the development of MWCNTs/TiO_2. As seen from the low and high magnification SEM images in figure 4.9 (a and b), the tubes are tangled together with smooth surfaces, and both exhibit a white layer on the surface of the nanotubes with a diameter of 20-30 nm and 170 nm in length. The increased diameter revealed that thioglycolic acid and hydrazine were deposited on the surface [5].

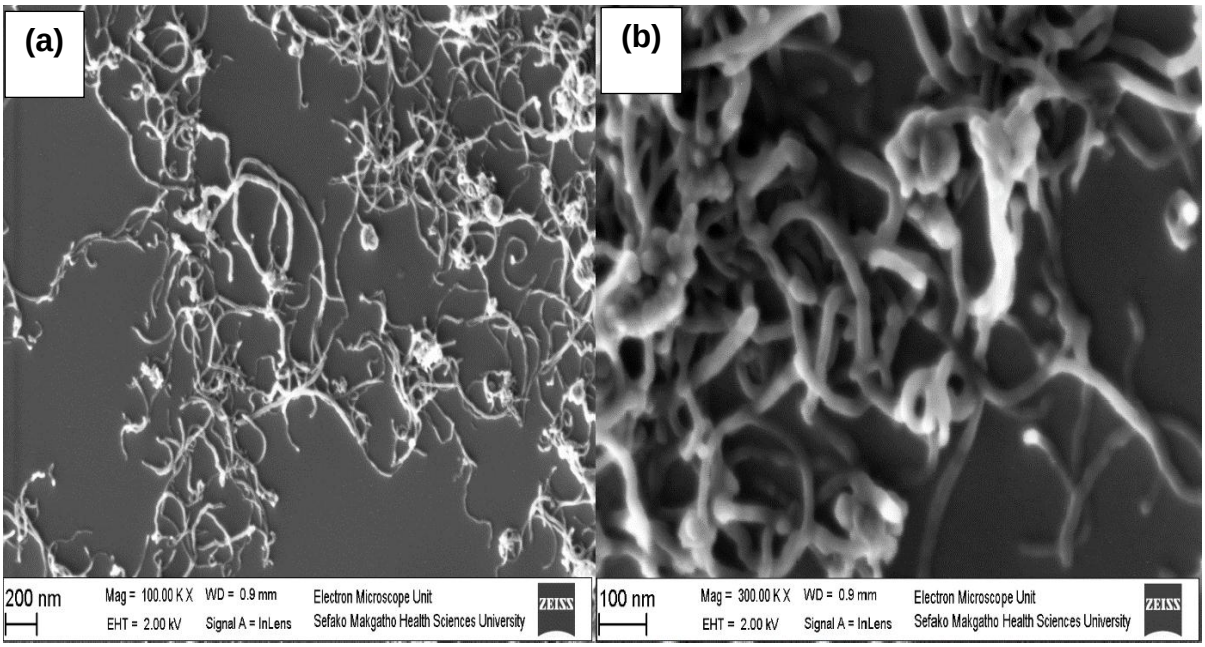

Figure 4.9: (a) Low and (b) high magnification SEM images of hydrazine-modified MWCNTs (N_2H_4-SH-Fe_3O_4/o-MWCNTs).

4.2.4 Transmission electron microscopy analysis

4.2.4.1 TEM images of o-N-MWCNTs, Fe_3O_4/o-N-MWCNTs and SH-Fe_3O_4/o-N-MWCNTs nanocomposites

A representative low and high magnification TEM image of the synthesised CNT is shown in figure 4.10. According to the high-resolution electron microscopic images in figure 4.10 (a and b), the obtained CNTs have a bamboo-like morphology [15,31,32]. It is well known that bamboo-shaped structures of nanotubes result from nitrogen doping since nitrogen plays a key role in generating compartment layers inside the nanotubes [15]. Nitrogen incorporation is demonstrated by the presence of bamboo-like structures in which the inside of the tube is divided into two or more compartments [21]. The inner diameter of N-MWCNT is between 10 and 20 nm, whereas the diameter was also confirmed from PXRD results in section 4.2.2.1. The TEM images confirm the high diversity of tubules structure [15]. Additionally, literature explained that purified MWCNTs were generally well dispersed, but agglomerates approximately 10 nm in diameter could often be observed owing to van der Waals forces. [33].

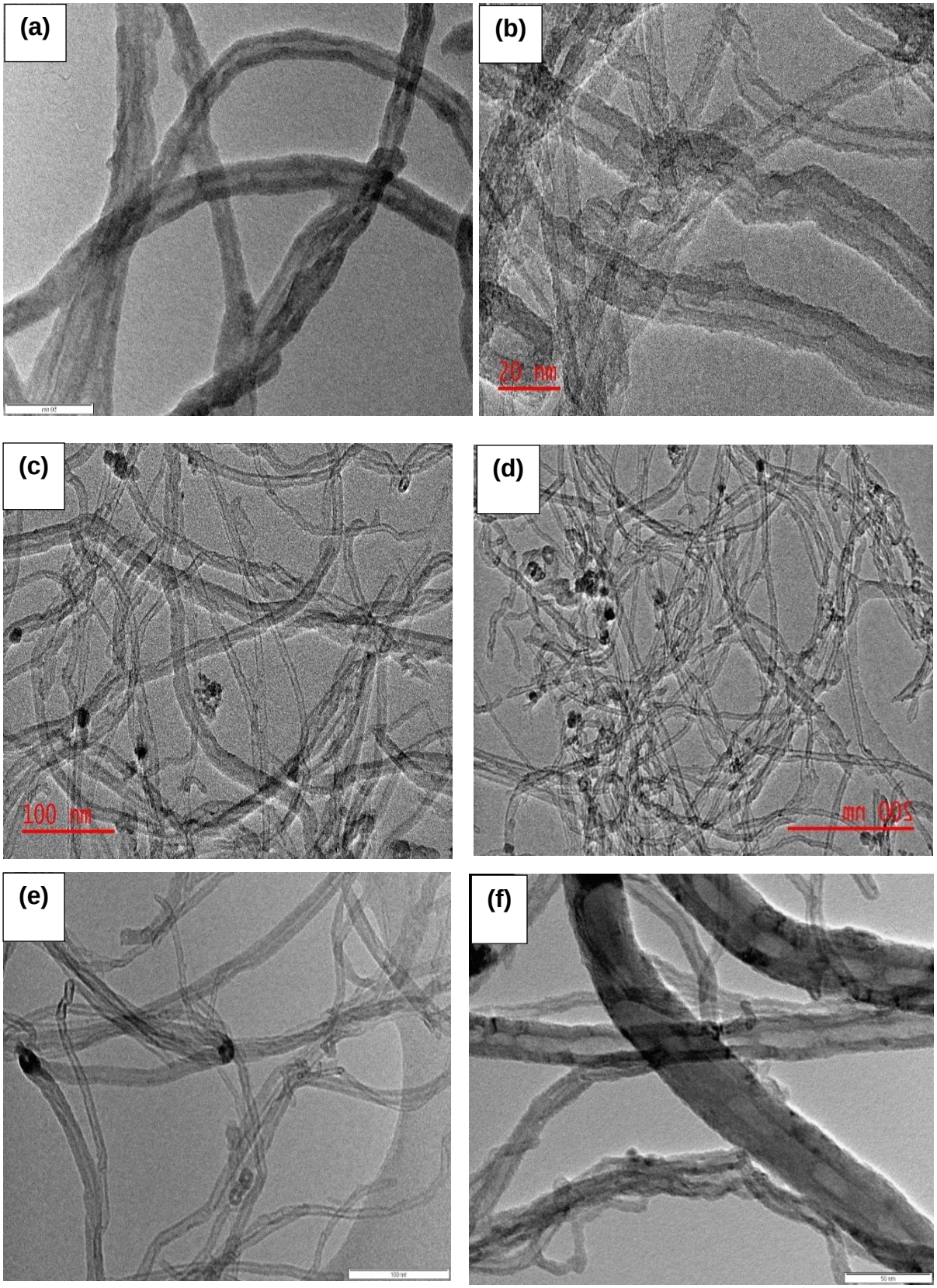

Figure 4.10: Low and high magnification TEM images of M-MWCNTs o-N-MWCNTs (a and b), Fe_3O_4/o-N-MWCNTs (c and d) and SH-Fe_3O_4/o-N-MWCNTs (e and f).

Figure 4.10 (c and d) shows the representative TEM images of the as-synthesised Fe_3O_4/o-N-MWCNTs. The TEM image of Fe_3O_4/o-N-MWCNTs nanocomposites indicate a clear tubular structure of the nanotubes with figure 4.10 d showing high resolution image with the N-MWCNTs displaying a bamboo-like structure in which the tube inside is separated into a series of compartments. The multi-walled nanotubes display a diameter range of 20–40 nm. Similar results were also reported by Lv et al. [31] by electrocatalysis towards oxidation of NO using Nitrogen-doped multiwalled carbon nanotubes. The MWCNTs nanoparticles size further corresponds with the crystallite sizes calculated from PXRD results in section 4.2.2.1. TEM images in figure 4.10 e show that the thiol groups were deposited on the surface of the Fe_3O_4/CNTs. It is indicated that the SH-Fe_3O_4/o-N-MWCNTs nanocomposite retained the spiral and bamboo-like structure of N-MWCNTs and has a larger surface than the raw N-MWCNTs (not shown) which may provide more active sorption sites for the target contaminant. In figure 4.11 f, the images of the SH-Fe_3O_4/o-N-MWCNTs proved that the N-doped MWNTs exhibit typical 'bamboo-like compartments with diameters of a range ~20-40 nm, while N-doped tubes consist of periodically curved graphitic layers. Literature also specified that substitutional nitrogen doping can modify the morphology of MWNTs drastically by introducing some pentagons and heptagons into the graphitic layers [32]. Figure 4.10 (e and f) TEM images indicate clearly that the N-MWCNTs are long and bamboo-shaped with some open tips. The inner diameter of the tubes was measured to be 29.27 nm (figure 4.11 f).

4.2.4.2 TEM images showing the effect of hydrazine and triethylenetetramine (TETA) substituted SH-Fe_3O_4/o-N-MWCNTs nanocomposites

No aggregation was observed as shown from TEM images in figure 4.12 (a and b) after hydrazine-functionalisation. The amino-functionalised SH-Fe_3O_4 nanoparticles attached to the surface of the CNTs were quite uniform. From the high-resolution TEM images (figure 4.11 b), the nanoparticles were observed to exhibit diameters of 20-30 nm attributed to the hydrazine-functionalisation. The findings are similar to those made by Zhan et al. [14] during the synthesis of Fe_3O_4/carboxylic multiwalled carbon nanotubes using amino-functionalisation. The increased diameter revealed that

hydrazine was deposited on the surface of MWCNTs (figure 4.11 b) when compared to TEM images in figure 4.10 (c and d) and 4.10 (e and f). The MWCNTs nanoparticles size further corresponds with the crystallite sizes calculated from PXRD results in section 4.2.2.1. TEM images as shown in figure 4.11 (c and d) revealed the diameter of TETA-functionalised SH-Fe_3O_4/o-N-MWCNTs increased from 25 to 40 nm to 41-70 nm after amination suggesting that the surface of the TETA-functionalised SH-Fe_3O_4/o-N-MWCNTs was densely covered by amino groups.

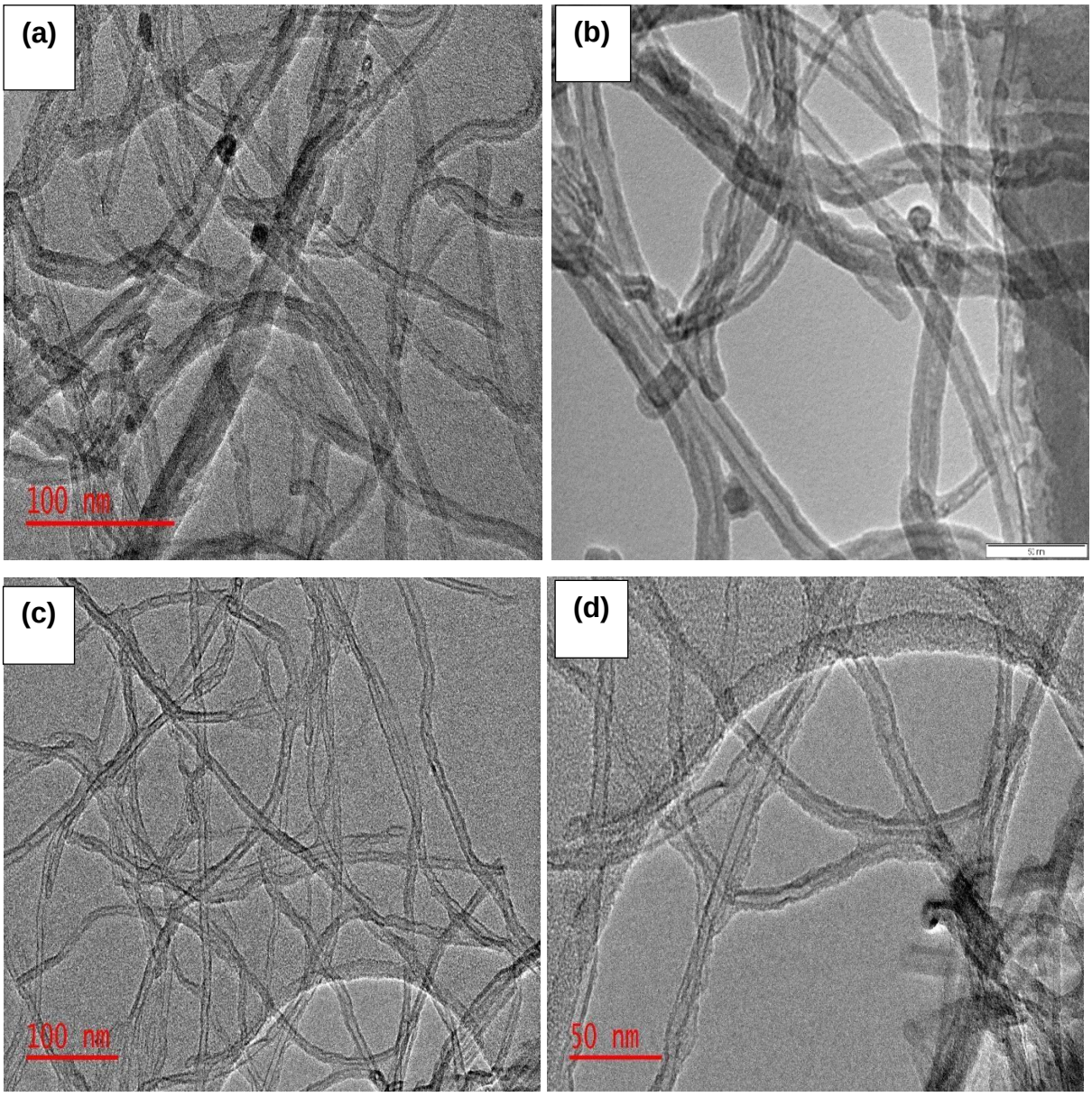

Figure 4.11: Low and high magnification TEM images of hydrazine-functionalised SH-Fe_3O_4/o-N-MWCNTs (a and b) and TETA-functionalised SH-Fe_3O_4/o-N-MWCNTs (c and d).

4.2.4.3 TEM images of N_2H_4-SH-Fe_3O_4/o-N-MWCNTs nanocomposite

Figure 4.12 shows the TEM images of the M-MWCNTs (N_2H_4-SH-Fe_3O_4/o-MWCNTs). The TEM images revealed the diameter of the N_2H_4-SH-Fe_3O_4/o-MWCNTs to 70-160 nm proving that Fe_3O_4, thiol and amino groups are successfully coated on the surface of the o-MWCNTs with an average diameter of 98 nm (figure 4.12 a and b). In accordance with the literature, our results are similar to those reported [5], which showed apparent evidence indicating that thiol-groups and hydrazine were modified on the surface of N_2H_4–SH–Fe_3O_4/o-MWCNTs. The reported facts agree with the TEM observations of N_2H_4-SH-Fe_3O_4/o-MWCNTs under similar treatment conditions and the work reported by Jiang et al [5]. In section 4.2.2.3, the size of the crystallites from the TEM analysis was found to be highly consistent with the diameter from the PXRD analysis.

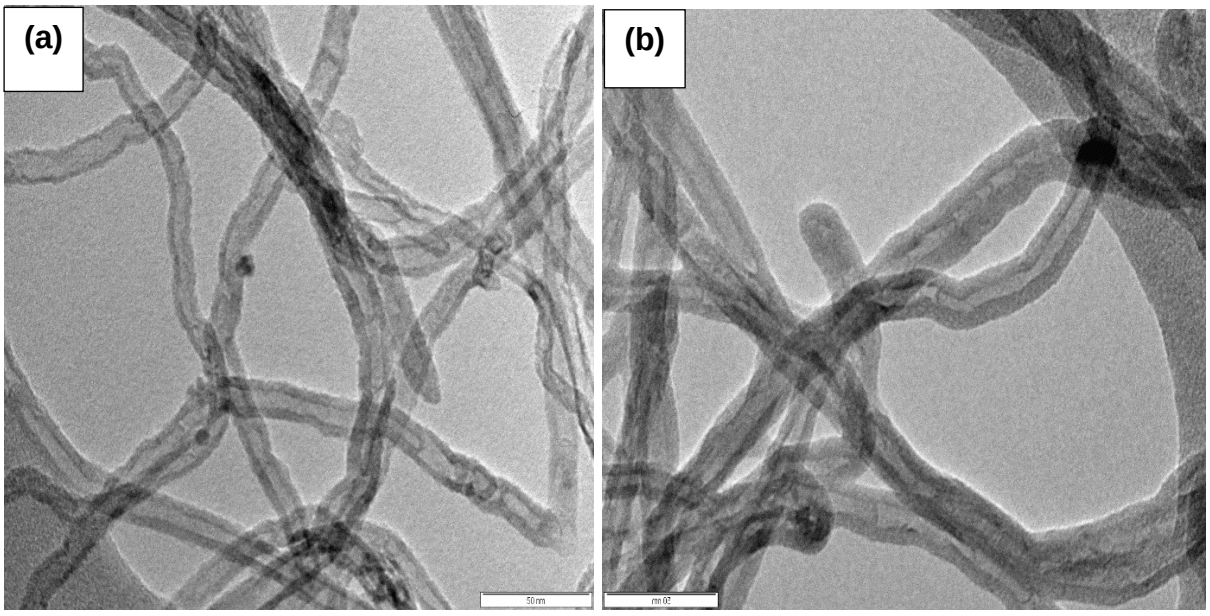

Figure 4.12: (a) Low and (b) high magnification TEM images of hydrazine-modified MWCNTs (N_2H_4-SH-Fe_3O_4/o-MWCNTs).

4.2.6 Brunauer-Emmett-Teller analysis

BET surface area, pore volume and average pore diameter of the as-synthesised nanocomposites are presented in Table 4.2.1. The results showed that the Fe_3O_4/o-N-MWCNTs had an average specific surface area of 233.2 m^2/g, which was larger than that of o-N-MWCNTs (1.134 m^2/g). This was mainly due to the addition of Fe_3O_4 nanoparticles onto the surface of the MWCNTs [34] and thus adsorption capability and adsorption active sites will be increased [8]. This result is in good agreement with the study by Lee et al. [34]. As is observed, the thiol treatment has led to a significant increase in the specific surface area and pore volume of the Fe_3O_4/o-N-MWCNTs. The surface area of SH-Fe_3O_4/o-N-MWCNTs was higher than other samples, which can be correlated to the formation of new pores and the extra surface on MWCNTs [35]. After the SH-Fe_3O_4/o-N-MWCNTs were treated with amine groups (hydrazine and triethylenetetramine), the surface area of amine-functionalised N-MWCNTs decreased to 213.1 and 114.5 m^2/g, respectively. Yang et al. [3] explained that the reason was that massive hydrophilic groups like -NH_2 covered the surface of amino-functionalised MWCNTs after amination, even filling part of the three-dimensional network structure and resulting in the significant decrease of the surface area and total pore volume detected by BET-N_2. This result confirmed the hydrophilic amino groups was successfully grafted on the N_2H_4-SH-Fe_3O_4/o-N-MWCNTs and $C_6H_{18}N_4$-SH-Fe_3O_4/o-N-MWCNTs [3]. The Fe_3O_4 and SH-functionalised N-MWCNTs had larger pore volume and smaller average pore diameter compared to o-N-MWCNTs. The surface area, average pore diameter and pore volume of CNTs decrease after purification. Following purification, CNTs may become short and confined spaces among isolated CNTs become smaller because of their short lengths [36]. The increase in the pore volume of modified N-MWCNTs may be due to the removal of impurities and moisture blocking the pores during the synthesis process [37]. The average pore volumes of the amine-functionalised N-MWCNTs decreased.

Table 4.1: BET results of o-N-MWCNTs, Fe_3O_4/o-N-MWCNTs, SH-Fe_3O_4/o-N-MWCNTs, N_2H_4-SH-Fe_3O_4/o-N-MWCNTs, $C_6H_{18}N_4$-SH-Fe_3O_4/o-N-MWCNTs, and N_2H_4-SH-Fe_3O_4/o-MWCNTs nanocomposites

Sample name	BET surface area (m^2g^{-1})	Pore volume (cm^3g^{-1})	Average pore diameter (nm)
o-N-MWCNTs	1.134	0.003131	11.04
Fe_3O_4/o-N-MWCNTs	233.2	0.4532	7.774
SH-Fe_3O_4/o-N-MWCNTs	242	0.5276	8.722
N_2H_4-SH-Fe_3O_4/o-N-MWCNTs	213.1	0.4606	8.645
$C_6H_{18}N_4$-SH-Fe_3O_4/o-N-MWCNTs	114.5	0.3167	11.06
N_2H_4-SH-Fe_3O_4/o-MWCNTs	172.5	0.2269	5.263

4.2.7 Thermogravimetric analysis

4.2.7.1 TGA results of raw N-MWCNTs and o-N-MWCNTs nanocomposites

Figure 4.13 displays the thermogravimetric curves of the as-prepared nanocomposite materials. Thermogravimetric analysis was carried out from 25 to 1000 °C. The decomposition of nanoadsorbents was evaluated by measuring the TGA profiles of the prepared materials with respect to temperature [25]. The weight loss curves for the as-prepared nanomaterials obtained from TGA are shown in figure 4.13.

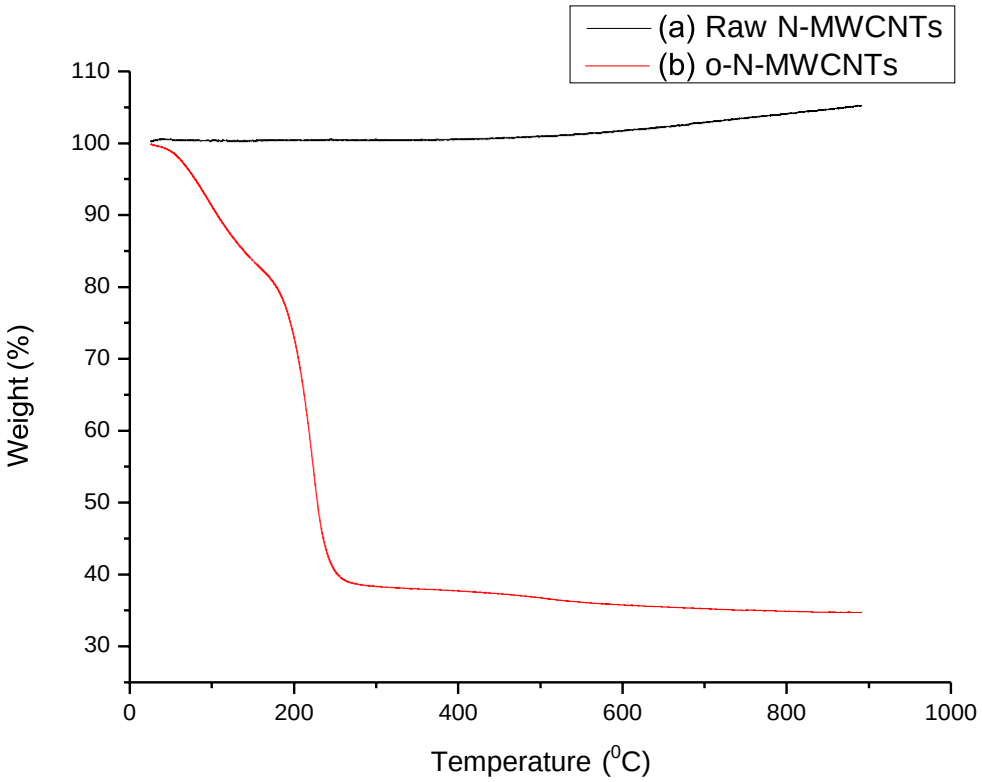

Figure 4. 13: TGA curves of (a) raw N-MWCNTs and (b) o-N-MWCNTs.

Figure 4.13 a shows weight loss stability with the raw N-MWCNTs remaining at 100% then showing a slight change from 600 to 900 °C with an increase of 2-4% as compared to the other materials which decreased with an increase in temperature. Rezaie et al. [38] observed a slight weight gain on magnetorheological studies of polymer nanocomposites and explained it to be as a result of the oxidation of magnetic particles. Figure 4.13 b shows the first stage of weight loss (20 wt%) below 190 °C. The degradation at low temperature can be attributed to the damaging effect that the acid mixture (H_2SO_4:HNO_3) had on the walls of the CNTs decreasing the thermal stability of the MWCNTs [1]. The second stage of weight loss (40 wt%) is from 200 °C to 250 °C and as the temperature increased to 900 °C a weight loss of 2 wt% was observed. Compared with the weight loss of raw N-MWCNTs, the weight loss in figure 4.13b is due to the decomposition of the -COOH and OH groups on the surface of o-N-MWCNTs [5]. The o-N-MWCNTs nanoparticles (figure 4.13b) are thermally unstable and decompose at lower temperature of less than 300 °C.

4.2.7.2 TGA results of Fe_3O_4/o-N-MWCNTs, SH-Fe_3O_4/o-N-MWCNTs, N_2H_4-SH-Fe_3O_4/o-N-MWCNTs and $C_6H_{18}N_4$-SH-Fe_3O_4/o-N-MWCNTs nanocomposites

Figure 4.14 shows TGA curves of the modified N-doped MWCNTs. The initial weight loss of (6 wt%) in figure 4.14a below 500 °C was due to the evaporation of the adsorbed moisture. As the temperature is further increased, weight loss is at approximately (2 wt%) from 500 °C to 880 °C. The last stage of decomposition at 880°C to 1000°C was 10 wt%. The introduction of thiol groups into Fe_3O_4/o-N-MWCNTs nanocomposites is also confirmed by TGA results shown in figure 4.14b, which exhibited a two-step decomposition process. In the first step, degradation of (8 wt%) occurred at temperatures below 770 °C, which can be due to the evaporation of absorbed water and ethanol, the removal of residual $C_2H_4O_2S$ as well as the combustion reaction of CNTs respectively [7]. The second step of degradation (5 wt%) occurred as the temperature increased from 770 °C to 900°C corresponding to the loss of thiol groups. An insignificant weight loss (4 wt%) that occurred below 900°C was observed in figure 4.14c and could be due to the decomposition of residual inorganic and organic moieties, followed by 10 wt% loss in weight as the temperature increased to 900 °C onwards which may attribute to the presence of amino groups [39].

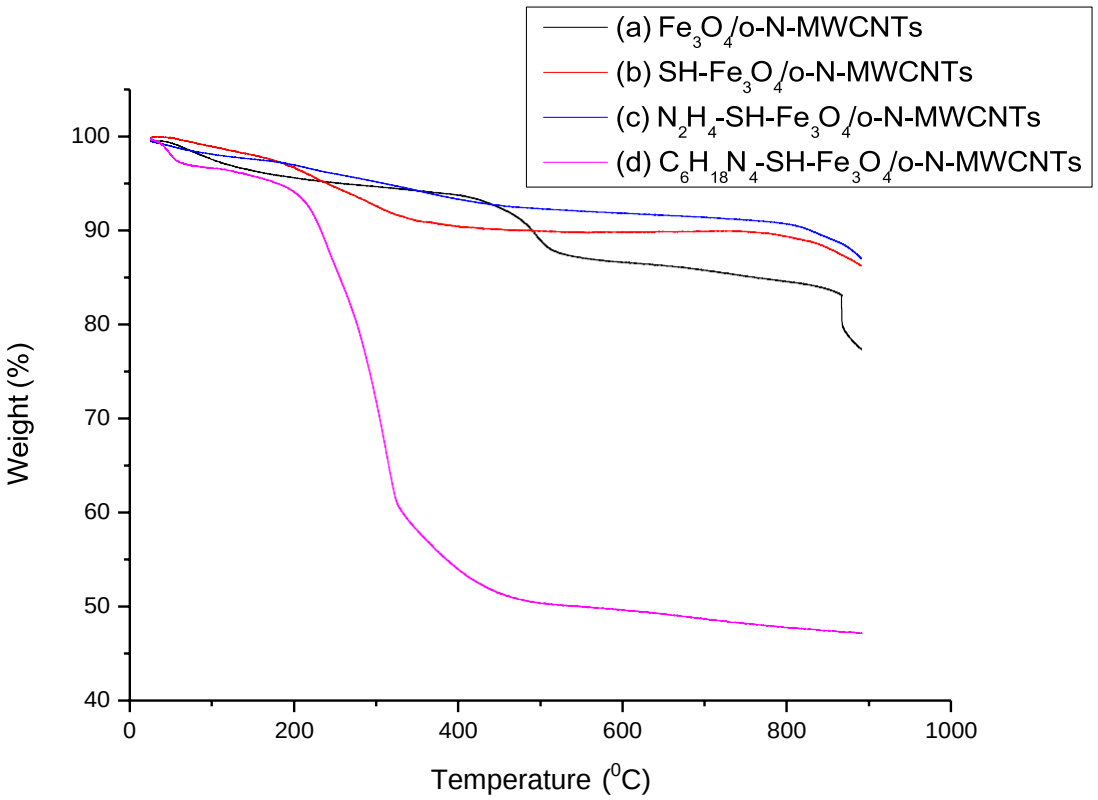

Figure 4.14: TGA curves of (a) Fe_3O_4/o-N-MWCNTs, (b) SH-Fe_3O_4/o-N-MWCNTs, (c) N_2H_4-SH-Fe_3O_4/o-N-MWCNTs and (d) $C_6H_{18}N_4$-SH-Fe_3O_4/o-N-MWCNTs.

Figure 4.14d shows a slight weight loss (4 wt%) below 230 °C followed by an obvious weight loss (40 wt%) from 230 to 400 °C. Based on all the results, it appears that the surface of the MWCNTs is successfully coated with the functional groups and that these results are in agreement with those of the FTIR analysis. As expected, Fe_3O_4/o-N-MWCNTs, SH-Fe_3O_4/o-N-MWCNTs and N_2H_4-SH-Fe_3O_4/o-N-MWCNTs are exceptionally thermally stable and over 85% of the nanocomposite masses remained even at 900 °C. However, the $C_6H_{18}N_4$-SH-Fe_3O_4/o-N-MWCNTs nanoparticles (figure 4.14d) is thermally unstable and decompose at a lower temperatures of less than 400°C with the nanocomposite material retaining 50% of the mass from 300 to 1000 °C.

4.2.7.3 TGA results showing the effects of Nitrogen doping on N_2H_4-SH-Fe_3O_4/o-MWCNTs nanocomposites

Figure 4.15 shows TGA curves of the N-doped MWCNTs (a) and undoped MWCNTs (b) after amination. The weight loss of 3 wt% and 15 wt% from (400 to 900 °C) and (850 to 900 °C) in figure 4.15(a and b) are attributed to the deamination reaction, respectively [5]. Similar results as those in figure 4.16b were obtained by Jiang et al. [5]. According to Silva et al. [40], the decomposition of the functional groups can be related to the decomposition of N-MWCNTs functionalised with TETA and the oxidation of residual oxygenated groups which did not react with TETA Both the N-doped and undoped N_2H_4-SH-Fe_3O_4/o-MWCNTs are thermally stable and over 85% of the nanocomposite masses remained even at 900 °C.

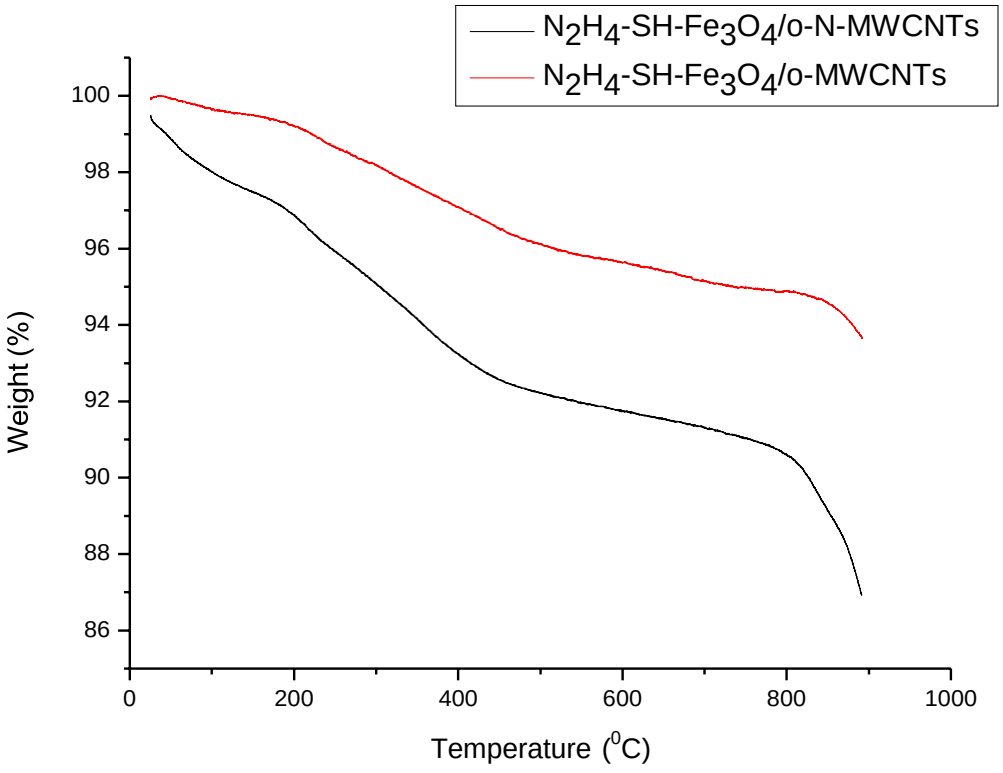

Figure 4.15: TGA curves of (a) N-doped N_2H_4-SH-Fe_3O_4/o-MWCNTs and (b) undoped N_2H_4-SH-Fe_3O_4/o-MWCNTs.

The rate of N-doped MWCNTs thermal stability appears to be much slower than that reported by others; reactants/conditions used in this study are however the same as

those reported by Jiang et al. [5] with minor differences wherein their case they only used undoped MWCNTs, and this study used N-doped MWCNTs. Other reported studies also showed different results as compared, for example, Ramesh et al. [33] used N-doped MWCNTs modified with GO/cellulose and cellulose with 3 stages of decomposition, and in his study, the first stage showed weight loss of ~ 10 wt% between 25 and 125 °C and the third stage (45 wt%) between 320 and 900 °C. This is about 100 times faster than the thermal stability noted in this study.

4.3 ADSORPTION STUDIES

4.3.1 Batch Adsorption studies of trivalent and hexavalent chromium

4.3.1.1 Effect of pH on the removal of Cr(III) and Cr(VI)

Figure 4.16 shows the effects of pH on the removal efficiencies of Cr(III) and Cr(VI). The pH value of a solution has a significant influence on the adsorption of chromium ions because it affects not only the adsorbent surface properties but also the distribution of the metal species [41]. The effect of pH on the removal of Cr(III) by oxidised MWCNTs was conducted in the pH range 2–8. This range was selected on the basis that Cr(III) precipitates at pH > 8 [42]. Figure 4.16 shows that the optimum pH for Cr(III) was reached at pH 5.5 with a percentage removal of 93% which was selected as the optimum condition to be used for further studies. In pH range of 2 to 5, the percentage removal was found to be between 87 and 89% and reached a maximum at pH 5.5 which then showed a decrease between pH of 5.5 and 8. Gupta et al. [41] reported that at pH less than 3.6, Cr(III) is present as Cr^{3+} while at higher than 4 and lower than 6.5, it is present as $Cr(OH)^{2+}$. However, it is present as neutral $Cr(OH)_3$ species at pH 7-12. Similar results were observed as previously reported in the literature [42,44]. The stability of Cr(VI) is dependent on the pH of the system. The pH of a solution has a considerable influence on adsorption capacity because it can convert the existing forms of chromium ions and change the binding capacity of the adsorbent for chromium ions [45].

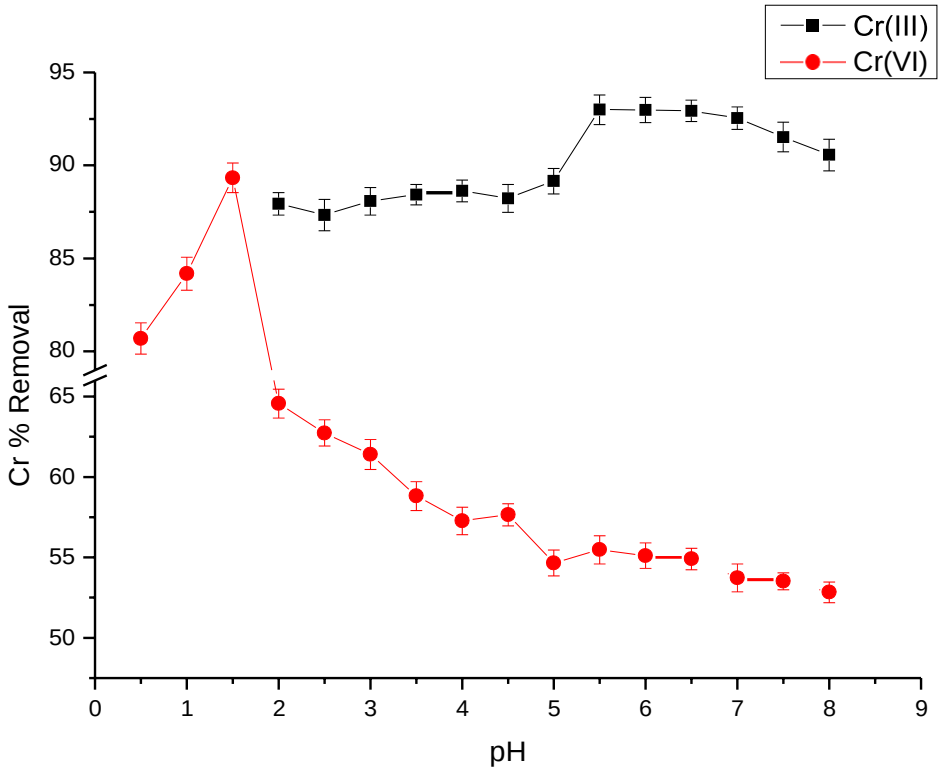

Figure 4. 16: Effect of pH on the removal of Cr species by o-MWCNTs. Experimental conditions: Cr(III) (pH = 5.5, dosage = 0.1 g/L, initial concentration = 50 mg/L and contact time = 80 minutes at room temperature) and Cr(VI) (pH = 0.5 - 8, dosage = 0.1 g/L, concentration = 50 mg/L and contact time = 80 minutes at room temperature).

Figure 4.16 illustrates that as pH increased from 0.5 to 6, Cr(VI) removal decreased. The percentage removal of Cr(VI) reached an optimum at pH 1.5 with 89% removal. Thereafter, a sharp decrease in percentage removal was observed with increasing pH. As the pH continued to rise to 8, the percentage removal decreased to 52.6%. The change in the adsorption with the solution pH can be explained based on the surface charge of the adsorbent and the ionic form of chromium [46]. In short, the literature pertaining to Cr(VI) removal strongly suggests that in aqueous mediums, Cr(VI) is known to exist in the form $HCrO_4^-$ and $Cr_2O_7^{2-}$ at pH < 6 and CrO_4^{2-} at pH > 6 [45]. At low pH of less than 2, Cr(VI) exists as $HCrO_4^-$, which binds effectively to the positively charged surface of MWCNTs. However, at high pH, the $HCrO_4^-$ converts to CrO_4^{2-} and $Cr_2O_7^{2-}$, which weakly binds to the adsorbent surface [41,42,47]. The high adsorption capacity at low initial pH, and a diminishing adsorption capacity at higher initial pH of

MWCNTs can be explained in terms of surface charge; a positive surface charge facilitates the adsorption of dichromate ions [41-47]. The redox mechanisms were considered and as suggested in the literature, Cr(III) forms at lower pH as a result of the reduction of Cr(VI) to Cr(III). Such a reduction is coupled to the oxidation of carbon surfaces resulting in carboxyl surface moieties. Thus, it can be argued that there are carboxyl functionalities on the oxidised carbon nanotube surface which are binding and adsorbing Cr(III) at low pH [41-47]. Therefore, pH 5.5 and 1.5 were considered as the optimum condition and were used for further studies for the removal of Cr(III) and Cr(VI), respectively.

4.3.1.2 Effect of contact time on the removal of Cr(III) and Cr(VI)

Figure 4.17 shows the effect of contact time on the removal efficiencies of Cr(III). The effect of contact time on the removal of Cr(III) by functionalised N-MWCNTs was studied in the range of 1-180 minutes at optimum pH of 5.5. Figure 4.17 shows the removal of over 86% for all nanocomposites. This can be explained by the additional adsorbing sites that are provided by the oxygen atoms of iron oxide nanoparticles [43]. The percentage removal was approximately 86-88% between t = 1 and 10 minutes which then increased with an increase in contact time until optimum was reached at 80 minutes for best adsorbent with removal above 96% and remained at equilibrium until 180 minutes. Adsorption onto the thiol-functionalised N-MWCNTs was slightly higher than adsorption onto the iron oxide and amino-functionalised N-MWCNTs. Notably, the higher removal efficiency onto the thiol-functionalised N-MWCNTs agrees with the higher BET surface area of the adsorbent in section 4.2.4 as compared to the iron oxide and amino-functionalised N-MWCNTs. Initially, the removal rate was fast and became slow until equilibrium was reached [48]. Equilibrium was reached at 80 min with adsorption of 93 and 96% onto the H_2O_2-HNO_3 and H_2SO_4-HNO_3 treated SH-Fe_3O_4/o-N-MWCNTs, respectively. Cr(III) removal by Gupta et al. [43] showed 90% adsorption by MWCNTs/nano-iron oxide after 60 min and dosage = 0.1 g/L at pH = 6 with removal starting at less than 20% which was poor compared to the current study where the removal from 1 min was above 86% and continued to increase with contact time. These data are consistent with similar studies in the literature [41-43]. Contact

time of 80 min was selected as the optimum based on the best performing nanocomposite (N_2H_4-SH-Fe_3O_4/o-N-MWCNTs treated with H_2SO_4-HNO_3). The H_2SO_4-HNO_3 treated N-MWCNTs were selected to continue with the rest of the studies due to their high removal efficiency as compared to the H_2O_2-HNO_3 treated N-MWCNTs.

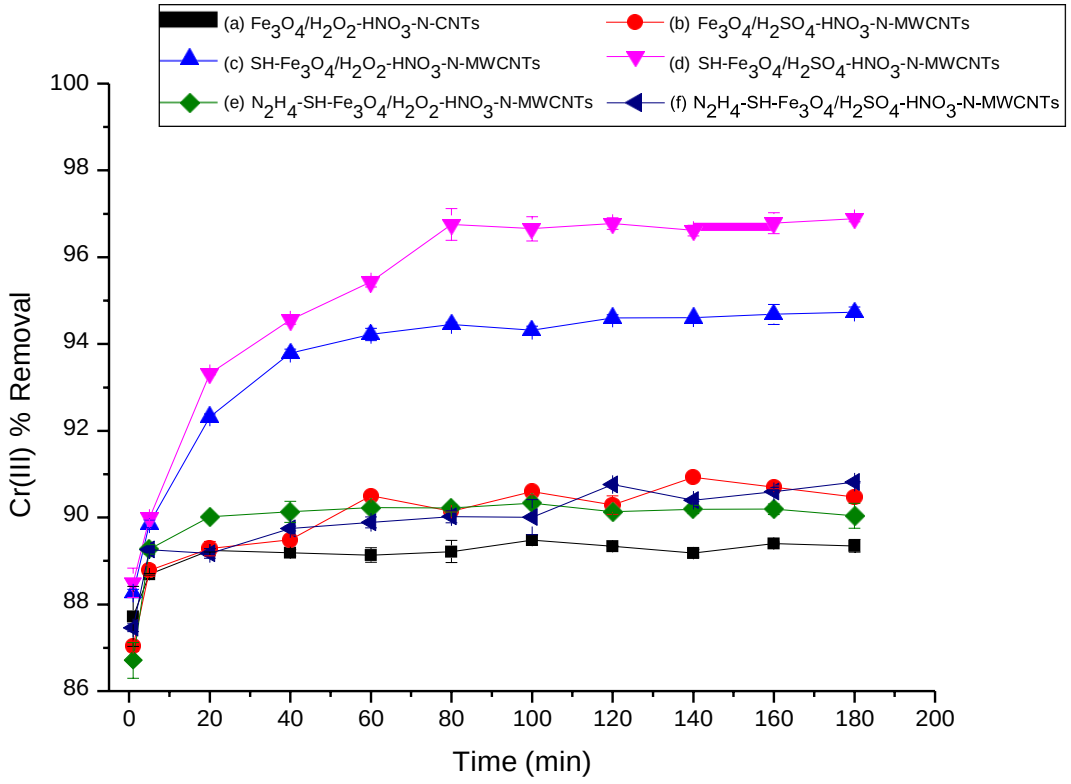

Figure 4.17: Effect of contact time on the removal of Cr(III) by (a) Fe_3O_4/o-N-MWCNTs, (b) SH-Fe_3O_4/o-N-MWCNTs and (f) N_2H_4-SH-Fe_3O_4/o-N-MWCNTs treated with H_2O_2-HNO_3 and H_2SO_4-HNO_3 respectively. Experimental conditions: pH = 5.5, dosage = 0.30 g/L, initial concentration = 50 mg/L and contact time = 1-180 minutes at room temperature.

Figure 4.18 shows the effect of contact time on the removal efficiencies of Cr(VI). Equilibrium time is an important parameter for economical water and wastewater treatment. As the contact time increases, the rate of adsorption decreases depending on the chemical characteristics of the surface and the properties of each adsorbent

[49]. The as-synthesised nanocomposites show a good ability to remove Cr(VI) from aqueous solution as depicted in figure 4.13. However, the amine treated N-MWCNTs show a greater ability with over 90% removal within the first ten minutes of adsorption as compared to the iron oxide and thiol treated N-MWCNTs, which also had over 84 and 86% removal within the first ten minutes. Initially, adsorption occurred fast because Cr(VI) ions adsorbed quickly onto the vacant adsorbent (NH-, SH- and Fe_3O_4) and exposed surface sites of N-MWCNTs. For all the adsorbents, the percentage removal increased from one minute of which an optimum was observed at approximately 10 minutes, after this time the percentage removals for all the six adsorbents reached equilibrium with a slight decrease and increase (< 0.02%) as time increased.

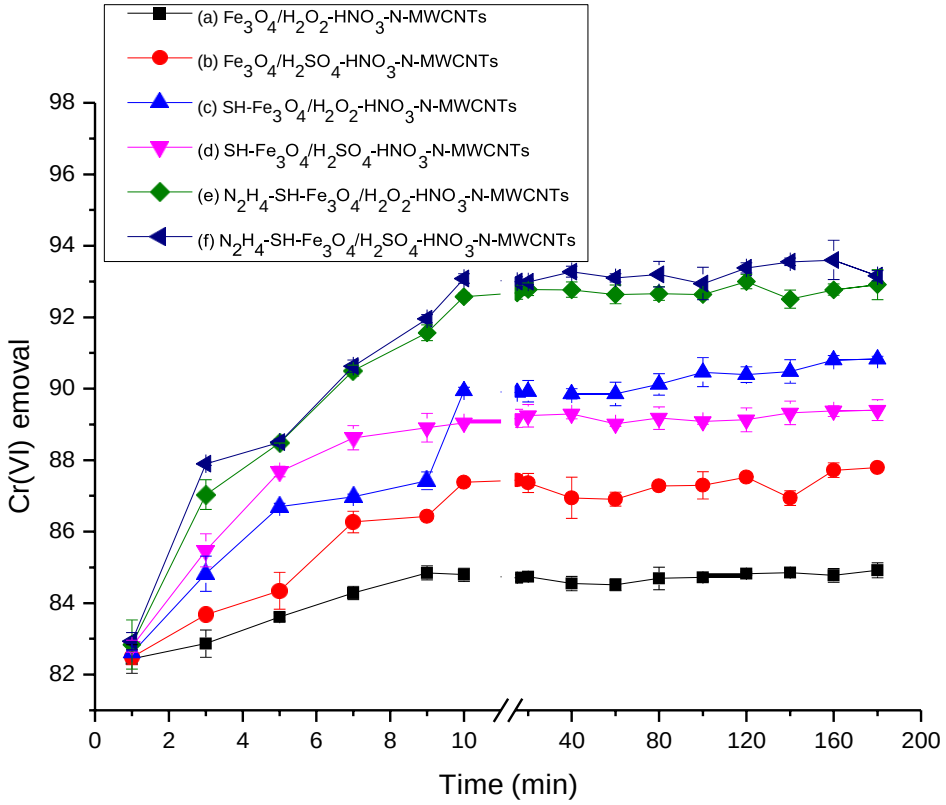

Figure 4.18: Effect of contact time on the removal of Cr(VI) by (a) Fe_3O_4/o-N-MWCNTs, (b) SH-Fe_3O_4/o-N-MWCNTs and (c) N_2H_4-SH-Fe_3O_4/o-N-MWCNTs treated with H_2O_2-HNO_3 and H_2SO_4-HNO_3. Experimental conditions: pH = 1.5, dosage = 0.35 g/L, initial concentration = 50 mg/L and contact time = 1-180 minutes at room temperature.

The modified N-MWCNTs used in this study had the highest removal (> 90%) of Cr(VI) ions onto hydrazine-functionalised N-MWCNTs compared to other studies. Jung et al. [10] achieved 40% removal with an initial Cr(VI) concentration of 0.5 mg/L using raw MWCNTs. In comparison to the acid treatment of the N-MWCNTs, the H_2SO_4-HNO_3 mixture was selected to continue with the rest of the study as the nanocomposite materials showed better removal efficiency for the iron oxide, thiol and amino-functionalised N-MWCNTs than the H_2O_2-HNO_3 mixture.

4.3.1.3 Effect of adsorbent dosage on the removal of Cr(III) and Cr(VI)

The effect of adsorbent dosage on the removal efficiency of Cr(III) is shown in figure 4.19. The amount of adsorbent in solution is an important parameter since it determines how effectively the adsorbent will remove Cr(III) at a certain initial concentration [44]. The effect of various dosages of a known mass of 0.05, 0.1, 0.15, 0.2, 0.25, 0.3 and 0.35 g/L on the removal of Cr(III) was investigated at optimum pH of 5.5 and 80 min in time with an initial concentration of 50 mg/L. These results indicate that the number of adsorption sites for Cr(III) was directly proportional to the dose applied where 79% removal was observed at 0.05 g/L, which increased to 84% at 0.30 g/L. However, no further increase in percentage removal was observed after 0.30 g/L dose which suggests that most Cr (III) molecules occupied surface sites [49] resulting in a slight decrease to 83.5% at 0.35 g/L. The 0.3 g/L dose was selected as the maximum dose and used for the remainder of the study. In comparison to literature with similar experimental conditions, the dosage is better than that of Gupta et al. [43] adsorbent (0.2 g/L) were in only 60% and 90% of Cr(III) ions adsorption was observed using o-MWCNTs and MWCNTs/nano-iron, respectively.

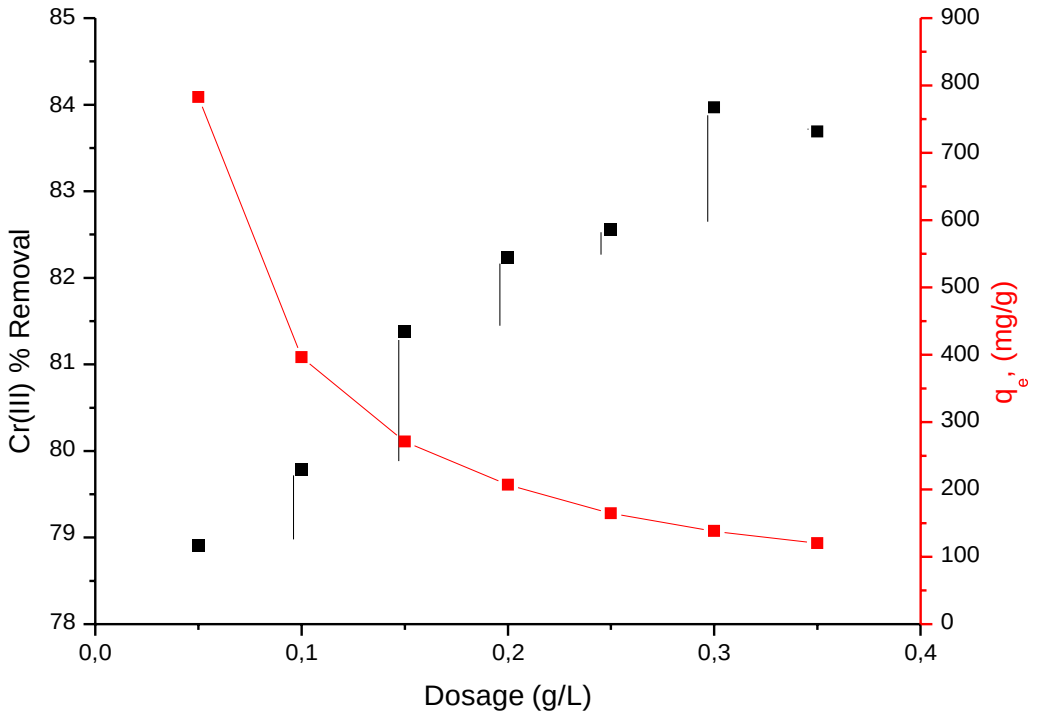

Figure 4. 19: Effect of adsorbent dosage on the removal of Cr(III) by o-MWCNTs. Experimental conditions: pH = 5.5, contact time = 60 min at room temperature and adsorbent dose varied from 0.05-0.35 g/L.

Adsorbent dosage and its effect on the removal efficiency of Cr(VI) is shown in figure 4.20. The effect of various dosages of known mass of 0.025-0.35 g/L on the removal of Cr(VI) was investigated at optimum pH and time with a concentration of 50 mg/L. The results in figure 4.20 show that the adsorption capacity of o-MWCNTs on chromium ions decreased from 1600 to 100 mg/g with an increase in dosage. As explained by Qiao et al. [45], the reason was that the chromium concentration was fixed and the number of unsaturated active sites on the nanocomposite increased more than the number of saturated active sites. On the other hand, the percentage removal increased sharply from 80.5 to 87% as the dose varied from 0.025 to 0.35 g/L. The highest removal was achieved at a dosage of 0.35 g/L which was selected as the optimum to continue with the rest of the study. Chen et al. [9], stated that both the reduction of the number of active sites after continuous adsorption of the metal ions and the neutralization of negative charges on the surface of the adsorbent cause

the descending of the adsorption capacity of the adsorbent. The obtained results were better compared to the study done by Dokmaj et al. [42].

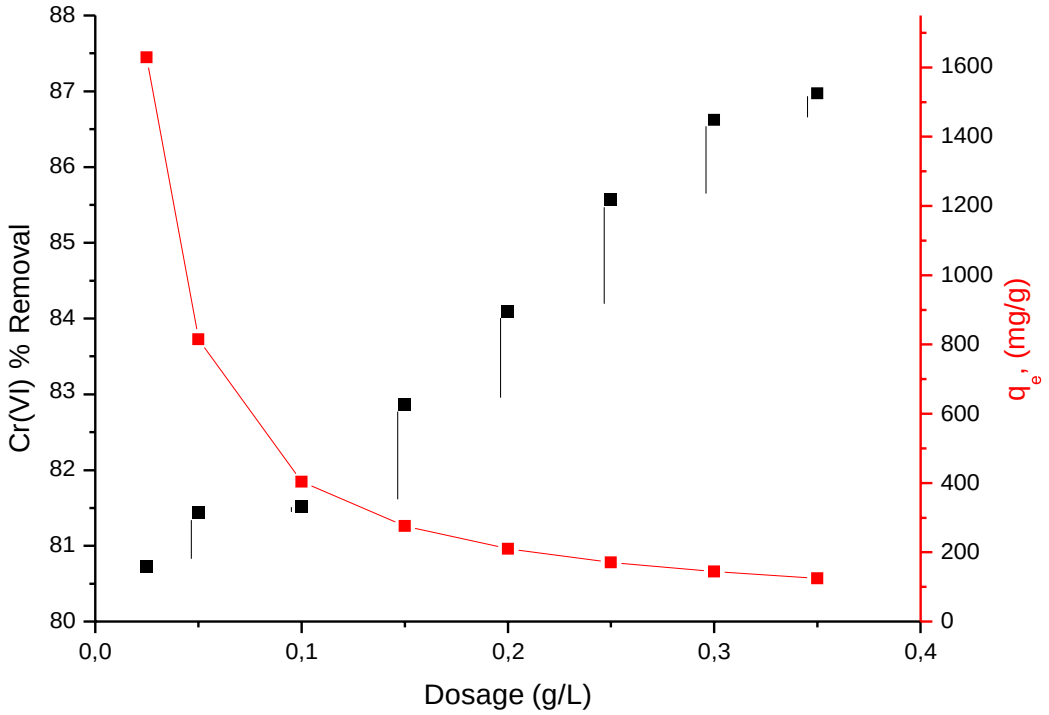

Figure 4. 20: Effect of adsorbent dosage on the removal of Cr(VI) by o-MWCNTs. Experimental conditions: pH = 1.5, contact time = 10 min at room temperature and adsorbent dose varied from 0.025-0.35 g/L.

4.3.1.4 Effect of initial concentration on the removal of Cr(III) and Cr(VI)

The effect of initial concentration (50–250 mg/L) (figure 4.22) on the removal efficiency and adsorption capacity of Cr(III) was investigated at optimum pH, contact time and adsorbent dosage. Figure 4.21a shows that as the concentration of the solution was increased, the percentage removal was decreased, and the adsorption capacity had a proportional relationship with increasing concentration. The percentage removal decreased from 83.3, 98.3 and 100% to 82.1, 83.5 and 91.2% from 20 to 250 mg/L

using o-MWCNTs, raw N-MWCNTs and o-N-MWCNTs, respectively. However, the adsorption capacity (figure 4.21b) increased from 500 to over 650 mg/g from 20-250 mg/L for all the adsorbents. Cr(III) concentration (20–250 mg/L), demonstrate that the percentage removal decreased as the initial concentration increased while the adsorption capacity (q_e) increased with increasing concentration. This has been confirmed by a great number of authors in the literature [8,42-44,50]. Since the quantity of the adsorbents used was fixed at 0.35 g/L, the number of active adsorption sites remained constant. These sites eventually become saturated with chromium ions and therefore are unable to accommodate any more ions at higher concentrations as observed from the study done by Pillay et al. [50]. The order of the adsorbent with the highest removal is as follows: o-N-MWCNTs > N-MWCNTs > o-MWCNTs which may be attributed to the high amount of sidewall pores observed in the MWCNTs limiting chromium diffusion and accounting for the slow diffusion rate [51]. N-MWCNTs were selected as the adsorbent to continue with going forth.

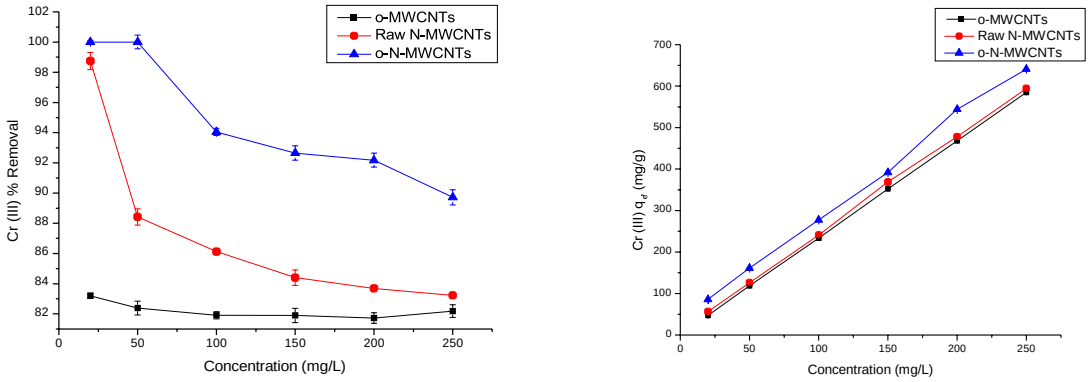

Figure 4.21: Effect of initial concentration on Cr(III) (a) removal and (b) adsorption capacity by o-MWCNTs, raw N-MWCNTs and o-N-MWCNTs. Experimental conditions: pH = 5.5, contact time = 80 min at room temperature, adsorbent dose = 0.30 g/L at varied concentrations 20-250 mg/L.

Figure 4.22 shows the effect of initial Cr(VI) concentration on the removal and adsorption capacities of the adsorbents. The percentage removal (figure 4.22a) decreased from 88.7, 89.3 and 100% to 86, 82.9 and 90.2% from 20 to 250 mg/L using

o-MWCNTs, raw N-MWCNTs and o-N-MWCNTs, respectively. Notably, the adsorption capacity (figure 4.22b) increased from 500 to over 650 mg/g from 20-250 mg/L for all the adsorbents. It was reported in literature that the increase in initial concentration of chromium results in the increased uptake capacity and decreased percentage removal since at high initial concentrations, the number of moles of chromium available to the surface area is high, number of collisions between chromium ions and adsorbent get increased and a driving force to overcome all mass transfer resistances between the aqueous and solid phases is developed [49]. The study done by Gupta et al. [52] on the removal of hexavalent chromium ions using CuO nanoparticles for water purification applications strongly suggests that at a lower concentration of Cr(VI) ions, the higher removal efficiency is obtained due to the presence of large surface area as well as binding sites of CuO nanoparticles, while the removal efficiency lowered for high initial metal ions concentration due to lesser available sites for Cr(VI) ions [52].

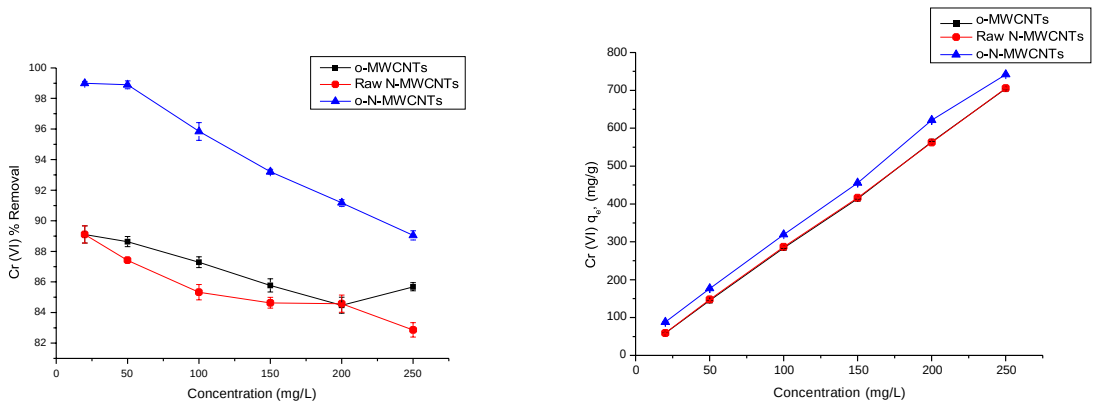

Figure 4.22: Effect of initial concentration on Cr(VI) (a) removal and (b) adsorption capacity by o-MWCNTs, raw N-MWCNTs and o-N-MWCNTs. Experimental conditions: pH = 1.5, contact time = 10 min at room temperature, adsorbent dose = 0.35 g/L at varied concentrations 20-250 mg/L.

The order of the adsorbent with the highest removal is as follows: o-N-MWCNTs > N-MWCNTs > o-MWCNTs as was also observed from Cr(III) removal. The high removal

of chromium by N-MWCNTs was explained by Perez-Aguilar [51] to be due to the short length, small and bamboo-type morphology observed with nitrogen-doped multiwall carbon nanotubes accounting for the relatively fast adsorption rate as this morphology prevents chromium diffusion through the internal tubular space of these nanotubes. These results are also supported by the SEM and TEM analysis in sections 4.2.3 and 4.2.4, respectively. After MWCNTs and N-MWCNTs comparison, N-MWCNTs were selected as the adsorbent to continue with going forth.

4.3.1.5 Effect of temperature on the removal of Cr(III) and Cr(VI)

Figure 4.23 shows the effect of temperature on the removal of chromium species using the as-prepared adsorbents at optimum pH, contact time and adsorbent dosage with an initial metal concentration of 50 mg/L. The temperature was varied from 20, 25, 30, 35 and 40 °C. As illustrated from both figure 4.23 (a and b), it can be observed that as the temperature of the solution was increased, percentage removal also increased. Kumar et al. [53] further explained that the fact that MWCNTs have multiple atomic layers, which require more energy for the diffusion of chromium and as the temperature of the solution is increased, the viscosity of the solution decreased while the velocity of chromium increased and broadened of the adsorbent pore may have taken place. From all the acid-treated N-MWCNTs, best removal was observed in the order amino (84.9 - 93.8%) > thiol (85 to 90%) > iron oxide (87 to 89%).

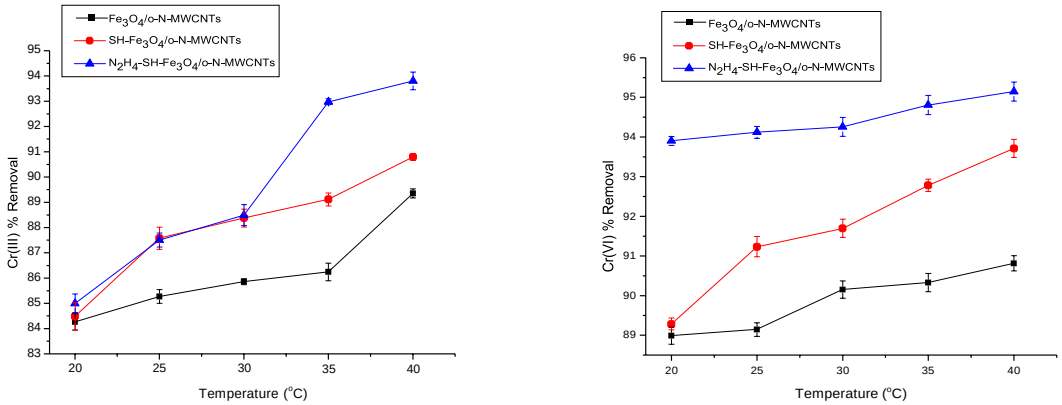

Figure 4.23: Effect of temperature on the removal of (a) Cr(III) and (b) Cr(VI) by Fe_3O_4/o-N-MWCNTs, SH-Fe_3O_4/o-N-MWCNTs and N_2H_4-SH-Fe_3O_4/o-N-MWCNTs. Experimental conditions: optimum pH, contact time, adsorbent dosage and initial concentration of 50 mg/L. The temperature varied from 20 – 40 °C.

From figure 4.23b, no significant difference was observed at all temperatures with a range between 93.9 and 95.1% for amino-functionalised N-MWCNTs. The same trend was observed for Cr(VI) as in Cr(III) results wherein the amino-functionalised N-MWCNTs showed good removal as compared to the removal by thiol and Fe_3O_4 with removal percentage ranging from (89 to 93.7%) and (87.4 to 92.9%) from 20 to 40 °C, respectively. The adsorption efficiencies of Cr(III) and Cr(VI) onto the prepared adsorbent were seen to have increased significantly with increasing temperature and a combination of different functional groups. A recent study by Obayomi et al. [54] concluded that at a higher temperature, there was an intraparticle diffusion increase resulting in more adsorption sites, leading to a higher adsorption capacity of Cr(III) and Cr(VI) ions, respectively. It is evident that the adsorption process is endothermic based on the increased adsorption capacity of both metal ions with increasing temperature. For convenience, 25 and 40 °C were selected as optimum temperatures to continue with the study for both ions.

4.3.1.6 Adsorption kinetics of Cr(III) and Cr(VI) ions removal

The linearised forms of the pseudo-first and pseudo-second order kinetic models of Cr(III) and Cr(VI) are given in figure 4.24, respectively. The kinetic parameters calculated by the above models for chromium ions are shown in Table 4.2. The coefficient of determination (R^2) is a parameter that can be used to judge the accuracy of kinetic models in data simulation [45]. As shown, the R^2 values predicted by the pseudo-second order equation for both Cr(III) and Cr(VI) were much higher (0.9986-0.9999) and (0.9999) than those predicted by the pseudo-first order equation in the ranges (0.5247-0.9257) and (0.09961–0.3471), respectively. The calculated q_e values were compared with the experimental q_e. The calculated q_e values and the low coefficients of determination obtained indicate that adsorption of Cr(III) and Cr(VI) onto the M-N-MWCNTs can't be classified as first-order [55]. The q_e values calculated from the pseudo-second order model are much closer to the experimental data indicating that the adsorption process follows the pseudo-second order model, which demonstrates that the rate-limiting step is chemisorption involving valence forces through the sharing and exchange of electrons between metal ions and adsorbents [55]. Similar findings were listed in the literature [45,55]. The Fe_3O_4-functionalised N-MWCNTs maintained a faster removal rate for Cr(VI) than Cr(III) because the values of k_1 and k_2 were higher for Cr(VI). However, a faster removal rate for Cr(III) than Cr(VI) was maintained using the thiol and amino-functionalised N-MWCNTs [45]. Several studies in the literature involving the adsorption of Cr(III) and Cr(VI) onto modified MWCNTs have shown that the pseudo-second order kinetics model gave the best fit for the experimental data [47,50,53].

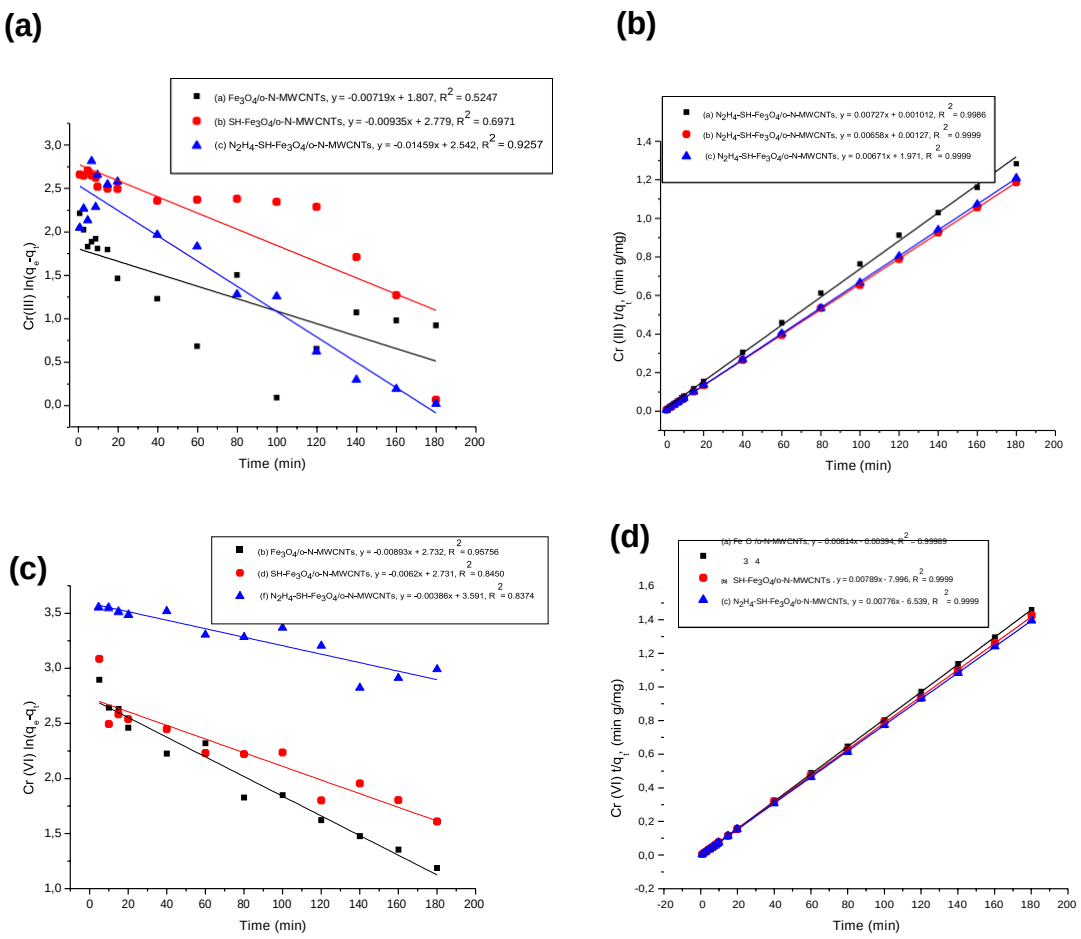

Figure 4.24: (i) Pseudo-first order and (ii) Pseudo-second order kinetic model for adsorption of Cr^{3+}(a and b) and Cr^{6+}(c and d) ions by Fe_3O_4-o-N-MWCNTs, SH-Fe_3O_4-o-N-MWCNTs and N_2H_4-SH-Fe_3O_4/o-N-MWCNTs nanocomposites.

Table 4.2: The parameters calculated by kinetic models for the adsorption of Cr(III) and Cr(VI) ions adsorption by f-N-MWCNTs nanocomposites

Adsorbent	Adsorbate	Experimental q_e (mg/g)	Pseudo-first order kinetic model			Pseudo-second order kinetic model		
			$q_{e.cal}$ (mg/g)	k_1 (min^{-1})	R^2	$q_{e.cal}$ (mg/g)	k_2 (g/mg/min)	R^2
Fe_3O_4 /o-N-	Cr(III)	154.2	0.9928	0.00719	0.5247	137.6	0.005223	0.9986

MWCNTs	Cr(VI)	157	1.012	0.01187	0.09961	122.9	-0.0168	0.9999
SH-Fe_3O_4/o-N-MWCNTs	Cr(III)	141.4	0.9907	0.00935	0.6971	152	0.03409	0.9999
	Cr(VI)	132.8	1.006	0.00634	0.3471	126.7	-0.0783	0.9999
N_2H_4-SH-Fe_3O_4/oN-MWCNTs	Cr(III)	152	0.9855	0.0146	0.9257	149.0	0.2284	0.9999
	Cr(VI)	137.8	1,001	0.00103	0.2487	128.866	-0.0899	0.9999

4.3.1.7 Adsorption isotherms of Cr(III) and Cr(VI) ions removal

The linear forms of the Langmuir and Freundlich isotherms of Cr(III) and Cr(VI) are shown in figure 4.25. The parameters obtained from the above isotherm equations for adsorption of chromium are listed in Table 4.3. As shown in Table 4.3, the coefficients of determination of the two isotherms are high and closer to each other (0.9591-0.9988). Both the Langmuir and Freundlich equations have a good linear relationship and fit the experimental data well assuming a monolayer coverage and heterogeneous adsorption of the adsorbate. A comparison of q_{max} values for Cr(III) and Cr(VI) adsorption by M-N-MWCNTs with those reported previously using different adsorbents reveal that the removal capacity of M-N-MWCNTs was higher than many other adsorbents such as carbon nanotubes and chitosan-modified adsorbents [10,42,47,56] among others. A separation factor $R_L > 1$ implies unfavourable adsorption, while values ranging from 0 to 1 indicate effective interaction between the adsorbent and adsorbate at the optimised experimental conditions [60,66]. In this study, all the R_L values were within the range 0.341-0.980 and 0.420-0.602 (Table 4.3), respectively. Furthermore, the values of n are greater than one indicating favourable Cr(III) and Cr(VI) adsorption on all modified adsorbents and obeyed the

Freundlich isotherm model. Similar results were reported by many researchers [8,42,47,56]

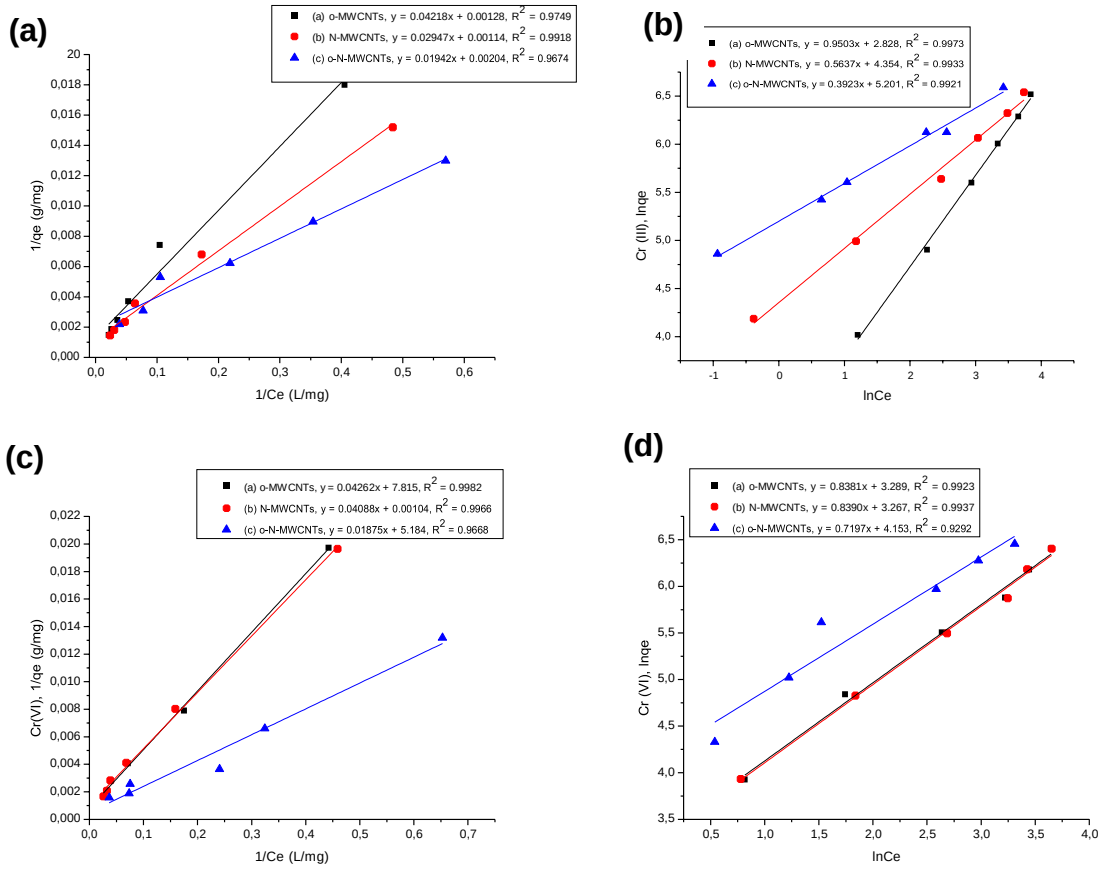

Figure 4.25: (i) Langmuir isotherm and (ii) Freundlich isotherm for adsorption of Cr^{3+}(a and b) and Cr^{6+}(c and d) ions by Fe_3O_4/o-N-MWCNTs, SH-Fe_3O_4/o-N- and N_2H_4-SH-Fe_3O_4/o-N-MWCNTs nanocomposites.

Table 4.3: The parameters calculated by isotherm models for adsorption of Cr(III) and Cr(VI) ions adsorption by f-N-MWCNTs nanocomposites

Adsorbent	Adsorbate	q_{max} (mg/g	Langmuir model			Freundlich model		
			b (L/mg)	R_L	R^2	K_f (mg/g)	N	R^2
o-MWCNTs	Cr(III)	1990	0.00854	0.701	0.9952	16.91	1.052	0.9973
	Cr(VI)	1280	0.0183	0.522	0.9982	26.81	1.193	0.9923
	Cr(III)	877	0.0387	0.341	0.9918	77.81	1.774	0.9933

Raw N-MWCNTs	Cr(VI)	962	0.0254	0.440	0.9966	26.24	1.192	0.9937
o-N-MWCNTs	Cr(III)	1720	0.0344	0.367	0.9591	181.5	2.549	0.9921
	Cr(VI)	1930	0.0276	0.420	0.9668	63.62	1.390	0.9292

The adsorption performance of Cr(III) and Cr(VI) by different adsorbents are shown in Table 4.4. Table 4.4 shows a comparison between the as-prepared adsorbents with various similar adsorbents reported in the literature at optimised conditions. The removal capacity for Cr(III) and Cr(VI) has proven to be greater than those of other reported similar materials. The nanocomposites in our study meet standard requirements and could remove most of the chromium ions from water at a lower dose of 0.30 and 0.35 g/L even at low pH of 1.5 for Cr(VI) with less time required. In this study, results obtained from the Langmuir equation showed a superior adsorption capacity when compared to those obtained from previous studies using different adsorbents. The findings are presented in Table 4.4. The adsorbents used in this study have shown better adsorption capacity when compared to the other adsorbents including chitosan, nitrogen-doped carbon sheet, activated carbon and other carbon-based materials. M-N-MWCNTs seem to have a higher adsorption capacity than most adsorbents, however, this could be explained by the dosage used (0.30 and 0.35 g/L) compared to the dosage used in the literature (0.36 to 5 g/L).

Table 4.4: Comparison of chromium ions adsorption capacity by various adsorbents

Adsorbent	Adsorbate	Optimised parameters			Adsorption capacity q_{max} (mg/g)	References
		pH	Time (min)	Dosage (g/L)		
MWCNTs-M-SLS	Cr(III)	5	60	2	66.2	[42]
MWCNTs-CTAB	Cr(VI)	4.5	30	5	27.8	
chitosan/MWCNTs-COOH	Cr(VI)	2	30	50	142.9	[47]

PAC chitosan SWNTs MWCNTs	Cr(VI)	4	30	0.05	46.9 35.6 20.3 2.48	[10]
Nitrogen and sulfur codoped micro-mesoporous carbon sheets (N,S-MMCSs)	Cr(VI)	2	720	0.36	217.4	[57]
nitrogen-doped carbon sheet (NDCS)	Cr(VI)	3	150		432	[58]
MWCNTs o-MWCNTs Activated carbon	Cr(III)		180	1	8.4 5 9	[59]
Magnetic nanoparticle MNP/MWCNTs	Cr(VI)	2	60	1	19.65	[60]
Carbon nanotubes	Cr(III)	7	120	3	0.3853	[44]
Magnetron sputtered CuO nanoparticles	Cr(VI)	3	60	5	15.63	[52]
MWCNTs from Co–Fe/AC	Cr	2	20	0.3	243.9	[54]
MWCNTs	Cr(III)	2	900	5	18.24	[45]
	Cr(VI)	4			11.13	
o-MWCNTs Raw N-MWCNTs o-N-MWCNTs	Cr(III)	5.5	60	0.30	1990 877 1720	This study
o-MWCNTs Raw N-MWCNTs o-N-MWCNTs	Cr(VI)	1.5	10	0.35	1280 962 1930	This study

4.3.1.8 Adsorption thermodynamics of Cr(III) and Cr(VI) ions removal

Figure 4.26 shows the thermodynamic analysis for adsorption of Cr(III) ions onto M-N-MWCNTs. The change in the Gibbs free energy (ΔG), enthalpy (ΔH), and entropy (ΔS) of the adsorption system were evaluated to determine the thermodynamic parameters of the adsorption process. The adsorption thermodynamics is one of the most powerful techniques for determining the mode of interactions between an adsorbent and an adsorbate. The Gibbs free energy ΔG is the accepted criteria for assessing the type of adsorption whether it is chemisorption or physisorption. Physisorption processes are present when ΔG is in the −20.0 to 0.0 kJ/mol range and chemisorption processes are present if the range is −80.0 to −400 kJ/mol [42]. The equilibrium constant, ΔH and ΔS were obtained from the slope and intercept of the van't Hoff plot of ln K against 1/T (figure 4.26). Typical slopes of exothermic reactions are positive, and equilibrium constants decrease with increasing temperature [61].

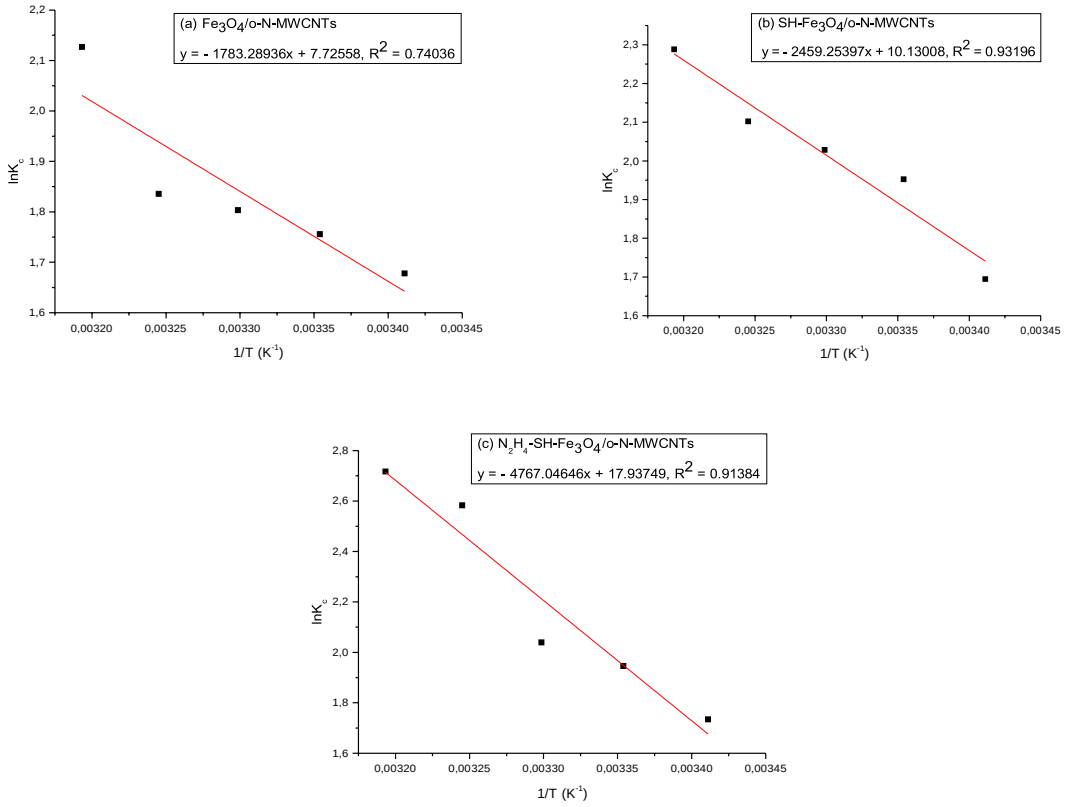

Figure 4.26: Thermodynamic analysis for adsorption of Cr(III) ions by (a) Fe_3O_4/o-N-MWCNTs, (b) SH-Fe_3O_4/o-N-MWCNTs and (c) N_2H_4-SH-Fe_3O_4/o-N-MWCNTs nanocomposites.

The thermodynamic parameter changes ΔG, ΔH, and ΔS, for the adsorption of Cr(III) ions onto respective adsorbents are given in Table 4.5. showed a negative value in all temperature ranges. The negative values may be interpreted as representing both the spontaneous nature of the reaction as well as the feasibility of the process [62]. The negative values of ΔG increase with an increase in temperature indicating the increase in the spontaneity of adsorption process with temperature [46]. Negative free energy is a good indication of spontaneous adsorption. The positive value of changes in both enthalpy and entropy revealed that the adsorption process is endothermic in nature and that there is randomness during the adsorbate-adsorbent interaction in the adsorption process, respectively. The Gibbs free energy obtained in this study is similar to the results obtained by Yahya et al. [62], which confirmed that the adsorption processes for chromium ions were physical. The study by Kumar et al. [53] and Huang et al. [47] were in contradiction since the free energy values decreased with an increase in temperature and the enthalpy change (ΔH) was found to be negative indicating the exothermic nature of adsorption. The sign and degree of ΔS describe whether the arrangement of the metal at solid-liquid phase was more likely (ΔS > 0) or less random (ΔS < 0) [25]. The high values of ΔS imply that a noticeable change in entropy occurs during the adsorption process of the metal as observed by Jiang et al. [5].

Table 4.5: Thermodynamic parameters for Cr(III) ions adsorption by f-N-MWCNTs nanoparticles at different temperatures

Adsorbent	Thermodynamic parameters			
	Temperature (K)	ΔG (kJ/mol)	ΔH (KJ/mol)	ΔS (J/mol/K)
Fe_3O_4/o-N-MWCNTs	293.15	-4.227	14.83	67.23
	298.15	-4.824		
	303.15	-5.141		
	308.15	-6.617		
	313.15	-7.073		
SH-Fe_3O_4/o-N-MWCNTs	293.15	-4.377	20.45	84.22
	298.15	-4.709		

	303.15	-5.045		
	308.15	-5.261		
	313.15	-5.912		
N_2H_4-SH-Fe_3O_4/o-N-MWCNTs	293.15	-4.823	39.63	149.1
	298.15	-5.124		
	303.15	-5.409		
	308.15	-5.614		
	313.15	-5.762		

Figure 4.27 shows thermodynamic analysis for adsorption of Cr(VI) ions onto M-N-MWCNTs. The value of ΔH and ΔS were obtained from the slope and intercept of the plot of ln K against 1/T, respectively [46,56]. The values of thermodynamic parameters are given in Table 4.6. A decrease in ΔG with temperature increase shows better sorption at an increased temperature [71]. Positive values of ΔH verify the endothermic nature of Cr(VI) adsorption process and the positive ΔS value reflects the affinity of the M-N-MWCNTs for Cr(VI) as well as an increase of randomness at solid-solution interface during metal ion adsorption. The magnitude of ΔH also gives information about the type of adsorption i.e., physical, chemical or physicochemical [46]. The enthalpy change for Cr(VI) adsorption onto M-N-MWCNTs was found to be 43.772 kJ/mol as shown in Table 4.6, implying that the adsorption was chemisorption. These results are in agreement with the study conducted by Kumar et al. [46]. A recent study by Hosseinkhani et al. [63] showed that ΔH > 0 illustrated that the adsorption process of Cr(VI) by the synthesised adsorbent was considered endothermic. In addition, this process was considered physical after obtaining ΔH values. Chen et al. [57] also agree. In contrast to this study, Kahu et al. [56] reported negative enthalpy change indicating that the adsorption process was exothermic and negative entropy change indicating the decrease in the randomness of Cr(VI) as it passed from solution to adsorbed state. Thus, a decrease in the negative value of ΔG was also attained with an increase in temperature.

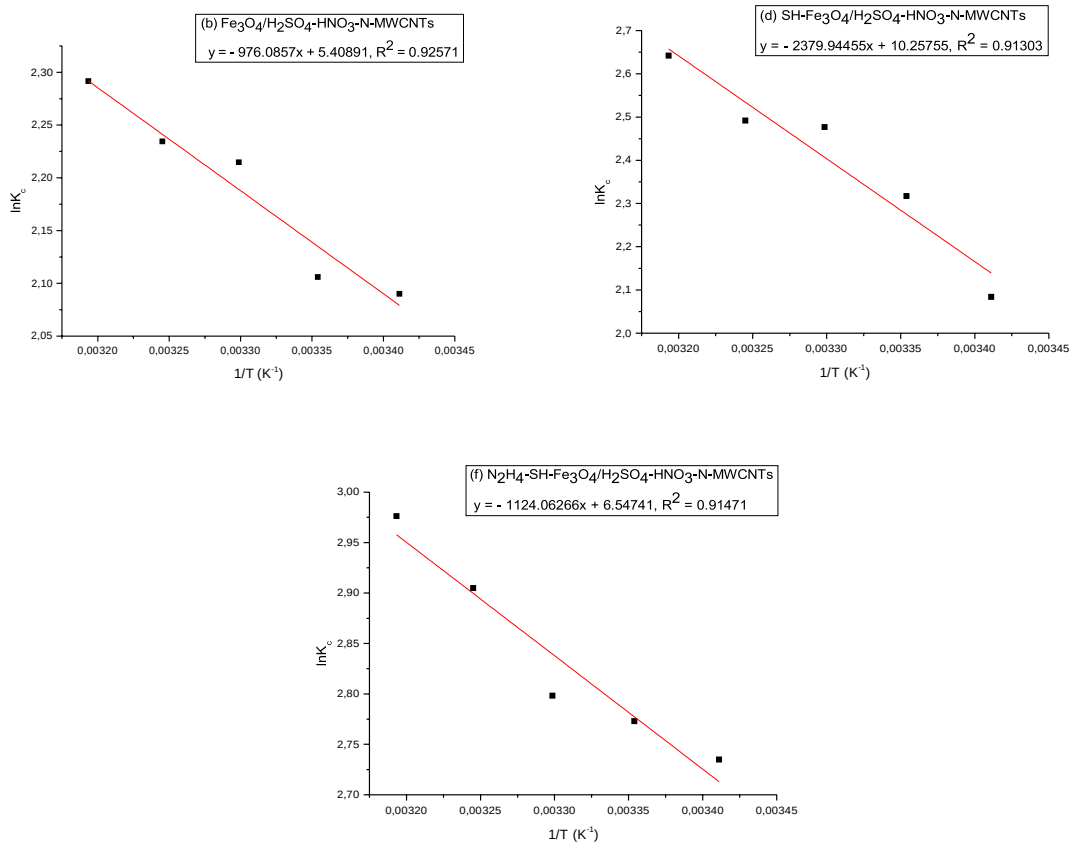

Figure 4.27: Thermodynamic analysis for adsorption of Cr(VI) ions by (a) Fe_3O_4/o-N-MWCNTs, (b) SH-Fe_3O_4/o-N-MWCNTs and (c) N_2H_4-SH-Fe_3O_4/o-N-MWCNTs nanocomposites.

Table 4.6: Thermodynamic parameters for Cr(VI) ions adsorption by f-N-MWCNTs nanoparticles at different temperatures

Adsorbent	Thermodynamic parameters			
	Temperature (K)	ΔG (kJ/mol)	ΔH (KJ/mol)	ΔS° (J/mol/K)
Fe_3O_4/o-N-MWCNTs	293.15	-5.167	8.132	45
	298.15	-5.807		
	303.15	-6.054		
	308.15	-6.542		

	313.15	-7.035		
SH-Fe_3O_4/o-N-MWCNTs	293.15	-6.665	19.79	85.28
	298.15	-6.874		
	303.15	-7.053		
	308.15	-7.442		
	313.15	-7.749		
N_2H_4-SH-Fe_3O_4/o-N-MWCNTs	293.15	-5.721	9.345	54.44
	298.15	-5.985		
	303.15	-6.251		
	308.15	-6.424		
	313.15	-6.539		

4.4.1.9 Effect of competing ions on the removal of Cr(III) and Cr(VI)

Figure 4.28 shows the effect of interfering anions on the removal of Cr(III). Competing anions are known to influence Cr(III) uptake. The Cl^-, HCO_3^-, NO_3^- and SO_4^{2-} were selected as possible competing anions and among them, the chloride ion was mainly selected as mentioned by Pillay et al. [50], that ions such as this are often added to industrial effluents for water treatment, where they have shown to potentially impede chromium adsorption. Figure 4.28 clearly shows that the removal of trivalent chromium onto the as-prepared nanocomposites in a single-solute system of 50 mg/L Cr(III) was good with a percentage removal of greater than 90% for all adsorbents. From figure 4.28, it can be stated that some counterions interfere with the removal of Cr(III) to a lesser extent in comparison to others. For instance, Cr(III) in a single-solute system has a percentage removal of over 80% for all the adsorbents but in a binary-solute system containing chloride ions, the percentage removal is lower with an average of 40% for all adsorbents. The results show great removal in a multi-solute system which is great since in real wastewater we expect multiple elements at the same time. The removal was also excellent in the presence of carbonates for two of the adsorbents except for Fe_3O_4/o-N-MWCNTs, which had removal of less than 50%. The following sequence was observed starting from anions that interfere at a greater extent to a lesser extent on the removal of Cr(III): $Cl^- > NO_3^- > SO_4^{2-} > HCO_3^-$ > multi-solute. From

the above results, the presence of competing ions on the removal of Cr(III) using functionalised adsorbents is good for simulated water and proves that it will be beneficial in real wastewater treatment.

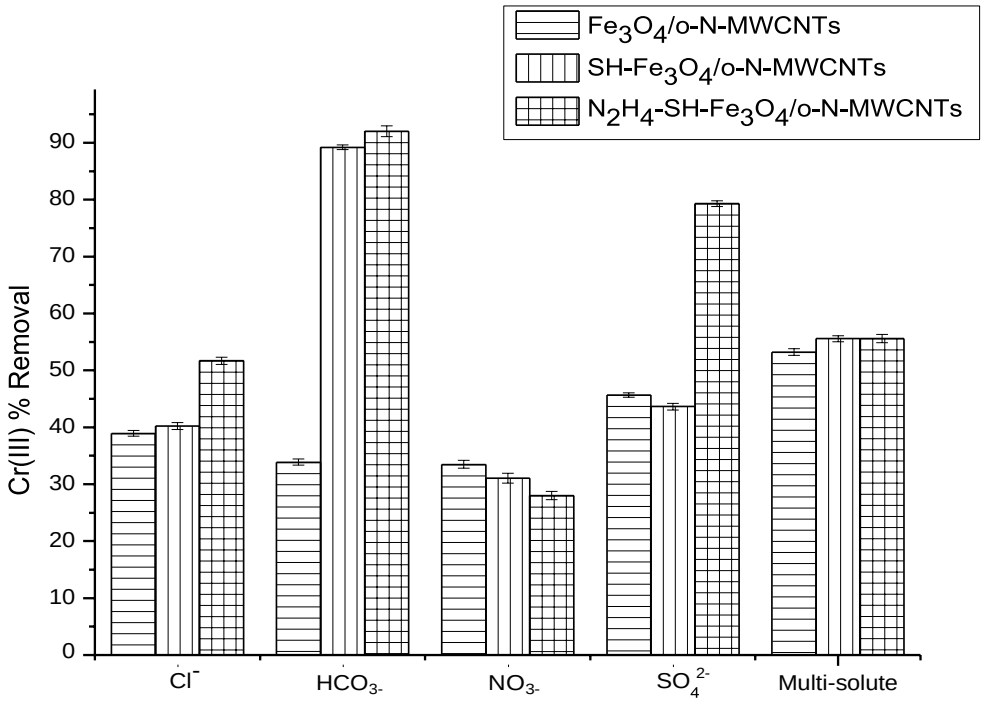

Figure 4.28: Effect of the presence of competing ions on the removal of Cr(III) by (a) Fe_3O_4/o-N-MWCNTs, (b) SH-Fe_3O_4/o-N-MWCNTs and (c) N_2H_4-SH-Fe_3O_4/o-N-MWCNTs. Experimental conditions: optimum pH, contact time, adsorbent dosage, Cr (III) concentration and temperature. ($[NO_3^-]_0$ = 20 mg/L, $[Cl^-]_0$ = 355 mg/L, $[HCO_3^-]_0$ = 610 mg/L and $[SO_4^{2-}]_0$ = 960 mg/L).

The effect of interfering anions on the removal of Cr(VI) is presented in figure 4.29. Zhou et al. [64], stated that in reality, the coexisting anions (CO_3^{2-}, SO_4^{2-} and PO_4^{2-}) and humic acid (HA) contained in water would interfere with the removal of the metal ion of interest. Hence, a study is required for the effects of various anions and organic matter on the removal of hexavalent chromium [64]. Figure 4.29 shows that from a simulated single-system that contained 50 mg/L Cr(VI), the percentage removal was between 17.3 and 95.5% using Fe_3O_4/o-N-MWCNTs, SH-Fe_3O_4/o-N-MWCNTs and N_2H_4-SH-Fe_3O_4/o-N-MWCNTs nanocomposites. The removal percentages of the as-prepared nanocomposites towards the removal of Cr(VI) in a binary-solute system containing Cl^-, HCO_3^-, NO_3^-, SO_4^{2-} and multi-system containing (Cl^-, HCO_3^-, NO_3^- and

SO_4^{2-}) were investigated with the chloride system showing the greatest interference. From the above results, the removal of Cr(VI) is favoured by the use of Fe_3O_4/o-N-MWCNTs in a binary-solute system, which shows good results whereas toxic elements exist in a multi-system in real wastewater. Although the removal is good in a binary-solute system, it showed poor results in the presence of multiple anions as compared to other adsorbents which showed great Cr(VI) removal of about 65% and above. Therefore, the percentage removal of Cr(VI) in the simulated water is slightly lower than that in the single-solute system which may be due to the presence of the competing ions but greater than that in a binary-solute system. These added functional groups provided numerous chemical sorption sites on MWCNTs surface, hence the adsorption capability increased with higher number of functional groups on the surface of MWCNTs.

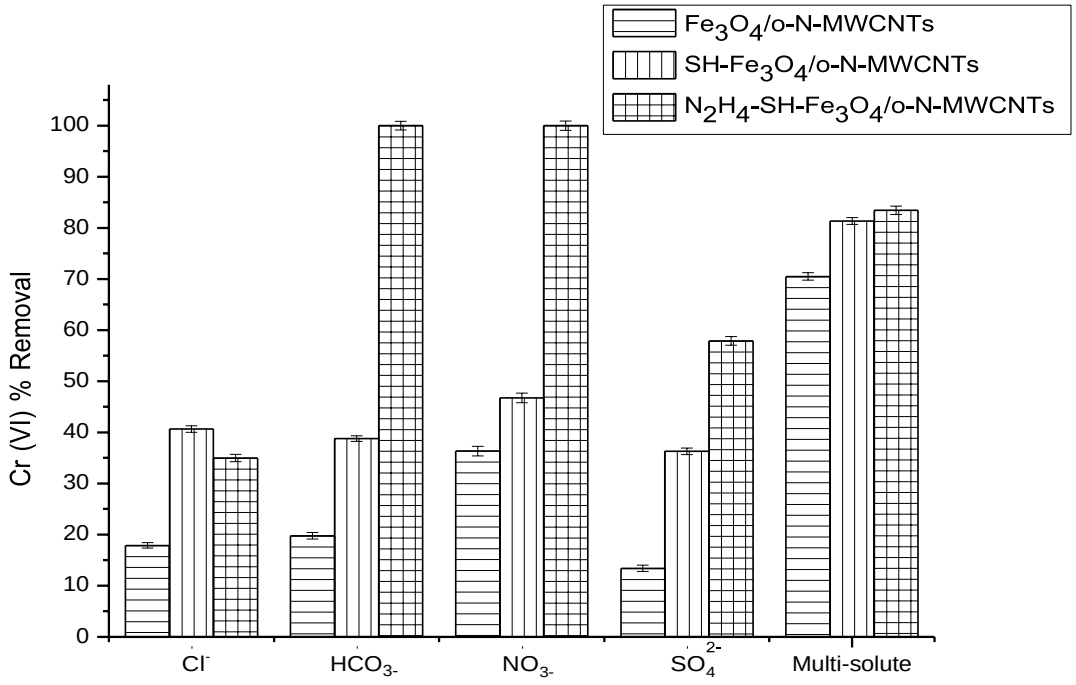

Figure 4.29: Effect of the presence of competing ions on the removal of Cr(VI) by (a) Fe_3O_4/o-N-MWCNTs, (b) SH-Fe_3O_4/o-N-MWCNTs and (c) N_2H_4-SH-Fe_3O_4/o-N-MWCNTs. Experimental conditions: optimum pH, contact time, adsorbent dosage, Cr(VI) concentration and temperature. ($[NO_3^-]_0$ = 20 mg/L, $[Cl^-]_0$ = 355 mg/L, $[HCO_3^-]_0$ = 610 mg/L and $[SO_4^{2-}]_0$ = 960 mg/L).

The presence of some of the competing anions was found to interfere to a lesser extent as compared to others which can be observed from the following sequence starting from anions that interfere at a greater extent to a lesser extent on the removal of Cr(VI): Cl^- > SO_4^{2-}> HCO_3^- > NO_3^- > multi-solute. The removal of Cr(VI) in a binary-solute system containing chloride ions using all the adsorbents showed a decrease of over 50% as compared to the multi-solute system. As stated by Huang et al. [47], Cl^- and NO_3^- are monovalent anions, their competition with the chromium anions for the positively-charged sorption sites on the surface of chitosan/MWCNTsCOOH was relatively small. PO_4^{3-} and SO_4^{2-} however, are multivalent anions, thus competing more extensively with Cr(VI) for the positively-charged sorption sites. In contrast, amino- and thiol-functionalised N-MWCNTs showed better removal in the presence of SO_4^{2-} compared to Cl^- and NO_3^- containing solution. This may be due to the type of adsorbent and modification of adsorbent.

4.4.1.10 Reusability studies on Cr(III) and Cr(VI) removal

Along with the adsorption capacity, the regeneration and reusability potential should be considered when evaluating an adsorbent [64]. To assess the feasibility of the material for a potential application, the removal of metal ions from solution is not just a criterion of adsorptive ability but is also one of regeneration and reusability. Previous studies have reported various regeneration methods such as using HCl [65], NaCl [64] and NaOH [67].

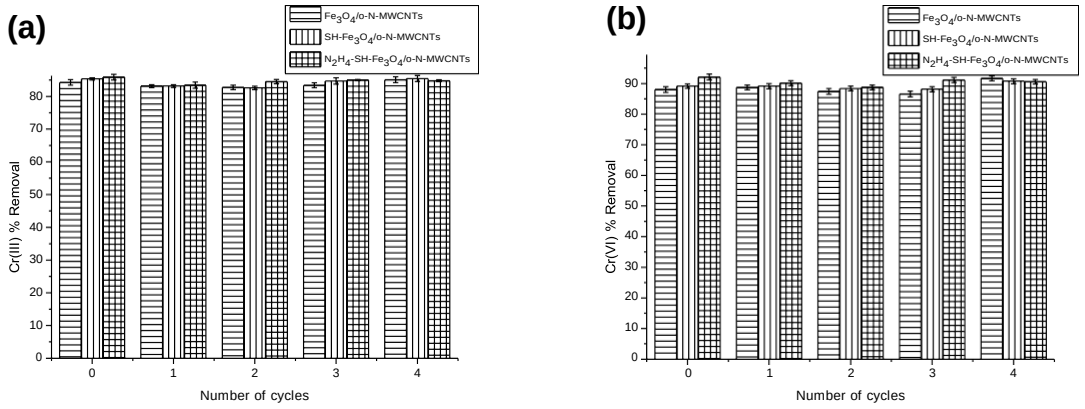

Figure 4.30: Reusability on Cr(III) and Cr(VI) removal by (a) Fe_3O_4/o-N-MWCNTs, (b) SH-Fe_3O_4/o-N-MWCNTs and (c) N_2H_4-SH-Fe_3O_4/o-N-MWCNTs. Experimental conditions: optimum pH, contact time, adsorbent dosage, Cr concentration and temperature.

In this study, the regeneration of modified N-MWCTs was examined using HCl (0.5 M). If the expended adsorbent is discharged into the environment without regeneration, it may cause another environmental concern. Regeneration of adsorbents is carried out by desorbing the adsorbent using an eluent [68,69]. The reusability study shows the percentage removal of trivalent chromium almost remains unchanged after four cycles as shown in figure 4.31a. After regeneration with a hydrochloric acid solution, the removal decreased by approximately less than 5% after the fourth cycle. The N-MWNCTs could still adsorb and retain removal of over 86% (figure 4.30b) after the fourth cycle. Thus, the adsorbent is promising for practical application in chromium treatment and the results suggest that modified o-N-MWCNTs can be repeatedly used for the removal of chromium species from wastewater. The functionalisation of sorbent using a chemical bond between the sorbent and the new functional groups can significantly enhance the sorbent's chemical stability. As a result, the possibility of sorbent regeneration and its reusability increase [69].

4.3.2 Batch Adsorption studies of Nickel (II) ions

4.3.2.1 Effect of pH on the removal of Ni(II) ions

Figure 4.31 shows the effect of pH on the removal of Ni (II) from the prepared o/o-MWCNTs at a contact time of 30 minutes, Initial concentration of 20 mg/L and adsorbent dosage of 0.05 g/L. The study was carried out by evaluating the maximum percentage uptake of Ni(II) onto the adsorbent (o-N-MWCNTs) in an aqueous solution. The percentage removal increased from 64 to 76% between pH of 3 and 4.5, then slightly decreased to 68% at pH = 6.5 from that point going up the% removal increased up to 92% at pH = 11. The removal of Ni(II) is not favourable at acidic pH range thus the optimum pH for Ni(II) ions is at pH = 11.

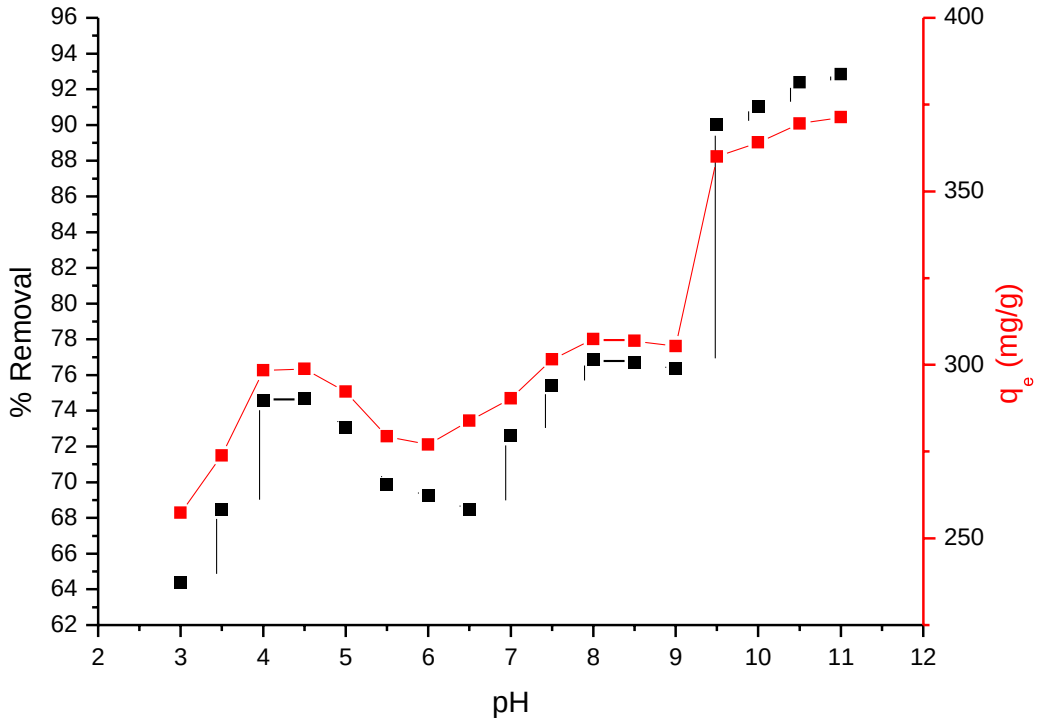

Figure 4.31: Effect of pH on Ni(II) removal using o-N-MWCNTs. Experimental conditions: concentration = 20 mg/L, contact time 30 min at room temperature, adsorbent dose = 0.05 g/L at varied pH values 3-11.

Ni(II) ions are positively charged and the surface of MWCNTs is negatively charged thus electrostatic attraction is increased between them leading to increased % removal [48]. At lower pH, the hydroxyl and carboxyl groups are more likely to bind to a large amount of H_3O^+ that strongly compete with metal ions for adsorption sites. On the other hand, after protonation, the nanocomposites become positively charged, resulting in electrostatic repulsion between the cationic metal ions and the adsorbent [70]. The adsorption capacity and % removal are both directly proportional to pH, as one parameter increases the other also increases [70]. This result is consistent with other studies [48]. Adolph et al. [70] observed a similar trend for Ni(II) removal by phosphine functionalised multiwalled carbon nanotubes with only 80 mg/g which was lower as compared to 375 mg/g from this study. Therefore, pH 11 was considered as the optimum condition and was used for further study for the removal of Ni(II).

4.3.2.2 Effect of contact time on the removal of Ni(II) ions

Figure 4.32a shows the removal of Ni(II) from aqueous solution on three adsorbents functionalised with metal oxide, thiol- and amino- groups. The percentage removal increases at a rapid rate during the first few minutes and thereafter at a slower rate until an equilibrium is reached. The removal increased from 95.2 and 99.9% reaching equilibrium at 60 min for the best performing adsorbents with the removal of above 99%. The difference can be explained due to the added functional groups on the oxidised N-MWCNTs. The amine treated N-MWCNTs showed greater removal as compared to the iron oxide and thiol treated N-MWCNTs and thus the optimum time was selected as 60 minutes based on the best performing adsorbent (N_2H_4-SH-Fe_3O_4/o-N-MWCNTs). Similar findings were reported in previous studies of nickel removal by CNTs, stating that CNTs have a fast equilibrium time and have a great potential for Ni(II) adsorption applications [69]. Ahmadi et al. [48] reported similar findings with only 40% Ni(II) at 25 mg/L. Removal was continued over a longer period (figure 4.32b). After 72 hours the percentage removal by Fe_3O_4/o-N-MWCNTs, SH-Fe_3O_4/o-N-MWCNTs and N_2H_4-SH-Fe_3O_4/N-MWCNTs were at 89, 92 and 91% respectively. Over longer periods, as contact time increases the removal percentage decreases which can be observed by over 9% decrease in removal for all the adsorbents.

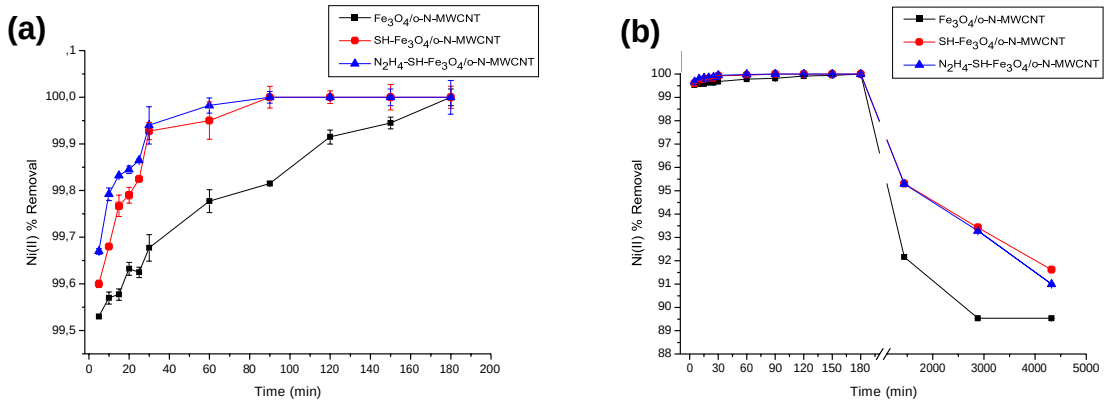

Figure 4.32: Effect of contact time on Ni(II) removal by (a) Fe_3O_4/o-N-MWCNTs, (b) SH-Fe_3O_4/o-N-MWCNTs and (c) N_2H_4-SH-Fe_3O_4/N-MWCNTs. Experimental conditions: pH = 11, dosage = 0.05 g/L, concentration = 20 mg/L and contact time = 5-180 minutes at room temperature (25 °*C*).

4.3.2.3 Effect of adsorbent dosage on the removal of Ni(II) ions

Figure 4.33 shows the effect of adsorbent dosage on the removal efficiency of Ni(II). The effect of various dosages of a known mass of 0.01, 0.02, 0.03, 0.04 and 0.05 g/L on the removal of Ni(II) was investigated at optimum pH and time with Ni(II) initial concentration of 20 mg/L.

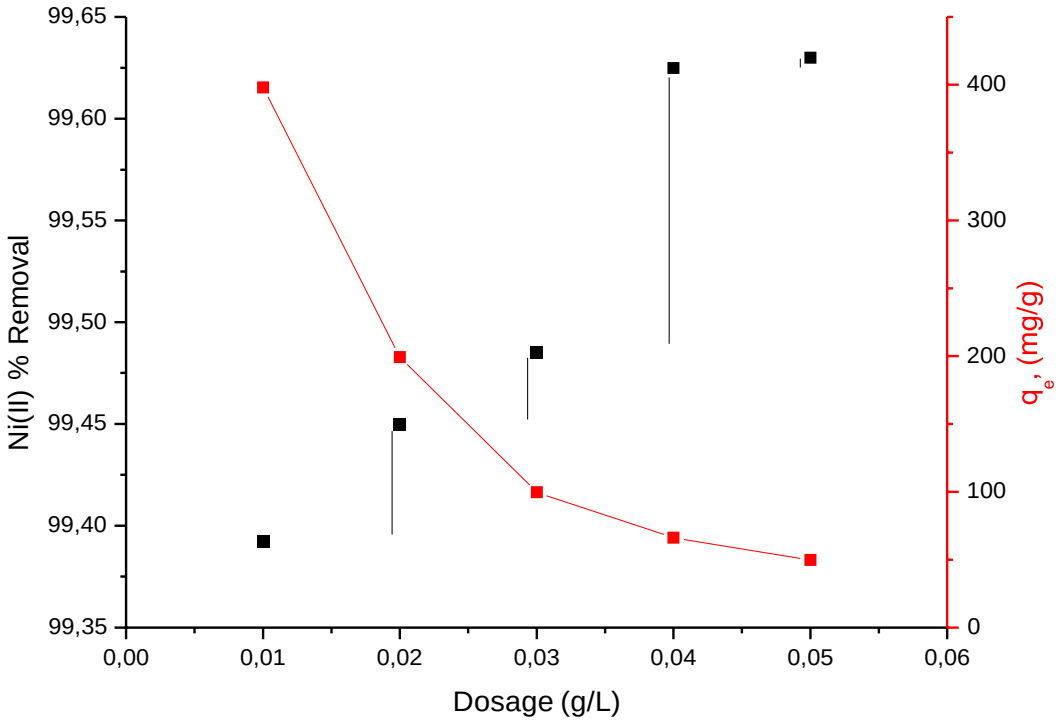

Figure 4. 33: Effect of adsorbent dosage on the removal of Ni(II) by o-N-MWCNTs. Experimental conditions: pH = 11, contact time = 60 min at room temperature (25 °C), concentrations = 20 mg/L and dosage varied between 0.01 to 0.05 g/L.

Figure 4.33 shows that as the adsorbent dosage was increased from 0.01 to 0.05 g/L, the percentage removal increased from 99.4 to 99.6%, whereas a decrease was observed with the adsorption capacity. As the adsorbent dosage increased, the adsorption capacity decreased from 425 to 50 mg/g. Similar findings were observed by Dong et al. [72] explaining that at lower solid dosage, the functionalised MWCNTs particles disperse well in the solution. Hence, all the surface sites are completely exposed for Ni(II) removal amount. In contrast, the functionalised MWCNTs particles tend to collide with each other at higher solid dosage causing the formation of aggregation and the decrease of their dispersion in solution. This would decrease the total specific surface area and increase the diffusional path length, which is expected to reduce the availability of binding sites and further decrease the removal of Ni(II) on MWCNTs. A 0.05 g/L was selected as the optimum adsorbent dosage to continue with the study. The dosage is better than that of Dong et al. [72] adsorbent was only 74%

and 7 mg/g of Ni(II) ions adsorption was observed at a very high adsorbent dosage of 1.0 g/L.

4.3.2.4 Effect of initial concentration on the removal of Ni(II) ions

Figure 4.34 shows the effect of initial concentrations (20, 40, 60, 80, 100 and 120 mg/L) on the removal of Ni(II) at optimum pH = 11, contact time = 60 minutes and dosage = 0.05 g/L. As illustrated in figure 4.34a from the graph, the removal decreased with increasing concentration from 20-120 mg/L. No significant change was observed between 20 and 60 mg/L for all adsorbents with removal ranging between 99.8 and 99.9%. A slight decrease was observed from 99.7 at 20 mg/L to 99.1% at 120 mg/L using Fe_3O_4/o-MWCNTs. However, N_2H_4-SH-Fe_3O_4/o-N-MWCNTs showed greater percentage removal between 20 and 80 mg/L followed by a noticeable decrease at 80 to 120 mg/L. When the concentration was increased from 20-120 mg/L the adsorption capacity increased from 350 mg/g to 2400 mg/g as indicated by figure 4.34b which is because, during the adsorption process, the surface of the adsorbent was easily saturated by the molecules with higher concentration. A similar trend was observed by Ahmadi et al. [48] because the increase in the amount of Ni(II) ions increased collision between ions and the active sites on the adsorbent. Therefore, 20 mg/L concentration was selected as the maximum initial concentration and used for the remainder of the study. The current study was compared to studies by other authors, the study by Adolph et al. showed similar trends with a maximum adsorption capacity of 30 mg/g at a higher dose of 0.4 g/L [71]. Another study by Dong et al. showed a maximum of 13 mg/g which is very low compared to the current study at a dosage of 0.5 g/L [72]. The low adsorption capacity of both the studies could also be due to the pH of 6 used.

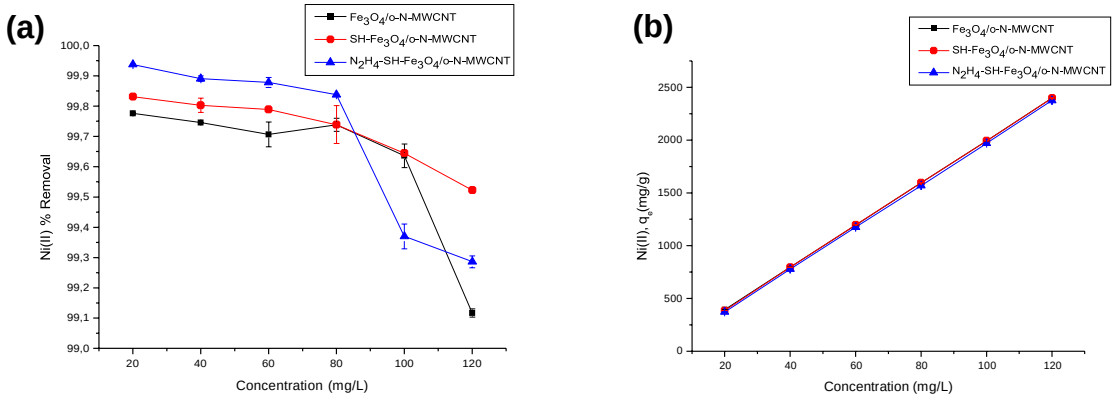

Figure 4.34: Effect of initial concentration on Ni(II) (a) removal and (b) adsorption capacity by Fe_3O_4/o-MWCNTs, SH-Fe_3O_4/o-N-MWCNTs and N_2H_4-SH-Fe_3O_4/o-N-MWCNTs. Experimental conditions: pH = 11, dosage = 0.05 g/L, concentration = 20-120 mg/L and contact time = 60 minutes at room temperature (25 °C).

4.3.2.5 Effect of temperature on the removal of Ni(II) ions

The effect of temperature (20, 25, 30, 35 and 40 °C) on the removal of Ni(II) was investigated as shown in figure 4.35 while other adsorption parameters were kept constant (pH, time, dosage and concentration). From figure 4.35, as the temperature of the solution is increased from 20°C to 40°C, the percentage removal increases from a minimum of 99.2 to 99.8% using Fe_3O_4/o-N-MWCNTs, SH-Fe_3O_4/o-N-MWCNTs and N_2H_4-SH-Fe_3O_4/o-N-MWCNTs, respectively. Therefore, 25 °C was selected as the temperature to be used for the remainder of the study because for all adsorbents the removal was above 99.3% at room temperature, which shows good removal qualities.

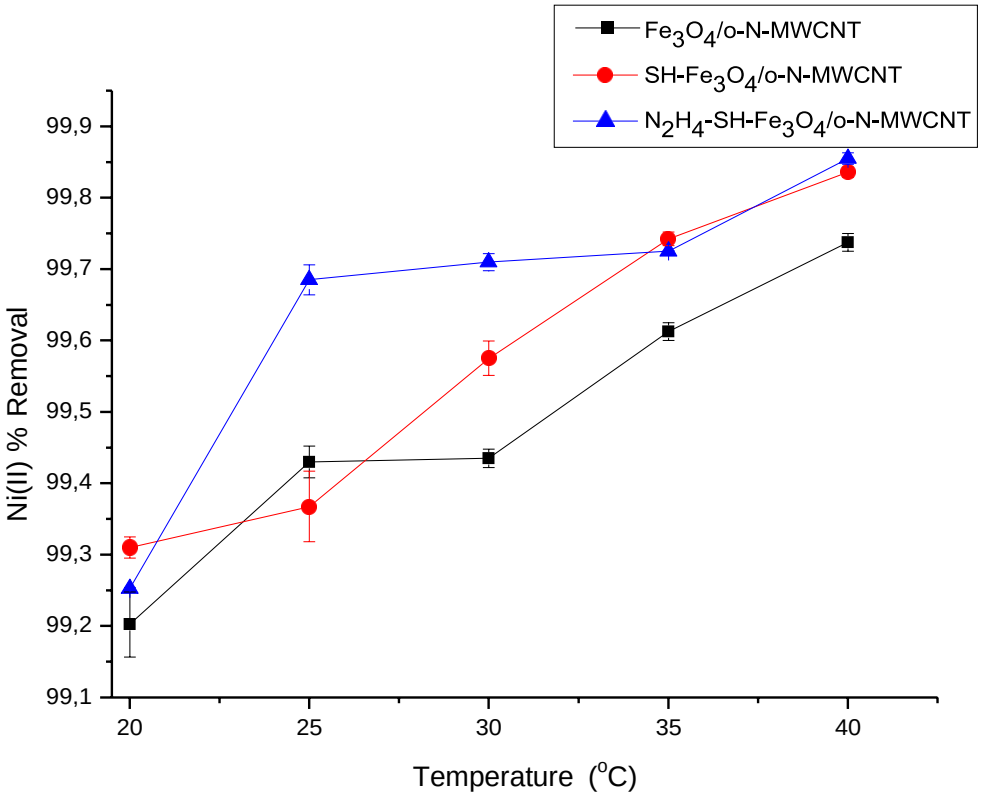

Figure 4.35: Effect of temperature on Ni(II) removal by (a) Fe_3O_4/o-N-MWCNTs, (b) SH-Fe_3O_4/o-N-MWCNTs and (c) N_2H_4-SH-Fe_3O_4/o-N-MWCNTs. Experimental conditions: pH = 11, dosage = 0.05 g/L, concentration = 20 mg/L, contact time = 60 minutes and temperature = 20, 25, 30, 35 and 40 °C.

4.3.2.6 Adsorption kinetics of Ni(II) ions

Figure 4.36 shows the linear fitting results of the kinetic data of Ni(II) ions removal on M-N-MWCNTs. The kinetic parameters are presented in Table 4.7. kinetic experimental results for M-N-MWCNTS adsorbents with the linearity in the ranges R^2 = (-0.08689 to 0.1123) for pseudo-first order and (R^2 = 0.9999 to 1) for the pseudo-second model indicate that pseudo-second order kinetic model is better fitting with the experimental data and proves that kinetic behaviour of nickel adsorption on the as-prepared adsorbents follows pseudo second order equation. However, the calculated q_e values were compared with the experimental values which were far different and could not be fitted with the pseudo-first order equations. Furthermore, the calculated

q_e (adsorption capacity) of M-N-MWCNTs adsorbent in the pseudo-second order model was closely fitted to the experimental values. The parameters q_e and k_2 were determined from the intercept and slope of the plot t/qt versus t. The results demonstrate that the adsorption data has a correlation coefficient close to 1 for all the adsorbents suggesting that the adsorption mechanism of Ni^{2+} could be chemisorption (rate-limiting step) [71]. This indicates that the pseudo-second order model is more valid to describe the kinetics of the undergoing adsorption process [70]. The above results agree with those reported in the literature [70-74]. K_1 values from our study contradict values from literature. K_1 values from most studies are greater than k_2 values, whereas the opposite was observed from the above results.

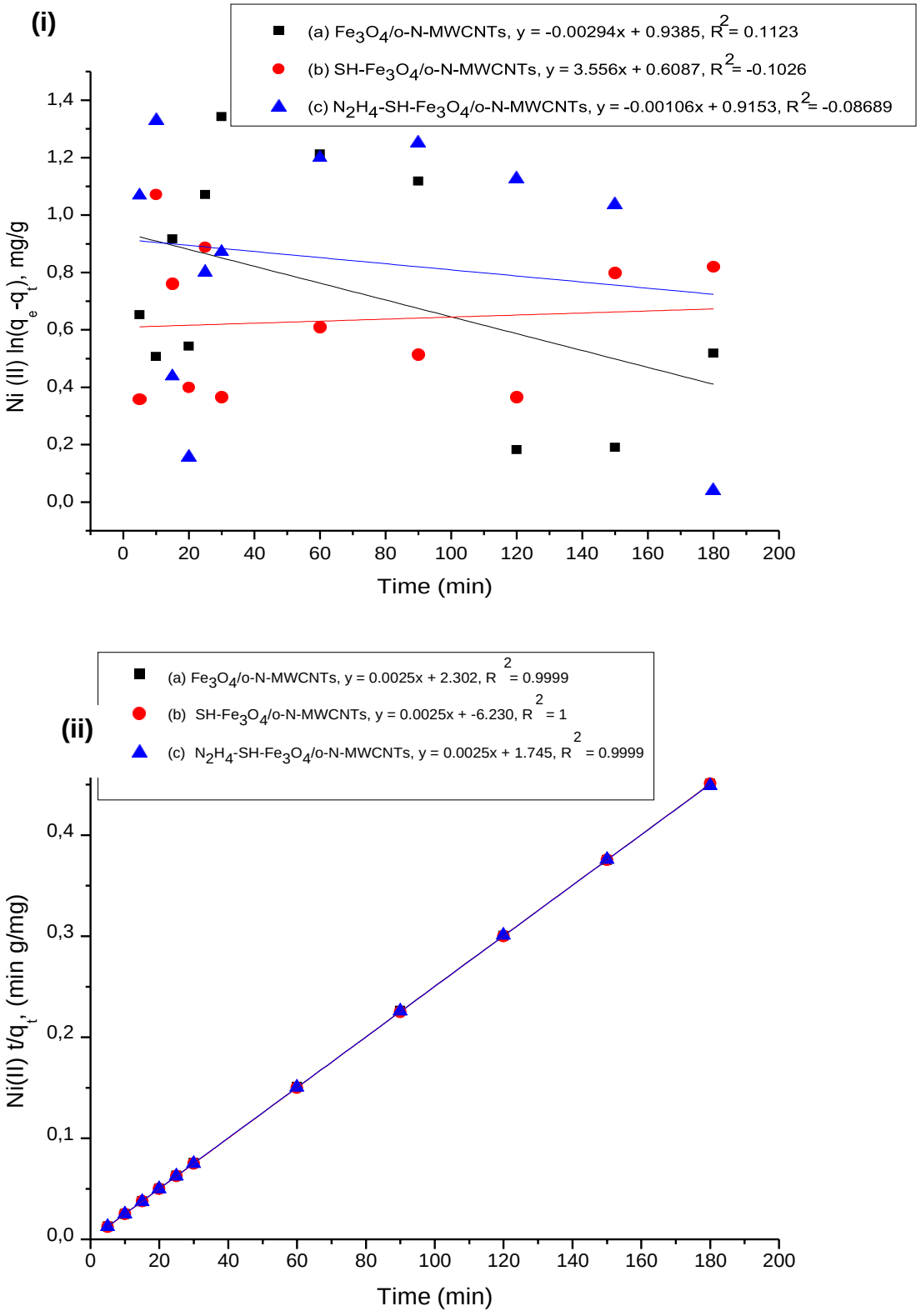

Figure 4.36: (i) Pseudo-first order and (ii) Pseudo-second order kinetic model for adsorption of Ni(II) ions by (a) Fe_3O_4/o-N-MWCNTs, (b) SH-Fe_3O_4/o-N-MWCNTs and (c) N_2H_4-SH-Fe_3O_4/o-N-MWCNTs nanocomposites.

Table 4.7: The parameters calculated by kinetic models for adsorption of Ni(II) ions adsorption by f-N-MWCNTs nanoparticles

Adsorbent	Experimental q_e (mg/g)	Pseudo-first order kinetic model			Pseudo-second order kinetic model		
		$q_{e.cal}$ (mg/g)	k_1 (min^{-1})	R^2	$q_{e.cal}$ (mg/g)	k_2 (g/mg/min)	R^2
Fe_3O_4/o-N-MWCNTs	401	2.556	0.00294	0.1123	398.4	0.261	0.9999
SH-Fe_3O_4/o-N-MWCNTs	401.6	1.838	-3.556	-0.1026	398.4	0.261	1
N_2H_4-SH-Fe_3O_4/o-N-MWCNTs	402	2.497	0.00106	-0.08689	398.4	0.261	0.9999

4.3.2.7 Adsorption isotherms of Ni(II) ions

The Ni(II) adsorption isotherms for M-N-MWCNTs is illustrated in figure 4.37. The adsorption data of Ni(II) onto the synthesised nanomaterials were modelled using the linearised Langmuir and Freundlich isotherms. The constants (q_{max} and b) were calculated from the slope and intercept of plot between $1/C_e$ and $1/q_e$ (figure 4.37) [3]. The values for various constants are listed in Table 4.8. The maximum adsorption capacity of the M-N-MWCNTs was obtained for Ni(II) adsorption. For Langmuir adsorption, the value of R_L indicates the isotherm shapes to be favourable ($0< R_L <1$), linear ($R_L = 1$), irreversible $R_L = 0$) and unfavourable ($R_L >1$) [1]. R_L values were found to be in the ranges (0.0142-0.0444) which is a favourable process. Langmuir isotherm model suitably described the adsorption of Ni(II) ions onto o-N-MWCNTs (0.8528) due to the larger value of R^2 which was higher than that of the Freundlich isotherm model

(0.760). These results imply that the adsorption of Ni(II) ions occurred by chemisorption controlled monolayer coverage of the homogeneous surface of the nanoparticles [75]. Figure 4.37 reveals that the adsorption of Ni(II) using M-N-MWCNTS fit the Freundlich isotherm well onto o-MWCNTs (0.9381) and raw N-MWCNTs (0.9601). The obtained maximum adsorption capacity values for investigated adsorbents were compared to other studies reported in the literature on Ni(II) removal (Table 4.9). From the literature surveyed, MWCNTs adsorption data were predominantly described by Langmuir and Freundlich isotherm models.

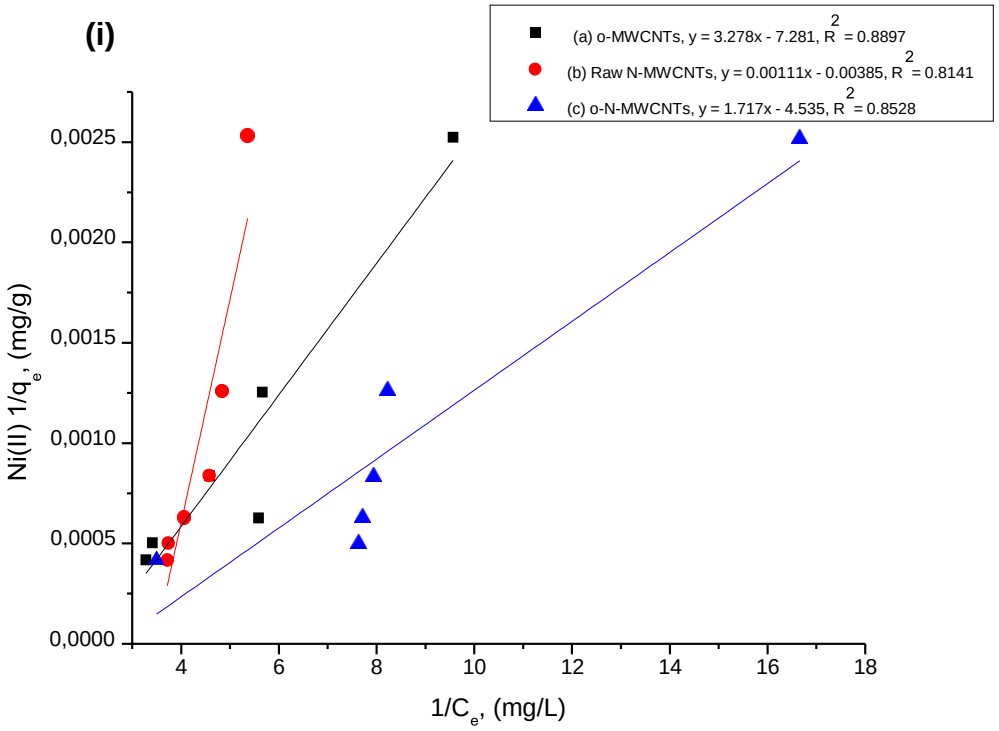

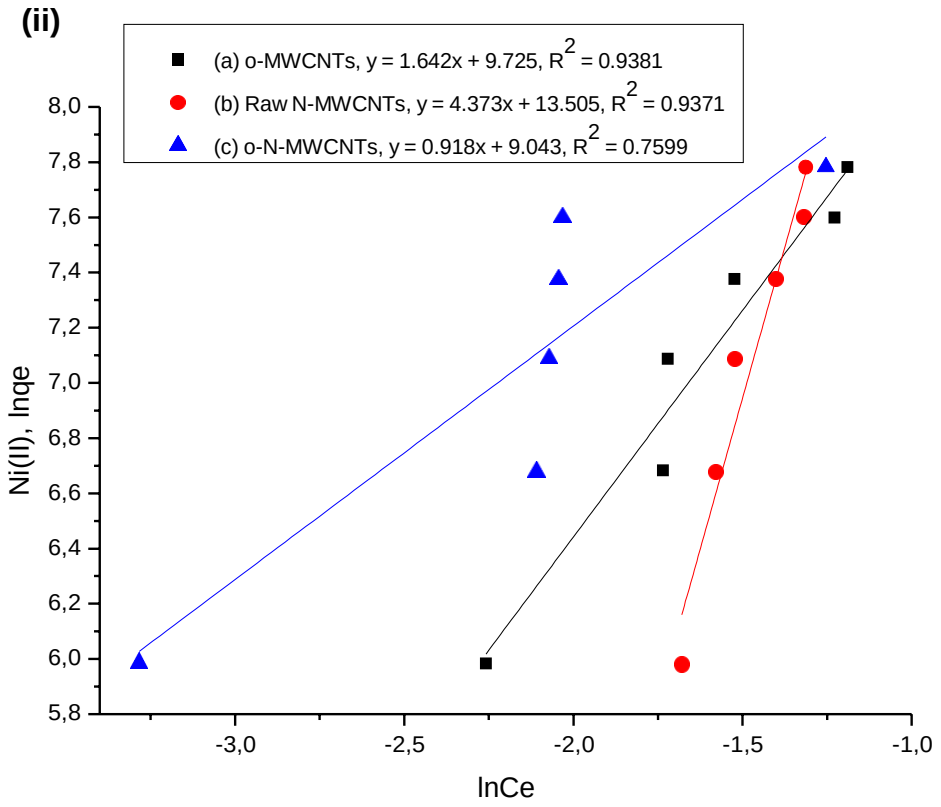

Figure 4.37: (i) Langmuir isotherm and (ii) Freundlich isotherm for adsorption of Ni(II) ions by (a) o-N-MWCNTs, (b) Raw N-MWCNTs and (c) o-N-MWCNTs nanocomposites.

Table 4.8: The parameters calculated by isotherm models for adsorption of Ni(II) ions adsorption by f-N-MWCNTs nanocomposites

Adsorbent	q_{max} (mg/g)	Langmuir model			Freundlich model		
		b (L/mg)	R_L	R^2	K_f (mg/g)	N	R^2
o-MWCNTs	1370	2.22	0.022	0.8897	16730	0.609	0.9381
Raw N-MWCNTs	260	3.47	0.0142	0.8141	733073	0.2287	0.9690
o-N-MWCNTs	5410	1.08	0.0444	0.8528	8459	1.0893	0.760

The maximum adsorption capacity (q_{max}) derived from the Langmuir model fitting of the as-prepared M-N-MWCNT onto Ni(II) was compared with other various adsorbents

to verify the potential of using the nanomaterials in water purification. As depicted in Table 4.9, the q_{max} value of Ni(II) onto o-N-MWCNTs is higher than a series of adsorbent materials such as CD/MWCNT/iron oxide [70], (Phosphine-functionalised MWCNTs and Tpp-MWCNTs) [71], MWCNTs [71], ɣ-PGA-Fe3O4-GO-(o-MWCNTs) [67] and Fe_3O_4-GO-(o-MWCNTs) [70]. The higher adsorption capacities of M-N-MWCNTs may be partly attributed to the higher solution pH (11) used in the sorption isotherm experiments.

Table 4.9: Comparison of Ni(II) ions adsorption capacity by various adsorbents

Adsorbent	Optimised parameters			Adsorption capacity q_{max} (mg/g)	References
	pH	Time (min)	Dosage (g/L)		
ɣ-PGA-Fe_3O_4-GO-(o-MWCNTs) Fe_3O_4-GO-(o-MWCNTs)	5	60	0.13	384.62 59.52	[70]
CD/MWCNT/iron oxide	6.5	240	0.8	38.24	[72]
Phosphine-functionalised MWCNTs Tpp-MWCNTs(1) Tpp-MWCNTs (2)	6 12 12	60	0.4	55.55 83.33 100	[71]
MWCNTs	7	60	0.03	230.78	[74]
oxidised porous carbon (PC-KF)	8	5	0.25	0.01	[76]

o-MWCNTs Raw N-MWCNTs o-N-MWCNTs	11	60	0.05	1370 260 5410	This study

4.3.2.8 Adsorption thermodynamics of Ni(II) ions

K_C was plotted versus 1/T at the temperature of 20, 25, 30, 35 and 40°C to determine the thermodynamic parameters of adsorption of Ni(II) by the synthesised adsorbents. Van't Hoff equation was used to calculate the change in enthalpy (ΔH) and entropy (ΔS) from the slope and intercept of the plot of ln Kc versus 1/T as shown in figure 4.38 and the other thermodynamic parameters are listed in Table 4.10. According to Table. 3.10, the negative value of free Gibbs energy indicates that the process of Ni(II) removal was spontaneous and thermodynamically favourable [77]. The positive change in enthalpy correlates to an endothermic reaction. The positive amount of entropy represents an increase in irregularities in the solid-liquid boundary layer, which is a beneficial factor for the spontaneous development of the removal process of nickel ions [77]. The free energy changes (ΔG) values were negative, confirming that the adsorption of nickel onto the adsorbents was spontaneous and thermodynamically favourable. However, the study by Siddiqui et al. [76] contradicts the results obtained in the current study. Their study showed negative value of ΔH (−45.32 J/mol); indicating adsorption was spontaneous and exothermic. Thus, increased randomness at the solid-solution interface during the adsorption process. The decrease in free energy changes (ΔG) values with the increase in temperature indicated that the adsorption decreased with rising in temperature and the decrease in ΔG values were

due to the increase in the degree of freedom which might have enhanced desorption rather than adsorption at higher temperatures [76].

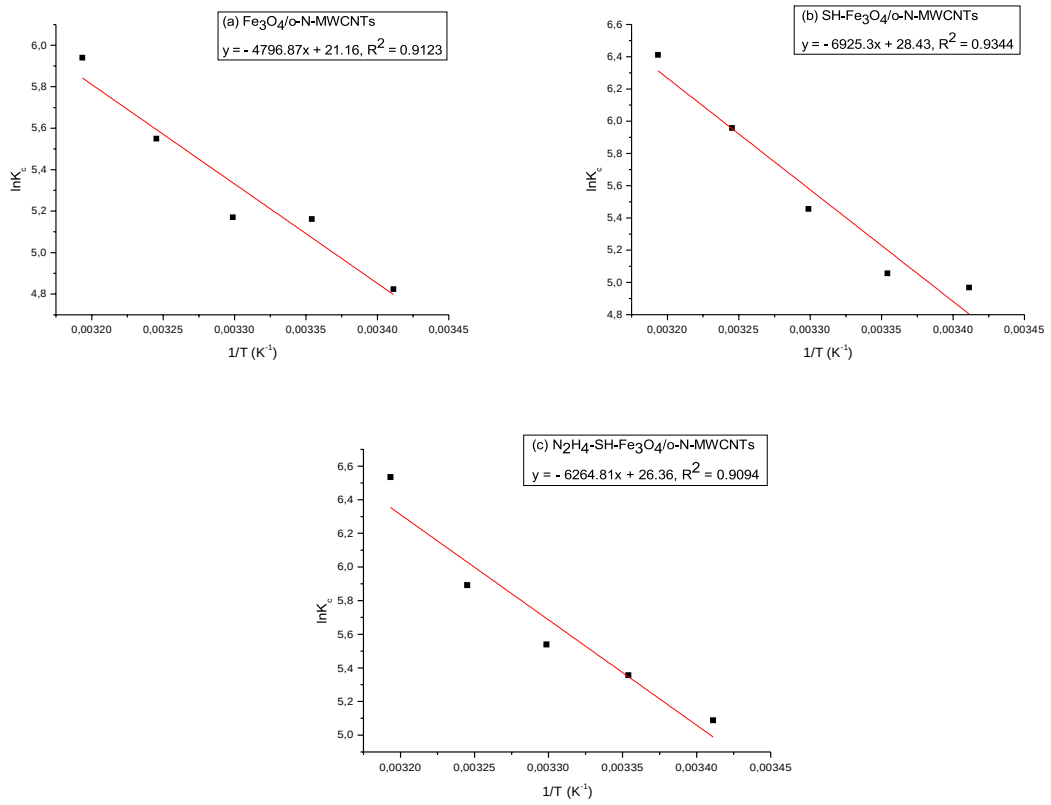

Figure 4.38: Thermodynamic analysis for adsorption of Ni(II) ions by (a) Fe_3O_4/o-N-MWCNTs, (b) SH-Fe_3O_4/o-N-MWCNTs and (c) N_2H_4-SH-Fe_3O_4/o-N-MWCNTs nanocomposites.

Table 4.10: Thermodynamic parameters for Ni(II) ions adsorption by functionalised N-MWCNTs nanoparticles at different temperatures

Adsorbent	Thermodynamic parameters			
	Temperature (K)	ΔG (kJ/mol)	ΔH (KJ/mol)	ΔS (J/mol/K)
Fe_3O_4/o-N-MWCNTs	293.15	-12.10	39.88	175.9
	298.15	-13.16		

	303.15	-13.42		
	308.15	-15.0		
	313.15	-18.12		
SH-Fe_3O_4/o-N-MWCNTs	293.15	-11.92	57.58	236.3
	298.15	-14.27		
	303.15	-14.72		
	308.15	-15.10		
	313.15	-17.01		
N_2H_4-SH-Fe_3O_4/o_3-N-MWCNTs	293.15	-11.27	52.09	219.2
	298.15	-12.77		
	303.15	-13.57		
	308.15	-13.96		
	313.15	-15.63		

4.3.1.9 Effect of competing ions on the removal of Ni(II) ions

Figure 4.39 shows the removal of Ni(II) on six prepared adsorbents in the presence of competing ions at optimum pH, contact time, adsorbent dosage and concentration. The actual environment is a complicated and heterogeneous system due to the simultaneous presence of different components such as toxic elements, organic pollutants, electrolyte ions, microorganisms, natural minerals, etc. [72]. The removal of Ni(II) was evaluated in a binary-solute system and multi-solute system containing four different anions together with the metal of interest. The simulated aqueous solution contained $[NO_3^-]_0$ = 20 mg/L, $[Cl^-]_0$ = 355 mg/L, $[HCO_3^-]_0$ = 610 mg/L, $[SO_4^{2-}]_0$ = 960 mg/L and $[Cr_2O_7^{2-}]_0$ = 50 mg/L. Most ions were selected as potential competing anions, since they are frequently used in industrial effluent water treatment and have proven a potential to inhibit metal ion adsorption on selected adsorbents. Ni(II) has no ability to compete with anions that adsorb on the same sites as it is considered to be the most weakly adsorbed species and has lower affinities than other ions. The competitive adsorption may be related to ion exchange and electrochemical properties of the cations. The higher the complex redox properties and ion exchange processes,

the higher is the polarizability of the ion, and the greater the affinity between the ions and functional groups [8].

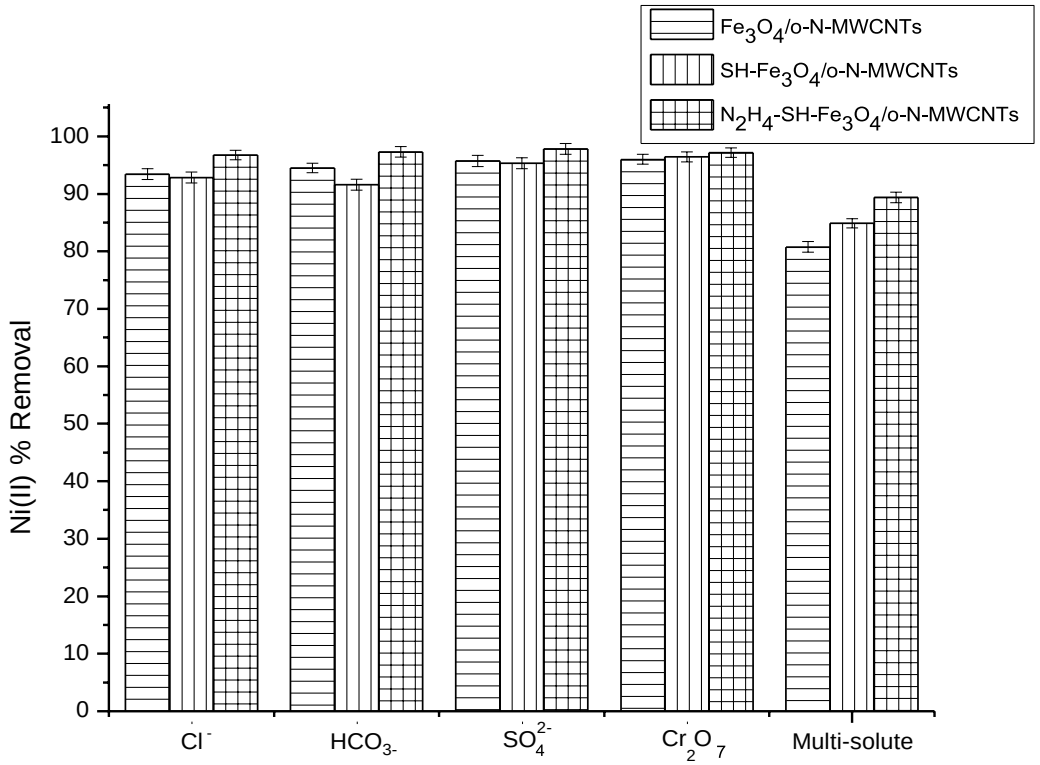

Figure 4.39: Effect of the presence of competing ions on Ni(II) removal by (a) Fe_3O_4/o-N-MWCNTs, (b) SH-Fe_3O_4/o-N-MWCNTs and (c) N_2H_4-SH-Fe_3O_4/o-N-MWCNTs. ($[NO_3^-]_0$ = 20 mg/L, $[Cl^-]_0$ = 355 mg/L, $[HCO_3^-]_0$ = 610 mg/L, $[SO_4^{2-}]_0$ = 960 mg/L and $[Cr_2O_7^{2-}]_0$ = 50 mg/L).

The removal of Ni(II) in the presence of chloride, carbonate, sulphates and dichromate in a binary-solute system retained over 90% removal for all the adsorbents with the N_2H_4-SH-Fe_3O_4/o-N-MWCNTs showing maximum removal of over 95% in all the binary systems. The Fe_3O_4 and thiol-functionalised N-MWCNTs performed lower than the amine treated N-MWCNTs in both the binary and multi-solute systems. A noticeable decrease was observed in the removal of Ni(II) in a multi-solute system whereby removal of over 75 to 89% was achieved as compared to the single-solute system with percentage removals of greater than 99%. The presence of competing anions in a binary-solute system was found to interfere to a lesser extent as compared to a multi-solute system which corresponds to the work done by Egbosiuba et al. [74]

and can be observed from the following sequence starting from anions that interfere at a greater extent to a lesser extent on the removal of Ni(II): multi-solute > HCO_3^- > Cl^- > SO_4^{2-}> $Cr_2O_7^{2-}$. The prepared adsorbents show good results even in the presence of competing ions and will be suitable for use in real wastewater treatment.

4.3.1.10 Reusability studies on Ni(II) removal

As shown in figure 4.40, initially the removal of Ni(II) using the as-prepared adsorbents was greater than 97% for all the adsorbents. After regeneration with a hydrochloric acid solution, a slight decrease in percentage removal can be observed with the removal remaining above 90% for all the adsorbents after cycle one with the SH-Fe_3O_4/o-N-MWCNTs showing maximum removal of 97%. The adsorbents remained viable even after three cycles retaining a removal of 70% and above. Overall, three adsorbents performed well retaining over 80% removal even after three cycles namely, the SH-Fe_3O_4/o-N-MWCNTs and the amine-N-MWCNTs. Dong et al. [69] maintained an adsorption capacity of 13 mg/g after ten cycles while Wang et al. [67] obtained 90% removal after three cycles both of which were lower compared to the current study. The large adsorption capacity of the functionalised N-MWCNTs for Ni(II) ions is mainly due to the oxygenous functional groups on its surface which react with metals to form salt or complex deposits on the surface of the N-MWCNTs [8]. Thus, the adsorbent is promising for practical application in Ni(II) treatment.

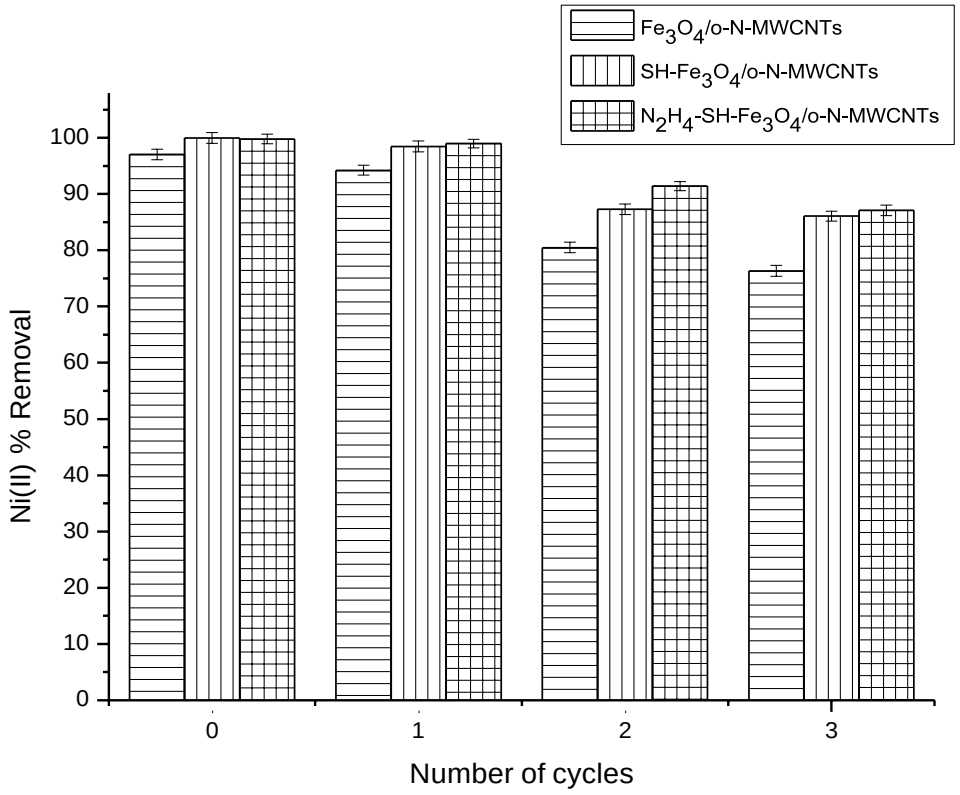

Figure 4.40: Reusability of (a) Fe_3O_4/o-N-MWCNTs, (b) SH-Fe_3O_4/o-N-MWCNTs and (c) N_2H_4-SH-Fe_3O_4/o-N-MWCNTs on Ni(II) removal.

4.3.3 Batch Adsorption studies of lead ions

4.3.3.1 Effect of pH on the removal of Pb(II) ions

As shown in figure 4.41, the effect of pH on the removal of Pb(II) using Fe_3O_4/o-N-MWCNTs, SH-Fe_3O_4/o-N-MWCNTs and N_2H_4-SH-Fe_3O_4/o-N-MWCNTs ranging from 2-9 was investigated. The pH of a solution is one of the dominant parameters for the adsorption of metal ions [27]. When pH is kept below 3.3, Pb(II) mainly exists in the form of Pb^{2+} ions. Only a small fraction of Pb(II) can hydrolyse into $Pb(OH)^{+}$ when the pH is raised to 4.2–6.2, but still mainly in Pb^{2+} form. According to the solubility product constant of $Pb(OH)_2$ and the initial Pb(II) concentration, Pb(II) would start to generate $Pb(OH)_2$ which precipitate at pH 6.7 [3]. Figure 4.41 shows that the removal of Pb(II) increase with an increase in pH until pH 6 is reached then start to decrease at pH

values above 6. Maximum removal was reached at pH 6 with 86.6, 88.2 and 90.4% using Fe_3O_4/o-N-MWCNTs, SH-Fe_3O_4/o-N-MWCNTs and N_2H_4-SH-Fe_3O_4/o-N-MWCNTs, respectively.

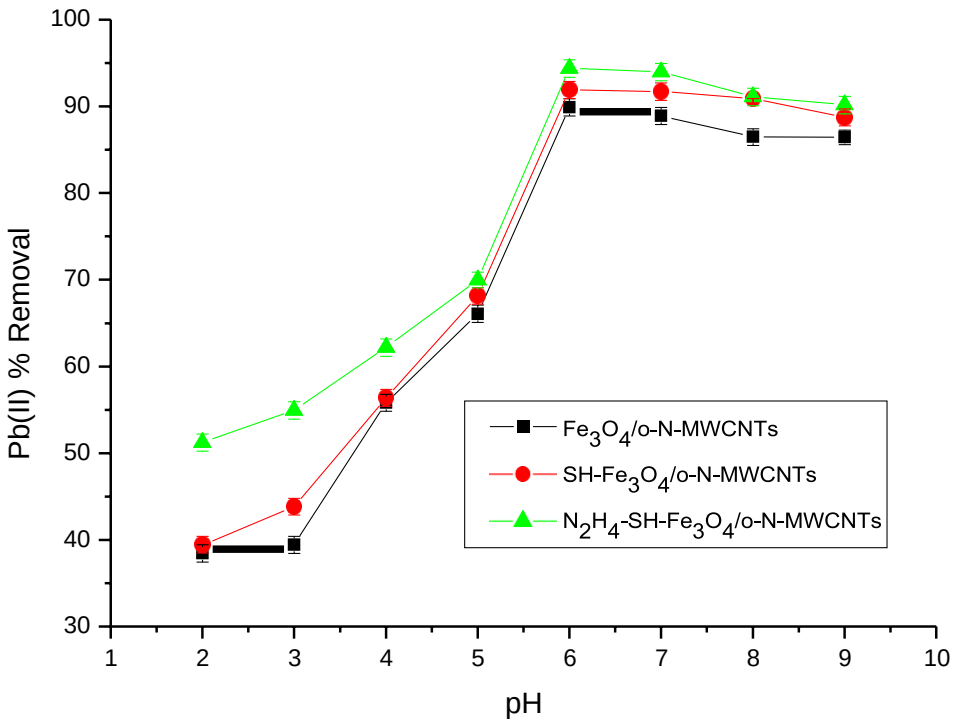

Figure 4.41: Effect of pH on Pb(II) removal by (a) Fe_3O_4/o-N-MWCNTs, (b) SH-Fe_3O_4/o-N-MWCNTs and (c) N_2H_4-SH-Fe_3O_4/o-N-MWCNTs. Experimental conditions: adsorbent dosage = 0.2 g/L, concentration = 40 mg/L, contact time = 30 minutes at room temperature and pH value 2-9.

The adsorption capacity was also observed to be at a maximum of 129.6, 130.1 and 130.8 mg/g. In this case, the hydrazine-treated nanocomposite showed greater results among the three followed by the thiol and then the iron oxide treated nanocomposite. The greater performance of the amine treated nanocomposite was further elaborated by Yang et al. [3] suggesting that this occurred because the amino groups grafted on the N_2H_4-SH-Fe_3O_4/o-N-MWCNTs were combined with hydronium ions under strongly acidic conditions, which made amino groups protonated. The protonated $-NH_3^+$ would reject Pb(II) according to the theory of the same electric charge mutual repulsion, leading to the low Pb(II) adsorption efficiencies at low pH. The H^+ concentration

decreased quickly as the pH increased from 2 to 4, and the deprotonation reaction enhanced, which made the repulsive interaction between NH_3^+ and Pb(II) weakened and the Pb(II) adsorption enhanced sharply. As the pH increased from 4 to 6, most of the adsorptive sites on the N_2H_4-SH-Fe_3O_4/o-N-MWCNTs were occupied, and the adsorption capacity of Pb(II) slightly changed. Thus, at pH 6, the Pb(II) adsorption capacity was maximum. The optimal pH was therefore chosen to be 6 and used for the continuation of the study.

4.3.3.2 Effect of contact time on the removal of Pb(II)

The effect of contact time on the removal of Pb(II) using Fe_3O_4/o-N-MWCNTs, SH-Fe_3O_4/o-N-MWCNTs and N_2H_4-SH-Fe_3O_4/o-N-MWCNTs is shown in figure 4.42 at optimum pH = 6 with 0.2 g/L adsorbent and initial Pb(II) concentration of 40 mg/L. The required time for an adsorbent to become saturated is crucial, i.e., the better the adsorbent, the faster the removal [78]. The adsorption was increasing at a fast rate from the beginning of the reaction and continued to increase rapidly with increasing contact time.

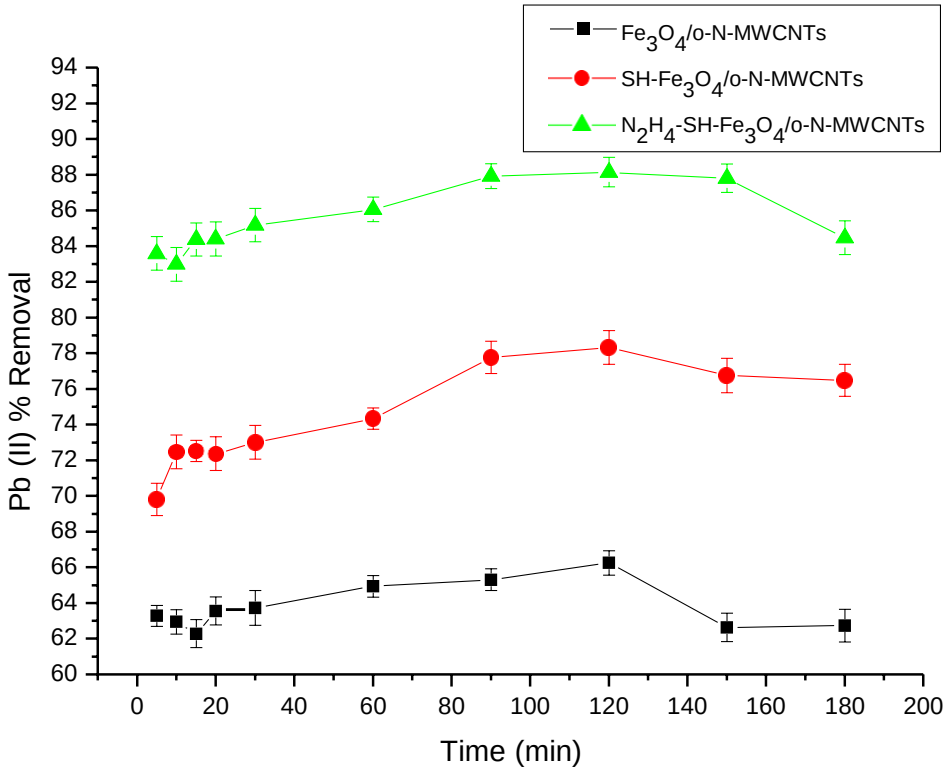

Figure 4.42: Effect of contact time on the removal of Pb(II) by (a) Fe_3O_4/o-N-MWCNTs, (b) SH-Fe_3O_4/o-N-MWCNTs and (c) N_2H_4-SH-Fe_3O_4/o-N-MWCNTs. Experimental conditions: pH = 6, adsorbent dosage = 0.2 g/L, initial concentration = 40 mg/L, contact time = 5-180 minutes at room temperature.

From the graph, the removal of Pb(II) ions increases with an increase in contact time for all the three adsorbents until equilibrium is reached at 120 minutes (maximum removal) with a slight decrease in removal afterwards. The amine treated adsorbent, N_2H_4-SH-Fe_3O_4/o-N-MWCNTs showed the greatest removal of the three materials with removal between 82.5 and 87.8%. The thiol treated adsorbent, SH-Fe_3O_4/o-N-MWCNTs also showed good results with removal between 69 and 79% as compared to the iron oxide treated adsorbents, Fe_3O_4/o-N-MWCNTs with removal between 62 and 66%. Contact time of 120 minutes was selected as the optimum time and used throughout the study. For instance, the following studies were conducted on Pb(II) removal using same experimental conditions (pH = 5-6) such as the study by Vukovic et al. (35 mg/g) [79], Laus et al. (35 mg/g) [80], Alizadeh et al. (100% removal and 450 mg/g adsorption capacity) [78], Jiang et al. (200 mg/g) [5], Wang et al. (75%) [27] and

Yang et al. (120 mg/g) [3]. The current study has the advantage of which the removal of 85% was achieved as the maximum. The 130 adsorption capacity (130 mg/g) was poor as compared to the study by Alizadeh et al. [78] and Jiang et al [5].

4.3.3.3 Effect of initial concentration on the removal of Pb(II)

Figure 4.44 shows the effect of initial concentration on the removal efficiency and adsorption capacity of Pb(II). Concentration of metal ions in solution is critical to overcome mass transfer resistance between solids and aqueous phases [3]. Figure 4.44a shows the effect of initial concentration on the removal and adsorption capacity of Pb(II) using Fe_3O_4/o-N-MWCNTs, SH-Fe_3O_4/o-N-MWCNTs and N_2H_4-SH-Fe_3O_4/o-N-MWCNTs at optimum pH = 6, contact time = 120 min and adsorbent dosage = 0.6 g/L.

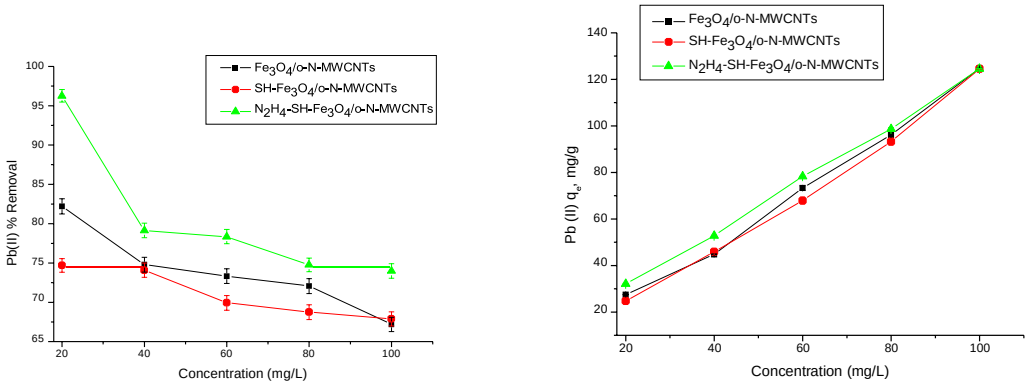

Figure 4.43: Effect of initial concentration on the removal and adsorption capacity of Pb(II) by (a) Fe_3O_4/o-N-MWCNTs, (b) SH-Fe_3O_4/o-N-MWCNTs and (c) N_2H_4-SH-Fe_3O_4/o-N-MWCNTs. Experimental conditions: pH = 6, contact time = 120 minutes, adsorbent dosage = 0.6 g/L, initial concentration = 40-100 mg/L at room temperature.

As observed from figure 4.44a, when the initial concentration of Pb(II) is increased from 20-100 mg/L, the removal decreases from 83.3, 74.9 and 97.2% to 66.3, 68 and 75.9% respectively with the amino-modified nanocomposite showing greater results followed by the iron oxide and thiol-modified nanocomposites. The results obtained using hydrazine-modified MWCNTs may be due to the greater particle size of 72.02 nm as shown from PXRD data in section 4.2.2.2. In lower initial concentrations, Pb(II)

ions could simply attach to the abundant adsorption sites on the surface of the as-prepared N-MWCNTs. Since the number of adsorption sites remains the same at higher initial concentrations (adsorbent dosage did not change), Pb(II) ions are not able to access adsorption sites and as a result, removal is reduced [78]. Unlike removal, the adsorption capacity increases with increasing initial concentration as shown in figure 4.43b which is expected. The adsorption capacity increased from 30 to 128 mg/g same as the results obtained by other authors [5,80] and higher than the maximum values obtained by Wang et al. [27] and Alizadeh et al. [78].

4.3.3.4 Effect of temperature on the removal of Pb(II)

Figure 4.44 shows the effect of temperature on the removal of Pb(II) using Fe_3O_4/o-N-MWCNTs, SH-Fe_3O_4/o-N-MWCNTs and N_2H_4-SH-Fe_3O_4/o-N-MWCNTs at optimum pH = 6, contact time = 120 min, adsorbent dosage = 0.4 g/L and initial concentration = 40 mg/L. Adsorption is primarily influenced by temperature, which increases the diffusion rate of adsorbate molecules in the internal porosity and across the external boundary layer of the adsorbent because the solution viscosity and mass transfer resistance decreases with increasing temperature [81].

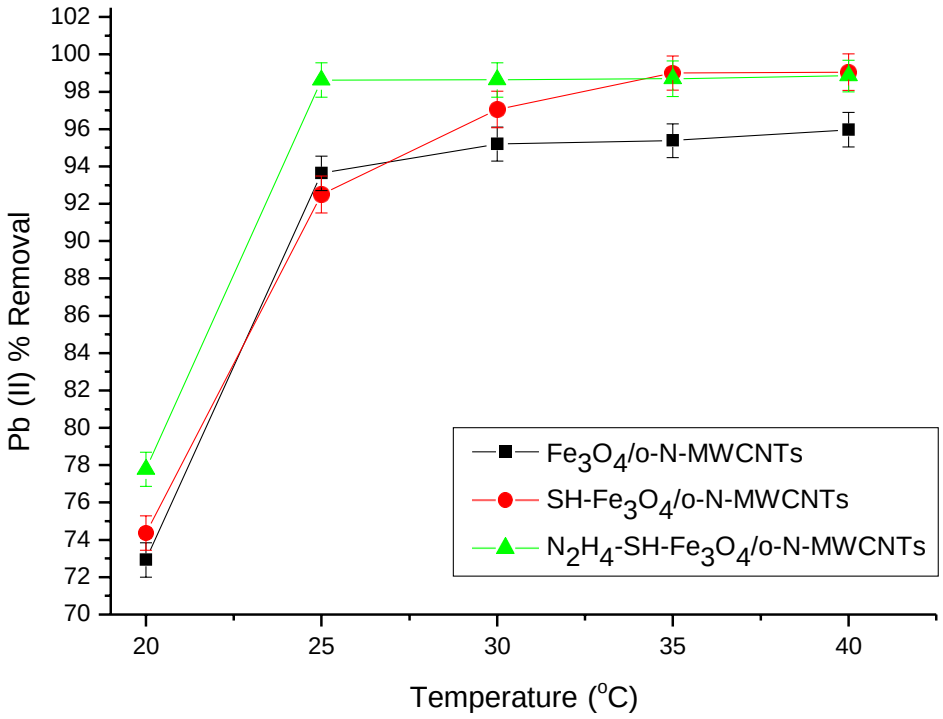

Figure 4.44: Effect of temperature on the removal of Pb(II) by (a) Fe_3O_4/o-N-MWCNTs, (b) SH-Fe_3O_4/o-N-MWCNTs and (c) N_2H_4-SH-Fe_3O_4/o-N-MWCNTs. Experimental conditions: pH = 6, contact time = 120 minutes, adsorbent dosage = 0.6 g/L, initial concentration = 40 mg/L and varied temperature from 20-40 °C.

As observed from figure 4.44, when the temperature is increased from 20-40 °C, the removal increases from 72.4, 74.1 and 76.8% to 93.2, 98.1 and 98.2% respectively. The iron oxide nanocomposite had less removal compared to the other materials and reached equilibrium at 30 °C with the removal becoming constant as the temperature increased. The thiol treated nanocomposite removal continued to increase with increasing temperature until no change was observed after reaching 35 °C while in the case of the amine treated nanocomposite, no significant change was observed from 25 °C until 40 °C. The amine treated nanocomposite showed better results as in the previously shown results for the other adsorption parameters. The same trend was also observed in the literature showing an increase in removal with increasing temperature [14,74,82]. The greater removal efficiency for all the nanocomposites at higher temperatures is due to the high thermal stability of greater than 800 °C as confirmed by the TGA analysis in section 4.2.5.2.

4.3.3.5 Adsorption kinetics of Pb(II) ions removal

As shown by the fitted curves and calculated parameters in figure 4.45 and Table 4.11, the pseudo-second order model (0.9988-0.9993) fit the experimental data better than the pseudo-first order (0.9435-0.9592) due to the observed high values of the R^2. Also, the value of calculated adsorption capacity (q_{ecal}) using pseudo-second order model for Fe_3O_4/o-N-MWCNTs (126.7 mg/g) SH-Fe_3O_4/o-N-MWCNTs (155 mg/g) and N_2H_4-SH-Fe_3O_4/o-N-MWCNTs (172.4 mg/g) are closely correlated with the experimental values compared to those of the pseudo-first order. The rate constant k_2 values were -0,01724, 0,005253 and 0,03581 g/mg/min for the adsorption of Pb(II) onto M-N-MWCNTs. The pseudo-second-order kinetic model results indicated that the adsorption of Ni(II) ions onto the nanoparticles were chemisorption controlled, suggesting the formation of chemical bonds in the adsorption process through sharing, relocation and transfer of electrons [73]. The kinetic parameters were calculated from the slope of the plot of t/q_t vs. t by linear regression analysis [79]. The results are consistent with the reports from literature [74,79].

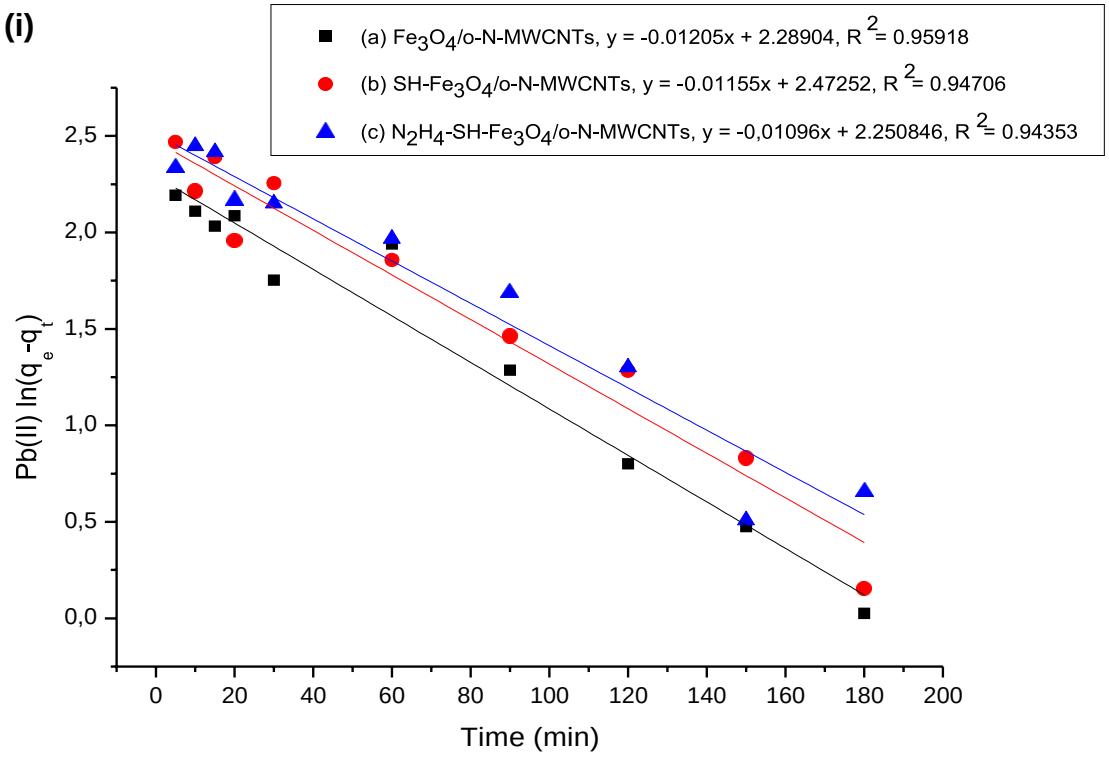

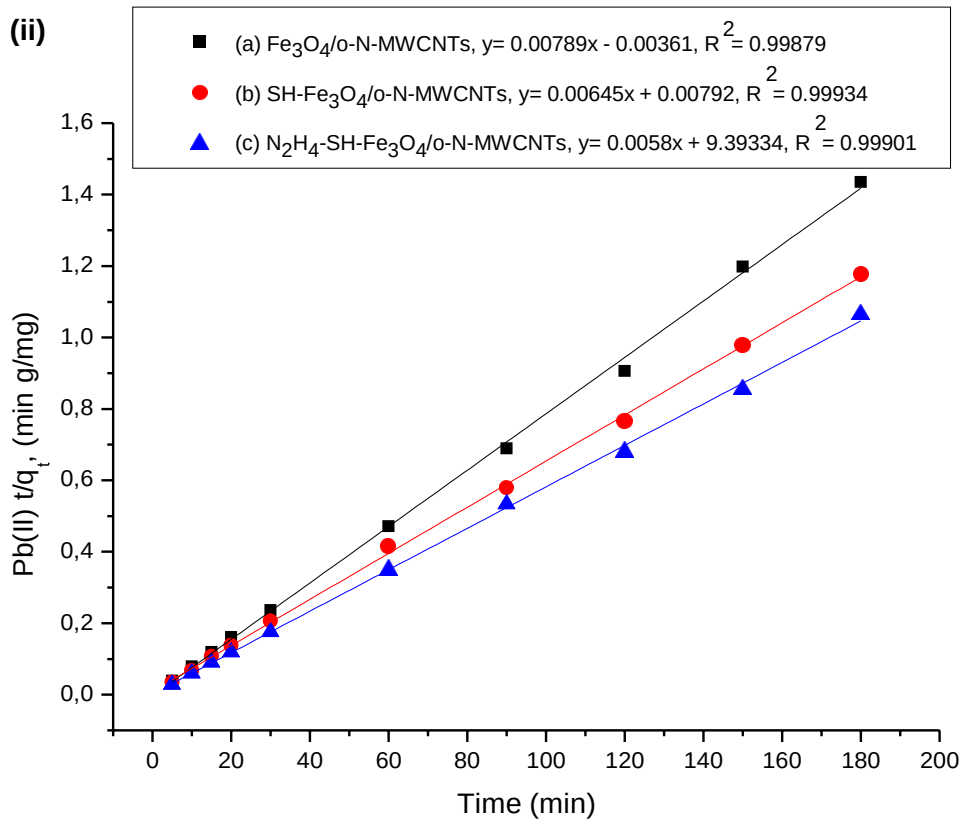

Figure 4.45: (i) Pseudo-first order and (ii) Pseudo-second order kinetic model for adsorption of Pb(II) ions by (a) Fe_3O_4/o-N-MWCNTs (b) SH-Fe_3O_4/o-N-MWCNTs and (c) N_2H_4-SH-Fe_3O_4/o-N-MWCNTs nanocomposites.

Table 4.11: The parameters calculated by kinetic models for adsorption of Pb(II) ions adsorption by f-N-MWCNTs nanocomposites

Adsorbent	Experimental q_e (mg/g)	Pseudo-first order kinetic model			Pseudo-second order kinetic model		
		$q_{e.cal}$ (mg/g)	k_1 (min^{-1})	R^2	$q_{e.cal}$ (mg/g)	k_2 (g/mg/min)	R^2
Fe_3O_4/o-N-MWCNTs	133.5	1,012	0.01205	0.9592	126,7	-0,01724	0.9988
SH-Fe_3O_4/o-	157.8	1,012	0.01155	0.9471	155,0	0,005253	0.9993

N-MWCNTs							
N_2H_4-SH-Fe_3O_4/o-N-MWCNTs	177.5	1,011	0.01096	0.9435	172,4	0,03581	0.9990

4.3.3.6 Adsorption isotherms of Pb(II) ions removal

The experimental data reveal that all the isotherms gave good linearity. Langmuir isotherm gave a better fit with Q_{max} values of 330, 179.9 and 317.5 mg/g onto Fe_3O_4/o-N-MWCNTs, SH-Fe_3O_4/o-N-MWCNTs and N_2H_4-SH-Fe_3O_4/o-N-MWCNTs respectively. The fitting results of the adsorption isotherms are listed in Table 4.12. It was demonstrated that both isotherms have high R^2 values of 0.9616, 0.9830 and 0.9895 for the Langmuir model and R^2 values of 0.9271, 0.9805 and 0.9587 for the Freundlich model. The maximum adsorption capacity from Langmuir fitting results showed a lower q_{max} value for the three adsorbents compared to Zhan et al. [14] who obtained 350.88 mg/g and higher q_{max} than Jiang et al. [5] who obtained 40 mg/g. Generally, MWCNTs are able to aggregate and form bundles by van der Waals forces in the solution due to their hydrophobic properties. These bundles lead to the formation of grooves, gaps, and inner areas. The cluster structure provides heterogeneous adsorption sites for Pb(II) [5]. For Freundlich model, the n indicates the productivity of adsorption; the adsorption is considered desirable if $1 < n < 10$ [77]. R_L values in this study were less than 1.0 and greater than zero indicating favourable adsorption. On the other hand, Freundlich adsorption isotherm constants K_F and n signify the heterogeneous adsorption capacity and adsorption intensity, respectively. These are calculated from the intercept and slope of the log q_e vs log C_e [76]. Therefore, by checking the values of the different parameters in Table 4.3.10, one can say that the adsorption of Pb(II) onto the adsorbent is better fitted to Langmuir model since the R^2 values are higher than of Freundlich model, thus indicating that Langmuir model better

describes adsorption on MWCNTs. Similarity in results was observed by Vukovic et al. [79].

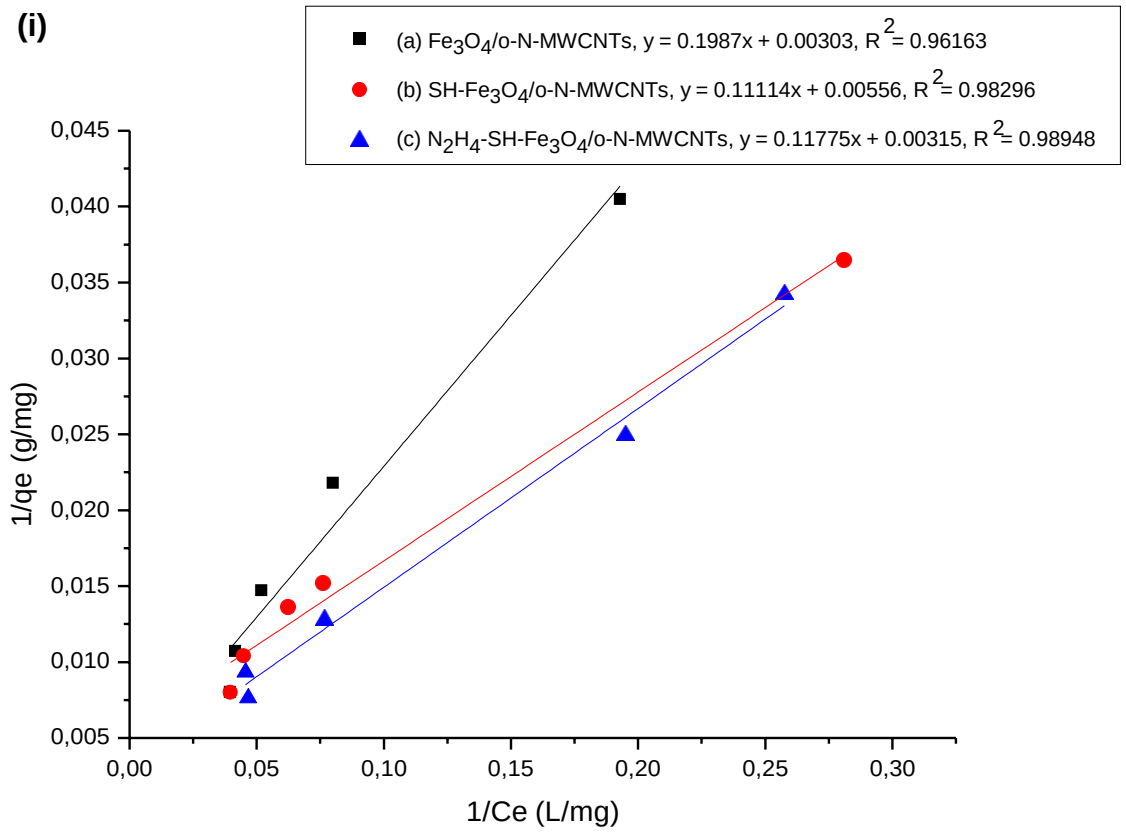

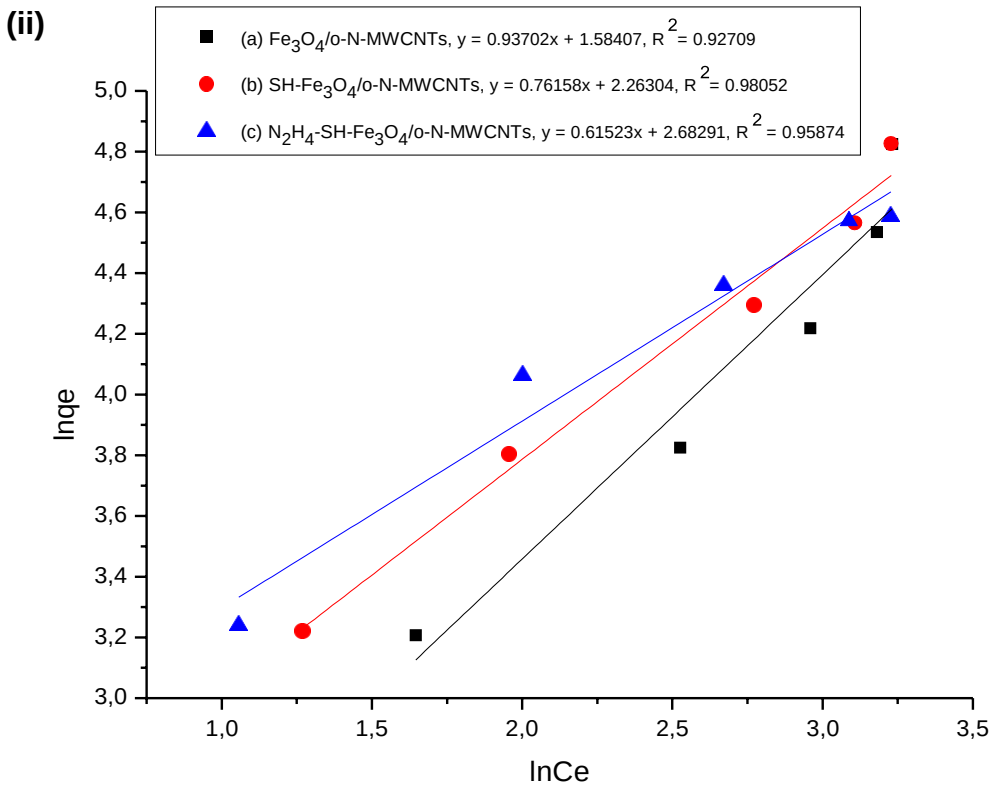

Figure 4.46: (i) Langmuir isotherm analysis and (ii) Freundlich isotherm analysis for adsorption of Pb(II) ions by (a) Fe_3O_4/o-N-MWCNTs, (b) SH-Fe_3O_4/o-N-MWCNTs and (c) N_2H_4-SH-Fe_3O_4/o-N-MWCNTs nanocomposites.

Table 4.12: Parameters calculated by isotherm models for Pb(II) adsorption by modified N-MWCNTs nanocomposites

Adsorbent	q_{max} (mg/g)	Langmuir model			Freundlich model		
		b (L/mg)	R_L	R^2	K_f (mg/g)	N	R^2
Fe_3O_4/o-N-MWCNTs	330	0.01525	0.6211	0.9616	4.875	1.067	0.9271
SH-Fe_3O_4/o-N-MWCNTs	179.9	0.05002	0.3332	0.9830	9.612	1.313	0.9805
N_2H_4-SH-Fe_3O_4/o-N-MWCNTs	317.5	0.02675	0.4831	0.9895	14.63	1.625	0.9587

Comparison with other adsorbents

The maximum adsorption capacities of Pb(II) on M-N-MWCNTs were compared with other previously used adsorbents reported in the literature as given in Table 4.13. The MWCNTs in the experiments showed higher removal efficiencies of Pb(II) than many other adsorbents, which could be attributed to their larger specific surface areas. In spite of this, MWCNTs offer a significant advantage in terms of potential applications in water and wastewater treatment since they can be separated from the solution effectively and conveniently and have higher uptake capacities than other adsorbents.

Table 4.13: The parameters calculated by isotherm models for adsorption of Pb(II) ions adsorption by f-N-MWCNTs nanocomposites

Adsorbent	Optimised parameters			Adsorption capacity q_{max} (mg/g)	References
	pH	Time (min)	Dosage (g/L)		
Graphene/polydopamine (MWCNT-PDA) aerogels	6	600	0.5	350.87	[14]
N_2H_4-SH-Fe_3O_4/o-MWCNTs	6	720	0.01	40	[5]
DETA-MWCNTs e-MWCNTs	6.2	40	0.1	54.27 40.12	[79]
CTS-ECH-TPP	5	720	1	166.94	[80]
MWCNTs/polyrhodanine	4	120	0.25	8118	[78]
Chitosan/o-MWCNTs (MHC/OMWCNTs)	5	120	0.4	116.3	[27]
MWCNTs@SiO_2-NH_2	5		Not specified	147	[3]
NiO/CNTs	5	10	Not specified	24.62	[83]
Fe_3O_4/CNTs	5	40	Not specified	21.55	[81]

MWCNTs–SeP(O)(O-t-Bu)2	5	60	0.5	156.25	[30]
Fe_3O_4/o-N-MWCNTs	6	120	0.6	330.0	This study [Pb(II)]
SH-Fe_3O_4/o-N-MWCNTs				179.9	
N_2H_4-SH-Fe_3O_4/o-N-MWCNTs				317.5	
o-MWCNTs Raw N-MWCNTs o-N-MWCNTs	5.5	80	0.30	1990 877 1720	This study [Cr(III)]
o-MWCNTs Raw N-MWCNTs o-N-MWCNTs	1.5	10	0.35	1280 962 1930	This study [Cr(VI)]
o-MWCNTs Raw N-MWCNTs o-N-MWCNTs	11	60	0.05	1370 260 5410	This study [Ni(II)]

4.3.3.7 Adsorption thermodynamics of Pb(II) ions removal

The adsorption thermodynamic studies were conducted from 288.15K to 313.15K with 40 mg/L of Pb(II) to investigate the thermodynamic parameters. Figure 4.47 shows the linear plot of $\ln K_d$ against 1/T. The values of ΔH and ΔS are evaluated from the slope and intercept [5]. The plot is linear with good correlation coefficients ($R^2 > 0.98$).

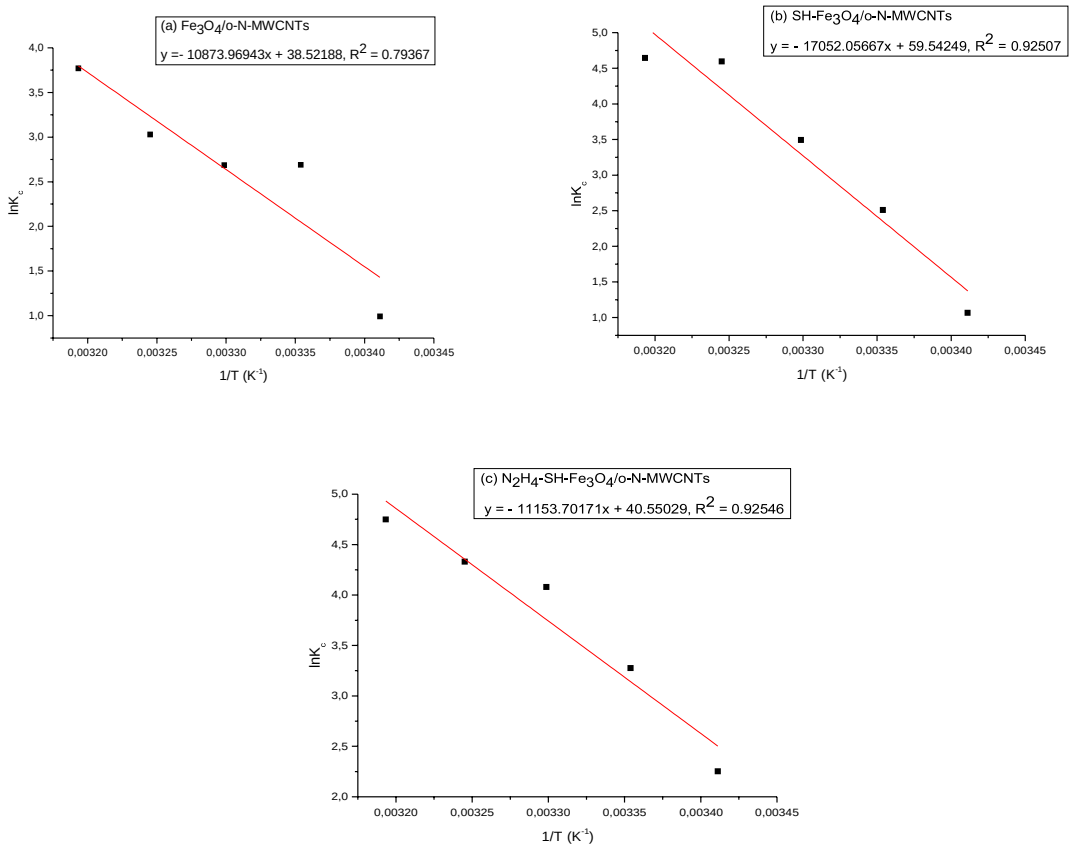

Figure 4.47: Thermodynamic analysis for adsorption of Pb(II) ions by (a) Fe_3O_4/o-N-MWCNTs (b) SH-Fe_3O_4/o-N-MWCNTs and (c) N_2H_4-SH-Fe_3O_4/o-N-MWCNTs nanocomposites.

The calculated thermodynamic parameters are displayed in Table 4.14. The negative values of ΔG in the temperature range of 298.15–313.15 K indicate that Pb(II) adsorption onto M-N-MWCNTs is spontaneous and is more favourable at higher temperatures. The positive ΔH value reveals an endothermic adsorption process and this can be supported by the increase of the adsorption capacity with elevated temperature. Besides, the positive value of ΔS indicated an increase in randomness at the solid/solution interface during the adsorption process. Also, the positive value for ΔH indicated the endothermic nature of Pb(II) adsorption by M-N-MWCNTs. In addition, positive values of ΔH implies an increase in spontaneity due to Pb(II) interaction with M-N-MWCNTs during the adsorption [25]. Konczyk et al. [30] reported

similar results for the thermodynamic parameters ΔG, ΔH and ΔS indicating the spontaneous and endothermic physisorption of Pb(II) on the used carbon nanotubes. The change of ΔG for physisorption occurs between −20 and 0 kJ/mol, while the physisorption and chemisorption occur together over the range of −20 to −80 kJ/mol, with chemisorption occurring in the range of −80 to −400 kJ/mol [5]. From this information, it can be said that the obtained ΔG values indicate that the interactions between Pb(II) and M-N-MWCNTs could be considered to undergo physisorption mechanisms. These can be explained by the fact that the functional groups (i.e., Fe_3O_4, thiol and amine), on the surface of M-N-MWCNTs can form chemical bonds with Pb(II) to increase the adsorption capacity [5]. Egbosiuba et al. [25] also reported that the values of ΔH are in the range of 1-40 kJ/mol for adsorption controlled by physisorption, while the values higher than 40 kJ/mol indicate chemisorption. Therefore, the adsorption of Pb(II) onto M-N-MWCNTs was chemisorption controlled because the obtained values of ΔH are 90.41, 141.8 and 92.73 kJ/mol by Fe_3O_4/o-N-MWCNTs, SH-Fe_3O_4/o-N-MWCNTs and N_2H_4-SH-Fe_3O_4/o-N-MWCNTs nanocomposites respectively

Table 4.14: Thermodynamic parameters for Pb(II) ions adsorption by functionalised N-MWCNTs nanoparticles at different temperatures

Adsorbent	Thermodynamic parameters			
	Temperature (K)	ΔG (kJ/mol)	ΔH (kJ/mol)	ΔS (J/mol/K)
Fe_3O_4/o-N-MWCNTs	293.15	-2.415	90.41	320.3
	298.15	-6.663		
	303.15	-7.524		
	308.15	-7.759		
	313.15	-8.251		
SH-Fe_3O_4/o-N-MWCNTs	293.15	-2.595	141.8	495
	298.15	-6.224		
	303.15	-8.806		
	308.15	-11.779		
	313.15	-12.092		

N_2H_4-SH-Fe_3O_4/o-N-MWCNTs	293.15	-3.053	92.73	337.1
	298.15	-10.599		
	303.15	-10.786		
	308.15	-11.098		
	313.15	-11.581		

4.4.3.8 Effect of competing ions on the removal of Pb(II)

Figure 4.48 shows the effect of interfering anions on the removal efficiency of Pb(II). Both natural water and industrial wastewater contain different kinds of ions and organics, which may co-exist with Pb(II) like K(I), Ca(II), Na(I) and Mg(II). The existence of these metal ions may affect the removal efficiency of lead ions in the adsorption process [3,27]. Other anions include chlorides, carbonates, humic acid, phosphates, sulphates, and nitrates just to name a few. Figure 4.48 shows the removal of Pb (II) using the three prepared adsorbents in the presence of competing ions at optimum pH, contact time, adsorbent dosage, and initial concentration. The removal of Pb(II) was evaluated in a binary-solute system and multi-solute system containing four different anions together with the metal of interest. The simulated aqueous solution contained $[Pb^{2+}]_0$ = 40 mg/L, $[Cl^-]_0$ = 355 mg/L, $[HCO_3^-]_0$ = 61.02 mg/L, $[SO_4^{2-}]_0$ = 96.06 mg/L and $[PO_4^{3-}]_0$ = 94.97 mg/L.

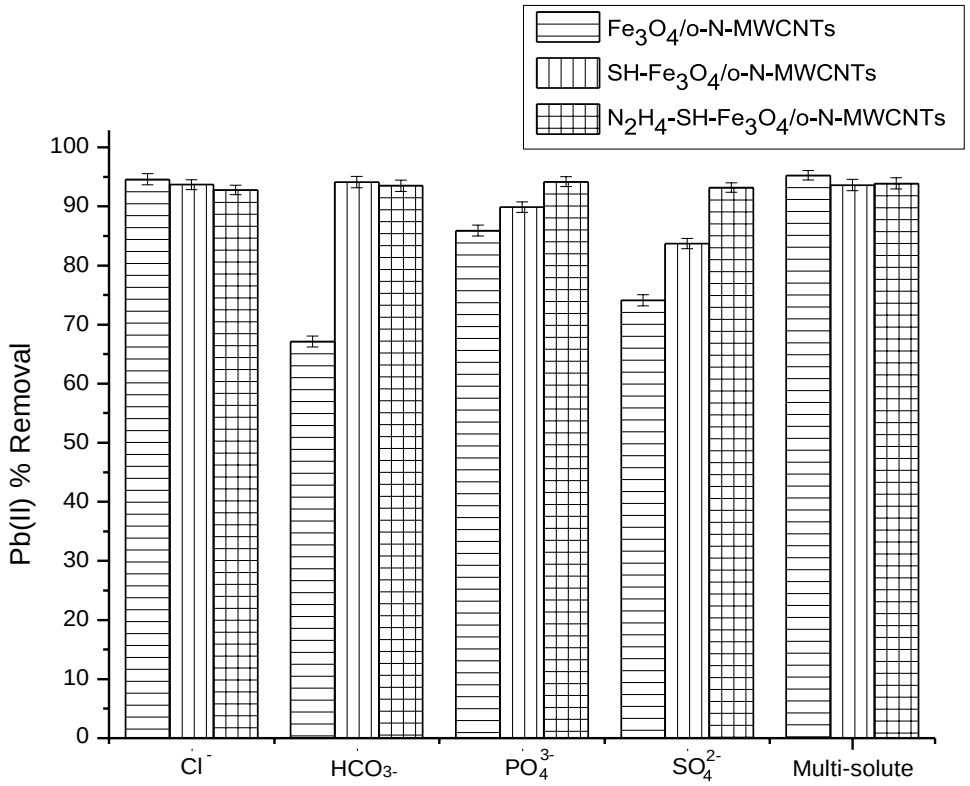

Figure 4.48: Effect of the presence of competing ions on Pb(II) removal by (a) Fe_3O_4/o-N-MWCNTs, (b) SH-Fe_3O_4/o-N-MWCNTs and (c) N_2H_4-SH-Fe_3O_4/o-N-MWCNTs. ($[PO_4^{3-}]_0$ = 94.97 mg/L, $[Cl^-]_0$ = 355 mg/L, $[HCO_3^-]_0$ = 61.02 mg/L and $[SO_4^{2-}]_0$ = 96.06 mg/L).

The removal of Pb(II) in the presence of chloride, carbonate, sulphate, and phosphate in a binary-solute system retained over 90% removal for all the adsorbents in the presence of competing ions. The results show that the presence of other anions has no greater influence on the removal of Pb(II). The thiol and amine treated nanocomposites showed no significant difference in the presence of counterions with the removal of over 80% in both binary and multi-solute systems. For all three nanocomposites, maximum removal was observed in the multi-solute system showing that the adsorbents were best suited for the removal of Pb(II) ions in water and wastewater. The presence of competing anions in a multi-solute system was found to interfere to a lesser extent as compared to a binary-solute system.

4.3.3.9 Reusability studies on Pb(II) removal

Figure 4.49 shows the effect of the reusability of the adsorbent on Pb(II) removal. For an industrial scale metal removal process, studies on the reusability of adsorbents are particularly important [30]. As shown in figure 4.49, initially the removal of Pb(II) using Fe_3O_4/o-N-MWCNTs, SH-Fe_3O_4/o-N-MWCNTs and N_2H_4-SH-Fe_3O_4/o-N-MWCNTs was 77.2, 79.3 and 88.2% respectively. After desorption studies were conducted by regenerating the adsorbents in a 5 M hydrochloric acid solution. A slight decrease in percentage removal can be observed with the percentage removal remaining over 70% for all the adsorbents. After four cycles, the percentage removal decreased by over 15% for all the nanocomposites with the amine treated nanocomposite still showing maximum removal compared to the thiol and iron oxide treated nanocomposites. The removal after four cycles was 64.2, 50.4 and 69.8% by Fe_3O_4/o-N-MWCNTs, SH-Fe_3O_4/o-N-MWCNTs and N_2H_4-SH-Fe_3O_4/o-N-MWCNTs respectively. Even though after four cycles the removal was between 50 and 60%, the adsorbents show good quality and could be helpful for practical applications.

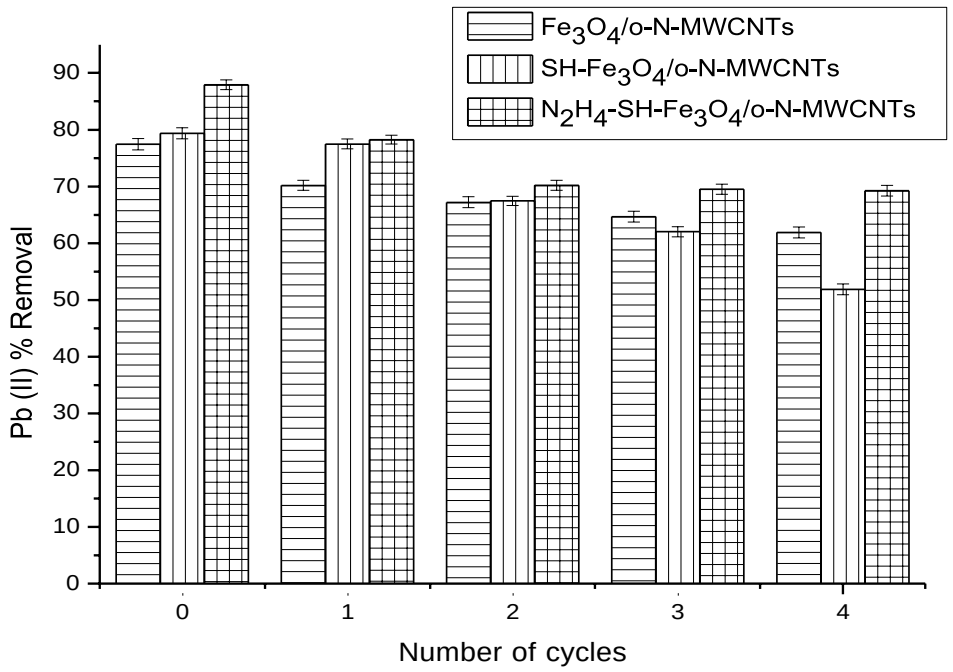

Figure 4.49: Reusability of adsorbents on Pb(II) removal by (a) Fe_3O_4/o-N-MWCNTs, (b) SH-Fe_3O_4/o-N-MWCNTs and (c) N_2H_4-SH-Fe_3O_4/o-N-MWCNTs).

4.3.4 Isotherm analysis of chromium(VI), nickel(II) and lead(II) ions

4.3.4.1 Effect of initial concentration on the removal and adsorption capacity of Cr(VI), Ni(II) and Pb(II) ions on hydrazine and triethylenetetramine-substituted SH-Fe_3O_4/o-N-MWCNTs nanocomposites

In relation to the study conducted by Jiang et al. [5], the same procedure was followed for the preparation of the adsorbents at the same experimental conditions. The relationship between the removal efficiencies and adsorption capacities of Cr(VI), Ni(II) and Pb(II) is presented in figure 4.51. The removal of the three metal ions increased with increasing initial concentration. When the concentration was varied from 20-250, 20-120 and 20-100 mg/L, the removal decreased from 93%, 99.9% and 84% to 84, 99.9 and 65% for chromium, nickel and lead respectively onto the hydrazine-functionalised SH-Fe_3O_4/o-N-MWCNTs with the adsorption capacity increasing by approximately 500 mg/g. However, the existing research has a lower Pb(II) 135 mg/g adsorption capacity in comparison to 196 mg/g obtained by Jiang et al. [5] under the same conditions.

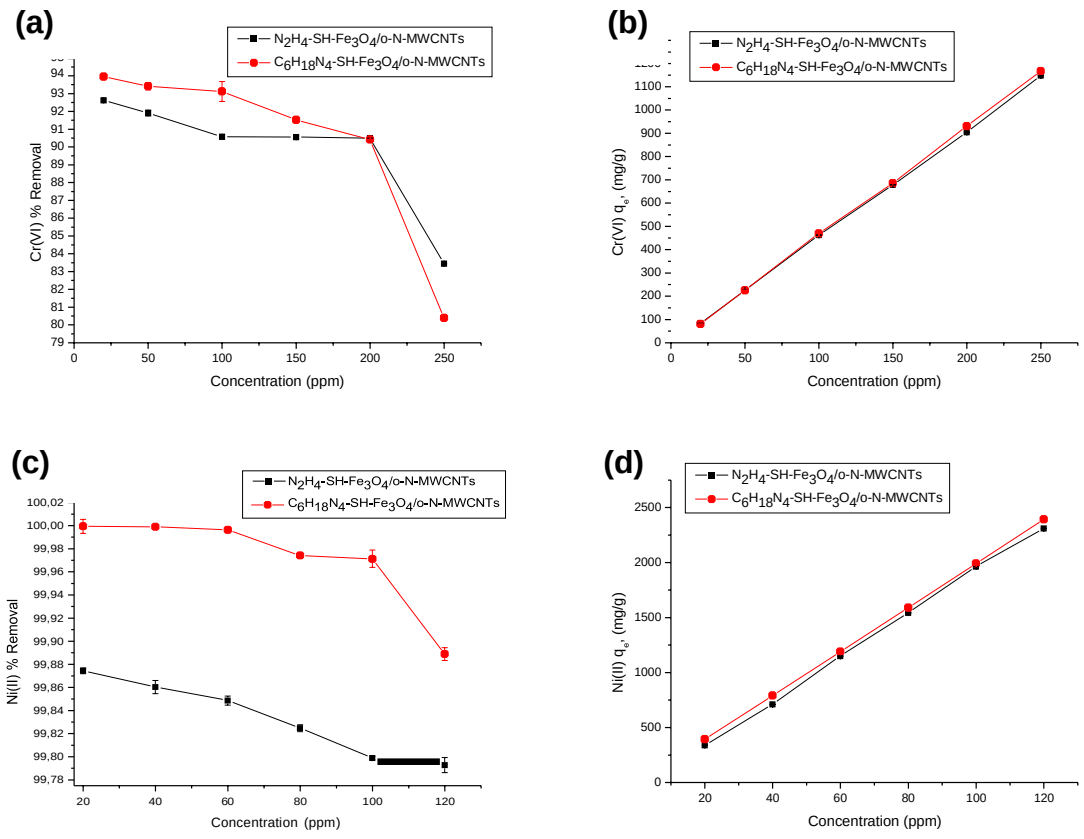

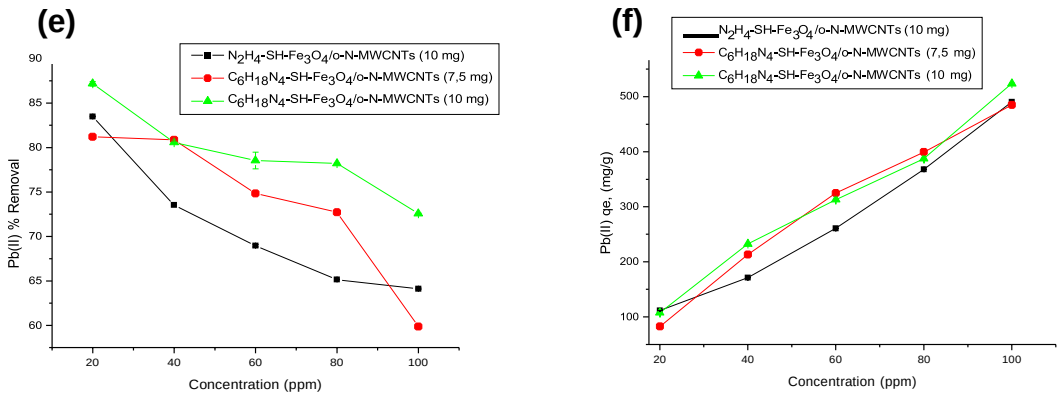

Figure 4.50: Effect of concentration on the (a) removal and (b) adsorption capacity of Cr(VI), Ni(II) and Pb(II) onto hydrazine and TETA-functionalised SH-Fe_3O_4/o-N-MWCNTs at specific optimum conditions with adsorbent dosage of 0.2 g/L.

The removal efficiency, as well as the adsorption capacity onto the TETA-functionalised SH-Fe_3O_4/o-N-MWCNTs for Cr(VI), Ni(II) and Pb(II) metal ions, showed the same trend as that onto hydrazine-functionalised SH-Fe_3O_4/o-N-MWCNTs with an increase in the removal of up to 2%, 0.08% and 10% respectively. A recent study by Qiao et al. [45] concluded that when the initial concentration was low, metal ions could react with enough active sites; therefore, the removal process was less affected by initial concentration. With the increase in concentration, the active sites tend to gradually become saturated, and the adsorption capacity was able to reach equilibrium accordingly.

4.3.4.2 Adsorption isotherm on the removal of Cr(VI), Ni(II) and Pb(II) ions onto hydrazine and triethylenetetramine-substituted SH-Fe_3O_4/o-N-MWCNTs nanocomposites

The parameters and correlation coefficients of the Langmuir and Freundlich models are listed in Table 4.15. It indicates that the values of n are bigger than 1, suggesting that Cr(VI), Ni(II) and Pb(II) are favourably adsorbed by the M-N-MWCNTs as shown in figure 4.51. This was further explained by Luo et al. [16] that the higher value of n suggests the formation of stronger bonds between heavy metal ions and M-N-MWCNTs adsorbents. Based on q_{max} value, the adsorption process using hydrazine-

functionalised SH-Fe_3O_4/o-N-MWCNTs nanocomposite is very good because it has the highest maximum monolayer adsorption capacity (q_{max}) values for Cr(VI) and Pb(II) ions than the TETA-functionalised SH-Fe_3O_4/o-N-MWCNTs nanocomposite. The opposite was observed for Ni(II). Higher K_L values indicate strong adsorbate-adsorbent interaction while smaller K_L values indicate weak interaction between adsorbate molecule and adsorbent surface [84]. High correlation coefficients for Langmuir models were found to be greater than those obtained from Freundlich model using both adsorbents onto Cr(VI) informing that N_2H_4-SH-Fe_3O_4/o-N-MWCNTs and $C_6H_{18}N_4$-SH-Fe_3O_4/o-N-MWCNTs are well represented by Langmuir isotherm assuming a monolayer coverage of the adsorbate over a homogeneous adsorbent surface [47]. R^2 values were also found to be better fitted with Langmuir model for Pb(II) adsorption using the hydrazine-functionalised SH-Fe_3O_4/o-N-MWCNTs and adsorption onto the TETA-functionalised SH-Fe_3O_4/o-N-MWCNTs were better fitted to Freundlich model with higher R^2 values which meet the heterogeneous adsorption process [47]. Ni(II) adsorption was better fitted to Freundlich isotherm based on the R^2 values. Since n indicates the productivity of adsorption, the adsorption is considered desirable if 1 < n < 10 but the Ni(II) values were both less than 1 and greater than 10 assuming a non-desirable state [77].

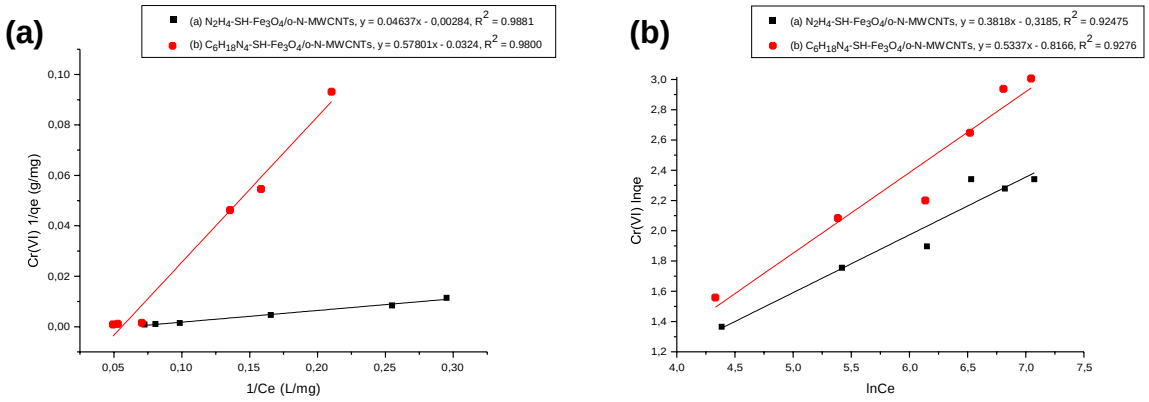

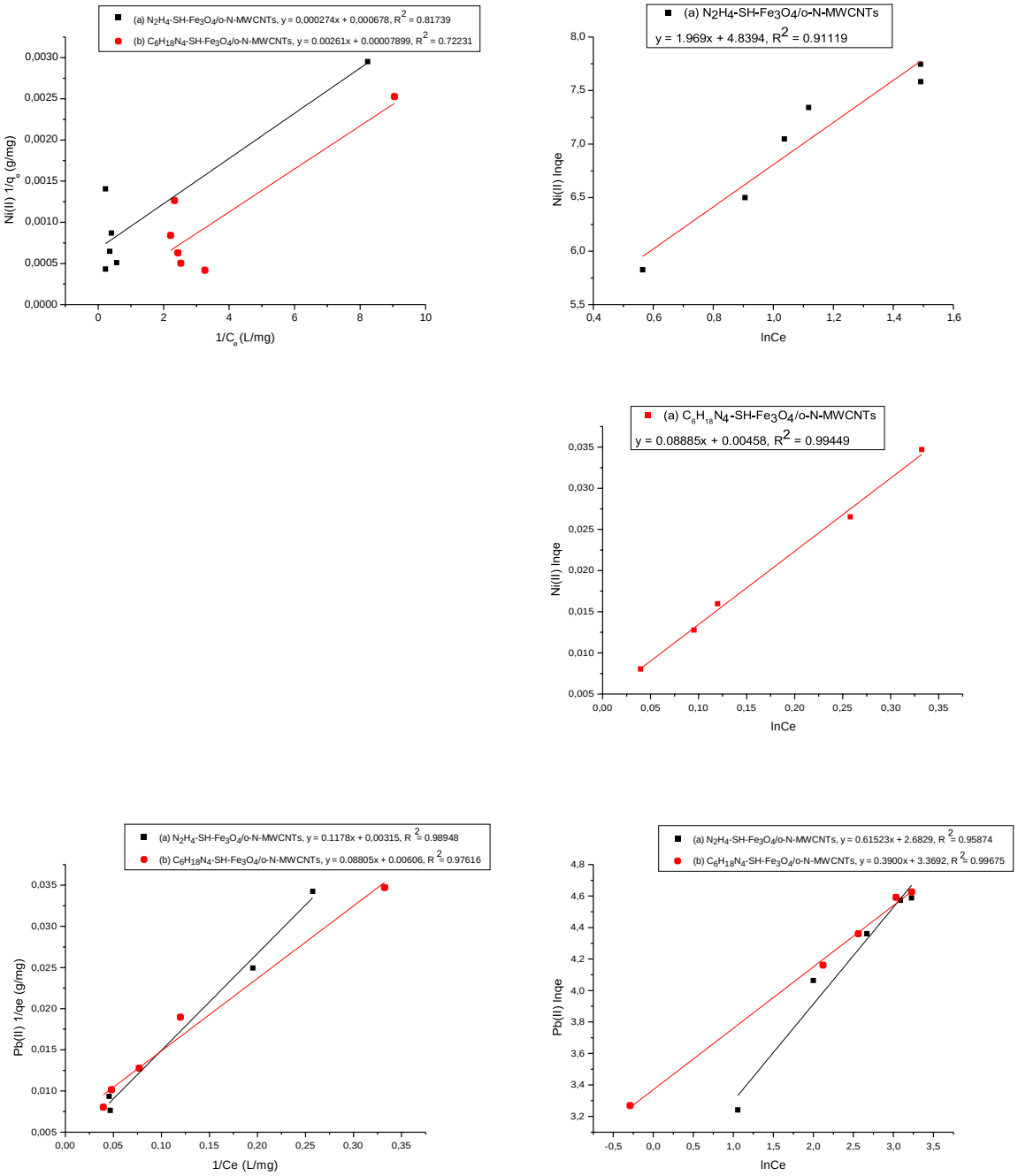

Figure 4.51: (i) Langmuir isotherm analysis and (ii) Freundlich isotherm analysis on adsorption of Cr(VI), Ni(II) and Pb(II) ions onto (a) hydrazine-functionalised SH-Fe_3O_4/o-N-MWCNTs and (b) TETA-functionalised SH-Fe_3O_4/o-N-MWCNTs nanocomposites

Table 4.15: Equilibrium adsorption isotherm parameters of Cr(VI), Ni(II) and Pb(II) onto hydrazine and TETA-functionalised SH-Fe_3O_4/o-N-MWCNTs nanocomposites

Isotherm	Equation	N_2H_4-SH-Fe_3O_4/o-N-MWCNTs			$C_6H_{18}N_4$-SH-Fe_3O_4/o-N-MWCNTs		
		Cr(VI)	Ni(II)	Pb(II)	Cr(VI)	Ni(II)	Pb(II)
Langmuir	q_{max} (mg/g)	352	1470	317.5	30.9	12700	165
	b (L/mg)	0.0612	2.47	0.02674	0.0561	0.0303	0.06883
	R_L	0.246	0.0198	0.4832	0.263	0.623	0.2665
	R^2	0.9881	0.8174	0.9895	0.9800	0.7223	0.9761
Freundlich	K_f (mg/g)	0.7272	126.4	14.63	0.4419	1.005	29.06
	N	2.619	0.5079	1.625	1.874	11.25	2.564
	R^2	0.9248	0.9276	0.9587	0.9276	0.9945	0.9968

As compared with the results of Fe_3O_4/o-N-MWCNTs and SH-Fe_3O_4/o-N-MWCNTs nanocomposites, the amount of Cr(VI), Ni(II) and Pb(II) adsorbed progressively increased with large number of functional groups added. In addition, amino groups (hydrazine and triethylenetetramine) were grafted on the surface of SH-Fe_3O_4/o-N-MWCNTs nanocomposite for enhancement of adsorption capabilities. Therefore, amine groups play an important role in the removal of Cr(VI), Ni(II) and Pb(II). The removal process of the metals is related to the surface chemistry of functionalised MWCNTs.

4.4 SURFACE AND GROUNDWATER SAMPLE ANALYSIS

4.4.1 Physico-chemical properties of the collected surface and groundwater samples

Table 4.16 indicates the acceptable limits of toxic metals in drinking water set by national and international organisations. The table also shows the physical and chemical parameters of the collected surface and groundwater.

Table 4.16: Surface and groundwater contaminants and maximum permissible limit set by different national and international organisations.

Sample names	Physical parameters	Chemical parameters			
	Conductivity (mS/m)	pH	Total Cr (mg/L)	Pb(II) (mg/L)	Ni(II) (mg/L)
SANS 241 [86,87]	≤ 170	≥ 5 to ≤ 9.7	≤ 0.05	≤ 0.01	≤ 0.07
USEPA [88,89]	Not stated	6.5 -8.5	≤ 0.05	≤ 0.015	≤ 0.1
WHO [40,90]	≤ 250	≥ 6.5 to ≤ 8.5	≤ 0.05	≤ 0.01	≤ 0.07

The metal ion concentrations and significant physicochemical parameters of all water samples (river and borehole) are presented in figure 4.48 and Table 4.17 respectively. Table 4.17 shows the physical and chemical parameters of the collected surface and groundwater before analysis or nanocomposite treatment. As discussed in section 3.7.1, water samples were collected along the Steelpoort and Olifants Rivers and at a borehole in the Sekhukhune district namely Burgersfort and Steelpoort. Samples of both ground and surface water were taken from nearby water resources that are used for domestic purposes by local communities.

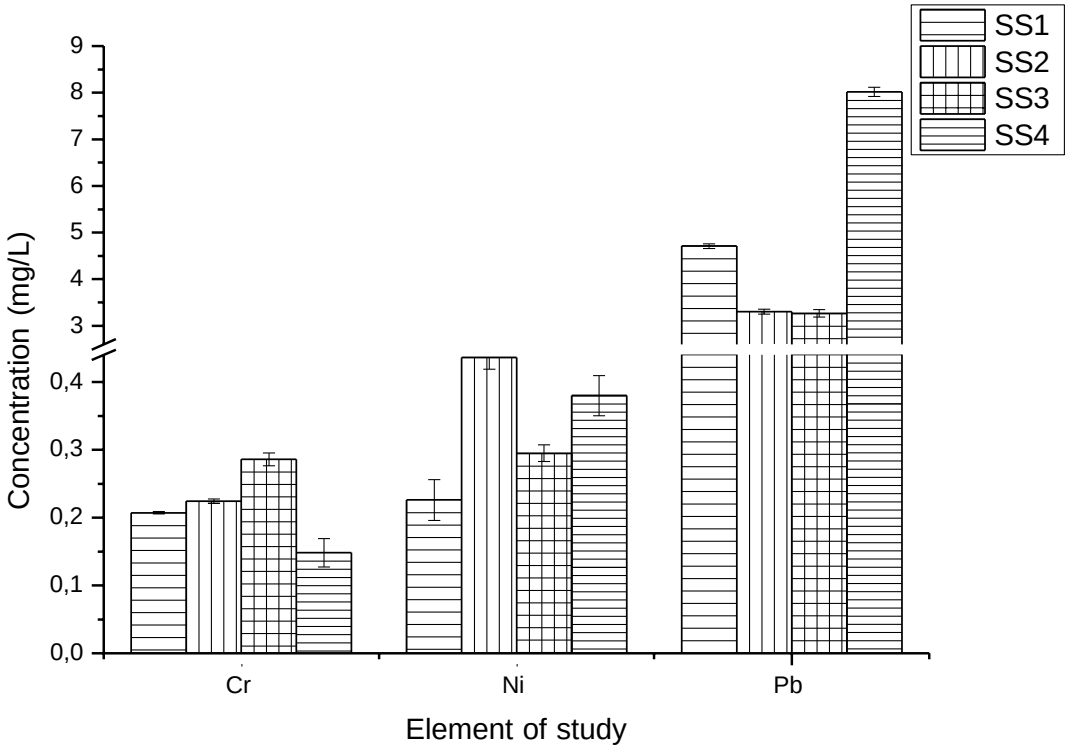

Figure 4.52: Toxic element content in surface and groundwater samples

Table 4.17: Analysis of surface and groundwater samples before nanocomposite treatment

Sampling Location	Conductivity (mS/m)	pH	Concentration (mg/L)		
			Total Cr	Pb	Ni
Steelpoort^{SS1}	79	8.49	0.207 ± 0.0028	4.71 ± 0.071	0.226 ± 0.071
Steelpoort^{SS2}	98	8.86	0.224 ± 0.0042	3.30 ± 0.40	0.436 ± 0.081
Olifants^{SS3}	85	8.67	0.286 ± 0.013	3.27 ± 0.82	0.295 ± 0.018
Burgersfort^{SS4} 75meters	43	7.69	0.148 ± 0.029	8.02 ± 1.02	0.380 ± 0.07

SS: Sampling site, Steelpoort^{SS1} (upstream river), Steelpoort^{SS2} (midstream river), Olifants^{SS3} (downstream of Steelpoort River) and Burgersfort^{SS4} (borehole)

4.4.1.1 Physical parameters

Electrical conductivity

Electrical conductivity measures the ability of water to conduct an electrical current and indicates the amount of total dissolved salts in the system which is an acceptable indicator for water quality [91,92]. The conductivity of the surface and groundwater samples ranged from 43 to 98 mS/m and similarly was within standards set by the SANS (≤ 170), WHO (≤ 250) and there is no stated limit in the USEPA. From the measured data, the electrical conductivity of surface water (river water) from all three sampling sites was greater than the groundwater samples (borehole water). EC values exceeding 500 µS cm^{-1} indicate that groundwater is likely polluted, although values as high as 2000 µS cm^{-1} may be acceptable for irrigation water [93].

4.4.1.2 Chemical parameters

pH

Acidity levels (pH) of the ambient media (water) are a key indicator of the extent of metal enrichment, affecting everything from drinking water to aquaculture growth. The pH of an environment is the most significant factor in determining how metals behave. The most stable and important metal complexes are those that contain sulfates, fluorides, chlorides and phosphates below pH 7, while metal complexes that contain carbonates and hydroxides gain importance above pH 6-8. Contrarily, oxyanions of arsenic, molybdenum, selenium and chromium tend to be desorbed from hydrous ferric oxide (HFeO) with increasing pH because of competition between the oxyanions and OH-ions for sorption sites. Moreover, most minerals containing metals are most soluble under acidic conditions, decreasing with increasing pH [94]. As shown in Table 4.16, the water samples had pH values varying between 7.69 and 8.86. The SANS [86,87], USEPA [86,88,89] and WHO [86,89,90] standards stated that the pH of drinking water should be in the pH ranges of 5-9.7, 6.5–8.5 and 6.5–8.5, respectively. The pH values of all water samples fell within the recommended range determined by the SANS, USEPA and WHO (Table 4.17).

4.4.2. Toxic element analysis of the collected surface and groundwater samples

Metal ion concentration

The concentration of toxic elements in the water samples (river and borehole) taken from the Sekhukhune district area and the permissible limits set by the SANS, USEPA and WHO for these metals are represented in Table 4.17. Elements of interest (chromium, nickel and lead) were detected in all water samples. As shown in figure 4.52, the results obtained from this study showed overall concentrations of total Cr, Ni and Pb. After sample analysis, the analytical data were assessed and related with the water quality guidelines. The mean concentration followed the sequence: Pb > Ni > Cr, moreover, the concentration of each element (total Cr, Ni and Pb) was higher than the permissible limit set by SANS (0.05, 0.07 and 0.01 mg/L), USEPA (0.05, 0.1 and 0.015 mg/L) and WHO (0.05, 0.07 and 0.01 mg/L) for drinking water.

4.4.2.1 Chromium results

Chromium levels varied from 0.207 to 0.286 mg/L in the Steelpoort and Olifants River with mean values of 0.207, 0.224 and 0.286 mg/L at SS1, SS2 and SS3. At SS4 the mean concentration was 0.148 mg/L in a borehole at Burgersfort which was above the maximum admissible limit of Cr in drinking water (0.05 mg/L). All the analysed samples contain chromium levels above the maximum admissible limit (0.05 mg/L) set by the SANS, USEPA and WHO, with the highest level of chromium recorded for samples from downstream of the Steelpoort River with a mean concentration of 0.286 mg/L and the lowest level recorded (0.148 mg/L) from Burgersfort borehole. According to the typical surface water and groundwater, the waters of these sites were slightly enriched in metal constituents. Moreover, Cr concentrations in the stream waters of sampling site 2 (SS2) were slightly higher than the concentrations of 0.06 mg/L reported by Magala for Aquatic Health Assessment of the Steelpoort River System (doctoral dissertation) at the same location in 2014 [90]. This indicated that surface and groundwater resources at Steelpoort River and boreholes could be significantly contaminated.

Table 4.18 shows the F-AAS results of the water samples after treatment with three nanocomposites. The nanocomposites were selected based on their higher removal efficiencies as observed from the spiked solutions in comparison to the oxidised and iron oxide functionalised nanocomposites. For all the nanocomposite materials, the final concentration of chromium species conducted at optimum conditions was measured below the detection limits (< 0.001 mg/L) in all samples after nanocomposite treatment. The results suggest that Cr concentration was reduced to permissible limits for both surface and groundwater.

Table 4.18: Analysis of surface and groundwater samples after nanocomposite treatment

Sampling Location	Total Cr, Concentration (mg/L)			
	Initial (C_o)	Final (C_e) nanocomposite[1]	Final (C_e) nanocomposite[2]	Final (C_e) nanocomposite[3]
Steelpoort^{SS1}	0.207	< 0.001	< 0.001	< 0.001
Steelpoort^{SS2}	0.224	< 0.001	< 0.001	< 0.001
Steelpoort^{SS3}	0.256	< 0.001	< 0.001	< 0.001
Burgersfort^{SS4} 75meters	0.148	< 0.001	< 0.001	< 0.001

SS: Sampling site, Steelpoort^{SS1} (upstream river), Steelpoort^{SS2} (midstream river), Olifants^{SS3} (downstream of Steelpoort River) and Burgersfort^{SS4} (borehole), Nanocomposite^{1}: SH-Fe_3O_4/o-N-MWCNTs, Nanocomposite^{2}: N_2H_4-SH-Fe_3O_4/o-N-MWCNTs and Nanocomposite^{3}: $C_6H_{18}N_4$-SH-Fe_3O_4/o-N-MWCNTs

4.4.2.2 Nickel results

The concentrations of nickel in the water samples at SS1, SS2, SS3 and SS4 were 0.226, 0.436, 0.295 and 0.380 mg/L, respectively. These values are above the permissible limit set by the SANS (0.07 mg/L), USEPA (0.1 mg/L) and WHO (0.07 mg/L). Nickel was detected at all sampling sites with a mean concentration of 0.319 mg/L at Steelpoort River and 0.380 mg/L at Burgersfort borehole. The highest level of nickel was recorded for samples from midstream of Steelpoort River with a mean

concentration of 0.436 mg/L and the lowest (0.226 mg/L) was recorded upstream of the Steelpoort River.

Figure 4.53(a and b) illustrates the results obtained from F-AAS analysis using two nanocomposites at room temperature (25 °C) and optimum temperature (40 °C). The final concentrations figure 4.53a after treatment for some of the sampling sites was above and some below the permissible limit using SH-Fe_3O_4/o-N-MWCNTs.

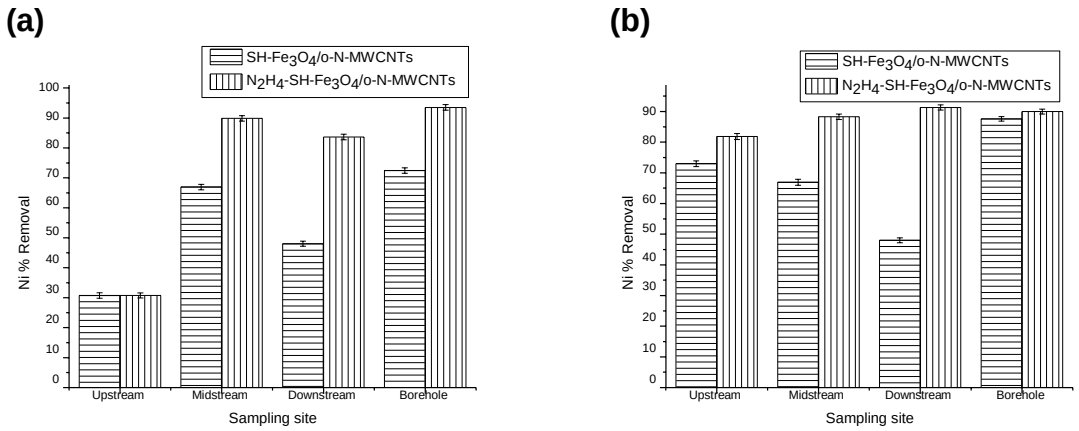

Figure 4.53: Effect of SH-Fe_3O_4/o-N-MWCNTs and N_2H_4-SH-Fe_3O_4/o-N-MWCNTs on the removal of Ni. Experimental conditions: pH =11, dosage = 2.5 mg/50 mL, concentration = 0.226-0.436 mg/L, contact time = 120 minutes and temperature = 25°C (a) and 40°C (b).

Different results were obtained after treatment with N_2H_4-SH-Fe_3O_4/o-N-MWCNTs and $C_6H_{18}N_4$-SH-Fe_3O_4/o-N-MWCNTs nanocomposites with concentrations of nickel measured below the detection limits. In comparison, figure 4.53b showed a better reduction. The final concentration was reduced especially with nanocomposite 2 (N_2H_4-SH-Fe_3O_4/o-N-MWCNTs) as compared to nanocomposite 1 (SH-Fe_3O_4/o-N-MWCNTs) with concentrations of (0.051 and 0.047) SS1, (0.043 and 0.04) SS2, (0.0457 and 0.023) SS3 and (0.025 and 0.001) SS4 respectively at 25 and 40 °C for N_2H_4--SH-Fe_3O_4/o-N-MWCNTs. Concentrations of permissible limits were obtained after treatment with $C_6H_{18}N_4$-SH-Fe_3O_4/o-N-MWCNTs nanocomposite with measured concentrations of < 0.001 mg/L (below detection limit) of nickel.

4.4.2.3 Lead results

Lead is a toxic and quite common metal. It occurs in the environment mainly as Pb^{2+} [95]. Kacmaz et al. [95] reported that both surface water and groundwater rarely contain Pb over 10 µg/L. However, in a Pb mineralisation area, the concentration of Pb may be ten-fold that of an unmineralised area. Additionally, depending on the proximity to sources, elevated Pb concentrations in river water are expected. In this study, a maximum level of Pb (8.017 mg/L) was found at SS4 in borehole drinking water from Burgersfort household. Lead concentrations from the Steelpoort River were found to be 4.709, 3.301 and 3.268 mg/L at SS1, SS2 and SS3 respectively. All the analysed samples were above the maximum permissible limit in drinking water set by the SANS (0.01 mg/L), USEPA (0.015 mg/L) and WHO (0.01 mg/L). The mean value of lead from all sampling sites ranged from 3.301 to 8.017 mg/L with the highest concentration recorded at Burgersfort borehole and the lowest at the Steelpoort River, midstream. The level of concentration for Pb was found to be higher at SS2 by 10 folds as compared to literature from the same sampling site. The study conducted by Magala [91] found the concentration of Pb to be below the detection limit with values of < 0.001 mg/L as compared to the values measured in this study, which exceed the permissible guidelines.

Table 4.19: Analysis of surface and groundwater samples after nanocomposite treatment

Sampling Location	Pb, Concentration (mg/L)			
	Initial (C_o)	Final (C_e) Nanocomposite[1]	Final (C_e) Nanocomposite[2]	Final (C_e) Nanocomposite[3]
Steelpoort^{SS1}	4.709	1.073	0.999	< 0.001
Steelpoort^{SS2}	3.301	0.617	0.499	< 0.001
Steelpoort^{SS3}	3.268	0.573	0.0482	< 0.001
Burgersfort^{SS4} 75meters	8.019	0.539	0.550	< 0.001

SS: Sampling site, Steelpoort^{SS1} (upstream river), Steelpoort^{SS2} (midstream river), Steelpoort^{SS3} (downstream river) and Burgersfort^{SS4} (borehole), Nanocomposite[1]: SH-Fe_3O_4/o-N-MWCNTs, Nanocomposite[2]: N_2H_4-SH-Fe_3O_4/o-N-MWCNTs, Nanocomposite[3]: $C_6H_{18}N_4$-SH-Fe_3O_4/o-N-MWCNTs.

A similarity in results after F-AAS analysis of Pb after the water samples were treated with three nanocomposites was observed for nanocomposites 1 and 2. As illustrated in both figure 4.55 (a and b), the final concentration of Pb was reduced after treatment with SH-Fe_3O_4/o-N-MWCNTs and N_2H_4-SH-Fe_3O_4/o-N-MWCNTs with concentration still above the permissible limits. Better reduction was observed for removal onto nanocomposite 3. Concentrations of Pb were below the detection limit as indicated in Table 4.19 after treatment with $C_6H_{18}N_4$-SH-Fe_3O_4/o-N-MWCNTs nanocomposite at both room and obtained optimum temperatures.

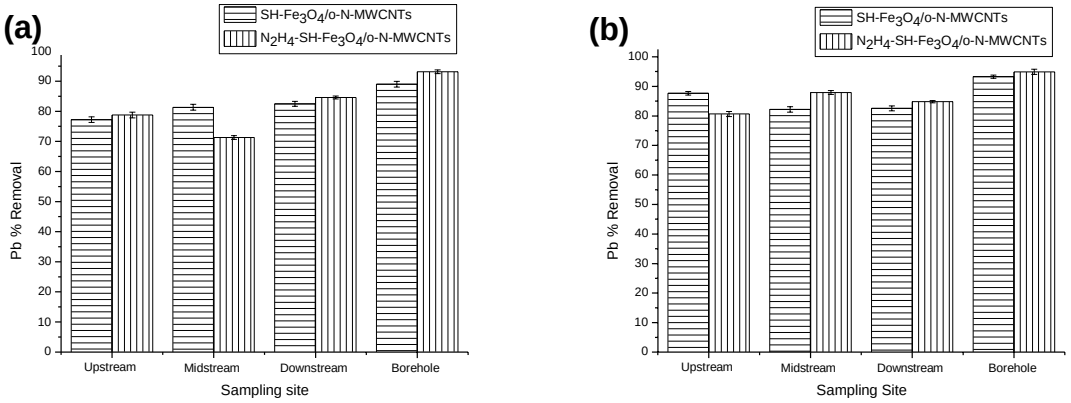

Figure 4.54: Effect of SH-Fe_3O_4/o-N-MWCNTs and N_2H_4-SH-Fe_3O_4/o-N-MWCNTs on the removal of Pb. Experimental conditions: pH = 6, dosage = 0.6 g/L, concentration = 3.301-8.017 mg/L and contact time = 120 minutes and temperature = 25°C (a) and 40°C (b).

The obtained results indicate that both the surface and groundwater in the Sekhukhune area should be treated before consumption due to the contamination of toxic elements. Moreover, the sampled borehole at Driekop (Burgersfort) was highly contaminated with toxic levels of lead ions and hence not suitable for human consumption. Studies conducted by Mathipa [95] and Magala [91] reported an increase in the level of toxic elements in surface water which may be due to contamination by effluents from surrounding mines. In the study by Mathipa [96] for analysis of bio-physicochemical quality of surface and groundwater in the Tubatse Municipality, chromium concentrations were found in the range of (< 0.001 – 0.45 mg/L). The aquatic health assessment of the Steelpoort river system study conducted

by Magala [91] indicated chromium levels of 0.007-0.06 mg/L due to effluent emanating from various chrome mines and smelters within the study area. Pb levels of < 0.001 which was below detection limits were also observed to be lower than the concentrations in this study. Other toxic elements in the area were also observed at high levels. As an example, contamination of groundwater by arsenic and other toxic elements due to operational activities of Foskor phosphate mines downstream of Greater Letaba was reported by Letsoalo et al. [97]. These reports support findings in the current study.

4.4.3 Reusability of adsorbent on samples surface and groundwater

Figure 4.55 shows the effect of reusability of the adsorbent on the removal efficiency of Cr(III), Cr(VI), Ni(II) and Pb(II). The use of the adsorbent multiple times is regarded as an important factor to determine whether the adsorbent can be widely used [9]. The effectiveness of the adsorption process is attributed to the fact that the adsorbent can be repeatedly re-used in industrial applications [42]. The removal of Cr, Ni and Pb are shown in figure 4.55. After regeneration with HCl solution, the percentage removal for chromium was reported as 100% using optimum conditions for both Cr(III) and Cr(VI) for the first cycle. After four cycles, the nanoadsorbents could still adsorb 100%.

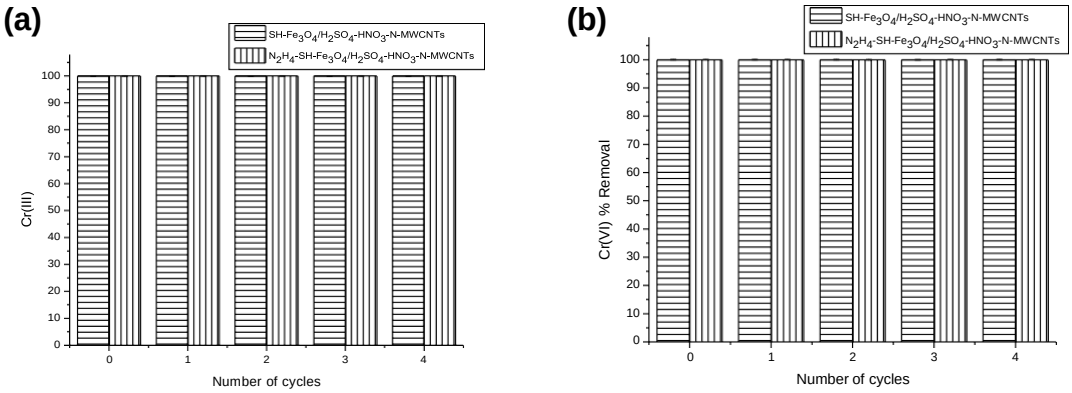

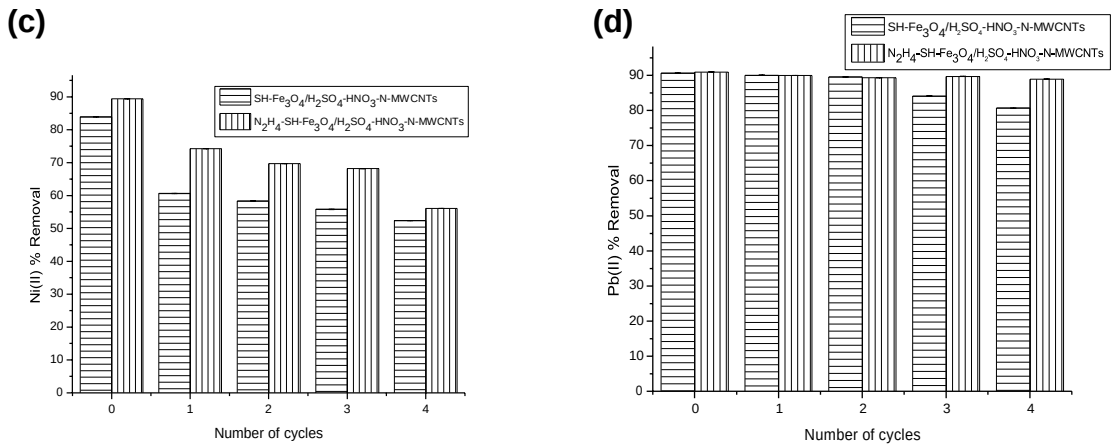

Figure 4.55: The adsorption behaviour of SH-Fe_3O_4/o-N-MWCNTs and N_2H_4-SH-Fe_3O_4/o-N-MWCNTs on the removal of (a) Cr(III), (b) Cr(VI), (c) Ni and (d) Pb at optimised conditions.

As shown in figure 4.55c, initially the removal of Ni(II) was greater than 80% for all the adsorbents. After regeneration with a hydrochloric acid solution, a slight decrease in percentage removal can be observed after four cycles retaining a removal of over 50% and above for both the thiol and amino treated o-N-MWCNTs. Figure 4.55d shows good results in lead removal. Initially, the removal of Pb(II) using the two best-prepared adsorbents from synthetic studies 90.6 and 90.9% using the SH-Fe_3O_4/o-N-MWCNTs and N_2H_4-SH-Fe_3O_4/o-N-MWCNTs respectively. After desorption studies were conducted a slight decrease in percentage removal can be observed with the removal of 80.7% and 88.9% after four cycles using the thiol and amino treated N-MWCNTs. Even after four cycles the removal for lead ions was over 80% for both the adsorbents. The adsorbents show good quality and could be helpful for practical applications. The N-MWNCTs could still adsorb chromium ions effectively after the fourth cycle. The results suggest that modified o-N-MWCNTs can be repeatedly used for the removal of selected toxic elements from water samples. Thus, both the adsorbents are promising for practical application in metal ion treatment.

4.4.4 SEM and TEM analysis of the $C_6H_{18}N_4$-SH-Fe_3O_4/o-N-MWCNTs composite before and after surface and borehole water sample adsorption

The SEM images of $C_6H_{18}N_4$-SH-Fe_3O_4/o-N-MWCNTs after borehole water adsorption are shown in figures 4.56b. The images show that carbon nanotubes generate an abundant network structure of MWCNTs. In comparison to the nanomaterial in figure 4.56a which showed no presence of impurities, after adsorption of chromium, nickel and lead agglomerates of small pieces of material appeared indicating the physical adsorption of the selected toxic elements by the prepared nanocomposite. Bright spots on a uniform surface can be observed in figure 4.56b which indicate persuasive interaction of the metal ion with the adsorbent. As observed by Egbosiuba et al. [25], for the adsorption of As(V) and Mn(II), after adsorption, the SEM and TEM images revealed the closely packed tubular morphology and deposition of the adsorbed As(V) and Mn(VII) ions. It can be observed that the surface of the adsorbent after adsorption changed, and the visible pores of the adsorbent had disappeared or had been filled up. TEM images as shown in figure 4.10(c and d) revealed the diameter of carbon nanotubes decreased after adsorption suggesting that the surface of the $C_6H_{18}N_4$-SH-Fe_3O_4/o-N-MWCNTs was densely covered by amino groups. Figure 4.56d showed black spots on the surface of the nanotubes after adsorption corresponding to chromium, nickel and lead ions. These results are in agreement with the work conducted by Zhan et al. [10].

Before **After**

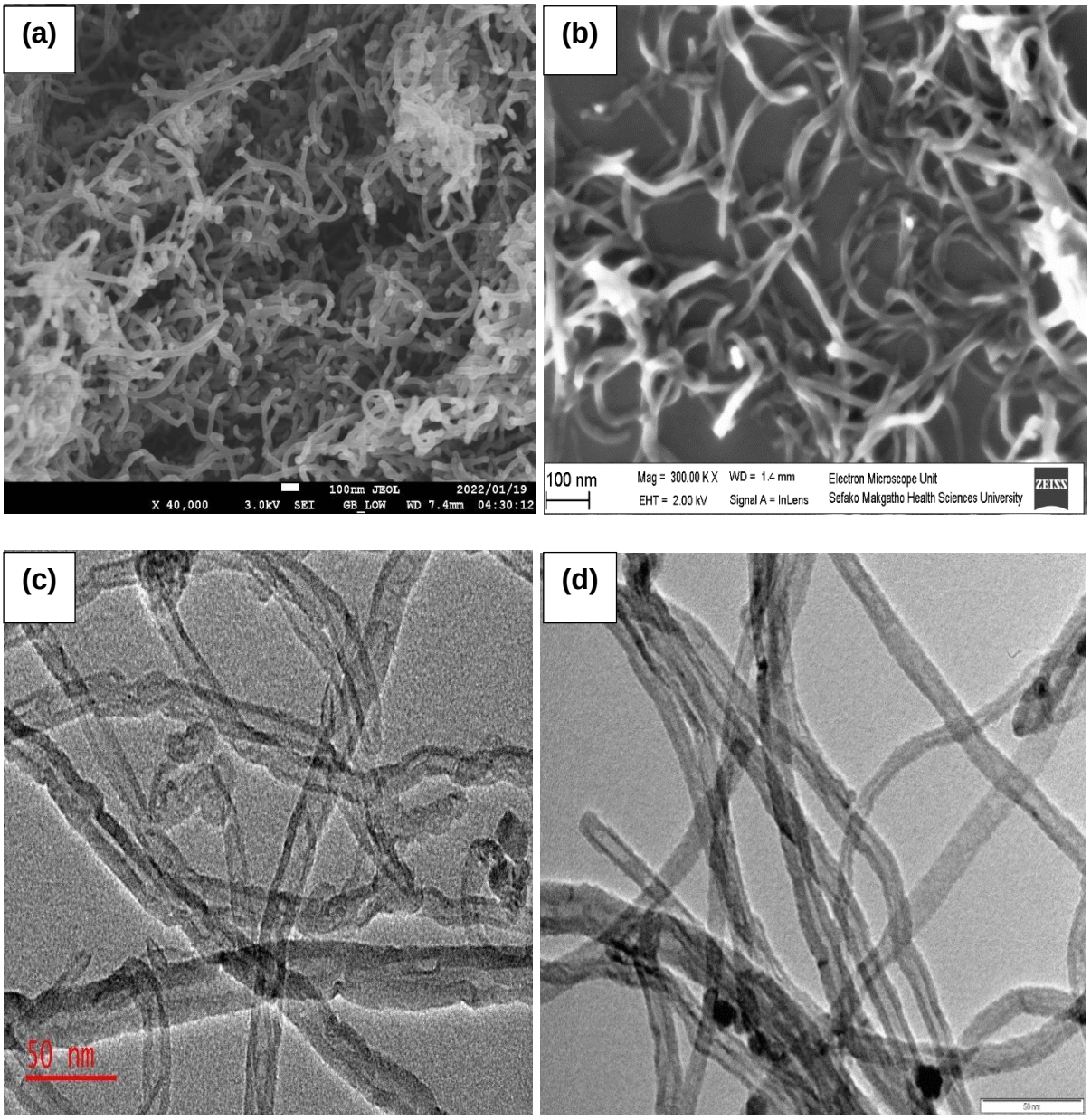

Figure 4.56: SEM and TEM images of triethylenetetramine-substituted N-MWCNTs $C_6H_{18}N_4$-SH-Fe_3O_4/o-N-MWCNTs before adsorption (a and c) and after adsorption (b & d).

REFERENCES

1. Mkhondo, N.B. and Magadzu, T., 2014. Effects of different acid-treatment on the nanostructure and performance of carbon nanotubes in electrochemical hydrogen storage. Dig. J. Nanomater. Bios, 9(4), pp.1331-1338.
2. Rananga, L.E., 2013. Synthesis, characters and application of silver-doped cabon Nanotubes and nanoporous polymers for purification of water samples (Doctoral dissertation, University of Limpopo (Turfloop Campus)).
3. Yang, K., Lou, Z., Fu, R., Zhou, J., Xu, J., Baig, S.A. and Xu, X., 2018. Multiwalled carbon nanotubes incorporated with or without amino groups for aqueous Pb (II) removal: Comparison and mechanism study. Journal of Molecular Liquids, 260, pp.149-158.
4. Singh, B.P., Choudhary, V., Teotia, S., Gupta, T.K., Singh, V.N., Dhakate, S.R. and Mathur, R.B., 2015. Solvent free, efficient, industrially viable, fast dispersion process based amine modified MWCNT reinforced epoxy composites of superior mechanical properties. Adv Mater Lett, 6(2), pp.104-113.
5. Jiang, L., Li, S., Yu, H., Zou, Z., Hou, X., Shen, F., Li, C. and Yao, X., 2016. Amino and thiol modified magnetic multi-walled carbon nanotubes for the simultaneous removal of lead, zinc, and phenol from aqueous solutions. Applied Surface Science, 369, pp.398-413.
6. Siregar, M.Z., Alfian, Z., Agusnar, H. and Marpaung, H., 2015. Preparation and Characterization Carbon Nanotubes–Chitosan Nanocomposite by Using Oil Palm Shell and Horseshoe Crab Shell. International Journal of Advanced Research in Chemical Science (IJARCS) Volume, 2, pp.6-13.
7. Zhang, C., Sui, J., Li, J., Tang, Y. and Cai, W., 2012. Efficient removal of heavy metal ions by thiol-functionalized superparamagnetic carbon nanotubes. Chemical Engineering Journal, 210, pp.45-52.
8. Farghali, A.A., Tawab, H.A., Moaty, S.A. and Khaled, R., 2017. Functionalization of acidified multi-walled carbon nanotubes for removal of heavy metals in aqueous solutions. Journal of Nanostructure in Chemistry, 7(2), pp.101-111.
9. Chen, K., Zhang, Z., Xia, K., Zhou, X., Guo, Y. and Huang, T., 2019. Facile synthesis of thiol-functionalized magnetic activated carbon and application for

the removal of mercury (II) from aqueous solution. ACS omega, 4(5), pp.8568-8579.

10. Jung, C., Heo, J., Han, J., Her, N., Lee, S.J., Oh, J., Ryu, J. and Yoon, Y., 2013. Hexavalent chromium removal by various adsorbents: powdered activated carbon, chitosan, and single/multi-walled carbon nanotubes. Separation and Purification Technology, 106, pp.63-71.
11. Fu, K., Wang, Y., Qian, Y., Mao, L., Jin, J., Yang, S. and Li, G., 2018. Synergistic effect of nitrogen doping and MWCNT intercalation for the graphene hybrid support for nanoparticles with exemplary oxygen reduction reaction performance. Materials, 11(4), p.642.
12. Ganesan, Y., Peng, C., Lu, Y., Ci, L., Srivastava, A., Ajayan, P.M. and Lou, J., 2010. Effect of nitrogen doping on the mechanical properties of carbon nanotubes. Acs Nano, 4(12), pp.7637-7643.
13. Ahangari, A., Raygan, S. and Ataie, A., 2019. Capabilities of nickel zinc ferrite and its nanocomposite with CNT for adsorption of arsenic (V) ions from wastewater. Journal of Environmental Chemical Engineering, 7(6), p.103493.
14. Zhan, W., Gao, L., Fu, X., Siyal, S.H., Sui, G. and Yang, X., 2019. Green synthesis of amino-functionalized carbon nanotube-graphene hybrid aerogels for high performance heavy metal ions removal. Applied Surface Science, 467, pp.1122-1133.
15. Ritter, U., Tsierkezos, N.G., Prylutskyy, Y.I., Matzui, L.Y., Gubanov, V.O., Bilyi, M.M. and Davydenko, M.O., 2012. Structure–electrical resistivity relationship of N-doped multi-walled carbon nanotubes. Journal of Materials Science, 47(5), pp.2390-2395.
16. Kariim, I., Abdulkareem, A.S., Tijani, J.O. and Abubakre, O.K., 2020. Development of MWCNTs/TiO2 nanoadsorbent for Simultaneous removal of Phenol and Cyanide from refinery wastewater. Scientific African, p.e00593.
17. Luo, X., Lei, X., Cai, N., Xie, X., Xue, Y. and Yu, F., 2016. Removal of heavy metal ions from water by magnetic cellulose-based beads with embedded chemically modified magnetite nanoparticles and activated carbon. ACS Sustainable Chemistry & Engineering, 4(7), pp.3960-3969.
18. Zhang, L., Pan, Z. and Huang, Q., 2013. Effect of primary particle size on colloidal stability of multiwall carbon nanotubes. Water science and technology, 68(10), pp.2249-2256.

19. Zhan, Y., Hu, H., He, Y., Long, Z., Wan, X. and Zeng, G., 2016. Novel amino-functionalized Fe 3 O 4/carboxylic multi-walled carbon nanotubes: one-pot synthesis, characterization and removal for Cu (II). Russian Journal of Applied Chemistry, 89(11), pp.1894-1902.
20. Mihalchik, A.L., Ding, W., Porter, D.W., McLoughlin, C., Schwegler-Berry, D., Sisler, J.D., Stefaniak, A.B., Snyder-Talkington, B.N., Cruz-Silva, R., Terrones, M. and Tsuruoka, S., 2015. Effects of nitrogen-doped multi-walled carbon nanotubes compared to pristine multi-walled carbon nanotubes on human small airway epithelial cells. Toxicology, 333, pp.25-36.
21. Tetana, Z.N., Mhlanga, S.D., Bepete, G., Krause, R.W.M. and Coville, N.J., 2012. The synthesis of nitrogen-doped multiwalled carbon nanotubes using an Fe-Co/CaCO3 catalyst. South African Journal of Chemistry, 65, pp.39-49.
22. Kaur, A.P., 2013. N-doped Multiwalled Carbon Nanotubes: Functionalization, Characterization and Application in Li Ion Batteries, (Doctoral dissertation, University of Kentucky, Department of Chemistry).
23. Simon, V., Manilo, M., Vanyorek, L., Csoma, Z. and Barany, S., 2020. Comparative Study of Cu (II) Adsorption by As-prepared and Oxidized Multi-walled N-Doped Carbon Nanotubes. Colloid Journal, 82(4), pp.427-436.
24. Huang, Z.N., Wang, X.L. and Yang, D.S., 2015. Adsorption of Cr (VI) in wastewater using magnetic multi-wall carbon nanotubes. Water Science and Engineering, 8(3), pp.226-232.
25. Egbosiuba, T.C., Abdulkareem, A.S., Kovo, A.S., Afolabi, E.A., Tijani, J.O. and Roos, W.D., 2020. Enhanced adsorption of As (V) and Mn (VII) from industrial wastewater using multi-walled carbon nanotubes and carboxylated multi-walled carbon nanotubes. Chemosphere, p.126780.
26. Fan, L., Zhou, A., Zhong, L., Zhang, Z. and Liu, Y., 2019. Selective and effective adsorption of Hg (II) from aqueous solution over wide pH range by thiol functionalized magnetic carbon nanotubes. Chemosphere, 226, pp.405-412.
27. Wang, Y., Shi, L., Gao, L., Wei, Q., Cui, L., Hu, L., Yan, L. and Du, B., 2015. The removal of lead ions from aqueous solution by using magnetic hydroxypropyl chitosan/oxidized multiwalled carbon nanotubes composites. Journal of colloid and interface science, 451, pp.7-14.
28. Silva, N.F., Netto, M.S., Silva, L.F., Mallmann, E.S., Lima, E.C., Ferrari, V. and Dotto, G.L., 2021. Composite carbon materials from winery composted waste

for the treatment of effluents contaminated with ketoprofen and 2-nitrophenol. Journal of Environmental Chemical Engineering, 9(4), p.105421.

29. Kashyap, A., Singh, N.P., Arora, S., Singh, V. and Gupta, V.K., 2020. Effect of amino-functionalization of MWCNTs on the mechanical and thermal properties of MWCNTs/epoxy composites. Bulletin of Materials Science, 43(1), pp.1-9.
30. Kończyk, J., Żarska, S. and Ciesielski, W., 2019. Adsorptive removal of Pb (II) ions from aqueous solutions by multi-walled carbon nanotubes functionalised by selenophosphoryl groups: Kinetic, mechanism, and thermodynamic studies. Colloids and Surfaces A: Physicochemical and Engineering Aspects, 575, pp.271-282.
31. Lv, W., Shi, K., Li, L. and Shao, S., 2010. Nitrogen-doped multiwalled carbon nanotubes and their electrocatalysis towards oxidation of NO. Microchimica Acta, 170(1-2), pp.91-98.
32. Zhang, Y., Liu, C., Wen, B., Song, X. and Li, T., 2011. Preparation and electrochemical properties of nitrogen-doped multi-walled carbon nanotubes. Materials letters, 65(1), pp.49-52.
33. Ramesh, S., Sivasamy, A., Kim, H.S. and Kim, J.H., 2017. High-performance N-doped MWCNT/GO/cellulose hybrid composites for supercapacitor electrodes. RSC advances, 7(78), pp.49799-49809.
34. Lee, E.C., 2020. Simultaneous Adsorption And Degradation Of Methylene Blue Using Magnetic Carbon Nanotubes (Doctoral dissertation, UTAR).
35. Doğan, M., Selek, A., Turhan, O., Kızılduman, B.K. and Bicil, Z., 2021. Different functional groups functionalized hexagonal boron nitride (h-BN) nanoparticles and multi-walled carbon nanotubes (MWCNT) for hydrogen storage. Fuel, 303, p.121335.
36. Lu, C. and Chiu, H., 2006. Adsorption of zinc (II) from water with purified carbon nanotubes. Chemical Engineering Science, 61(4), pp.1138-1145.
37. Moazzen, M., Khaneghah, A.M., Shariatifar, N., Ahmadloo, M., Eş, I., Baghani, A.N., Yousefinejad, S., Alimohammadi, M., Azari, A., Dobaradaran, S. and Rastkari, N., 2019. Multi-walled carbon nanotubes modified with iron oxide and silver nanoparticles (MWCNT-Fe3O4/Ag) as a novel adsorbent for determining PAEs in carbonated soft drinks using magnetic SPE-GC/MS method. Arabian Journal of Chemistry, 12(4), pp.476-488.

38. Rezaie, E., Hajalilou, A., Rezanezhad, A., Abouzari-Lotf, E. and Arsalani, N., 2020. Magnetorheological studies of polymer nanocomposites. In Rheology of Polymer Blends and Nanocomposites (pp. 263-294). Elsevier
39. Huang, Z., Huang, Z., Feng, L., Luo, X., Wu, P., Cui, L. and Mao, X., 2018. Modified cellulose by polyethyleneimine and ethylenediamine with induced Cu (II) and Pb (II) adsorption potentialities. Carbohydrate polymers, 202, pp.470-478.
40. Silva, W.M., Ribeiro, H., Seara, L.M., Calado, H.D., Ferlauto, A.S., Paniago, R.M., Leite, C.F. and Silva, G.G., 2012. Surface properties of oxidized and aminated multi-walled carbon nanotubes. Journal of the Brazilian Chemical Society, 23, pp.1078-1086.
41. Yu, H., Sun, W., Zhu, X., Zhu, X. and Wei, J., 2012. Study on multi-walled carbon nanotubes on-line separation/preconcentration of chromium (III) and chromium speciation. Analytical Sciences, 28(12), pp.1219-1224.
42. Dokmaj, T., Ibrahim, T., Khamis, M., Abouleish, M. and Alam, I., 2020. Chemically Modified Nanoparticles Usage for Removal of Chromium from Sewer Water. Environmental Nanotechnology, Monitoring & Management, p.100319.
43. Gupta, V.K., Agarwal, S. and Saleh, T.A., 2011. Chromium removal by combining the magnetic properties of iron oxide with adsorption properties of carbon nanotubes. Water research, 45(6), pp.2207-2212.
44. Atieh, M.A., Bakather, O.Y., Tawabini, B.S., Bukhari, A.A., Khaled, M., Alharthi, M., Fettouhi, M. and Abuilaiwi, F.A., 2010. Removal of chromium (III) from water by using modified and nonmodified carbon nanotubes. Journal of Nanomaterials, 2010.
45. Qiao, K., Tian, W., Bai, J., Zhao, J., Du, Z., Song, T., Chu, M., Wang, L. and Xie, W., 2020. Synthesis of floatable magnetic iron/biochar beads for the removal of chromium from aqueous solutions. Environmental Technology & Innovation, p.100907.
46. Kumar, R., Ansari, M.O. and Barakat, M.A., 2013. DBSA doped polyaniline/multi-walled carbon nanotubes composite for high efficiency removal of Cr (VI) from aqueous solution. Chemical Engineering Journal, 228, pp.748-755.

47. Huang, Y., Lee, X., Macazo, F.C., Grattieri, M., Cai, R. and Minteer, S.D., 2018. Fast and efficient removal of chromium (VI) anionic species by a reusable chitosan-modified multi-walled carbon nanotube composite. Chemical Engineering Journal, 339, pp.259-267.
48. Ahmadi, S., Igwegbe, C.A., Rahdar, S. and Asadi, Z., 2019. The survey of application of the linear nonlinear kinetic models for the adsorption of nickel (II) by modified multi-walled carbon nanotubes. Applied Water Science, 9(4), pp.1-7.
49. Anupam, K., Dutta, S., Bhattacharjee, C. and Datta, S., 2011. Adsorptive removal of chromium (VI) from aqueous solution over powdered activated carbon: Optimisation through response surface methodology. Chemical Engineering Journal, 173(1), pp.135-143.
50. Pillay, K., Cukrowska, E.M. and Coville, N.J., 2009. Multi-walled carbon nanotubes as adsorbents for the removal of parts per billion levels of hexavalent chromium from aqueous solution. Journal of hazardous materials, 166(2-3), pp.1067-1075.
51. Perez-Aguilar, N.V., Diaz-Flores, P.E. and Rangel-Mendez, J.R., 2011. The adsorption kinetics of cadmium by three different types of carbon nanotubes. Journal of colloid and interface science, 364(2), pp.279-287.
52. Gupta, V.K., Chandra, R., Tyagi, I. and Verma, M., 2016. Removal of hexavalent chromium ions using CuO nanoparticles for water purification applications. Journal of colloid and interface science, 478, pp.54-62.
53. Kumar, A.S.K., Jiang, S.J. and Tseng, W.L., 2015. Effective adsorption of chromium (VI)/Cr (III) from aqueous solution using ionic liquid functionalized multiwalled carbon nanotubes as a super sorbent. Journal of Materials Chemistry A, 3(13), pp.7044-7057.
54. Obayomi, K.S., Bello, J.O., Yahya, M.D., Chukwunedum, E. and Adeoye, J.B., 2020. Statistical analyses on effective removal of cadmium and hexavalent chromium ions by multiwall carbon nanotubes (MWCNTs). Heliyon, 6(6), p.e04174.
55. Shi, T., Yang, D., Yang, H., Ye, J. and Cheng, Q., 2017. Preparation of chitosan crosslinked modified silicon material and its adsorption capability for chromium (VI). Applied Clay Science, 142, pp.100-108.

56. Kahu, S.S., Shekhawat, A., Saravanan, D. and Jugade, R.M., 2016. Two fold modified chitosan for enhanced adsorption of hexavalent chromium from simulated wastewater and industrial effluents. Carbohydrate polymers, 146, pp.264-273.
57. Chen, F., Zhang, M., Ma, L., Ren, J., Ma, P., Li, B., Wu, N., Song, Z. and Huang, L., 2020. Nitrogen and sulfur codoped micro-mesoporous carbon sheets derived from natural biomass for synergistic removal of chromium (VI): adsorption behavior and computing mechanism. Science of The Total Environment, p.138930.
58. Hussain, I., Qi, J., Sun, X., Wang, L. and Li, J., 2020. Melamine derived nitrogen-doped carbon sheet for the efficient removal of chromium (VI). Journal of Molecular Liquids, 318, p.114052.
59. Alguacil, F.J. and López, F.A., 2020. On the Active Adsorption of Chromium (III) from Alkaline Solutions Using Multiwalled Carbon Nanotubes. Applied Sciences, 10(1), p.36.
60. Lu, W., Li, J., Sheng, Y., Zhang, X., You, J. and Chen, L., 2017. One-pot synthesis of magnetic iron oxide nanoparticle-multiwalled carbon nanotube composites for enhanced removal of Cr (VI) from aqueous solution. Journal of colloid and interface science, 505, pp.1134-1146.
61. Zulfiqar, M., Lee, S.Y., Mafize, A.A., Kahar, N.A.M.A., Johari, K. and Rabat, N.E., 2020. Efficient removal of Pb (II) from aqueous solutions by using oil palm bio-waste/MWCNTs reinforced PVA hydrogel composites: Kinetic, isotherm and thermodynamic modeling. Polymers, 12(2), p.430.
62. Yahya, M.D., Obayomi, K.S., Abdulkadir, M.B., Iyaka, Y.A. and Olugbenga, A.G., 2020. Characterization of cobalt ferrite-supported activated carbon for removal of chromium and lead ions from tannery wastewater via adsorption equilibrium. Water Science and Engineering, 13(3), pp.202-213.
63. Hosseinkhani, A., Rad, B.F. and Baghdadi, M., 2020. Efficient removal of hexavalent chromium from electroplating wastewater using polypyrrole coated on cellulose sulfate fibers. Journal of Environmental Management, 274, p.111153.
64. Zhou, J., Zhou, X., Yang, K., Cao, Z., Wang, Z., Zhou, C., Baig, S.A. and Xu, X., 2020. Adsorption behavior and mechanism of arsenic on mesoporous silica

modified by iron-manganese binary oxide (FeMnOx/SBA-15) from aqueous systems. Journal of hazardous materials, 384, p.121229.

65. Awual, M.R., Hasan, M.M., Eldesoky, G.E., Khaleque, M.A., Rahman, M.M. and Naushad, M., 2016. Facile mercury detection and removal from aqueous media involving ligand impregnated conjugate nanomaterials. Chemical Engineering Journal, 290, pp.243-251.

66. Zhou, Y., Liu, X., Xiang, Y., Wang, P., Zhang, J., Zhang, F., Wei, J., Luo, L., Lei, M. and Tang, L., 2017. Modification of biochar derived from sawdust and its application in removal of tetracycline and copper from aqueous solution: adsorption mechanism and modelling. Bioresource technology, 245, pp.266-273.

67. Vakili, M., Deng, S., Cagnetta, G., Wang, W., Meng, P., Liu, D. and Yu, G., 2019. Regeneration of chitosan-based adsorbents used in heavy metal adsorption: A review. Separation and Purification Technology, 224, pp.373-387.

68. Igwegbe, C.A., Oba, S.N., Aniagor, C.O., Adeniyi, A.G. and Ighalo, J.O., 2020. Adsorption of ciprofloxacin from water: a comprehensive review. Journal of Industrial and Engineering Chemistry, 93, pp.57-77.
69. Ghorbani, M., Seyedin, O. and Aghamohammadhassan, M., 2020. Adsorptive removal of lead (II) ion from water and wastewater media using carbon-based nanomaterials as unique sorbents: A review. Journal of environmental management, 254, p.109814.
70. Wang, L., Hu, D., Kong, X., Liu, J., Li, X., Zhou, K., Zhao, H. and Zhou, C., 2018. Anionic polypeptide poly (γ-glutamic acid)-functionalized magnetic Fe3O4-GO-(o-MWCNTs) hybrid nanocomposite for high-efficiency removal of Cd (II), Cu (II) and Ni (II) heavy metal ions. Chemical Engineering Journal, 346, pp.38-49.
71. Adolph, M.A., Xavier, Y.M., Kriveshini, P. and Rui, K., 2012. Phosphine functionalised multiwalled carbon nanotubes: a new adsorbent for the removal of nickel from aqueous solution. Journal of Environmental Sciences, 24(6), pp.1133-1141.

72. Dong, P., Wu, X., Sun, Z., Hu, J. and Yang, S., 2014. Removal performance and the underlying mechanisms of plasma-induced CD/MWCNT/iron oxides towards Ni (II). Chemical Engineering Journal, 256, pp.128-136.
73. Zarghami, Z., Akbari, A., Latifi, A.M. and Amani, M.A., 2016. Design of a new integrated chitosan-PAMAM dendrimer biosorbent for heavy metals removing and study of its adsorption kinetics and thermodynamics. Bioresource technology, 205, pp.230-238.
74. Egbosiuba, T.C., Abdulkareem, A.S., Tijani, J.O., Ani, J.I., Krikstolaityte, V., Srinivasan, M., Veksha, A. and Lisak, G., 2021. Taguchi optimization design of diameter-controlled synthesis of multi walled carbon nanotubes for the adsorption of Pb (II) and Ni (II) from chemical industry wastewater. Chemosphere, 266, p.128937.
75. Gupta, A., Vidyarthi, S.R. and Sankararamakrishnan, N., 2014. Thiol functionalized sugarcane bagasse—A low cost adsorbent for mercury remediation from compact fluorescent bulbs and contaminated water streams. Journal of Environmental Chemical Engineering, 2(3), pp.1378-1385.
76. Siddiqui, M.N., Ali, I., Asim, M. and Chanbasha, B., 2020. Quick removal of nickel metal ions in water using asphalt-based porous carbon. Journal of Molecular Liquids, 308, p.113078.
77. Rahmati, N., Rahimnejad, M., Pourali, M. and Muallah, S.K., 2021. Effective removal of nickel ions from aqueous solution using multi-wall carbon nanotube functionalized by glycerol-based deep eutectic solvent. Colloid and Interface Science Communications, 40, p.100347.
78. Alizadeh, B., Ghorbani, M. and Salehi, M.A., 2016. Application of polyrhodanine modified multi-walled carbon nanotubes for high efficiency removal of Pb (II) from aqueous solution. Journal of Molecular Liquids, 220, pp.142-149.
79. Vuković, G.D., Marinković, A.D., Škapin, S.D., Ristić, M.Đ., Aleksić, R., Perić-Grujić, A.A. and Uskoković, P.S., 2011. Removal of lead from water by amino modified multi-walled carbon nanotubes. Chemical Engineering Journal, 173(3), pp.855-865.
80. Laus, R., Costa, T.G., Szpoganicz, B. and Fávere, V.T., 2010. Adsorption and desorption of Cu (II), Cd (II) and Pb (II) ions using chitosan crosslinked with epichlorohydrin-triphosphate as the adsorbent. Journal of hazardous materials, 183(1-3), pp.233-241.

81. Elmi, F., Hosseini, T., Taleshi, M.S. and Taleshi, F., 2017. Kinetic and thermodynamic investigation into the lead adsorption process from wastewater through magnetic nanocomposite Fe 3 O 4/CNT. Nanotechnology for Environmental Engineering, 2(1), pp.1-13.
82. Georgieva, V.G., Gonsalvesh, L. and Tavlieva, M.P., 2020. Thermodynamics and kinetics of the removal of nickel (II) ions from aqueous solutions by biochar adsorbent made from agro-waste walnut shells. Journal of Molecular Liquids, 312, p.112788.
83. Diva, T.N., Zare, K., Taleshi, F. and Yousefi, M., 2017. Synthesis, characterization, and application of nickel oxide/CNT nanocomposites to remove Pb 2+ from aqueous solution. Journal of Nanostructure in Chemistry, 7(3), pp.273-281.
84. Ragadhita, R. and Nandiyanto, A.B.D., 2021. How to calculate adsorption isotherms of particles using two-parameter monolayer adsorption models and equations. Indonesian Journal of Science and Technology, 6(1), pp.205-234.
85. Robati, D., Mirza, B., Ghazisaeidi, R., Rajabi, M., Moradi, O., Tyagi, I., Agarwal, S. and Gupta, V.K., 2016. Adsorption behavior of methylene blue dye on nanocomposite multi-walled carbon nanotube functionalized thiol (MWCNT-SH) as new adsorbent. Journal of Molecular Liquids, 216, pp.830-835.
86. SOUTH AFRICAN WATER QUALITY GUIDELINES Volume 1: Domestic Water Use Second Edition, 1996. (Department of Water Affairs and Forestry Second edition 1996).
87. Verlicchi, P. and Grillini, V., 2019. Surface and groundwater quality in South African area—Analysis of the most critical pollutants for drinking purposes. In Multidisciplinary Digital Publishing Institute Proceedings (Vol. 48, No. 1, p. 3).
88. Gautam, P.K., Gautam, R.K., Banerjee, S., Chattopadhyaya, M.C. and Pandey, J.D., 2016. Heavy metals in the environment: fate, transport, toxicity and remediation technologies. Nova Sci Publishers, 60, pp.101-130.
89. Kinuthia, G.K., Ngure, V., Beti, D., Lugalia, R., Wangila, A. and Kamau, L., 2020. Levels of heavy metals in wastewater and soil samples from open drainage channels in Nairobi, Kenya: Community health implication. Scientific reports, 10(1), pp.1-13.
90. Edition, F., 2011. Guidelines for drinking-water quality. WHO chronicle, 38(4), pp.104-108.

91. Magala, M., 2015. Aquatic Health Assessment of the Steelpoort River System, Limpopo, South Africa. University of Johannesburg (South Africa).
92. Macevele, L.E., 2019. Preparation and application of multi-walled carbon nanotubes/poly (vinylidene fluoride-co_hexafluropropylene) composite membranes for filtration and adsorption of contaminants in water (Doctoral dissertation, University of Limpopo, Department of Chemistry).
93. Nephalama, A. and Muzerengi, C., 2016. Assessment of the influence of coal mining on groundwater quality: Case of Masisi Village in the Limpopo Province of South Africa. Proceedings of the Freiberg/Germany, Mining Meets Water—Conflicts and Solutions (IMWA 2016), Leipzig, Germany, pp.11-15.
94. Sedibe, M., Achilonu, M.C., Tikilili, P., Shale, K. and Ebenebe, P.C., 2017. South African mine effluents: Heavy metal pollution and impact on the ecosystem. Int J Chem Sci. 2017;15(4), pp.198.
95. Kacmaz, H., 2020. Assessment of heavy metal contamination in natural waters of Dereli, Giresun: an area containing mineral deposits in northeastern Turkey. Environmental monitoring and assessment, 192(2), pp.1-12.
96. Mathipa, M.M., 2016. Analysis of the bio-physicochemical quality of surface and ground water in the Tubatse Municipality (Doctoral dissertation, University of Limpopo, Department of Microbiology).
97. Letsoalo, M.R., Godeto, T.W., Magadzu, T. and Ambushe, A.A., 2018. Quantitative Speciation of Arsenic in Water and Sediment Samples from the Mokolo River in Limpopo Province, South Africa. Analytical Letters, 51(17), pp.2763-2777.

CHAPTER 5

CONCLUSIONS AND RECOMMENDATIONS

5.1 CONCLUSIONS

The aims and objectives of this study were successfully satisfied by investigating the adsorption capabilities of the nanocomposite nanomaterials for the removal of toxic elements. Iron oxide, thiol and amino-functionalised MWCNT nanocomposites were successfully prepared and used for the adsorption of toxic elements such as Cr, Ni and Pb. The synthesised nanocomposites were characterised using techniques such as FTIR spectroscopy, PXRD, SEM, TEM, BET and TGA. FTIR spectroscopy confirmed that Fe_3O_4, -SH and -NH_2 functional groups were successfully grafted onto the acid-treated MWCNTs. PXRD showed that the as-prepared nanocomposites consist of the graphitic structure of CNTs and are in line with the standard XRD data for the inverse spine crystalline structure of Fe_3O_4 with a face-centered cubic (fcc) structure.

SEM and TEM images showed that the uniform Fe_3O_4 nanoparticles were evenly coated on the surface of N-doped bamboo-like carbon nanotubes with an increase in diameters after functional group modification. BET analysis showed that the surface area and pore volume increased after the acid-treated CNTs were modified with Fe_3O_4 and -SH. After amination, both the surface area and pore volume showed a slight decrease as compared to the Fe_3O_4 and -SH modified CNTs. Lastly, TGA results showed that the thermal decomposition of the o-N-MWCNTs and $C_6H_{18}N_4$-SH-Fe_3O_4/o-N-MWCNTs nanocomposite was between 300 and 400 °C while the raw N-MWCNTs, Fe_3O_4/o-N-MWCNTs, SH-Fe_3O_4/o-N-MWCNTs, N_2H_4-SH-Fe_3O_4/o-N-MWCNTs and N_2H_4-SH-Fe_3O_4/o-MWCNTs nanocomposites possess high thermal stability with decomposition occurring at around 800 to 900 °C.

Adsorption experiments demonstrated that the N_2H_4-SH-Fe_3O_4/o-N-MWCNTs nanocomposites adsorbed Cr(III), Cr(VI), Ni(II) and Pb(II) effectively at 94%, 95%, 99.8% and 98%, respectively under optimised conditions. The kinetics followed a pseudo-second order which gave a better correlation with the adsorptions of Cr(III), Cr(VI), Ni(II) and Pb(II) than the pseudo-first order. The maximum monolayer adsorption capacity of the o-N-MWCNTs and N_2H_4-SH-Fe_3O_4/o-N-MWCNTs onto Cr(III), Cr(VI), Ni(II) and Pb(II) which fitted the Langmuir isotherms was found to be

1720, 1930, 5410 and 317,5 mg/g, respectively and exceeding most nanocomposites. Thermodynamics studies proved that the adsorption of Cr(III), Cr(VI), Ni(II) and Pb(II) onto Fe_3O_4/o-N-MWCNTs, SH-Fe_3O_4/o-N-MWCNTs, and N_2H_4-SH-Fe_3O_4/o-N-MWCNTs have an endothermic and spontaneous nature and there is an increase in randomness at the solid/liquid interface during the adsorption process. The adsorption process was physisorption in nature with the negative free energy of adsorption.

All the modified N-MWCNTs could still remove over 50% of the adsorbate after regeneration. The removal efficiencies of Cr(III)), Cr(VI), Ni(II) and Pb(II) were 80, 90, 70 and 50% after four cycles, respectively. Cr(III) and Cr(VI) had as low as 10% removal efficiencies in the presence of some competing anions. However, even in the presence of interfering ions, the f-N-MWCNTs (f = functionalised) demonstrated to have high Ni(II) and Pb(II) removal.

Total concentrations of chromium, nickel and lead in surface and groundwater were determined to assess the level of contamination relative to water guidelines for trace elements. It was found that both the surface and groundwater were contaminated with chromium, nickel and lead at the Steelpoort and Olifants River as well as from a sampled borehole in Burgersfort. The concentration of each element from both river and borehole water was found to be higher than the permissible limit set by the SANS, USEPA and WHO for drinking water. After treatment, the concentration of all water samples was below the F-AAS detection limit. In conclusion, the as-prepared nanocomposites are a promising adsorbent for toxic element treatment in surface and groundwater. Therefore, there is a serious need to monitor surface and groundwater which is used for drinking purposes.

5.2 RECOMMENDATIONS

- Similar procedures for the preparation of metal oxides-functionalised MWCNTs nanocomposites can be followed to prepare other variants of metal oxides (M = Co_3O_4, TiO_2) modified MWCNTs.
- For better removal efficiencies and selection of treatment techniques, different species of Cr in surface and groundwater samples from the Sekhukhune area need to be quantified.
- Water sampling at the selected sampling points can be done seasonally to better monitor when higher concentrations of these toxic elements are recorded.
- Concerning the high removal efficiencies obtained for inorganic contaminants, the application of as-prepared nanocomposites can be extended for the treatment of organic and biological contaminants from the same areas.
- Sampled water should be quantified after treatment with inductively coupled plasma-mass spectrometry (ICP-MS) to determine total concentrations of chromium, nickel and lead accurately.
- The results of this study may be used by municipal authorities to control groundwater quality both domestically and commercially.

APPENDICES

Appendix A: Characterisation results

1. XRD patterns of oxidised-MWCNTs and (Fe_3O_4, thiol and amino) modified MWCNTs and N-MWCNTs

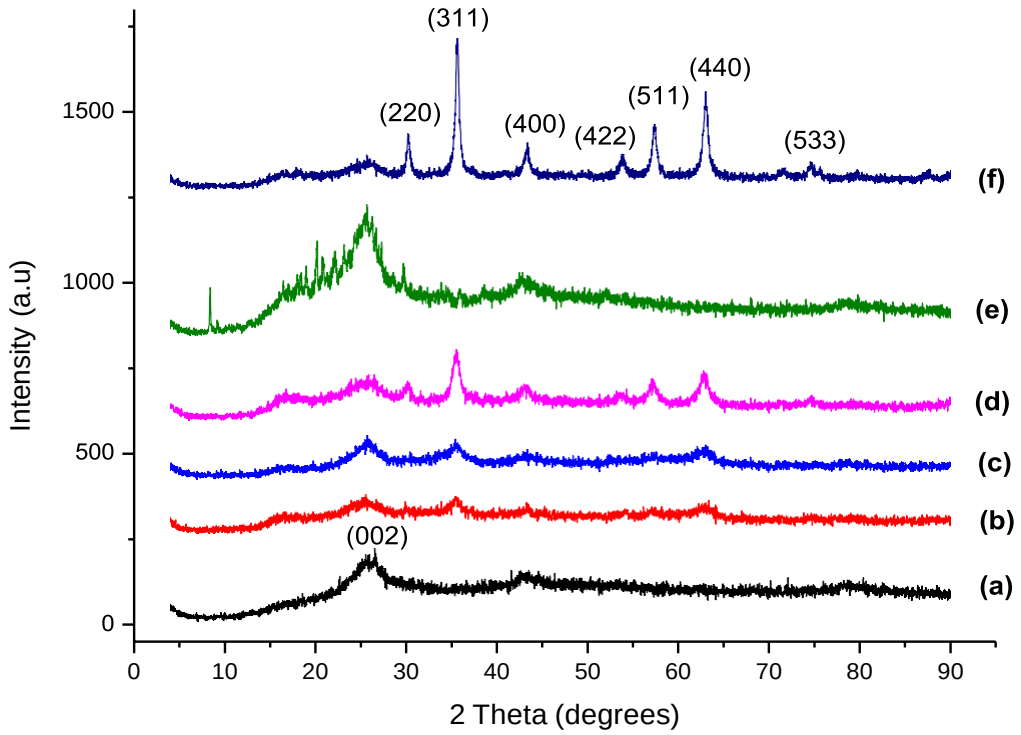

Figure 4.57: XRD patterns of H_2SO_4-HNO_3-N-MWCNTs (a), Fe_3O_4/H_2SO_4-HNO_3-N-MWCNTs (b), SH-Fe_3O_4/H_2SO_4-HNO_3-N-MWCNTs (c) N_2H_4-SH-Fe_3O_4/H_2SO_4-HNO_3-N-MWCNTs (d), $C_6H_{18}N_4$-SH-Fe_3O_4/H_2SO_4-HNO_3-N-MWCNTs (e) and N_2H_4-SH-Fe_3O_4/H_2SO_4-HNO_3-MWCNTs (f).

Appendix B: Adsorption studies by H_2O_2-HNO_3 and H_2SO_4-HNO_3 treated nanocomposites

1. Effect of initial concentration on the removal of Cr(III) and Cr(VI)

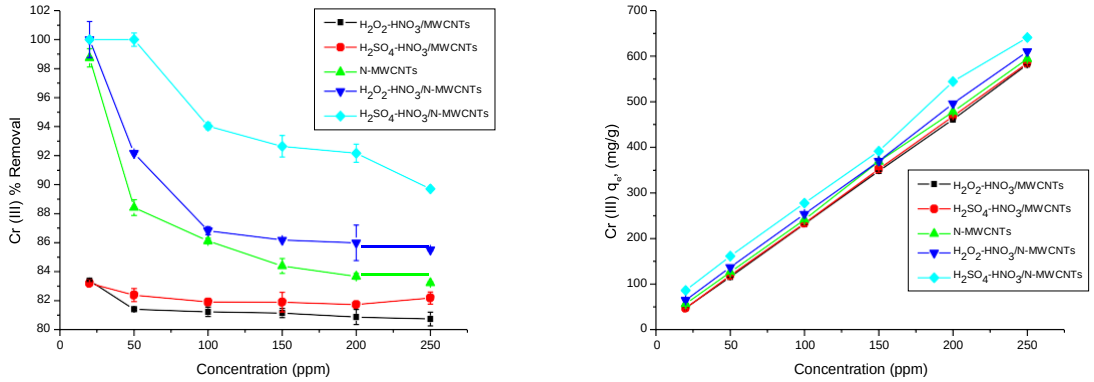

Figure 4.58: Effect of initial concentration on Cr(III) removal (a) and adsorption capacity (b) onto (a)H_2SO_4-HNO_3/MWCNTs, (b)H_2O_2-HNO_3/MWCNTs, (c)N-MWCNTs, (d)H_2SO_4-HNO_3/N-MWCNTs and (e)H_2O_2-HNO_3/N-MWCNTs.

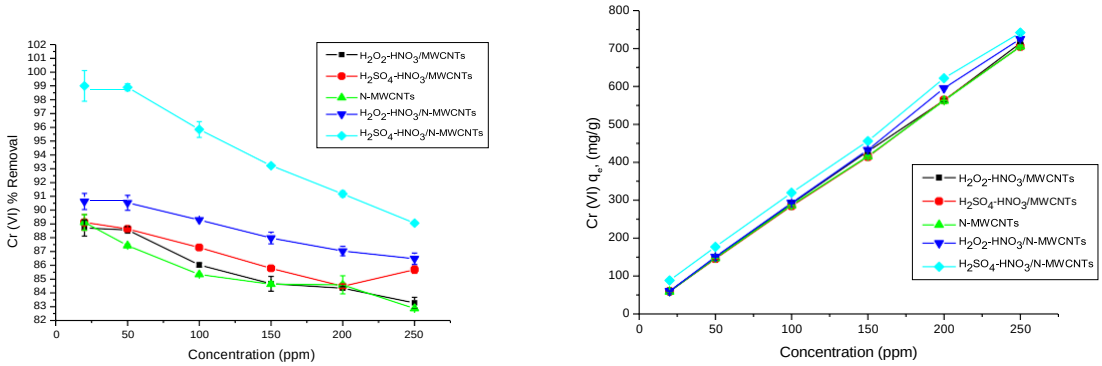

Figure 4.58: Effect of initial concentration on Cr(VI) removal (a) and adsorption capacity (b) onto (a)H_2O_2-HNO_3/MWCNTs, (b)H_2SO_4-HNO_3/MWCNTs, (c)N-MWCNTs, (d)H_2O_2-HNO_3/N-MWCNTs and (e)H_2SO_4-HNO_3/N-MWCNTs).

2. Effect of temperature on the removal of Cr(III) and Cr(VI)

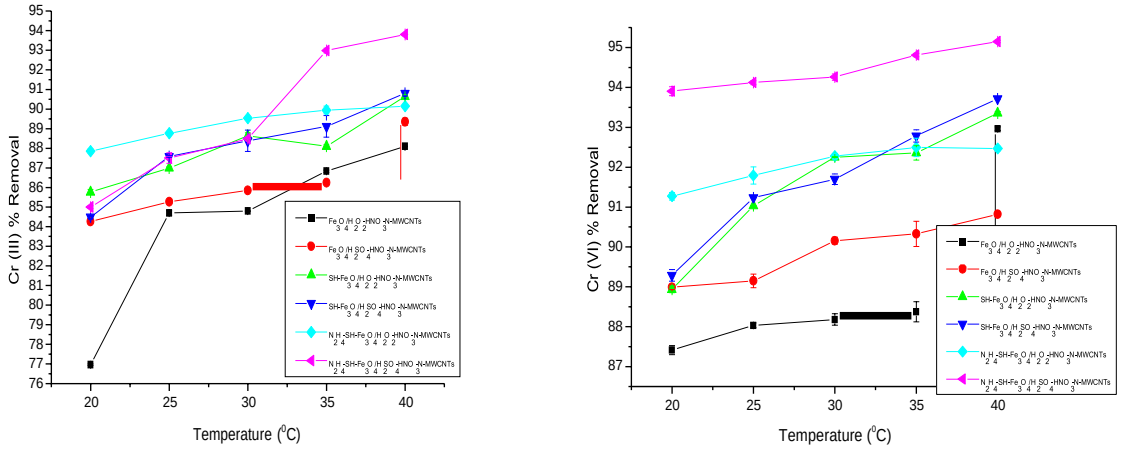

Figure 4.59: Effect of temperature on the removal of Cr(III) (a) and Cr(VI) (b) onto (a)Fe_3O_4/H_2O_2-HNO_3-N-MWCNTs, (b)Fe_3O_4-H_2SO_4-HNO_3-N-MWCNTs, (c)SH-Fe_3O_4/H_2O_2-HNO_3-N-MWCNTs, (d)SH-Fe_3O_4-H_2SO_4-HNO_3-N-MWCNTs, (e)N_2H_4-SH-Fe_3O_4/H_2O_2-HNO_3-N-MWCNTs and (f)N_2H_4-SH-Fe_3O_4/H_2SO_4-HNO_3-N-MWCNTs).

3. Adsorption kinetics of Cr(III) and Cr(VI) ions removal

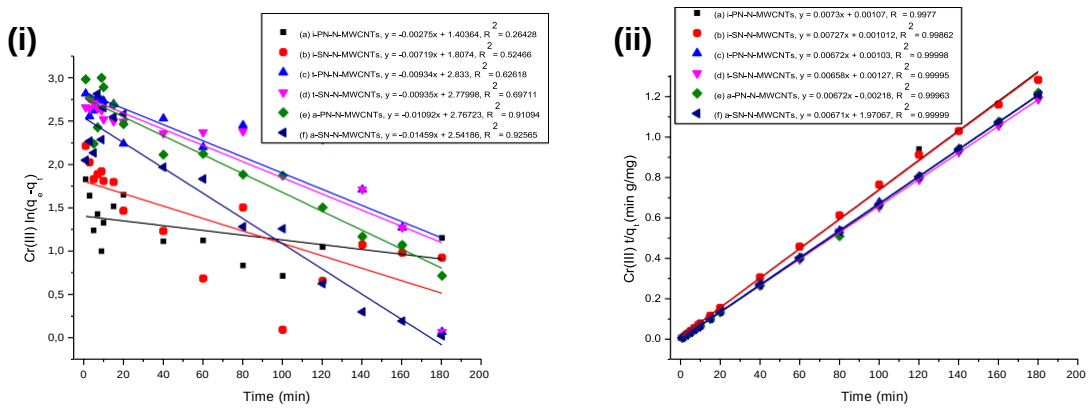

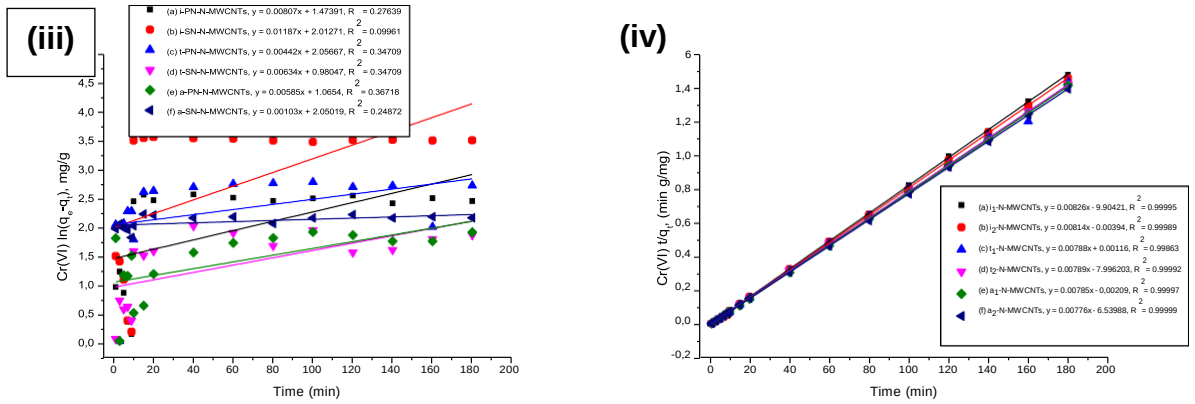

Figure 4.60: (i) Pseudo-first order and (ii) Pseudo-second order kinetic model for adsorption of Cr(III) and Cr(VI) ions onto Fe_3O_4/H_2O_2-HNO_3-N-MWCNTs (a), Fe_3O_4-H_2SO_4-HNO_3-N-MWCNTs (b), SH-Fe_3O_4/H_2O_2-HNO_3-N-MWCNTs (c), SH-Fe_3O_4-H_2SO_4-HNO_3-N-MWCNTs (d), N_2H_4-SH-Fe_3O_4/H_2O_2-HNO_3-N-MWCNTs (e) and N_2H_4-SH-Fe_3O_4/H_2SO_4-HNO_3-N-MWCNTs (f) nanocomposites.

4. Adsorption isotherms of Cr(III) and Cr(VI) ions removal

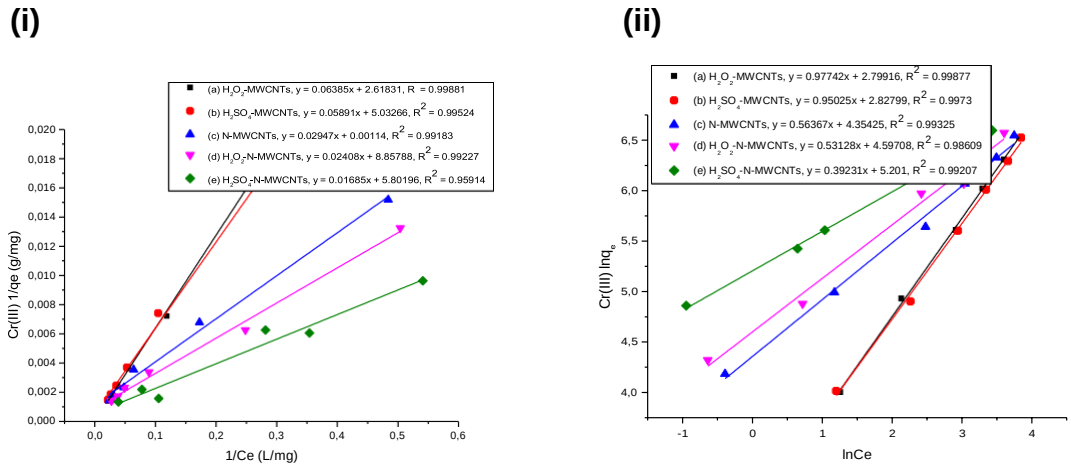

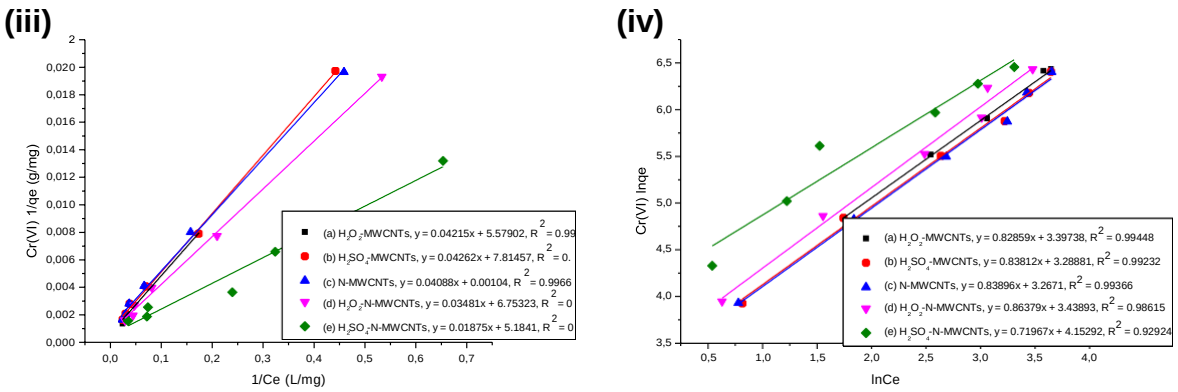

Figure 4.61: (i) Langmuir isotherm and (ii) Freundlich isotherm for adsorption of Cr(III) and Cr(VI) ions onto Fe_3O_4/H_2O_2-HNO_3-N-MWCNTs (a), Fe_3O_4-H_2SO_4-HNO_3-N-MWCNTs (b), SH-Fe_3O_4/H_2O_2-HNO_3-N-MWCNTs (c), SH-Fe_3O_4-H_2SO_4-HNO_3-N-MWCNTs (d), N_2H_4-SH-Fe_3O_4/H_2O_2-HNO_3-N-MWCNTs (e) and N_2H_4-SH-Fe_3O_4/H_2SO_4-HNO_3-N-MWCNTs (f) nanocomposites.

5. Adsorption thermodynamics of Cr(III) ions removal by H_2O_2-HNO_3 treated nanocomposites

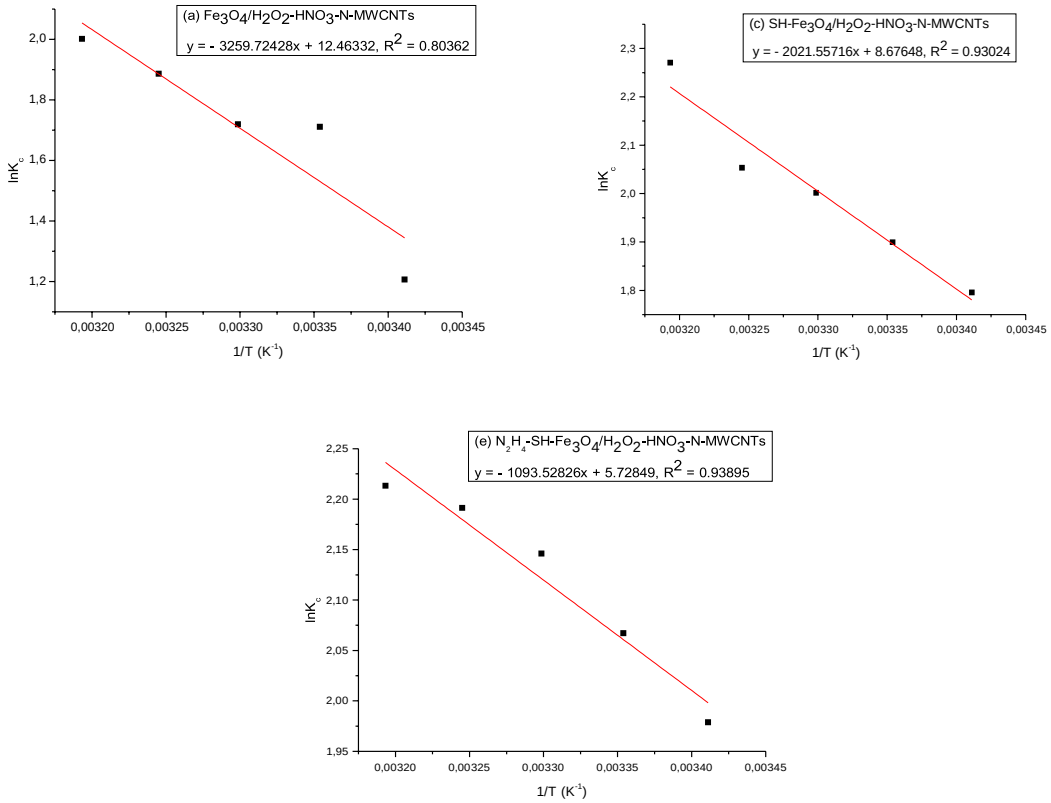

Figure 4.62: Thermodynamic analysis for adsorption of Cr(III) ions on Fe_3O_4/H_2O_2-HNO_3-N-MWCNTs (a), SH-Fe_3O_4/H_2O_2-HNO_3-N-MWCNTs (b), N_2H_4-SH-Fe_3O_4/H_2O_2-HNO_3-N-MWCNTs (c) nanocomposites.

6. Adsorption thermodynamics of Cr(VI) ions removal by H_2SO_4-HNO_3 treated nanocomposites

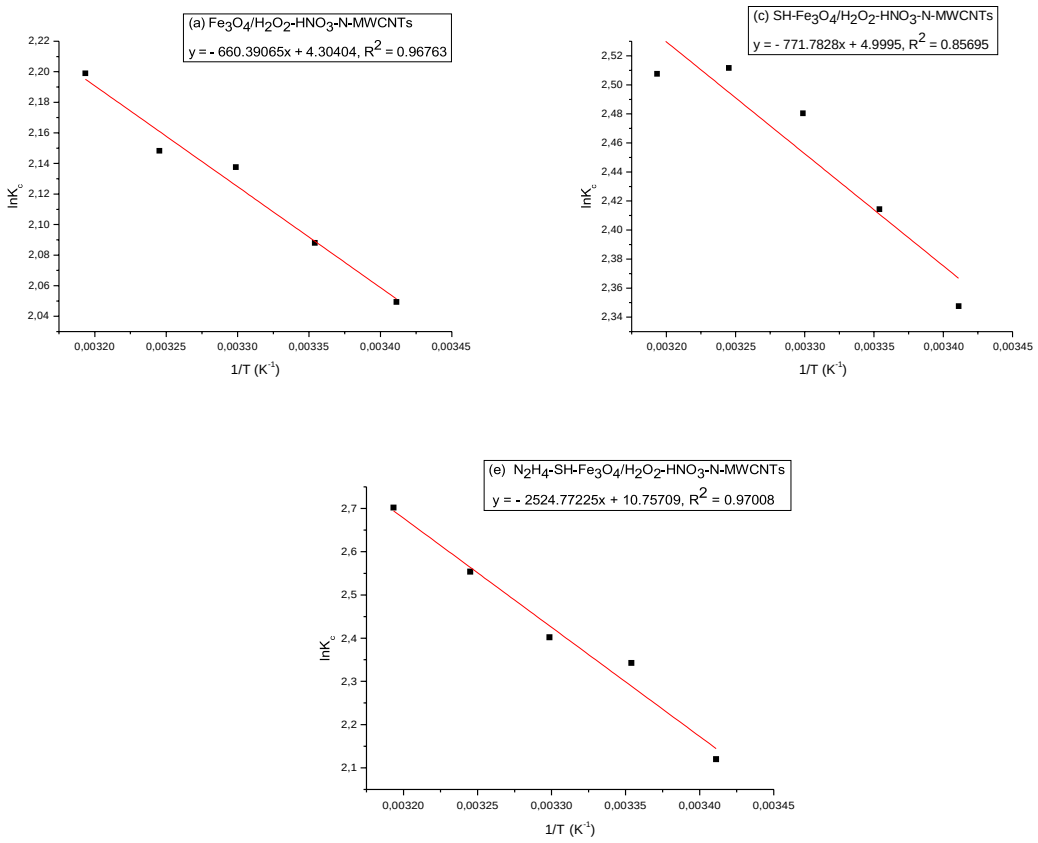

Figure 4.63: Thermodynamic analysis for adsorption of Cr(H_2O_2-HNO_3/MWCNTs, (c)N-MWCNTs, (d)H_2SO_4-HNO_3) ions on Fe_3O_4/H_2O_2-HNO_3-N-MWCNTs (a), SH-Fe_3O_4/H_2O_2-HNO_3-N-MWCNTs (b), N_2H_4-SH-Fe_3O_4/H_2O_2-HNO_3-N-MWCNTs (c) nanocomposites.

7. Effect of competing ions on the removal of Cr(III) and Cr(VI)

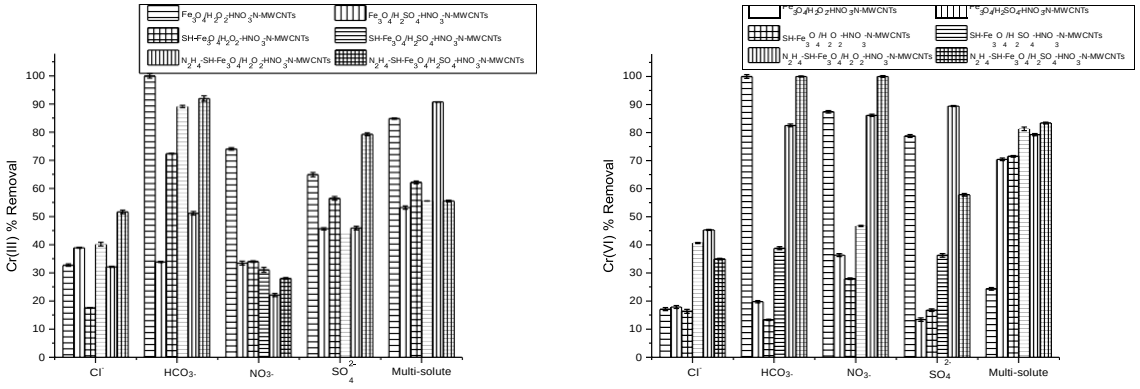

Figure 4.64: Effect of the presence of competing ions on the removal of Cr(III) andCr(VI) by H_2O_2-HNO_3 and H_2SO_4-HNO_3 treated nanocomposites

8. Reusability studies on Cr(III) and Cr(VI) removal

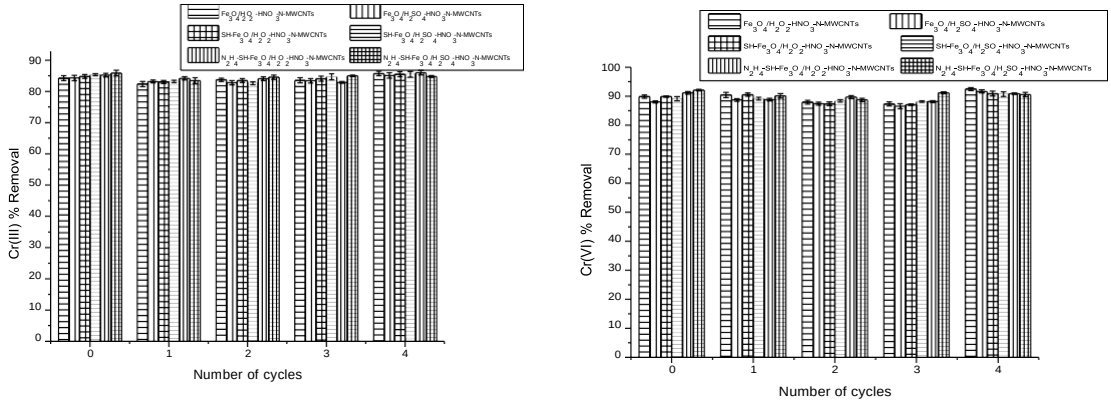

Figure 4.65: Reusability on Cr(III) and Cr(VI) removal onto H_2O_2-HNO_3 and H_2SO_4-HNO_3 treated nanocomposites

9. Effect of contact time on the removal of Ni(II) ions

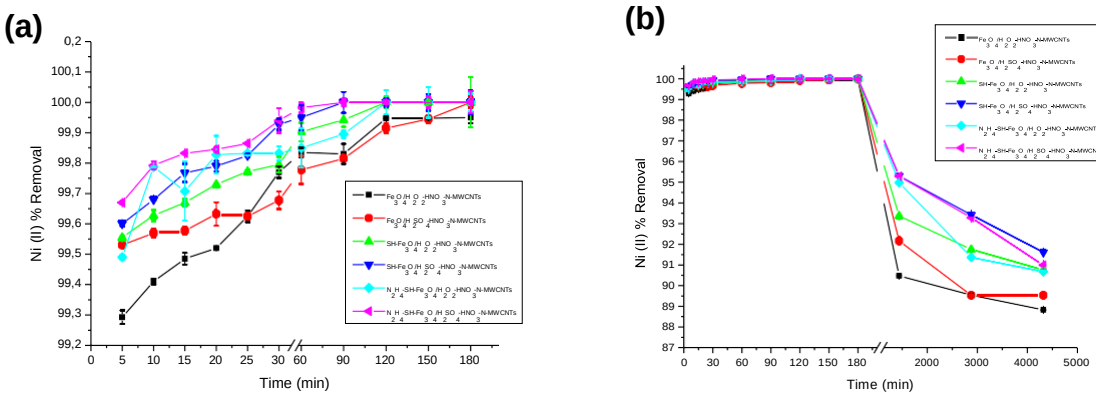

Figure 4.66: Effect of contact time on Ni(II) removal on Fe_3O_4/N-MWCNTs, SH-Fe_3O_4/N-MWCNTs and N_2H_4-SH-Fe_3O_4/N-MWCNTs treated with H_2SO_4-HNO_3 and H_2O_2-HNO_3.

10. Effect of initial concentration on the removal of Ni(II) ions

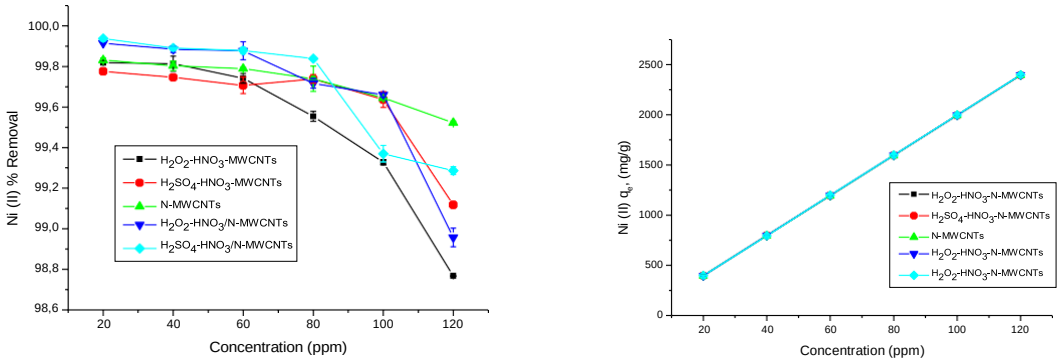

Figure 4.67: Effect of initial concentration on Ni(II) removal (a) and adsorption capacity (b) on H_2O_2-HNO_3/MWCNTs, H_2SO_4-HNO_3 /MWCNTs and N-MWCNTs, H_2O_2-HNO_3/N-MWCNTs, H_2SO_4-HNO_3 /N-MWCNTs.

11. Effect of temperature on the removal of Ni(II) ions

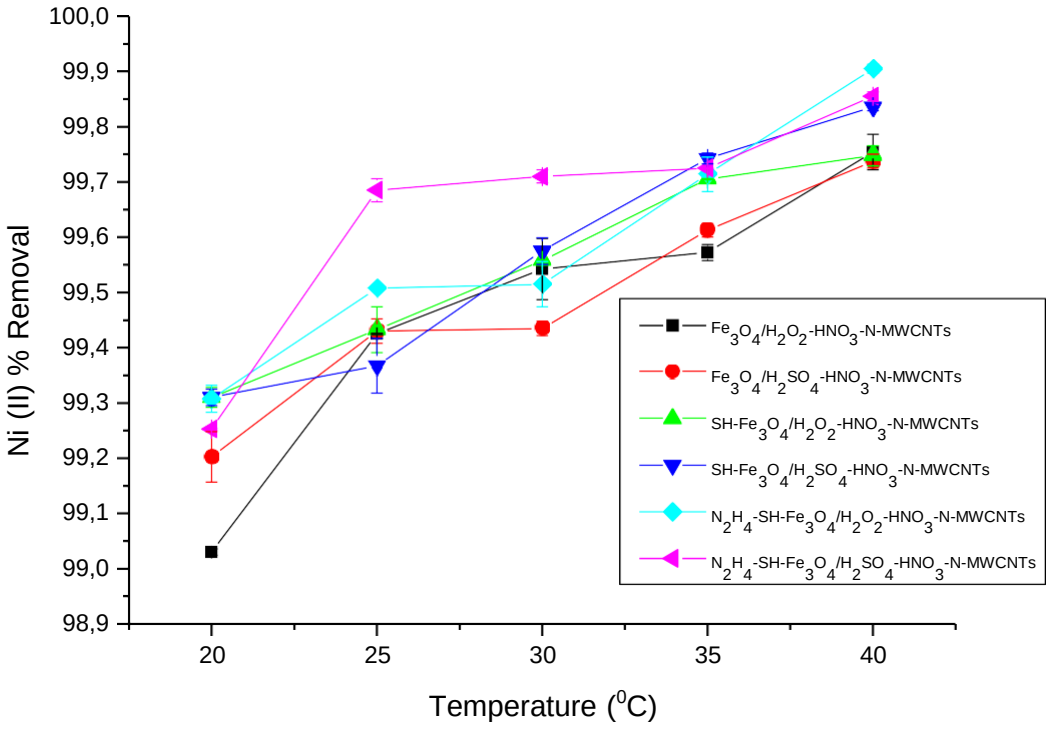

Figure 4.68: Effect of temperature on Ni(II) removal onto H_2O_2-HNO_3/N-MWCNTs and H_2SO_4-HNO_3 /N-MWCNTs nanocomposites.

12. Effect of competing ions on the removal of Ni(II) ions

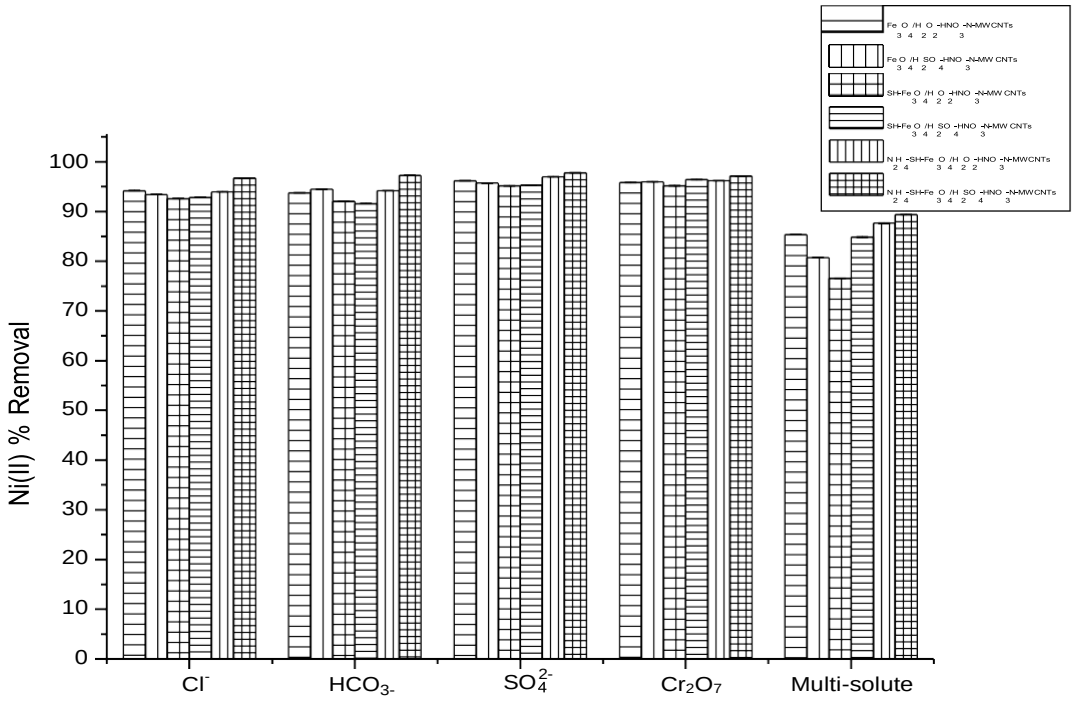

Figure 4.69: Effect of the presence of competing ions on Ni(II) removal onto H_2O_2-HNO_3/N-MWCNTs and H_2SO_4-HNO_3 /N-MWCNTs nanocomposites.

13. Reusability studies on Ni(II) removal

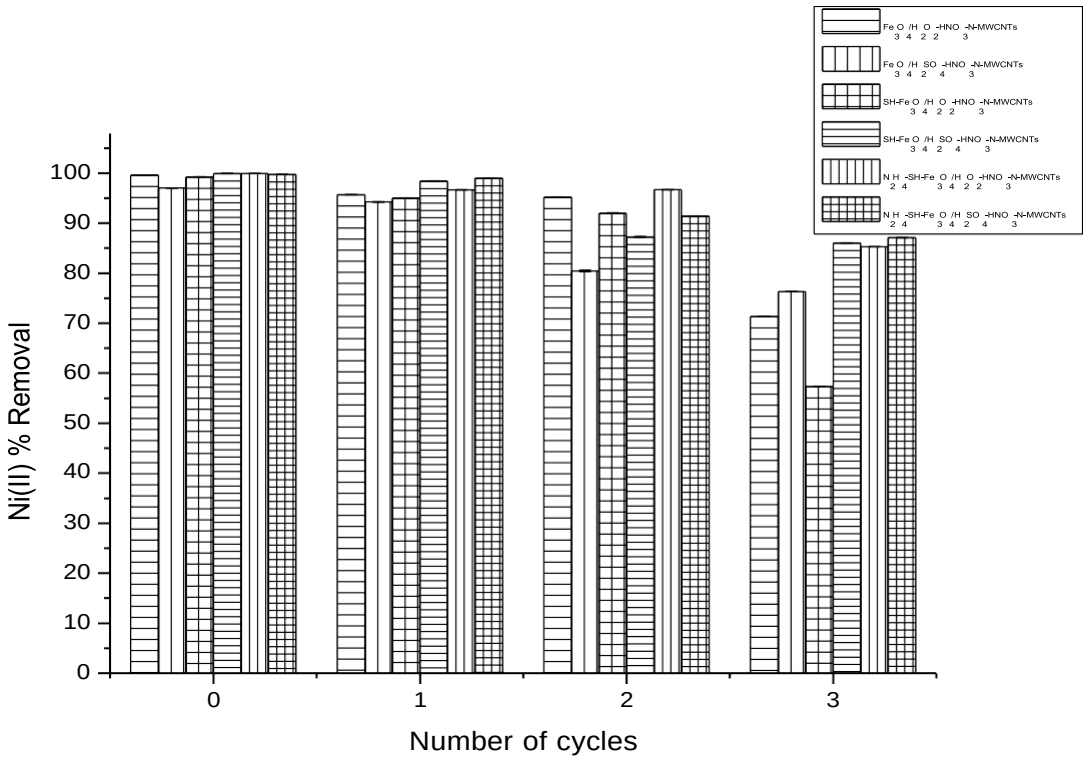

Figure 4.70: Reusability of adsorbents on Ni(II) by H_2O_2-HNO_3/N-MWCNTs and H_2SO_4-HNO_3 /N-MWCNTs nanocomposites.